Efficient Light-Induced pK(a) Modulation Coupled to Base-Catalyzed Photochromism

Johannes Gurke, Simon Budzak, Bernd M. Schmidt, Denis Jacquemin, Stefan Hecht

PROTONS AND PHOTONS

—

INTERCONNECTING PHOTOCHEMICAL AND ACID-BASE EQUILIBRIA

DISSERTATION

zur Erlangung des akademischen Grades

doctor rerum naturalium

Dr. rer. nat.

im Fach: Chemie
Spezialisierung: Organische und Bioorganische Chemie
eingereicht an der
Mathematisch-Naturwissenschaftlichen Fakultät
der Humboldt-Universität zu Berlin
von

Diplom-Chemiker Johannes Gurke

Präsidentin der Humboldt-Universität zu Berlin
Prof. Dr.-Ing. Dr. Sabine Kunst

Dekan der Mathematisch-Naturwissenschaftlichen Fakultät
Prof. Dr. Elmar Kulke

Gutachter/innen:	1. Prof. Stefan Hecht Ph.D.
	2. Prof. Dr. em. Werner Abraham
	3. Dr. habil. Christophe Coudret
Tag der mündlichen Prüfung:	19. Februar 2018

Die vorliegende Arbeit wurde in der Zeit von November 2013 bis November 2017 am Institut für Chemie der Humboldt-Universität zu Berlin unter der Anleitung von Prof. Stefan Hecht, Ph.D. angefertigt.

SELBSTÄNDIGKEITSERKLÄRUNG

„Ich erkläre, dass ich die Dissertation selbständig und nur unter Verwendung der von mir gemäß § 7 Abs. 3 der Promotionsordnung der Mathematisch-Naturwissenschaftlichen Fakultät, veröffentlicht im amtlichen Mitteilungsblatt der Humboldt-Universität zu Berlin Nr. 126/2014 am 18.11.2014 angegebenen Hilfsmittel angefertigt habe.“

Ort, Datum Unterschrift

Teile dieser Arbeit wurden bereits veröffentlicht oder eingereicht in: / Parts of this work have already been published or submitted in:

[1] J. Gurke, M. Quick, N. P. Ernsting, S. Hecht, *Chemical Communications* **2017**, *53*, 2150-2153.

[2] J. Gurke, Š. Budzák, B. M. Schmidt, D. Jacquemin, S. Hecht, *Angewandte Chemie International Edition* **2018**, *57*, 4797-4801.

VORWORT UND DANKSAGUNG

Wie so vieles in der deutschen Sprache entstammt das Wort „*promovieren*“ dem lateinischen, und bedeutet befördern, sich vorwärtsbewegen. Erst später bekam es die Bedeutung des Erlangen der Doktorwürde hinzu. Ich habe meine Promotion nie allein zum Zwecke der wissenschaftlichen Weiterentwicklung verstanden, sondern auch als Möglichkeit auszugleichen, was ein Chemiestudium mir nicht vermochte beizubringen. Ich verstand die vergangenen vier Jahre viel mehr als Zeit mich fachlich, persönlich und charakterlich „anzuheben“. Daher gilt die folgende Danksagung nicht nur den Personen meines wissenschaftlichen Umfeldes, sondern auch jenen, die mich in meiner persönlichen Weiterentwicklung begleitet haben.

Gleich zu Beginn möchte ich mit einer Konvention brechen, nicht zuerst meinem Doktorvater zu danken, sondern meiner Partnerin Manuela Risch, die alles ertragen hat. Jede extra Stunde in der Universität, denn persönliche Weiterentwicklung bedarf Zeit, die Sie mir gegeben hat.

Natürlich gilt mein Dank Professor Stefan Hecht für die optimalen Forschungs- und Promotionbedingungen. Selbstständiges Arbeiten, Denken und Forschen gehören für ihn zur Grundlage der Doktorarbeit und damit einher ging auch die beinahe uneingeschränkte Freiheit in der Bearbeitung und meines Forschungsthemas. Ich danke für ein immer offenes, aber auch kritisches Ohr für jede neue Idee, jedes Konzept was meinem Geist entsprungen ist. Mein größter Dank gilt seiner Geduld und Vertrauen in meine Fähigkeiten. Denn betrachtet man die vergangen vier Jahr kritisch, waren die ersten drei nicht von viel Erfolg getragen. Trotzdessen war ich mir seine Unterstützung sicher.

Mein Dank gilt auch der Arbeitsgruppe von Professor Hecht, für kritische Diskussion und eine sehr angenehme Arbeitsatmosphäre. Ins besondere danke ich Jutta Schwarz und Jana Hildebrandt für die praktische Syntheseunterstützung sowie dem Labor 3‘107. Dr. Bernd M. Schmidt, Dr. Alexis Goulet-Hanssens und Yves Garmshausen gilt mein Dank für das kritische Lesen dieser Arbeit. Nicht zuletzt danke ich meine Bachelorstudenten Luisa Lamberta Hantschke und Timo Pelchen sowie meinen Kooperationspartnern und Florian Römpp.

Dr. Robert Gurke, Dr. Celin Richter, Dr. Mario Gericke, Christan Helmut Kimmich, Yves Garmshausen und Dr. Thomas Kropp danke ich für kritische Diskussion über die Grenzen chemischer Fachdisziplinen hinaus und für ihre freundschaftliche Unterstützung.

Meiner Familie mit denen ich die vielen Misserfolge und wenigen Erfolge teilen konnte, danke ich. Zu guter Letzte möchte ich mich bei jene bedanken, die mich in meiner persönlichen Entwicklung begleitet haben: Fabian Kriegel, Sascha Hecker und Christian Weitzberg und der Gemeinschaft der Wasserwacht des DRK.

ABSTRACT

Two projects are implemented in this work, which share the goal to interconnect acid-base equilibria with the photoreactions of diarylethene (DAE) photoswitches. This task can be divided into two logic questions: How can photochemical equilibria be controlled or rather influenced *via* an acidic or basic stimulus and how can a photoreaction induce control over an acid-base equilibrium?

In the first project, "Acid-Catalyzed Cycloreversion", an externally tunable thermal back reaction was designed to influence a photochemical equilibrium. Upon addition of catalytic amounts of acid, a closed diarylethene derivative carrying a fluorenol moiety undergoes facile thermal ring opening. The underlying thermodynamics and kinetics of the entire system have been analyzed experimentally as well as computationally. Appling an excess of acid leads to a complete inhibition of the photoreaction through the introduction of a charge-transfer. My work suggests that acid catalysis provides a useful tool to bypass thermal barriers, by opening new reaction pathways, potentially usable to efficiently trigger the release of light energy stored in photoswitches.

In the second project, entitled "Light-induced pK_a Modulation", a significant pK_a change of 2.8 units in an aqueous medium was achieved by connecting two different acid-base equilibria. These thermodynamic equilibria are separated by a high activation barrier, overcome by a photoreaction. Furthermore, the developed system which is based on the incorporation of a 3-*H*-thiazol-2-one moiety into a DAE photoswitch, shows a strong dependency of the quantum yield and hence, of the photoconversion on the protonation state. Adjusting the pH within the range of the pK_a change (pH = 5 for this system), a substantial enhancement of the photoconversion is achievable as well as a distinct alteration of the performance of the photoreaction. In contrast to the first example, this effect does not originate from different reaction paths on the ground state potential energy surface (PES), but results presumably from a protonated state dependent difference in the excited PES.

It is noteworthy to point out that the questions addressed herein have already been discussed in the literature; however, through novel molecular designs it was possible to achieve significant progress and reach new insights.

ZUSAMMENFASSUNG

Gegenstand dieser Arbeit ist die Frage wie thermische und photochemische Gleichgewichte verbunden werden können und sich gegenseitig beeinflussen. Dazu wurden zwei Projekte bearbeitet, zum einen das Konzept der „säure-katalysierten Zykloreversion“ und zum anderen das Konzept der „licht-induzierten pK_a Veränderung“.

Im ersten der beiden Konzepte wurde eine extern steuerbare, thermische Rückreaktion genutzt, um die Zusammensetzung im photostationären Zustand zu kontrollieren. Durch Zugabe von katalytischen Mengen einer starken Säure wurde die Ringöffnung eines Diarylethens, welches mit einem Flurenol substituiert ist, eingeleitet. Der zugrundeliegende Prozess wurde kinetisch und thermodynamisch, sowohl durch Experimente als auch durch computergestützte Rechnungen beschrieben. Eine säure-induzierte Dehydratation öffnet einen neuen Reaktionspfad, wodurch die normalerweise sehr hohe Reaktionsbarriere der Ringöffnung umgangen werden kann. Die quantitative Umsetzung mit Säure führt zu einer kompletten Löschung der photochemischen Reaktivität. Dieses Konzept könnte in der Speicherung von Lichtenergie in photochromen metastabilen Systemen genutzt werden. Dabei liegt der Fokus nicht auf der absoluten Menge an speicherbarer Energie, sondern auf der Möglichkeit bei Bedarf gespeicherte Energie in thermische Energie umzuwandeln zu können.

Durch die Nutzung von 3-*H*-Thiazol-2-on als Arylrest im Diarylethen konnte eine signifikante pK_a Änderung von 2.8 Einheiten in wässriger Umgebung erreicht werden. Unter energetischer Betrachtung wurden dabei zwei Säure-Base Gleichgewichtssysteme miteinander gekoppelt, welche jedoch durch eine hohe Aktivierungsbarriere an der Umwandlung ineinander gehindert sind. Diese thermisch verbotene Reaktion kann jedoch photochemisch durchgeführt werden. Des Weiteren wurde eine hohe Abhängigkeit der Quantenausbeute von dem Protonierungszustand festgestellt. Diese wurde genutzt um die Performance der Photoreaktion zu beeinflussen. So führte die Einstellung auf pH 5, welcher genau zwischen den pKa Werten der Photoisomere liegt, dazu, dass eine vollständige Photokonversion bei der Zyklisierung induziert werden konnte. Im Gegensatz zum ersten Beispiel erfolgt die Beeinflussung der Photoreaktion nicht durch Veränderung der Energetik des Grundzustandes, sondern durch Veränderung der Potentialhyperfläche des angeregten Zustandes. Durch neue molekulare Designs konnte eine signifikante Verbesserung im Vergleich zu bekannter Molekülen und Konzepten in beiden Projekten erreicht werden.

TABLE OF CONTENTS

1 INTRODUCTION

Interconnecting equilibria, what does this mean and how can it be achieved? These questions can be approached either from an energetic or from a structural point of view, whereat a deep understanding of the concept of a potential energy surface (PES) is required.

The PES is defined as "a geometric hypersurface on which the potential energy of a set of reactants is plotted as a function of the coordinates representing the molecular geometries of the system."[3] Rephrasing this, every point on this multidimensional surface depicts one or the combination of several molecular entities, a plot of a particular multi-atom structure against its energy. "Moving" on this surface means that a chemical reaction is happening. The multi-atom conglomerate undergoes a distinct structural change, which necessarily correlates with an energy profile. The "navigation" on this surface is connected to a general goal of chemistry, controlling reactions and reactivity. In this context, the interconnection of equilibria or reactions can be understood as the linkage of two or more, formerly separated, PESs. To simplify this abstract concept of a multidimensional potential energy surface, phrases like "modulating" or "changing" the PES are often used, such as in the "decrease" of an activation barrier by a catalyst. In reality, a new reaction path opens up by introducing another dimension into this multidimensional surface. Unfortunately, the imaginativeness of the human brain is limited to three dimensions, and even this is mentally challenging to comprehend from a two-dimensional projection on a sheet of paper. Therefore, a potential energy diagram is used, which is literally a cut through the surface along the reaction path, giving a simple two-dimensional plane with an energy profile.

Even though not fully correct by physicochemical standards, an interconnection of equilibria will be considered either as a deformation in the energy profile of the first equilibrium by the second one and *vice versa* or as a distinct change in the population of the reactants *via* the second reaction. It does not only mean that two reactions occur in a sequential fashion, but that they influence each other.

To transfer this abstract line of thought into a molecular design, which can be synthesized, it is necessary to understand structure-property relations, the molecular/structural changes on the mentioned energy profiles and last but not least the effects, which can be introduced by geometrical changes during a reaction, electronic effects or delocalization paths within an organic molecule. Therefore, the aim of my work and research was not only to prove the concept, but also to understand the origins of the observed behavior.

The structural strategy to interconnect equilibria is rather simple; two reaction sides need to be incorporated into one structure, which in an ideal case, is triggered by two "*orthogonal*" stimuli.

Herein lies the first conscious decision: which trigger is going to be used. Le Chatelier's principle describes the possibility to influence a reaction in equilibrium, e.g. by temperature, by pressure or with chemical entities. The smallest chemical entities usable as stimuli are electrons or protons, defined as redox or acid-base reactions. The title of this work already suggests the selected trigger: a proton. It is the smallest possible Brønsted- and Lewis-acid, and always requires an electron-lone pair to interacte with.[3-4] Increasing electron density leads to a stronger lone pair-proton interaction, quantified by the pK_a of the molecule. The *orthogonal* stimulus is a photon, the particular form of light. An interaction of an atom or a molecule with a photon could lead to the process called absorption, where the chemical entity changes from its ground state to its excited state.[5] The interconnection of acid-base reactions and the absorption process is well known in literature. The change of the absorption spectra by an acid-base reaction is called acidochromism,[6] while the difference in the acidity between the ground and excited state is a concept employed for photoacids.[7] After excitation several processes might occur, e.g. emission, relaxation, interconversion and chemical conversion. The focus lies on the reactions occurring in the excited state, which are strongly connected to the observation of photochromism. As acidochromism is the change of the color by acid, the change by irradiation with light is called photochromism:

> *"[…] is a reversible transformation of a chemical species induced in one or both directions by absorption of electromagnetic radiation between two forms, A and B, having different absorption spectra"*[6a]

It is important to understand that the reversibility leads to a dynamic equilibrium driven by irradiation with light, which does not follow the law of mass action. The composition in the equilibrium state depends on the extinction coefficients of both photoisomers at the irradiation wavelength, on the quantum yields of both photoconversions (A→B, B→A) at the irradiation wavelength and on the rate constant of possible existing thermal isomerizations.

The interconnection of photochromism with chemical reactions in general,[8] including acid-base equilibria, have been a constant focus of past research. Our task was the improvement of known concepts by novel molecular designs. Therefore, diarylethenes (DAEs) as robust but also thermally irreversible photoswitches were employed. Superior photochromic behavior has been achieved with this class of photoswitches.

2 GENERAL PART

2.1 DIARYLETHENES (DAEs)

2.1.1 DAE Photochromism - Properties and Mechanism of Switching

The starting point of DAE research originates from the photochemistry of stilbenes.[9] Theoretical backgrounds have been largely elucidated by Woodward and Hoffmann with their publications on the stereochemistry of electrocyclic reactions[10] and the conservation of orbital symmetry.[11] Irie *et al.* did fundamental work to develop the stilbene type molecules to the molecules now known as DAEs.[12] With his highly-cited and well renowned review, Irie and his co-workers contributed the most comprehensive summary of DAEs.[13]

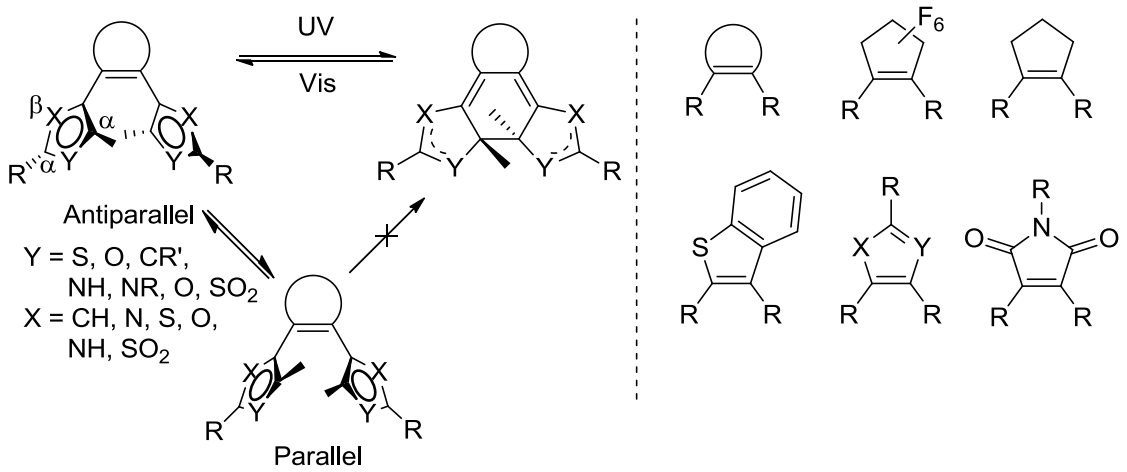

Scheme 2-1 Diarylethenes: structures and its thermal and photochemical reactions.

DAEs are photochromic compounds,[6a] which undergo a conrotatory 6π electrocyclization upon UV irradiation from the antiparallel conformation with high quantum yields, while cycloreversion is induced by visible light, yet occurring with much lower quantum yields. The disrotatory ring closure is not thermally favored and the parallel conformation does not lead to the photoreaction. The most used structural motif is the dithienyl hexafluorocyclopentene. The nomenclature of the aryl moiety stems from the use of thiophenes as the aryl components. The inner α carbon is termed active, since the new carbon-carbon bond is formed at this position. As shown in Scheme 2-1, a great diversity of DAE cores are literature known. Cyclization of DAEs by illumination with sunlight has been shown in the literature, although typical DAEs do not match the solar spectrum.[14] Due to the presence of UV light in combination with the more efficient cyclization, exposure upon sunlight leads to a significant, but less efficient conversion to the closed isomer compared to the irradiation with a single UV wavelength. In comparison to other photochromic molecules, typical DAEs show no thermal cycloreversion and are therefore

categorized as P-type photochromes(see chapter 3.2.1).[15] By using an appropriate substitution pattern, DAEs can be rendered highly fatigue resistant, even in solution (see chapter 2.1.2).

An important feature of DAEs is the change of the conjugation motif, e.g. the change from a hexatriene structure to a cyclohexadiene. It causes the substantial bathochromic shift of the closed absorption spectrum compared to the open. Negative photochromism has been realized *via* semi-inverse and inverse setup, where a linear conjugation in the open form changes to a cross-conjugated one, achieved by connecting the bridge to the thienyl moiety *via* the α carbon.[16] The alteration from a cross- to a linear-conjugated π-framework through the switching process in the classic DAE leads to the ability to modulate the electronic communication (use of this see chapter 4.2.1). The effect is amplified by the fact that the aryl moieties are twisted out of plane in the open form, while the closed isomer is more flat and rigid. This causes a significant change in the frontier orbital levels, which is the basis for the absorption shift. The mentioned transformation of the double bond structure results in the "disappearance" of aromaticity. This "loss" of aromatic stabilization energy is of central importance for this work and has been used in several literature examples, but also causes problems (see chapter 2.1.2). However, in this work it will be used to store energy (chapter 3) and to modulate an acid-base equilibrium (see chapter 4).

The aim of this work and science in general is not only the realization of concepts and reaction, but also the fundamental understanding of observations. This enables the transfer to other molecular systems and the application on not described molecules. Therefore, the following section will discuss the fundamentals of DAE photochemistry.

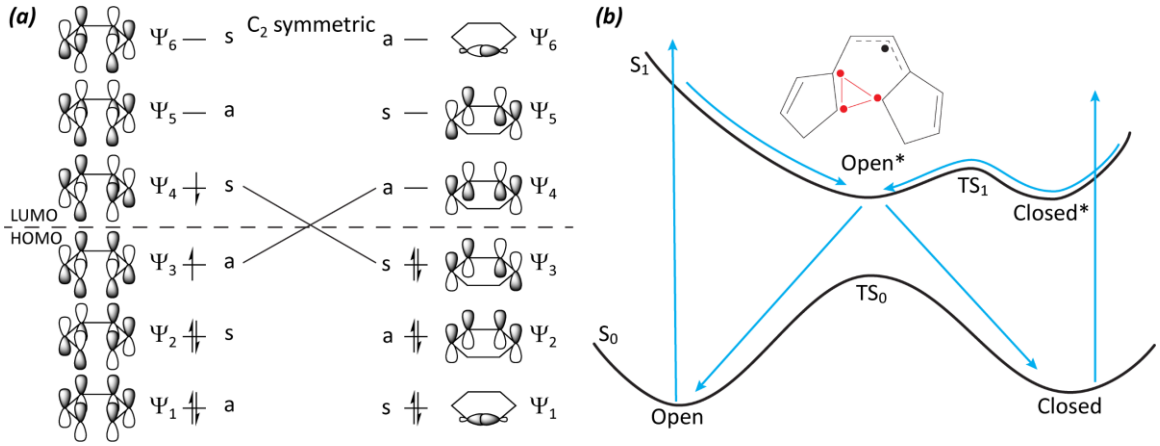

Figure 2-1 [11] [17] DAE switching mechanism: (a) orbital correlation diagram, including the frontier orbital of hexatriene on the left and cyclohexadiene on the right; (b) simplified potential energy surface including reaction paths of the cyclization and cycloreversion.

A first approximation of the mechanism of switching is provided by the orbital correlation diagram. Therefore the ideal frontier orbital of the photoreactive DAE core, the hexatriene and cyclohexadiene needs to be formulated (see Figure 2-1a).[18] The conrotatory cyclization appears

through preservation of C_2 symmetry, which leads to the classification of the orbitals as symmetric and asymmetric. According to the Woodward-Hoffmann rules, the reaction is thermally forbidden, but photochemically allowed and an activation barrier separates the reactants from the products of the reaction. Detailed theoretical analysis of a model compound agrees with this first approximation as it shows a barrier for the first excited state for the interconversion of the excited closed state to the excited open state.[17] The irradiation of the open isomer leads to a higher electronically excited state, which relaxes first into the S_1 and then to the excited state open isomer. From there, the system passes through the conical intersection to S_0 to reach either the closed form or to regenerate the open form. Similar to excitation of the open isomer, the closed isomer first reaches a higher excited state or a Franck-Condon (FC) state. After intersystem crossing or FC relaxation occurred, the excited molecule relaxes to the excited closed isomer. From there it must overcome the barrier TS_1 to reach the excited open structure and the conical intersection. Further detailed descriptions are summarized by Irie *et al.*.[13]

2.1.2 Design Principles for Robust DAEs

To avoid side reactions, distinct substitution motifs are required. This chapter will focus on the non-productive reaction, not on the structural dependence of the thermal stability (see chapter 3.2.1) or photochemical properties, e.g. absorption, band separation or quantum yield, which were the detailed focus of past reviews.[19] Different thermal, as well as photochemical reactions are reported, which occur almost exclusively from the closed isomer. For most of the reactions the recovery of the aromaticity is the main driving force. In the case of the hexafluorocyclopentene bridged DAEs a second possible driving force appears, the release of fluoride or the formation of hydrogen fluoride. The substitution of the active α carbons and by an appropriate group is essential for the stability. The oxidation of the closed isomer to a phenanthrene derivate is reported in case of unprotected α carbons, whereas a mono-substitution with a potential leaving group leads to elimination,[20] while an asymmetric substituent pattern by groups whiteout leaving character leads to a ring opening of the opposite heterocycle.[21] Slow thermal rearrangement of the α carbon substituent is rarely reported,[22] while photorearrangement[23] is more often observed, but can be prohibited by the addition of electron withdrawing groups.[24] Therefore, the hexafluorocyclopentene bridge is the most commonly used motif, which prevents the problem of photooxidation, frequently observed for electron rich structures like thiophene. Even though the photooxidation results mostly in undefined products, a ring expansion of the cyclohexadiene core *via* an endoperoxide and peroxide structure has been reported.[25] Furthermore, halogen-carbon bonds are known to be unstable under irradiation.[26]

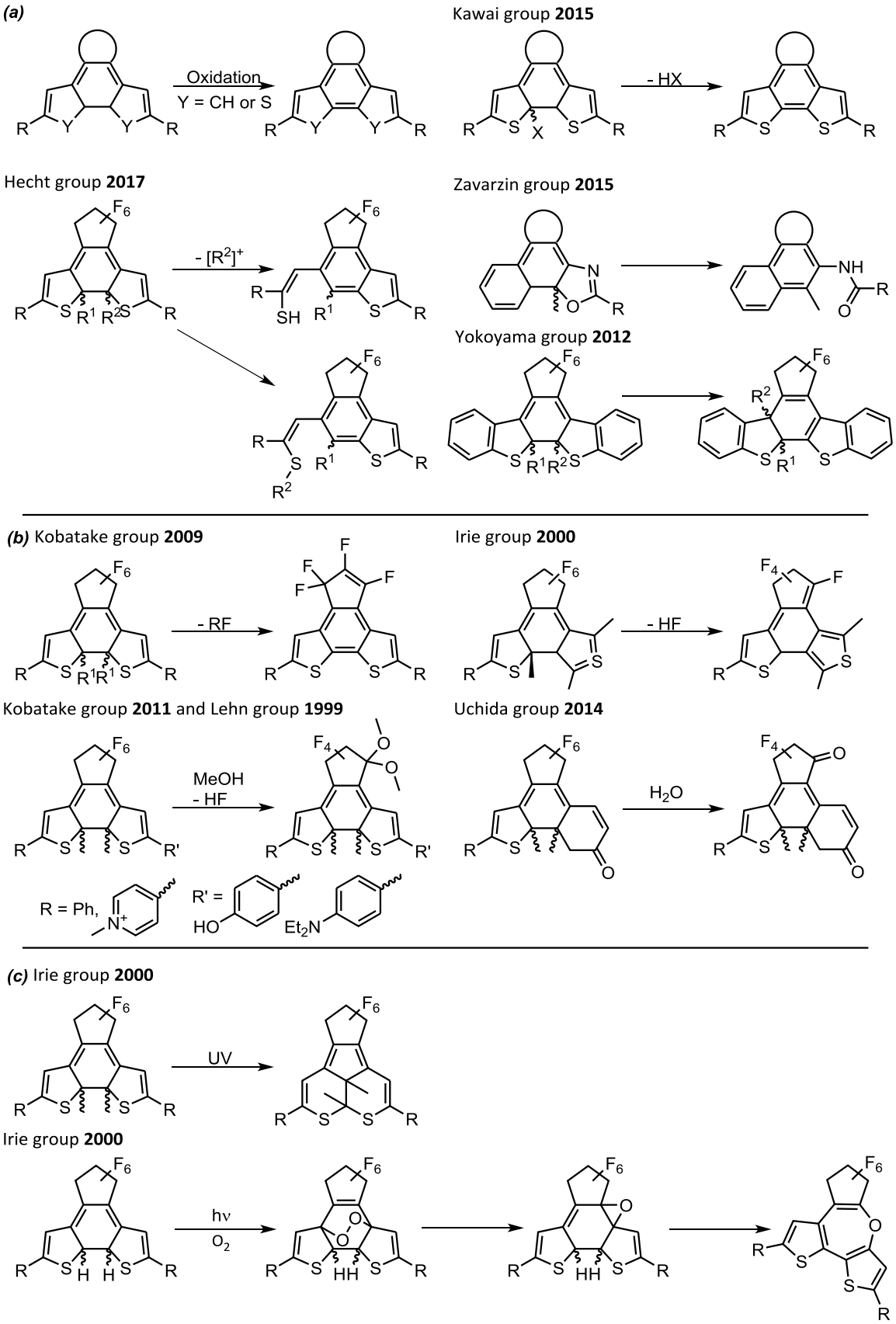

Scheme 2-2 Side reactions of DAE derivatives: ***(a)*** *thermal side reaction at the DAE core;* ***(b)*** *side reaction at the hexafluorocyclopente bridge;* ***(c)*** *photochemical side reactions at the DAE core.*

Fluorine substitution reactions are reported to occur in nucleophilic solvents. The reaction results the formation of an acyclic acetal[27] in the presence of methanol or a ketone[28] in the case of water as solvent. The electron accepting character of the pyridinium substitution has been discussed by Kawai *et. al* as a reason for the increased reactivity of the allylic position towards nucleophiles. Uchida and co-workers proposed a rather controversial mechanism, in which elemental fluorine is eliminated after a previous enhancement of an electron accepting effect at the DAE through a protonation. Kobatake and co-workers report a nucleophilic substitution of the fluorines in the bridge caused by electron donors.[29] Furthermore, an elimination of a fluorine yielding a vinylic structure has been published[23, 25] as well as a double fluorine elimination in the case of trimethyl silyl substitutions at the active *α* carbon.[30] The substitution of the *β* carbon could also be used to prevent fluoride elimination, occurring from a photo byproduct.[25]

2.1.3 Preparative Approach to Asymmetric DAE Cores

The dominant use of the fluorinated bridge is not only caused by the electronic character and the increased fatigue resistance, but also its straightforward and robust preparation.[13] Symmetric as well as non-symmetric DAE-cores are easily accessible, due to the use of lithiation and direct substitution at octafluorocyclopentene. The drawbacks of this strategy on the other hand lie in the required compatibility with lithiated species, low reaction yields as well as an expensive and volatile starting material. The dictated reactivity distribution, e.g. the aryl moiety is the nucleophile and the perfluorocyclopentene is the electrophile, is a further disadvantage. Cross-coupling reactions with 1,2-chloro-3,3,4,4,5,5-hexafluorocyclopentene as well as Friedel-Crafts/McMurry approaches are reported, but rarely used.[31] The perhydrobridge is mainly built-up *via* the Friedel-Crafts/McMurry approach, which allows the synthesis of asymmetric DAE-cores.[32] Furthermore, a cross-coupling with 1,2-dibromocyclopentene was used as well as a synthesis *via* a Michael-addition. Heterocyclic bridges are either synthesized *via* cross-coupling or the bridge is build-up after connecting the aryl moieties.

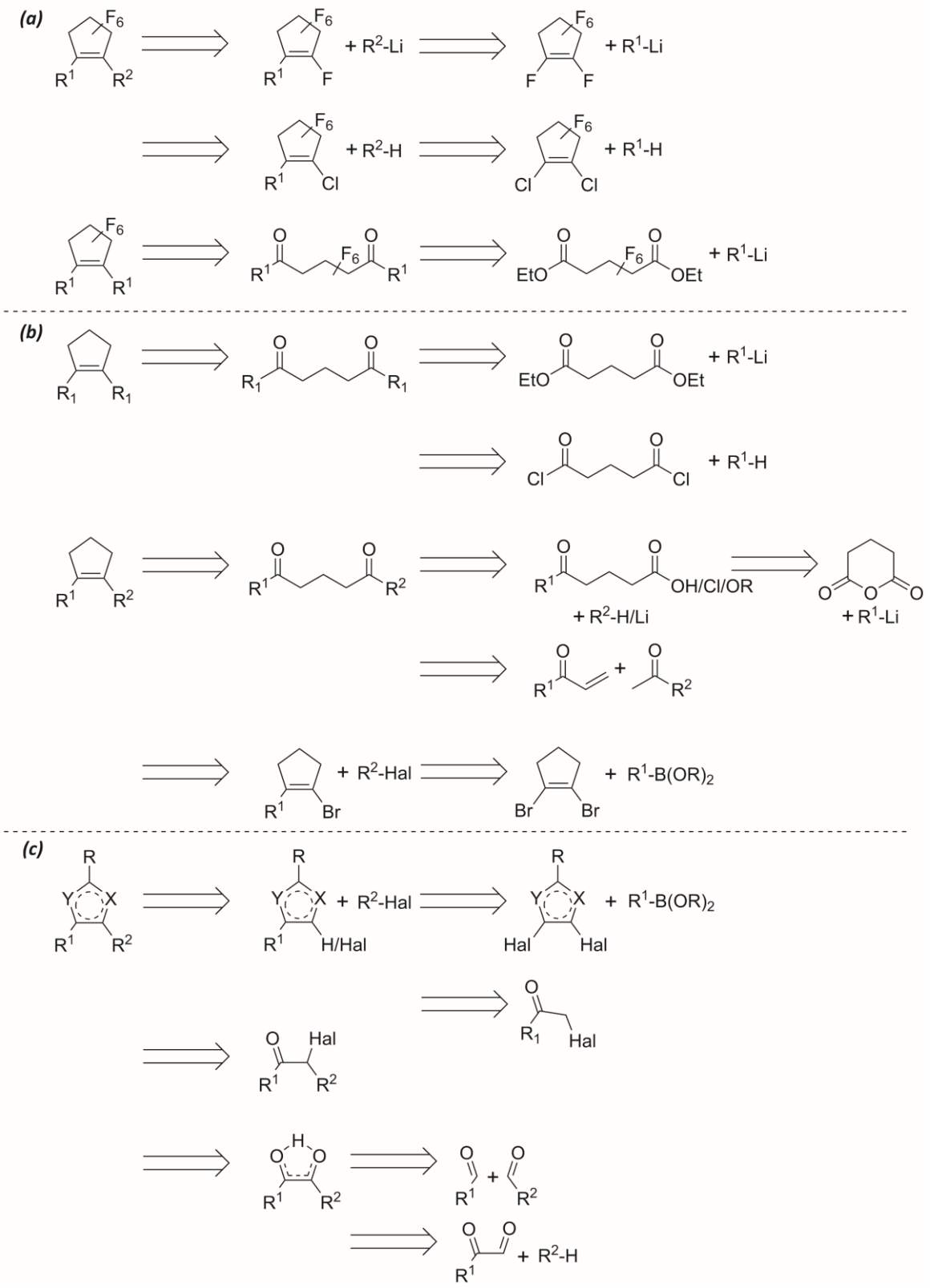

Scheme 2-3 Retrosynthetic approaches to symmetric and asymmetric DAE cores; ***(a)*** *hexafluorocyclopentene bridged DAEs;* ***(b)*** *cyclopentene bridged DAEs;* ***(c)*** *terarylene structures.*

2.2 pH AND pK_A OF ORGANIC MOLECULES IN AQUEOUS AND NON-AQUEOUS MEDIA

The pH was initially defined for pure water and so was the pK_a of a molecule. The limited solubility of organic molecules requires the substitution of the solvent. Furthermore, the importance of liquid chromatographic techniques, which are frequently used with a mixture of water and other organic water-miscible solvents, demands the quantification of pH in not-purely aqueous solution. The pharmaceutical industry has a need for the characterization of poorly soluble compounds, to estimate properties such as bioavailability.[33] Synthetic chemists need to estimate the reactivity of compounds, where the dissociation constant in organic solvents is of great importance. Due to the *leveling effect*, determination of dissociation constants in water are limited to a certain pH window (0-14).[3, 34] To overcome this problem the use of different solvents is necessary. The fundamental importance of this topic gives rise to a wide range of scientific models and approaches.[33a, 33b] Therefore, this chapter will focus on the acidity scales in water and water-acetonitrile mixtures. The determination of pK_a values by spectrophotometric titration will be briefly covered as well.

$$\boldsymbol{Acid} \rightleftharpoons \boldsymbol{Base} + \boldsymbol{Proton} \qquad \textbf{(E2-1)}$$

Equation 2-1 describes the Brønsted-Lowry theory of acids and bases. The equilibrium is formulated as a pair of corresponding acid and base, where the acid can be neutral (HA) or positively charged (HB^+). The solvent (SH) is mainly characterized by its relative permittivity (ε_r) and in the case of an amphiprotic solvent by its autoproteolytic equilibrium.[35]

$$\boldsymbol{SH} \rightleftharpoons \boldsymbol{SH_2^+} + \boldsymbol{S^-} \qquad \textbf{(E2-2)}$$

This leads to the rewriting of the equilibrium and the definition of the dissociation constant:

$$\boldsymbol{HA} + \boldsymbol{SH} \rightleftharpoons \boldsymbol{A^-} + \boldsymbol{SH_2^+} \qquad \textbf{(E2-3)}$$

$$\boldsymbol{K_a} = \frac{[\boldsymbol{A^-}][\boldsymbol{SH_2^+}]}{[\boldsymbol{HA}][\boldsymbol{SH}]} \qquad \textbf{(E2-4)}$$

$$\boldsymbol{HB^+} + \boldsymbol{SH} \rightleftharpoons \boldsymbol{B} + \boldsymbol{SH_2^+} \qquad \textbf{(E2-5)}$$

where *a* is the activity. The ionization of a neutral acid **HA** creates ions and is more sensitive to the polarity of the solvent, whereas the deprotonation of charged base $\mathbf{BH^+}$ does not involve charge separation and is less sensitive to polarity changes.[34] This equilibrium can be further splitted into two equilibria, which are strongly dependent on the polarity of the solvent; an ionization (E2-6) and a dissociation equilibrium for the formed ion pair. (E2-7):

$$\boldsymbol{HA} + \boldsymbol{SH} \rightleftharpoons \mathbf{ASH_2} \qquad \textbf{(E2-6)}$$

$$\mathbf{ASH_2} \rightleftharpoons \boldsymbol{A^-} + \boldsymbol{SH_2^+} \qquad \textbf{(E2-7)}$$

To standardize the dissociation constant, in water the pH scale resulting from the autoproteolytic equilibrium is used. To measure the pH, commonly a glass electrode is used,

where calibration of the Nernst equation with defined buffer solutions must be done. The use of a solvent mixture leads to a change of the pH and pK_a scale (labeled as ^{s}pH and $^{s}pK_a$), due to changes in autoproteolytic equilibrium and relative permittivity. An aqueous pH scale can be defined until 30 vol-% water. The preparation of buffer solutions in water-organic solvent mixtures are rarely reported and due to that not commercially available. This causes a limited feasibility and flexibility for different solvent mixtures, hence other techniques for standardization are required. The preparation of hydrogen chloride solutions with definite concentration can be used as well as a distinct change of the "proton" concertation *via* titration, whereat both options come up with a low feasibility.[33a, 36] A more practicable alternative approach was published by Bosch *et al.*, where the electrode is calibrated in aqueous buffer and the pH is measured as usual. To convert the resulting ${}_{w}^{s}pH$ scale (pH determined in solvent/water with electrodes calibrated in the water) to a ${}_{s}^{s}pH$ (pH determined in solvent/water with electrodes calibrated in the same acetonitrile/water mixture) a conversion parameter is used.[37] By ${}_{s}^{s}pK_a$ determination, a calculation of the pK_a in water is possible, by using the Yasuda-Shedlovsky plot, where ${}_{s}^{s}pK_a$--log[H_2O] is plotted against $1/\varepsilon_r$.[33a, 38] For determination in non-aqueous solutions, e.g. pure acetonitrile or dimethyl sulfoxide a reference base is used.[37, 39]

A variety of methods for the determination of pK_a values were developed in the past century, e.g. by potentiometry, the most popular and oldest method, by spectrometry,[40] conductometry, NMR, HPLC or by computation, which is rather challenging.[41]

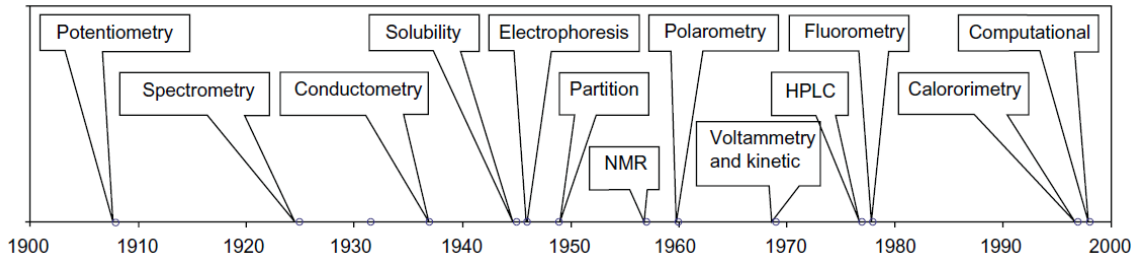

Figure 2-2[1] Timeline of the first notion of the various techniques to determine pK_a (dissociation constant, acid strength). [41]

Considering the initially discussed tasks within this work, the apparently most straight-forward method is the spectrometric determination of the pK_a value, which requires acidochromism of the target compound. To ensure this, the acidic or basic functionality needs to be attached near to the chromophore, e.g. an extended π-framework. The change of electronic properties, e.g. electron density or dipole moment, throughout the dissociation reaction and build-up of the charged or uncharged state, affect the frontier orbitals and consequently the HOMO-LUMO gap and absorption spectrum. Experimentally, the absorbance is measured in dependence of the pH or

[1] Reprinted with permission of © SAGE Publications

acid concertation, resulting in a sigmoidal curve where the pK_a can be determined from the inflection point.[42] This method is rather independent from the solvent, but susceptible to impurities. By measuring the whole spectral range, multi-component mixtures can be analyzed, even in the case of similar pK_a values. A concentration window, resulting from the Lambert-Beer law and the detection limit of the spectrometer, from approximately 10^{-6} M up to 10^{-3} M is achievable, which allows the determination of poorly soluble compounds. It is important, however, that the analyte does not affect the pH of the medium or interact with itself, which can be assumed in the case of low concentrations and the absence of medium effects, which can be neglected in the case of an existing isosbestic point within the acid or base induced spectral change.

3 Acid-Catalyzed Cycloreversion[2]

3.1 Introduction and Motivation

The use of a molecular photoswitch, that can be reversibly isomerized by light, constitutes a promising approach to chemically store solar energy and subsequently convert it to thermal energy on demand.[43] To store light energy efficiently, the molecular system has to fulfill certain design criteria:[44] 1) A high energy difference between the isomers combined with a low molecular mass to maximize the energy storage density; 2) a photoreaction with a high quantum yield (and no or negligible photochemical back reaction); 3) a matching absorption spectrum of the low energy isomer with the solar spectrum; 4) a sufficient thermal stability of the high energy isomer; 5) high fatigue resistance to assure recyclability of the system. While progress has been made in optimizing the energy storage density as well as long-time energy storage,[44] this work will focus on the issue of how to *release* the stored light energy using well-established DAEs.[45] Therefore a simple and universal trigger is needed. Furthermore, to enable the reusability of the system, the trigger must be easy to apply and remove from the system. An electron or a proton can be considered as such a trigger. Redox reactions, which induce a thermal back reaction are well-established for different photochromic molecule classes. Therefore, this chapter will focus on the use of an *acid-base reaction* to modulate the thermal reaction by bypassing the reaction barrier of the cycloreversion.

3.2 Theoretical Background

3.2.1 Thermal Stability of DAEs and Their Chemical Modulation

DAEs are known to be of P-type photochromes, which means that no thermal interconversion between the photoisomers is observed, meaning only irradiation with light leads to a conversion. Three different structure-properties relationships are known so far; the dependence on the aromatic stabilization energy of the aryl moieties, the influence of electron-withdrawing groups, and the effect of steric hindrance. (see Scheme 3-1)

[2] Parts of this work have already been published in: J. Gurke, M. Quick, N. P. Ernsting, S. Hecht, *Chemical Communications* **2017**, *53*, 2150-2153.

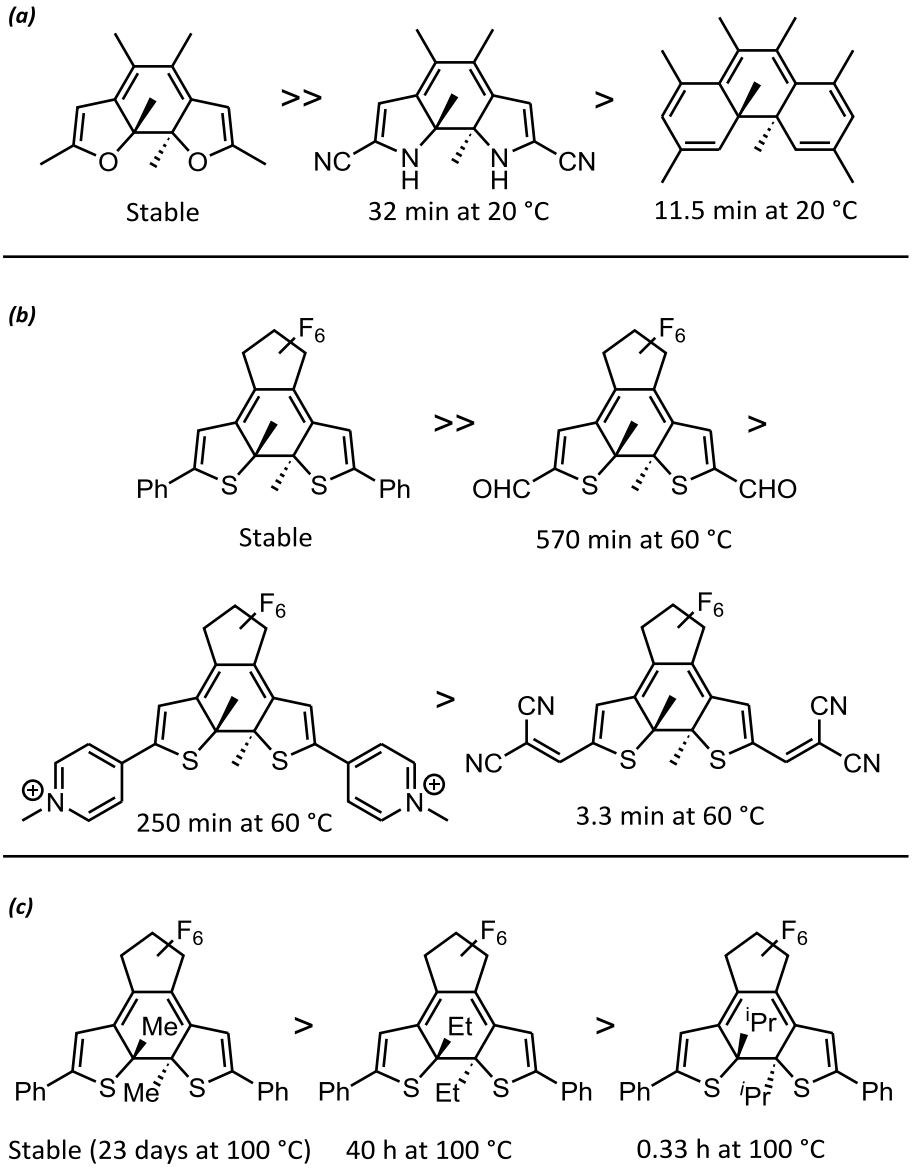

Scheme 3-1 Property-structure relationship of the thermal stability of DAEs: (a) increasing total aromatic stabilization energy leads to a decrease of the thermal stability; (b) substitution with strong electron withdrawing group decreases the thermal stability; (c) increasing steric hindrance at the α carbon decreases the thermal stability.

From the pioneering works of Irie and co-workers it is known that the closed DAE is typically the thermodynamically less stable isomer and the thermal back reaction is kinetically hindered due to an activation barrier, which increases upon decreasing the ground state energy difference.[12] DFT calculations of the thermal cycloreversion indicate a strong biradical character of the transition state[46] and therefore suggest a homolytic C-C-bond cleavage. It has been reported that the thermal stability decreases upon introduction of one or more aromatic moieties, which maximize the ground state energy difference.[47] For that reason thiophene and thiazole, with their low aromatic stabilization energy, were frequently employed as aryl moieties.[45]

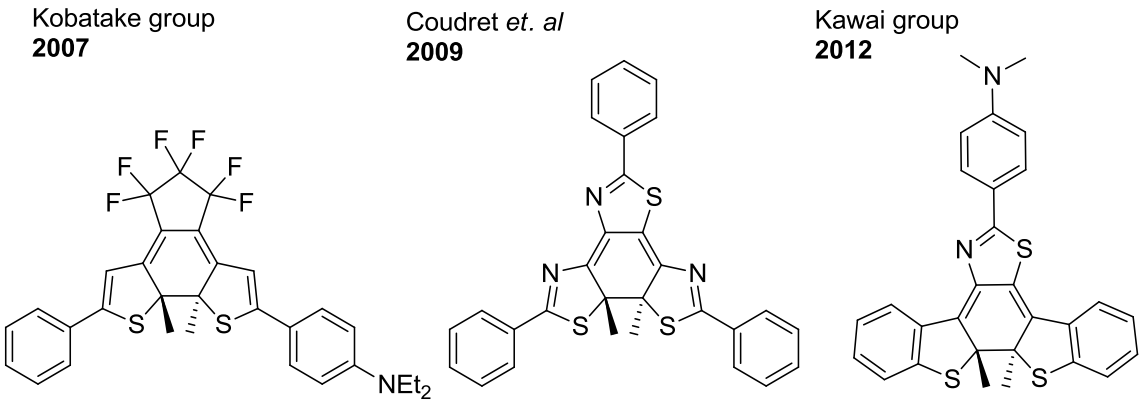

Figure 3-1 Modulation of the thermal stability by protonation of basic nitrogen atoms.

Furthermore, the substitution with electron-withdrawing groups leads to faster thermal cycloreversion.[48] This has been used to modulate the thermal back reaction by protonation of basic nitrogen or sulfur atoms.[49] The substitution of the *α* carbons with bulky substituents leads to a decrease of the thermal stability as reported by Kobatake *et al.*[50].

3.2.2 Gated Photochromism

The concept of gated photochromism has been defined in 2001 by Bouas-Laurent and Dürr[6a] and a summary of this field was published by Tian *et al.*[51] and Irie *et al.*[13]:

> *"Gated photochromism is a special type of photochromism in which one or both forms of the photochromic system* [Scheme 3-2a A and/or B] *are transformed (chemically or electrochemically) reversibly into a nonphotochromic form* [C]. *The photochromic process is controlled like the flow through a gate. The opening or closing of the gate may depend on external stimuli such as protonation, oxido-reduction, solvation, and temperature."*[6a]

While this definition describes the ideal case, it is now commonly used for systems showing significant deviations in terms of the overall performance, e.g. systems with low quantum yields or low photoconversion. To design a molecular system that fulfills this concept, two distinct questions need to be addressed: Which physico-organic processes inhibit a photoreaction and which chemical reaction is able to interconvert a photoresponsive state to a non-photoresponsive state?

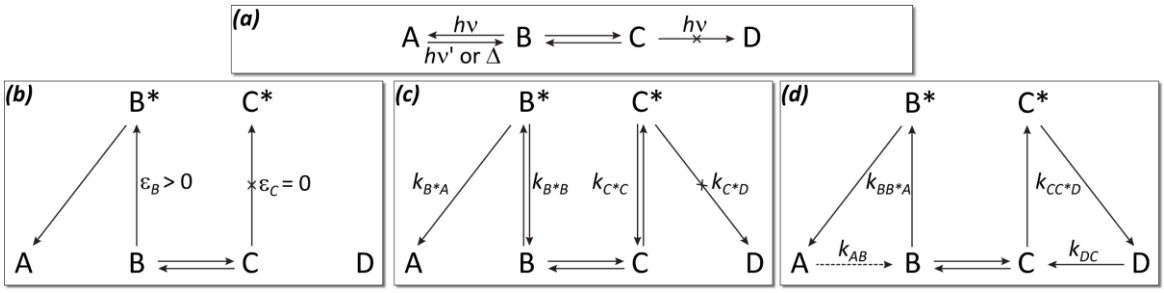

Scheme 3-2 Concept of gated photochromism and its possible mechanisms: (a) gated photochromism in general, (b) induced by differences in the absorption process ($\varepsilon_B >> \varepsilon_C$ or $\varepsilon_B \neq 0$, $\varepsilon_C = 0$), (c) induced by variation of the speed of the different relaxation processes ($k_{B*B} \leq k_{B*A}$ and $k_{C*C} >> k_{C*D}$ or $k_{C*D} = 0$), (d) induced by variation of the speed of the thermal backreaction and photoreaction ($k_{BB*A} \geq k_{AB}$ or $k_{AB} = 0$ and $k_{CC*D} << k_{DC}$).

The answer to the first question requires a general understanding of the excitation and photochemical process as well as a detailed knowledge of the switching mechanism, for DAEs provided by Woodward and Hoffman (see chapter 2.1.1).[10-11] The fundamental paradigm of molecular photochemistry is the state energy diagram[5] and the absorption of light is the starting point of every photoreaction. The energy of the electromagnetic irradiation has to overlap with the band gap. Amongst other, the rate of a photoreaction depends on the molar extinction coefficient at the irradiation wavelength. A change of the absorption spectra induced by a chemical reaction leads to a modulation of the photoreaction, if the irradiation wavelength stays constant (see Scheme 3-2b). The *classic* model to explain gated photochromism is the variation of the rate constant of the photoreaction (see Scheme 3-2c, k_{B*A} and k_{C*D}). The ideal case is the drastic decrease of the rate constant of the photoreaction ($k_{C*D} = 0$). Alternatively, the relaxation paths of the excitation energy could be accelerated ($k_{C*C} >> k_{C*D}$). Herein, the rate constant of the relaxation is the sum of all possible paths which do not result in a photo conversion, such as fluorescence, internal conversion as well as charge, electron and energy transfer paths. A change in the photochemical rate constants results in the modulation of the quantum yield, which describes the efficiency of the photoreaction. The conrotatory ring closure and opening of the DAE requires a distinct orbital structure, provided by the hexatriene structure and respectively, the cyclohexadiene structure. Therefore, the “shape” of the LUMO is of great importance (see 2.1.1). Variation of the central double bond motif however, leads to a loss of the photochromism.[52] Therefore redox-reactions (Figure 3-2a), the Diels-Alder reaction, as well as photoreactions were used. Furthermore, modulation of the electronics of the molecule influences the molecular orbital’s shape[53] and therefore the spectroscopic properties and overall switchability.[54] This has been used to enable and disable a photoreaction of a DAE by copper complexation.[55] The disrotatory cyclization occurs from the antiparallel conformation and manipulation of the corresponding equilibrium between antiparallel and parallel form results in the control over the switching process. Oxidation,[56] protonation,[57] and complexation[58] were reported to be employed as a trigger. As mentioned, charge and electron transfer were used, activated or

deactivated by redox-reactions,[59] protonation[60] or complexations.[53b] Intramolecular proton transfer was used as well to dissipate the excitation energy (Figure 3-2b).[61] Such proton transfer can be inhibited by acylation or phosphorylation of the proton donating phenol. Furthermore, the inhibition by triplet energy transfer to oxygen was reported.[62] Light as well as temperature were also used to gate a photochromic reaction.[52d, 63] In such case, the photoreaction occurs from a higher excited state, accessible by multiphoton absorption or two consecutive photoreactions, in a way that the first reaction enables the second. Further acid/base gated photochromic systems were reported, where the exact mechanism was not discussed.[49d, 64]

Another mechanism of gated photochromism (see Scheme 3-2d) is the acceleration of the thermal or photochemical back reaction ($k_{CC^*D} >> k_{DC}$ or $k_{CC^*D} >> k_{DD^*C}$) or the rapid stabilization of the one photoisomer C.[65]

Summarizing the above, gated photochromism is a well-established concept, in particular for DAEs. The same holds true for the use of protonation and deprotonation as an external trigger.

(a) Lehn group **1995**

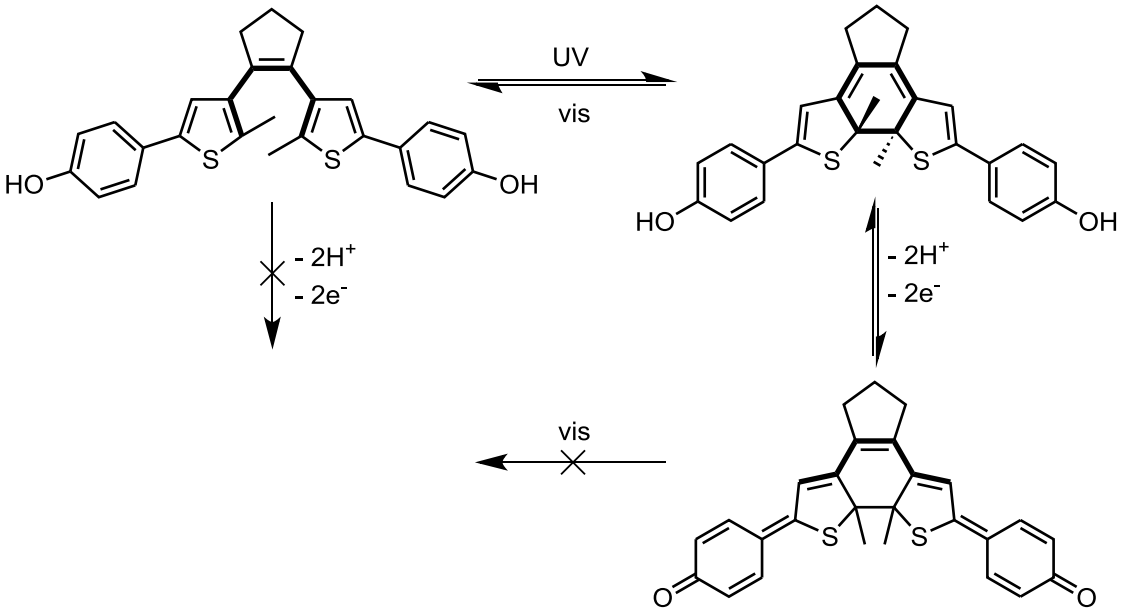

(b) Branda group **2011**

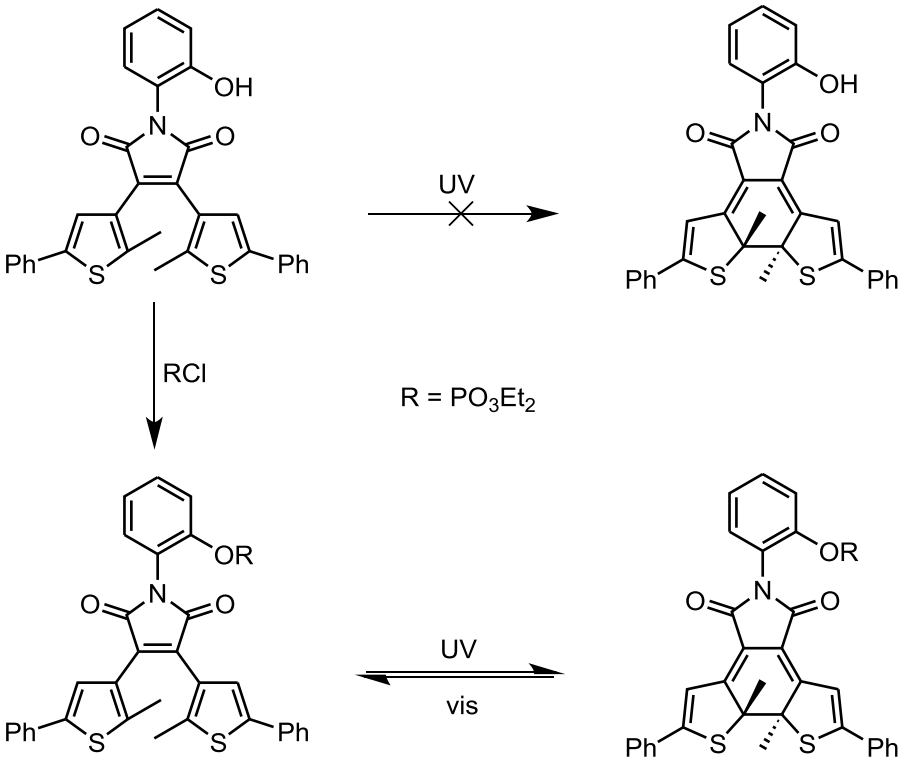

Figure 3-2 Two examples for gated photochromism of DAEs; (a) using a modulation of central double bond motif by a redox trigger to disable the photoreaction; (b) using a inhibition of a proton transfer to enable the photoreaction.[61b, 66]

3.3 Concept & Molecular Design

Target compound **3-1o** (Figure 3-3) was designed to feature the advantageous properties of DAEs while incorporating the possibility to generate a positive charge within the π-framework to effectively lower the thermal barrier. For this purpose the 3,3'-(3,3,4,4,5,5-hexafluoro-1-cyclopentene-1,2-diyl)bis(2-methylthiophene) core was substituted with a 4-methoxyphenyl unit on the one side and a 9-fluorenol moiety on the other side. Acid-driven dehydration leads to formation of the tertiary carbenium ion in both the open and closed isomers, i.e. **3-1o**$^+$ and **3-1c**$^+$, respectively. The thienyl moiety adjacent to the fluorenyl unit carries a β-methyl group to prevent side reactions of the free carbenium ion.[67] Comparing the two open ⇌ closed equilibria, the relative destabilization upon ring-closure should be more pronounced for the neutral isomers (**3-1o** ⇌ **3-1c**) as for the charged isomers (**3-1o**$^+$ ⇌ **3-1c**$^+$), which counterbalance this destabilization to some degree by the effective stabilization of the positive charge in the closed isomer **3-1c**$^+$ only. This should lead to a significant difference in the associated equilibrium constants (K_o and K_c). In an ideal scenario, an inversion of the dehydration equilibrium would occur during the course of the switching process; otherwise, the concept will be limited to a certain acid concentration range.

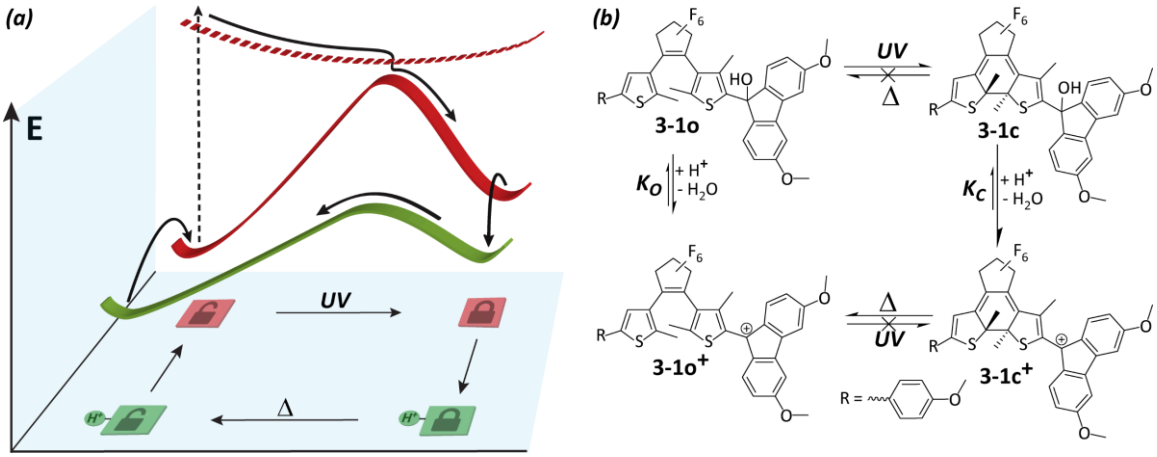

*Figure 3-3 Concept of acid-catalysed cycloreversion and energy release: **(a)** schematic potential energy diagram, **(b)** catalytic four-state reaction cycle of target molecule **3-1o**.*

3.4 Results and Discussion

3.4.1 Synthesis

The target structure was synthesized according to established procedures for hexafluorocyclopentene-bridged DAEs (Scheme 2-1). Compound **3-2** was synthesized following the literature procedure by lithiation and asymmetric substitution of perfluorocyclopentene, via an addition-elimination mechanism.[68] *Via* a second halogen-metal exchange with ^{n}butyl lithium on **3-3** followed by substitution at **3-2**, the DAE **3-4** has been prepared in good yield. The

trimethylsilyl group was converted quantitatively to a bromine substituent with N-bromosuccinimide to give **3-5**. Compound **3-6** was synthesized as reported via a palladium catalyzed C-H activation.[69] The addition of lithiated **3-5** to **3-6** furnishes the target structure **3-1o**.

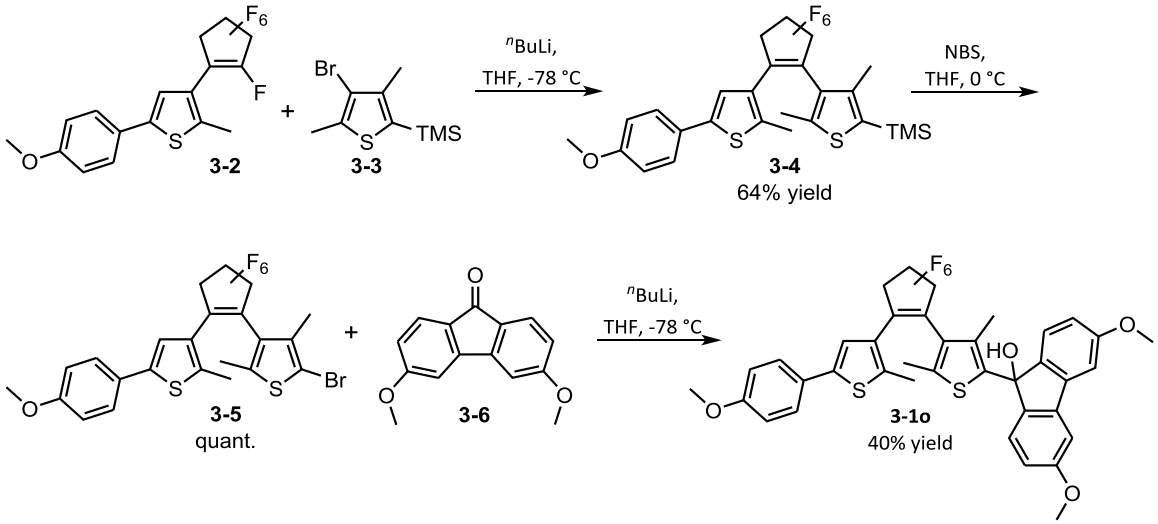

*Scheme 3-3 Synthesis of target molecule **3-1o**.*

3.4.2 Photochemical Analysis and Reaction with Acid

Compound **3-1o** shows a common photochemical behavior for DAEs (see Figure 3-4). The open isomer **3-1o** absorbs light solely in the UV region. By irradiation of a solution of **3-1o** in acetonitrile containing 1 vol% water with 302 nm, the band at 285 nm decreases and two bands at 330 nm and 576 nm emerge (Figure 3-4c). This results in a PSS composed of 94% of the closed isomer **3-1c,** associated with a relatively high quantum yield of photocyclization ($\Phi_{o\rightarrow c}$ = 0.6). Importantly, at 60 °C, no thermal back reaction is observed. Irradiation of the closed isomer's **3-1c** visible band at 546 nm leads to complete cycloreversion (Figure 3-4d) with a quantum yield of $\Phi_{c\rightarrow o}$ = 0.005, typical for DAEs.[45, 70] The sharp isosbestic points as well as the extinction difference diagrams (insets Figure 3-4c,d) indicate clean photoreactions for both ring closure and opening.[71] This is further supported by the observation that after several cycles of irradiation only marginal fatigue was observed (inset in Figure 3-4a).

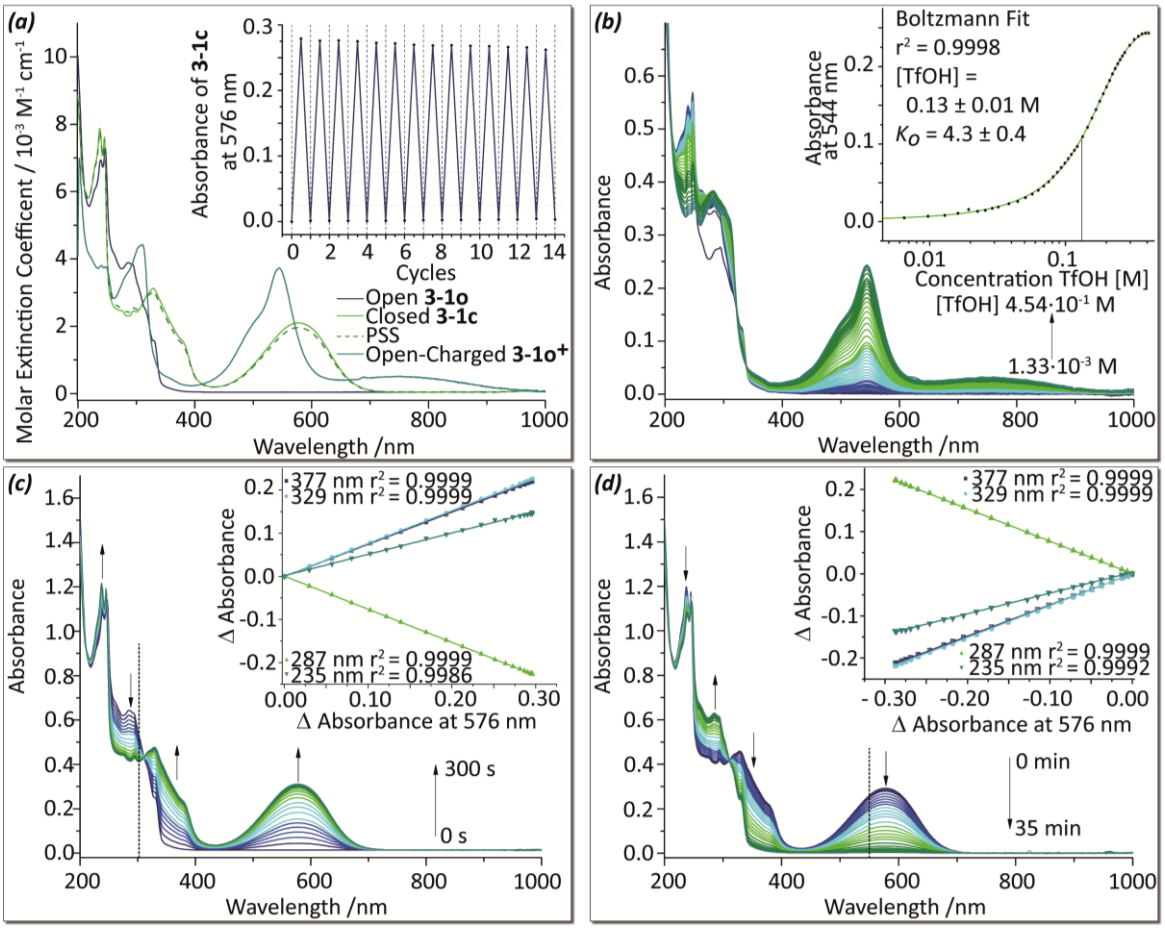

*Figure 3-4 Photo- and acidochromism of compound **3-1** at 25 °C: **(a)** Absorption spectra of **3-1o**, **3-1c**, PSS (305 nm) and the charged form **3-1o**⁺ in acetonitrile containing 1% water; irradiation cycles alternating 302 nm and 546 nm (inlet); **(b)** Titration of **3-1o** with 2 M TfOH solution; **(c)** Irradiation of **1o** with 302 nm; Mauser-diagram with linear fit (inset); **(d)** Irradiation of **3-1b** with 546 nm; Mauser-diagram with linear fit (inset).*

Treating the open isomer **3-1o** with trifluoromethanesulfonic acid (TfOH) leads to a hyperchromic as well as bathochromic shift of the absorption band at 285 nm and the appearance of a new band at 543 nm (Figure 3-4b). This new visible absorption band is attributed to the triarylmethyl cation **3-1o**⁺, which is formed by dehydration under the employed acidic conditions. This process can be reversed by the addition of base. Furthermore, the broad band extending from 600 nm to 1000 nm is assigned to a charge transfer from the p-methoxyphen-1-ylthiophene to the cationic fluorenol substituted thiophene, which is decoupled in the open isomer. Interestingly, irradiation of the strongly acidified solution does not induce any spectral changes, suggesting that the observed absence of photochromic behavior originates from this competing charge transfer. This is furthermore supported by transient absorption measurements, showing that the absence of the photoreaction is caused by thermal relaxation of the excited (charge transfer) state (chapter 5.3). Titration of **3-1o** in acetonitrile containing 1 vol% water with a 2 M TfOH solution in the same solvent mixture at 25 °C allowed us to determine the equilibrium constant for dehydration accompanied by formation of **3-1o**⁺ (K_o = 4.3 ± 0.4, see Figure 3-4b). As expected and key to this

concept, TfOH-induced dehydration of the closed isomer **3-1c** does *not* result in the formation of the elusive closed charged form **3-1c**$^+$ but in thermal ring opening. This acid-induced ring opening is accompanied by recovery of the absorption spectrum of **3-1o** and is clearly supported by UPLC-MS experiments. It is for that reason the equilibrium constant for the closed isomer **3-1c** (K_c) could not be determined.

3.4.3 Study of the Acid Dependent Cycloreversion

To get more insight into the observed acid-induced thermal ring opening the dependence of the kinetics on TfOH concentration was investigated by monitoring the decay of the band at 576 nm of **3-1c** at 60 °C (Figure 3-5a). An acceleration of the reaction with increasing acid concentration was observed and in all cases the reaction was of pseudo first order. Direct conversion to the neutral open form **3-1o** was observed, whereas the charged open form **3-1o**$^+$ could not be detected over the employed concentration window (10^{-5} M ≤ [TfOH] ≤ 10^{-3} M), which is below the one needed for dehydration (see Figure 3-4b). Studying the reverse process, i.e. the UV-induced ring-closure of **3-1o** in the presence of TfOH under the same reaction conditions, shows a clear dependence of the PSS composition on the acid concentration (Figure 3-5b). Increasing amounts of TfOH lead to the PSS being reached faster while the amount of the closed isomer **3-1c** is steadily shrinking in the PSS.

By measuring the photokinetics of the cyclization in the absence and the presence of acid, the molar fraction of **3-1c** at the PSS ($x_{PSS}(H^+)$), the rate constant of the photocyclization (k_{UV}) and photocycloreversion (k_{-UV}) as well as the overall rate constant of the thermal back reaction (k_t) can be determined, which are defined by the reaction below and in the equations **(E3-1)** and **(E3-2)**:

$$\boldsymbol{O} \underset{k_{-UV}+k_t}{\overset{k_{UV}}{\rightleftharpoons}} \boldsymbol{C}$$

$$[\dot{\boldsymbol{C}}] = \boldsymbol{k_{UV}}[\boldsymbol{O}] - (\boldsymbol{k_{-UV}} + \boldsymbol{k_t})[\boldsymbol{C}] \qquad \textbf{(E3-1)}$$

$$\boldsymbol{x_{PSS}} = \frac{[\boldsymbol{C}]}{[\boldsymbol{O}]+[\boldsymbol{C}]} = \frac{[\boldsymbol{C}]}{[\boldsymbol{O}]_0} = \frac{\boldsymbol{k_{UV}}}{\boldsymbol{k_{-UV}}+\boldsymbol{k_{UV}}+\boldsymbol{k_t}} \qquad \textbf{(E3-2)}$$

Integration of the photokinetic rate equations has been achieved using numerical methods. The Runge-Kutta-algorithm has been applied to fit concentration-time profiles from given starting conditions ($\boldsymbol{O}(0) = \boldsymbol{O}_0$ and $\boldsymbol{C}(0) = 0$). In the absence of acid, k_t has been neglected and k_{UV} and k_{-UV} could be determined. Data in the presence of acid gives k_{UV} and the total rate constant of the back reaction ($k_{-UV} + k_t$). Because k_{UV} *is* constant with increasing TfOH concentration, it has been assumed that the k_{-UV} is independent, too. Using this assumption, k_t has been calculated from $k_{-UV} + k_t$. The photokinetics calculated herein were verified using two independent data sets for analyzis. The experiments show a deviation from the linear behavior for high proton

concentrations (Figure 3-5 c & d). The rate constant of the thermal back reaction increases linearly, while the rate constant of the photochemical ring closure remains constant (Figure 3-5c). This verifies the assumption of $k_{-UV} = f([TfOH])$, since the reaction is pseudo first order in terms of the acid concentration. Importantly, the thermal ring opening reaction is observed well below the presence of one equivalent of TfOH, illustrating the catalytic nature of the process.

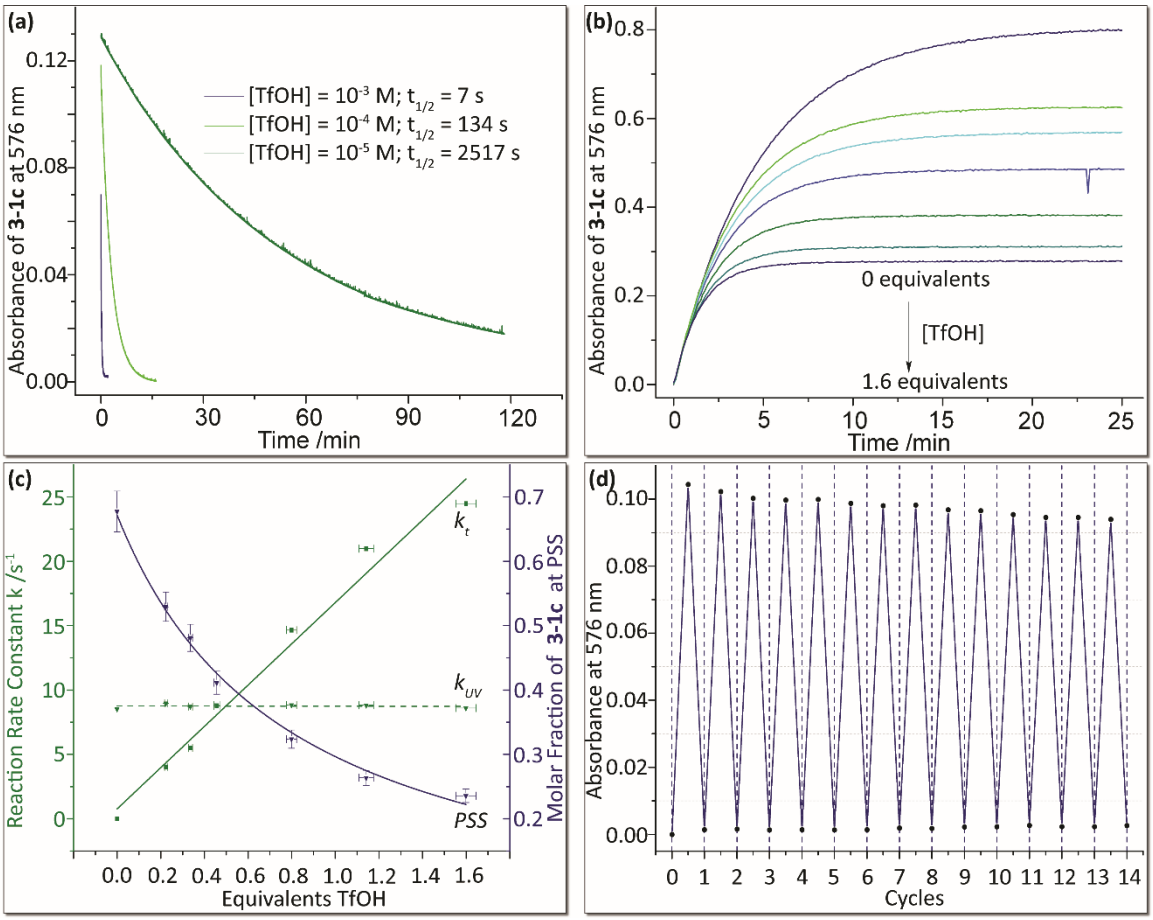

*Figure 3-5 Investigation of the thermal back reaction at 60°C in acetonitrile containing 1% water: (a) Kinetic plot of the thermal back reaction in different concentrations of TfOH; (b) Photo kinetic plot of the irradiation with 302 nm of **1o** in different concentrations of TfOH; (c) Dependence of the molar fraction of **1c** at the PSS during irradiation with 302 nm, the rate constant of the photo reaction k_{UV}, and the rate constant of the thermal back reaction k_t; (d) irradiation cycles in presence of TfOH alternating 302 nm and thermal cycloreversion.*

Considering the overall reaction cycle (see Figure 3-3), one can derive the following equation (**E3-3**, derivation see later in this chapter) describing the dependence of the molar fraction of **3-1c** at the PSS ($\boldsymbol{x_{PSS}(H^+)}$) on the acid concentration:

$$\frac{1}{x_{PSS}(H^+)} = \alpha[H^+] + \frac{1}{x^0_{PSS}} \qquad \textbf{(E3-3)}$$

Where x^0_{PSS} is the molar fraction of **3-1c** at the PSS without acid; $[H^+]$ is the acid's concentration and α is a linearity factor. By plotting the experimentally determined PSS compositions as a function of acid concentration we indeed find a reciprocal relationship (Figure 3-5c), proving the validity of the proposed mechanism. Furthermore, it should be mentioned that

even after several reaction cycles, including irradiation to the PSS and thermal back reaction, only insignificant fatigue was observed (Figure 3-5d).

3.4.4 Derivation of Equation E3-3

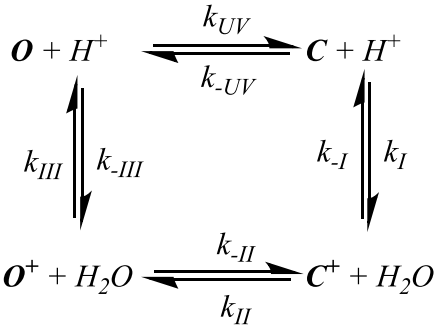

Scheme 3-4 Four-state reaction cycle with all important rate constants to simplify Figure 3-3b used to derivate E3-3.

As shown above, the experimental data suggest a linear dependence of 1/PSS and k_t on the acid's concentration. To describe the observations, the above shown reaction cycle is expected.

$$\boldsymbol{x_{PSS} = f([H^+])} \quad \textbf{(E3-4)}$$

$$\boldsymbol{k_t = f([H^+])} \quad \textbf{(E3-5)}$$

Due to the fact that no charged molecules, neither in the open form nor in the closed form, are observable in the UV/vis absorption spectrometry experiment and by taking the titration experiments into account, it is reasonable to assume that the hydration is much faster than the dehydration in the open state (at given acid concentration **(E3-6)**). Therefore, it can be assumed that the concentrations of the charged species are negligible **(E3-7).** In the PSS, under constant irradiation, we assume that the concentrations of all species are constant and the change of the concentrations over time is zero **(E3-8)**. Because of the absence of charged closed **3-1c**$^+$ form in the titration experiment, it is safe to assume that the charged ring opening is not reversible, neither thermally nor photochemically **(E3-9)**.

$$\boldsymbol{k_{-III}[H^+][O] \ll k_{III}[H_2O][O^+]} \quad \textbf{(E3-6)}$$

$$\boldsymbol{[O] + [C] \gg [O^+] + [C^+]} \quad \textbf{(E3-7)}$$

$$\boldsymbol{[\dot{C}] = [\dot{O}] = [\dot{O^+}] = [\dot{C^+}] = 0} \quad \textbf{(E3-8)}$$

$$\boldsymbol{k_{-II}[O^+] \approx 0} \quad \textbf{(E3-9)}$$

Furthermore, k_{aq}^{-I} is defined as following:

$$\boldsymbol{k_{aq}^{-I} = k_{-I}[H_2O]} \quad \textbf{(E3-10)}$$

Taking the latter into account, the rate equation for $[\dot{C}]$ and $[\dot{C^+}]$ can be expressed as in the equations **(E3-11)** and **(E3-12)**:

$$\boldsymbol{[\dot{C}] = k_{UV}[O] - k_{-UV}[C] + k_{aq}^{-I}[C^+] - k_I[C][H^+] = 0} \quad \textbf{(E3-11)}$$

$$[\dot{C^+}] = -k_{aq}^{-I}[C^+] + k_I[C][H^+] - k_{II}[C^+] = 0 \quad \textbf{(E3-12)}$$

From equation **(E3-12)** the concentration of the charged closed form can be expressed as following:

$$[C^+] = \frac{k_I[H^+]}{k_{aq}^{-I} + k_{II}}[C] \quad \textbf{(E3-13)}$$

The combination of **(E3-11)** and **(E3-13)** leads to **(E3-14),** which can be rearranged to **(E3-15)** by using the principle of mass conservation and the assumption **(E3-7)**:

$$k_{UV}[O] + ((\frac{k_{aq}^{-I}}{k_{aq}^{-I} + k_{II}} - 1)k_I[H^+] - k_{-UV})[C] = 0 \quad \textbf{(E3-14)}$$

$$\frac{[O]_0}{[C]} = \left(\frac{k_I}{k_{UV}} - \frac{k^I k_{aq}^{-I}}{(k_{aq}^{-I} + k^{II})k_{UV}}\right)[H^+] + \frac{k_{-UV} + k_{UV}}{k_{UV}} \quad \textbf{(E3-15)}$$

The combination of **(E3-15)** with the definition of the PSS **(E3-2)** leads to the linear equation **(E3-3)**, which expresses the dependence of the χ_{PSS} on the acid's concentration [H^+]. Furthermore, the equation **(E3-16)** can be formed and rearranged to **(E3-17)**, which leads to equation **(E3-18)**, describing the dependence of k_t on the acid's concentration [H^+] (see Figure 3-5c).

$$\frac{k_{-UV} + k_{UV} + k_t}{k_{UV}} = \left(\frac{k^I}{k_{UV}} - \frac{k^I k_{aq}^{-I}}{(k_{aq}^{-I} + k^{II})k_{UV}}\right)[H^+] + \frac{k_{-UV} + k_{UV}}{k_{UV}} \quad \textbf{(E3-16)}$$

$$k_t = \left(k^I - \frac{k^I k_{aq}^{-I}}{(k_{aq}^{-I} + k^{II})}\right)[H^+] \quad \textbf{(E3-17)}$$

$$k_t = \beta[H^+] \quad \textbf{(E3-18)}$$

Both α and β are linearity factors of the acid's concentration [H^+]. In contrast to β, α is dependent on the light intensity.

3.4.5 Computational Description

The energetics of the catalytic cycle, i.e. the stability of the involved intermediates as well as the key transition state of the thermal back reaction were investigated by DFT calculations on a UB3LYP 6-31G* SCFR SMD level in an acetonitrile-water (90:10) mixture (Figure 3-6).[72]

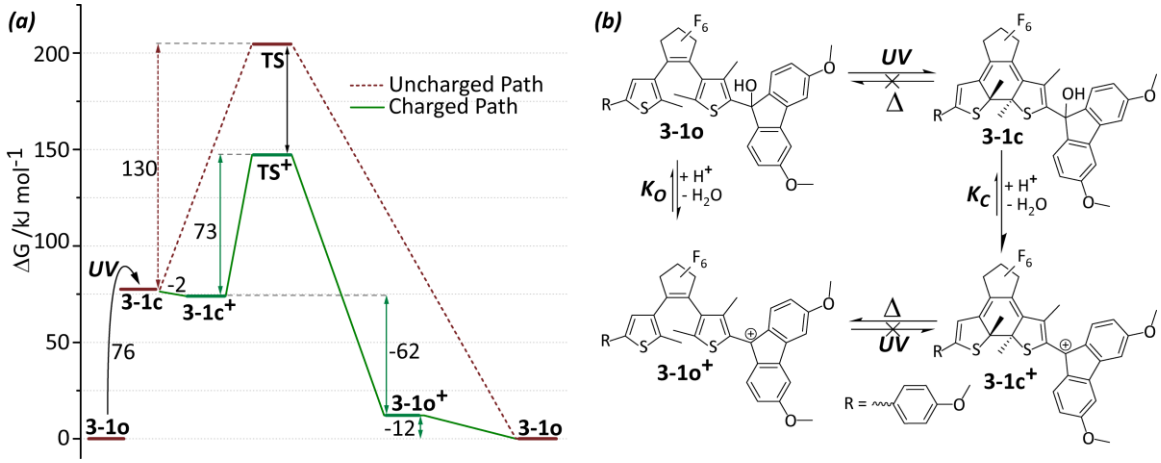

Figure 3-6 Energetics of the reaction cycle: (a) Energy diagram calculated by UB3LYP 6-31G SCFR SMD; (b) four-state reaction cycle.*

The photochemical 6π electrocyclic ring closing reaction of **3-1o** to **3-1c** leads to an increase in Gibbs free energy (+76 kJ·mol^{-1}). The following dehydration of **3-1c** to **3-1c$^+$** is more or less balanced (– 2 kJ·mol^{-1}) as calculated using a triphenylmethanol reference and is driven by the following reaction. Upon ring opening of the charged closed form **3-1c$^+$**, a significant amount of energy is released (– 62 kJ·mol^{-1}). Hydration of **3-1o$^+$** represents a slight downhill reaction (– 12 kJ·mol^{-1}) and closes the cycle. The calculated energies support the overall mechanistic proposal. In order to rationalize the significantly lower barrier for thermal ring opening in the charged form, (**3-1c$^+$** → **3-1o$^+$**) we investigated the corresponding transition states (Figure 3-7), which show an imaginary frequency for the dissociating bond between both thiophene moieties (Figure 3-7c and d). In comparison to the uncharged transition state, (**3-1TS**) the charged one (**3-1TS$^+$**) is computed to be significantly lower in energy ($\Delta\Delta G^{\ddagger}$ = –59 kJ·mol^{-1}). APT charge (Figure 3-7e and Table 3-1) as well as electrostatic charge population analysis[73] show a highly charged α-carbon atom of the cationic fluorenol substituted thiophene in **3-1TS$^+$**, while the population analyzis of **3-1TS** (Figure 3-7f) shows no polarization. The spin density of **3-1TS$^+$** shows no biradical character.[74] As expected, **3-1TS** has a clear biradical character with an unsymmetrical p-orbital on the central *α*-thiophene carbon atom and an alternating *α*- and *β*-spin density fraction within the π-conjugated framework of the DAE, calculated from the gas phase optimized structure.[46] (Figure 3-7g) Both of these findings are strong indications for a change from the homolytic mechanism in the neutral form **3-1TS** to a heterolytic bond cleavage in the charged form **3-1TS$^+$**.

*Table 3-1 Population analysis of the gas phase optimized structures for **3-1TS⁺** and **3-1TS**.[73b]*

#	*APT charges of **3-1TS⁺** (**3-1TS**)*		
1	1.511 (0.775)	7	-0.240 (-0.173)
2	-1.008 (0.003)	8	0.045 (0.082)
3	0.717 (-0.044)	9	0.719 (-0.219)
4	-0.711 (-0.143)	10	-0.713 (-0.048)
5	***1,43 (0,163)***	11	1.061 (0.226)
6	- 0.710 (-0.024)	12	-0.084 (-0.148)
		13	*-1,147 (0,029)*

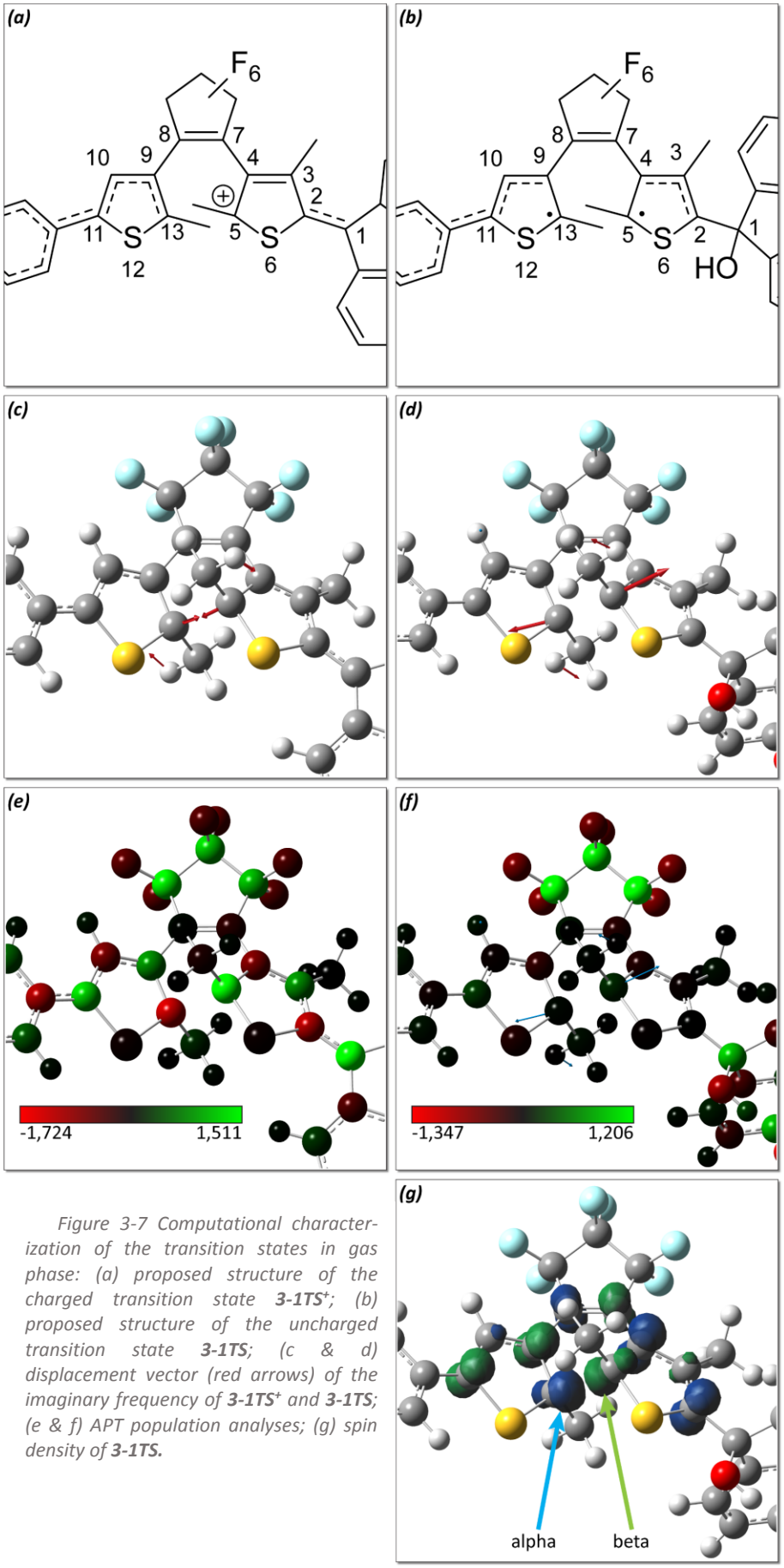

Figure 3-7 Computational characterization of the transition states in gas phase: (a) proposed structure of the charged transition state ***3-1TS***$^{+}$*; (b) proposed structure of the uncharged transition state* ***3-1TS****; (c & d) displacement vector (red arrows) of the imaginary frequency of* ***3-1TS***$^{+}$ *and* ***3-1TS****; (e & f) APT population analyses; (g) spin density of* ***3-1TS.***

3.5 Conclusion and Outlook

Title compound **3-1o** shows robust photochromism with a high fatigue resistance against (photo)chemical side reactions in both the uncharged and charged forms. The photochromism could be gated by an excess of acid due to formation of the charged open isomer, which is not photoreactive. Importantly, strong acids catalyze the thermal ring opening of the closed isomer, presumably *via* a heterolytic transition state. The light energy stored in the closed isomer ($\Delta H_{c\rightarrow o}$) equals to 59 kJ·mol^{-1}, giving rise to an energy density of 81 J·g^{-1}. This value clearly is not optimal for light energy storage since other photoresponsive materials, such as norbornadienes (1042 J·g^{-1}) and even normal azobenzene (228 J·g^{-1}) perform much better.[44d] Nevertheless, this work shows an alternative and promising pathway to catalytically trigger the release of the stored energy and efficiently recover the system. Importantly, the rate of the energy release can be tuned by the amount of acid added and the uncharged closed isomer is fully stable over long time. Future work should focus on applying this concept to other photochromic systems to maximize the energy that can be stored while the introduction of suitable functional groups should allow a minimization of the amount of acid needed for energy release. Therefore, the structure of the transition state is the key to enhance the molecular performance. A change of the methyl group attached at the *α* carbon to a methoxy group at the *α* carbon should lead to a stabilization of the positive charge and hence, of the transition state, resulting in a faster, more acid-sensitive, thermal back reaction. Additionally, the methoxy motif is known to decrease the quantum yield of the cycloreversion.[13] To increase the energy stored light energy, one thiophene moiety might be exchanged against a phenyl substituent. At last, the use of an unbridged DAE might be promising, resulting in the structural proposal shown in Scheme 3-1:

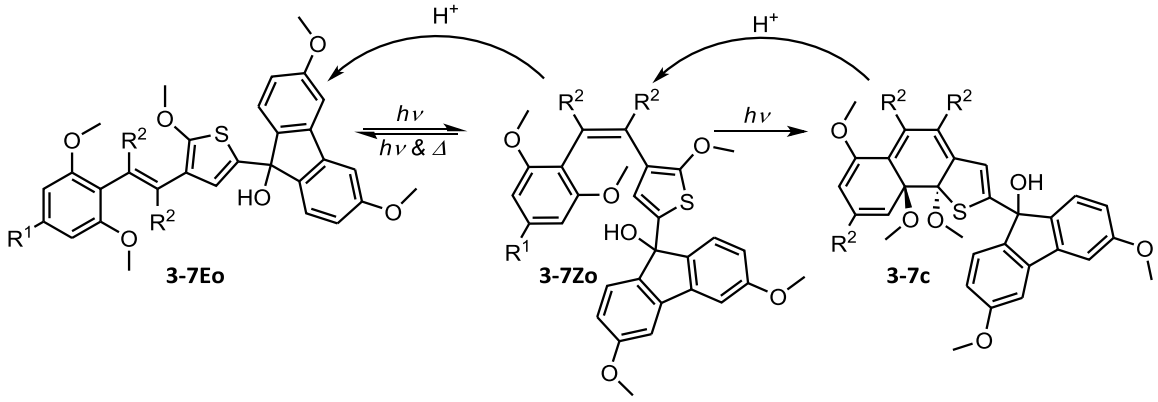

Scheme 3-5 The next molecular steps to improve the concept further. Proposed improved design of a next generation of energy storage photoswitches.

The E-Z isomerization is ideally gated by the cyclization and contributes to the stored light energy, which results in a higher energy density. The thermal *Z-E* isomerization of azobenzene is faster for push-pull systems and an acceleration by an acid-driven dehydration, which would result

in a strong acceptor, might be possible for **3-7** as well. The preparative approach is reasonably short (Scheme 3-6), starting with two Friedel-Crafts acylations, followed by formation of the carbon-carbon double bond and post-functionalization of the thiophene. The substituent R should be electron withdrawing to avoid photo-oxidation and its steric demand can be beneficial to tune the E-Z isomerization rate. The R' substituent can be used to introduce a light absorbing group to obtain a bathochromic shift.

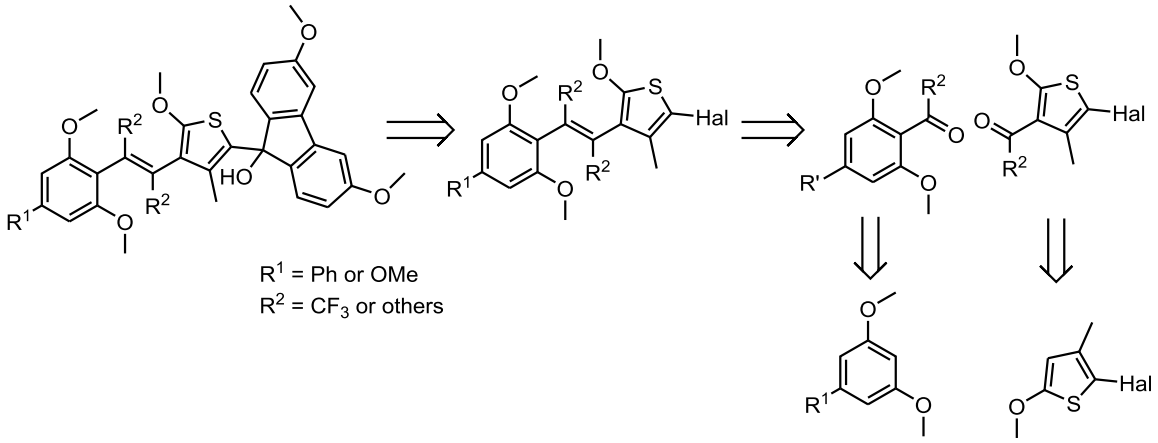

*Scheme 3-6 Retrosynthetic analysis of **3-7Eo**.*

4 LIGHT-INDUCED pK_A MODULATION[3]

4.1 INTRODUCTION & MOTIVATION

The acidity and respectively, basicity of an organic molecule is quantified by the pK_a, which describes one of the most fundamental properties of any organic compound and influences its chemical reactivity as well as its solubility, due to the polarity change within the protonation or deprotonation reaction. The correlation of basicity and nucleophilicity is a fundamental concept for every organic chemist. As a consequence, the activity of organocatalysts is strongly dependent on their pK_a value. The bioavailability of an active pharmaceutical ingredient is influenced by its membrane permeability, which depends on its polarity and therefore, on its pK_a and the pH of the receptive environment. Last but not least, the achievable pH range of a buffer system is dependent on the pK_a as well, as derived from the Henderson-Hasselbach equation. A simple molecular property like acidity influences chemistry, engineering and life science on the most fundamental level.

Why is it interesting to change the acidity or respectively basicity of an organic molecule by a non-invasive stimulus such as light? Which applications are achievable or imaginable if one would be able modulate this fundamental property?

The concept of photopharmacology has recently become a focus of research attention.[75] By changing the pK_a value, it might be possible to not only control the activity of a drug but also its availability. The activity depends on the interaction to a binding site, e.g. a target enzyme. Due to this binding of the drug a certain enzyme catalyzed reaction could be inhibited. This depends furthermore on the administration, e.g. oral, dermal, inhalation or intravenous. During an intravenous medication, the active agent is injected into the blood plasma, an extracellular space. To achieve its activity most drugs need to pass the bio-membrane, which usually occurs *via* diffusion (passive membrane transport), an active membrane transport or by an endocytosis. The phospholipid bilayer is considered polar on the outside due to charged head groups and non-polar on the inside in an aqueous environment. This causes differences in permeability depending on the organic molecule. Ions and other highly polar molecules cannot pass the membrane. By changing from a charged form to an uncharged form triggered with an external non-invasive stimulus alternative drug delivery concepts are achievable.

[3] Parts of this work have already been published in: J. Gurke, Š. Budzák, B. M. Schmidt, D. Jacquemin, S. Hecht, *Angewandte Chemie International Edition* **2018**, *57*, 4797-4801.

Supramolecular chemistry allows us to control assemblies beyond a single molecule, like host-guest interactions, micelle formation or liquid crystals. Originating from non-covalent interaction of molecules, e.g. hydrogen bonds, dipole-dipole interaction or the Coulombic force between charges. If we can control the protonation of a single molecule, not by changing the surrounding environment, but through an external stimulus, we might be able to modulate these fundamental non-covalent interactions and gain methods to influence the orientation of molecules to each other's or to an electric field, the size and shape of a micelle and its critical micelle concentration.

The membrane potential results from the difference of the ion concentration between the two sides of a bio membrane and is therefore strongly connected to the previously discussed permeability of charged species. The stimuli transfer in neurons, the transformation of chemical energy into heat, motion and metabolic processes consuming ATP as well as photosynthesis are coupled to membrane potentials. A way to potentially achieve an artificial change of the membrane potential, e.g. by an proton gradient, has been shown by Bakker and co-workers.[76]

As shown, a pK_a modulation in the biological window would be a highly promising application. How to define such a biological window and assessing the change of the pK_a necessary for efficient modulation needs to be addressed. The extracellular fluid, typically blood and the cerebrospinal fluid are buffered liquids with a precisely adjusted pH. The normal pH of blood is found to be between 7.34 and 7.45.[77] The pH of the cerebrospinal fluid is buffered to 7.3.[78] The intracellular pH differs with the cell type, but can be assumed to be mainly in the range of 7.0 to 7.4.[79] Therefore, pH 7.4 can be safely assumed as viable target pH value. Accordingly, a pK_a change around this value is necessary. To exemplify this, a thought experiment will be done:

The well-known Henderson-Hasselbalch equation (E4-2) describes the correlation of the pH and the dissociation equilibrium of a weak acid or base (E4-1).

$$HA + H_2O \rightleftharpoons A^- + H_3O^+ \qquad \textbf{(E4-1)}$$

$$pH = pK_A + log_{10}\frac{[A^-]}{[HA]} \qquad \textbf{(E4-2)}$$

If the aim is the change from 95% deprotonated to 95% protonated in a fixed pH, a modulation of the pK_a about *ca.* 2.6 units is required. Therefore, a change of the pK_a value in the range of 6.1 to 8.7 is necessary, if the pH is 7.4.

4.2 Theoretical Background

4.2.1 Controlling Reactions by Light

In general, a photoreaction opens PES regions or distributions of chemical entities, which are thermally not available, because it is either a thermodynamically unfavored or a kinetically hindered process. The interconnection of such a photoreaction with a thermal one, is used to

modulate the speed of a coupled reaction, by “decreasing” the activation barrier, which is equal to a new reaction path on the PES. Through increasing the reactant concentration by deflection of thermally unfavored, but photochemically addressable equilibrium state an acceleration of the absolute reaction speed or even the enabling of a reaction is possible. However, the modulation of a reaction kinetic always requires an exergonic process. Following the principles established by Le Chatelier, an interconnection of an endergonic process to a thermally irreversible photoreaction enables a deflection of the thermal equilibrium to the energetically unfavored side, by removing the high energy product from the thermal equilibrium (Figure 4-1).[80]

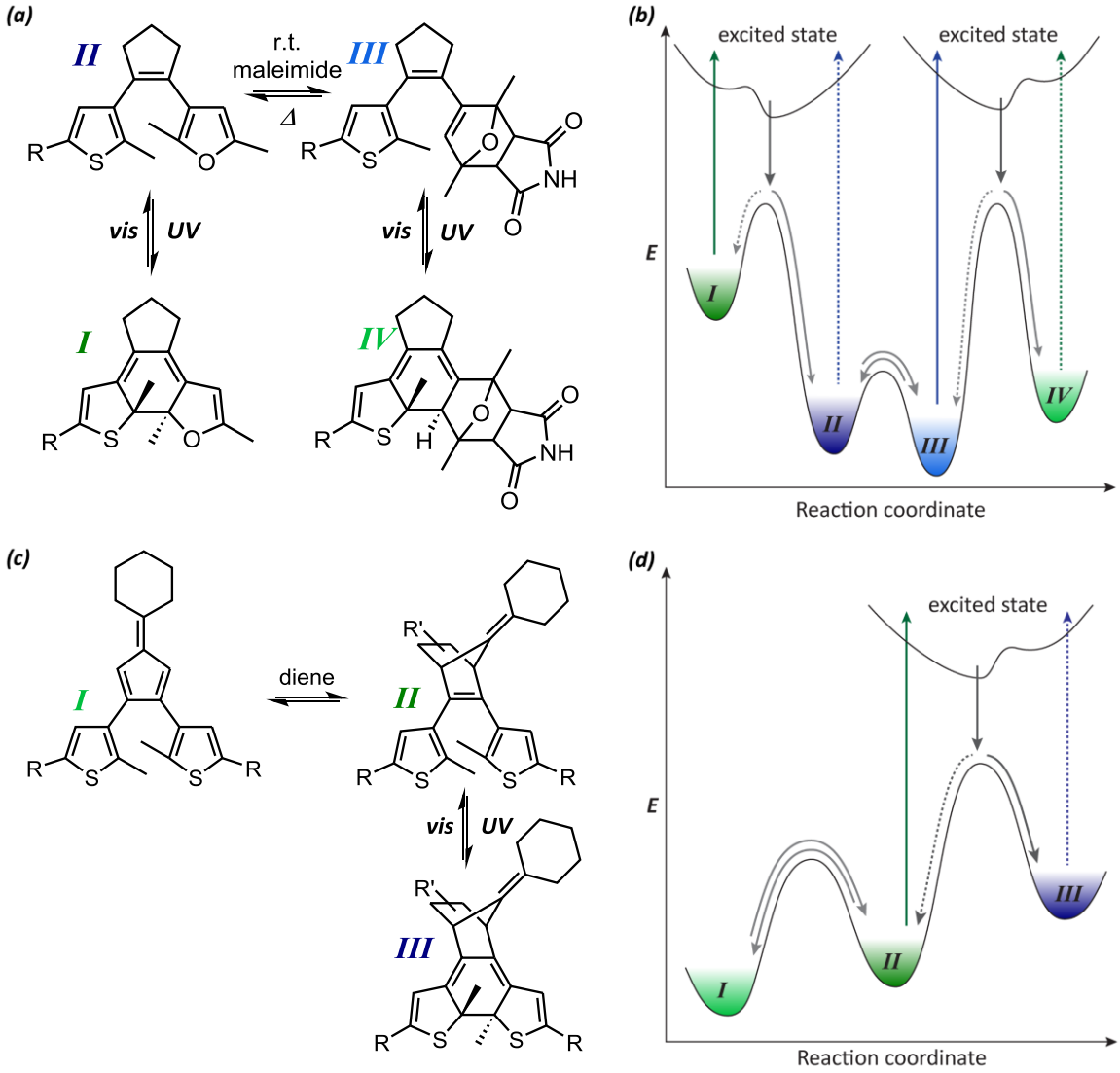

Figure 4-1 Energetic considerations for two examples of reaction control by light: (a + b) two approaches to control a Diels-Alder reaction with DAEs, (b+d) conceptual scheme of the corresponding potential energy diagram.[8a, 52c, 81]

The control over reactivity by light using DAEs has been well established, both by influencing the kinetics as well as the thermodynamics of a system. Three main concepts are used to control reactions by DAEs (Figure 4-2); first the change of the electron density by connecting or disconnecting a donor or acceptor *via* the DAE backbone or the aryl moiety; second, by using the

inherent change of the double bond location and therefore the aromaticity of the aryl moieties; third, by controlling the flexibility of the DAE.

By asymmetric substitution of a DAE with pyridinium, Branda and co-workers were able to activate an aldehyde, which was attached on the opposite side of a DAE.[82] The active DAE catalyzes the racemization and deuterium exchange of L-alanine. Using a similar concept Hecht and co-workers showed recently an acceleration of an imine-amine exchange (see Figure 4-2***a***),[83] using a bisformylated DAE switch. Upon ring-closure, the initially separated formyl groups, are electronically conjugated, which leads to a significant lower electron density in both aldehydes, accelerating the nucleophilic attack.

By exchanging the cyclohexene bridge with a 1,2,3-dioxaborole Branda and co-workers modulate the Lewis acidity of the boron(see Figure 4-2***b***).[84] In the open form, the 1,3,2-dioxaborole has a high aromatic character, and therefore the boron is Lewis "neutral". The electrocyclization by irradiation with 312 nm leads to a change of the double bond motif from hexatriene to cyclohexadiene. This causes a lower aromatic character of the bridge and cross-conjugation, which increases the Lewis acidity of the boron. Yam and co-workers used an imidazolium as the bridging unit,[85] where a positive charge in the open isomer is stabilized in a five-membered heterocycle, while the closed form exhibits no aromatic character. Due to the cross-conjugation the positive charge is not delocalized within the π-framework of the closed DAE, and so the stability is decreased, leading to a higher electrophilicity. Research including a similar concept has been conducted by Kawai and co-workers.[86] Instead of exchanging the bridge, the imidazolium was used as an aryl moiety. The ring closure leads to a destabilization of the positive charge. Due to the cross-conjugation of the positive charge in the closed form, no thermal back reaction is observed. Bielawski and co-workers used a related structure, a *N*-heterocyclic carbene (NHC) to modulate the catalytic activity by light.[87] Branda and co-workers as well as Hecht and co-workers showed the modulation and accordingly control of the Diels-Alder reactions by light (shown in Figure 4-1).[52c, 81] Former used a 2,3-thienyl substituted cyclopenta-1,3-diene, where the endergonic [4+2] cycloaddition[8a] forms the hexatriene motif of the DAE, which enables the photoreaction. The displacement of the open form to the thermally irreversible closed isomer, drives the Diels-Alder reaction. Hecht and co-workers improved this concept by using a furan as one aryl moiety. This leads to the possibility to *drive* the Diels-Alder reaction in both directions, by addressing different wavelengths.

The open DAE isomer can rotate around the carbon-carbon-bond between the bridge and the aryl moieties, resulting in a parallel and an antiparallel conformation, where only the antiparallel conformation is photo responsive. The closed isomer is build-up out of four annulated rings, which

induces a high rigidity. Würthner and co-workers designed this system to photocontrol self-assembled nanostructure.[88] Zhu and co-workers used a dithiazolyl ethene to complex borontrifluoride only in the open form(see Figure 4-2***c***).[88]

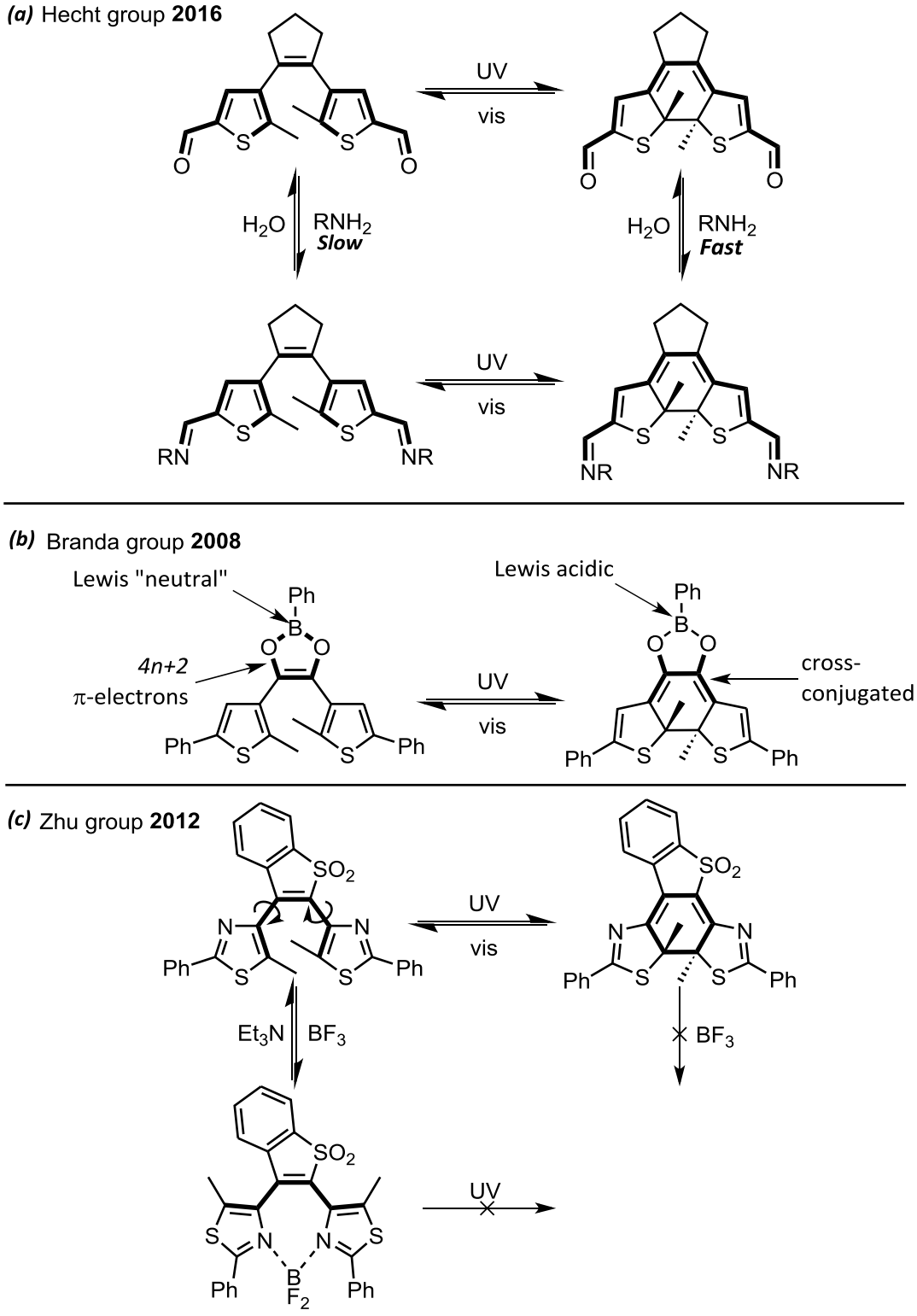

Figure 4-2 Molecular mechanisms of reactivity control with DAEs; ***(a)*** *using the change of linear to cross-conjugation within the switching of DAEs to accelerate a imine exchange;* ***(b)*** *using the alteration of the double bond motif to modulate Lewis acidity;* ***(c)*** *using the different rigidity of the open and the closed isomer to modulate a complexation reaction.[58a, 83-84]*

4.2.2 Photo Modulating pK_a-Values of Organic Molecules

The modulation of the pK_a-value by a non-invasive stimulus is a topic of high interest since many years. Initially, the difference of ground state to excited state pK_a was used to change the dissociation of a proton by light.[7, 89] To overcome the problem of the short lifetime different approaches were used, e.g. the irreversible release of an acid by irradiation, the so called "photoacid generator" as well as the use of photochromic molecules (Figure 4-3).[6a] The connection of an electron acceptor e.g. a stable positive charge or donor within the linear π-conjugated framework of the DAE is a literature known concept, for changing the pK_a-value of an acidic proton. Therefore, the property of connecting and disconnecting π-conjugated frameworks within the switching process of the DAE is used. A broad range of stabile organic cations, e.g. triphenylmethane cations, *N,N*-alkylated imidazolinium and benzimidazolium as well as tropylium ions, are potentially applicable to realize this concept. The approach described above suffers from a severe, intrinsic drawback, originating from two diametrical effects. To maximize the pK_a change triggered by a switching event, the positive charge needs to be directly attached at the DAE moiety or even within the switch, which results in a -*M*-effect affecting the proton directly through the π-framework of the closed DAE. As discussed and used previously a strong accepting group leads to a strong decrease of the thermal stability and converts the system effectively into a T-type photochrome. To avoid this, a separation of the positive charge from the DAE, by an aromatic linker or a weaker acceptor (e. g. pyridinium) could be substituted. This lead to a decrease of the acidity change, as conducted and discussed by Kawai and co-workers only a marginal pK_a change of 1 unit was observed (Figure 4-3*a*). The pronounced aromatic stability of the substituents has been discussed as a reason for this observation. Furthermore, a side reaction of the closed isomer with the nucleophilic solvent methanol has been observed (see chapter 2.1.2). A similar approach has been conducted by Irie and co-workers, where one thiophene moiety has been substituted with a donor or acceptor in the reactive *α* position and the hydroxyphenyl rest on the other *α* position,[90] which are disconnected upon electrocyclization. A pK_a change of 0.4 units was seen in a methanol-water mixture. An alternative molecular design was developed by Uchida and co-workers at the same time as this work was under preparation.[28] By activation of a keto-enol tautomerism a pH change could be induced. To achieve this, an asymmetric DAE with one phenol moiety instead of a thiophene was synthesized. The photochemical cyclization, and the accompanied structural change of a hexatriene to a cyclohexadiene, removes one double bond of the phenol moiety and consequently the aromaticity. The energetically favored carbon-oxygen double bond is formed, and the OH acidic proton is converted to a CH acidic proton, which is less acidic. Unfortunately, no pK_a-values have been determined and a similar side reaction related to the example of Kawai and co-workers has been observed.

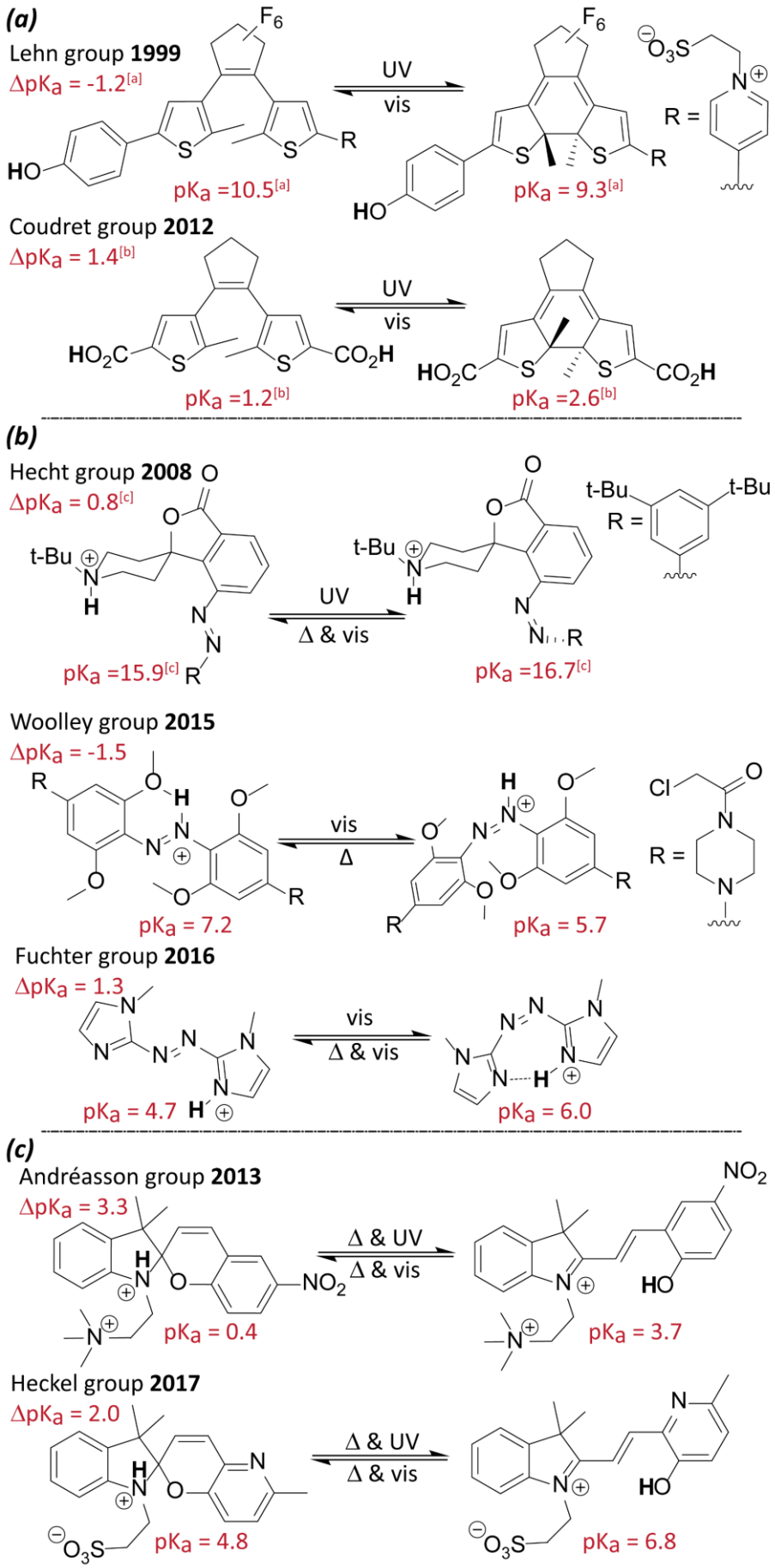

Figure 4-3 Molecular Structures of pKa switches in water, if not otherwise specified.
[a] methanol: water 5:2
[b] acetonitrile: water 8:2
[c] acetonitrile.

Azobenzene-based systems have been used for pK_a switches as well (Figure 4-3*b*). By removing the spatial hindrance of the basic piperidine nitrogen *via* the *EZ*-isomerization, Hecht and co-workers achieved a pK_a change of +0.8 units (*trans* 15.9 to *cis* 16.7) in non-aqueous solution.[91] Woolley and co-workers were able to acidify a protonated azobenzene by breaking a hydrogen bond between the proton and a neighboring methoxy group during the light-induced isomerization. In the meta-bismethoxy substituted azobenzene the pK_a decreases by about -1.5 units (E 7.2 to Z 5.7) in water. Above that, a strong bathochromic shift due to the protonation of the azobenzene occurs. The coupling of two *N*-methylimidazoles *via* a diazo-bond, as done by Fuchter and co-workers, leads to a pK_a shift of +1.3 units (E 4.7 to Z 6.0).[92]

As a last photochromic spiropyrans are frequently used, achieving significant pK_a changes in aqueous and non-aqueous media. The main drawback is their T-type photochromism (Figure 4-3*c*). Andréasson and co-workers investigated the physicochemical behavior of nitro substituted spiropyrans in aqueous solution.[93] The pK_a in the spiropyran form is 0.4, while the pK_a of the open merocyanine form is 3.7. In comparison to organic solvents, where the thermal equilibrium is almost completely on the spiropyran site, in water the thermal equilibrium constant $K_{c \rightleftharpoons o}$ has been determined to be 1.46. During irradiation with 254 nm light the photostationary distribution changes to 0.79. Bakker and co-workers described a pK_a change over six orders of magnitude by using spiropyrans as switch in an organic polymer matrix. The spiropyran form has a pK_a of 2.3, while the pK_a of merocyanine is 8.6.[94] The most recent approach to a pK_a switch using spiropyran was published by Heckel *et al.*, achieving a pK_a change of 2.0 units.

4.3 Concept And Molecular Design

4.3.1 Energetic Consideration of Light-induced pK_a Modulation

Summarizing the previous chapter, the main challenge concerning current photoacid research is the complete switching between two real metastable states with sufficient pK_a modulation, which includes ensuring that no thermal interconversion occurs. None of the three mentioned photochromic classes fulfills all of these requirements so far. There is a need for a new approach to reach a high pK_a change. Especially for biological applications, the possibility of switching around a neutral pH value is of great interest, since it would allow the experimenter to switch between uncharged and charged forms in a natural environment by a non-invasive trigger.

From an energetic point of view, the concept of light-induced pK_a-modulation needs a four-state potential energy diagram, containing two chemical equilibria separated by a high thermal barrier, overcome by a photochemical reaction. (Figure 4-4) The starting point of the four-state cycle is species $\boldsymbol{I}$ the most stable compound of the first dissociation equilibrium, which means it is

the most acidic compound. This requires the most potent stabilization of a negative charge, respectively, destabilization of a positive charge.

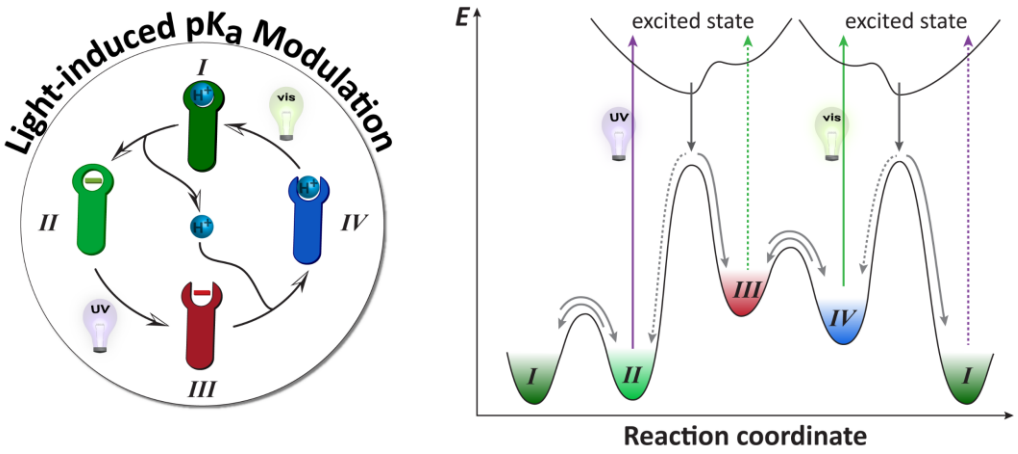

Figure 4-4 Conceptual four-state cycle of a light-induced pK_a-modulation with the corresponding potential energy diagram.

Species ***I*** is the most acidic species in the reaction cycle, whereat ***II*** is its corresponding base. ***II*** converts to species ***III***, the most unstable species in the whole cycle, by light irradiation. Within the first photoreaction a drastic destabilization of the negative charge is necessary. A protonation leads to compound ***IV***, which is hindered from further reactions by a second reaction barrier. The second photoreaction converts ***IV*** to ***I***. The ratio of species ***I*** to ***II*** and ***III*** to ***IV*** is directly dependent on the pH, while the ratio of the photoisomers (***II*** and ***III***; ***I*** and ***IV)*** is an intrinsic property of the photochromic unit and can possibly influenced by the irradiation wavelength.

To achieve the high activation barriers as described above, DAEs will be used in this concept. As show before, was the connection of a donor or acceptor *via* the DAE backbone an unsuccessful concept to gain a significant pK_a modulation. Therefore, the change of the double bond motif will be applied, as it was in modulation of other reactivities. The first step in the realization is the literature-search for a suitable aryl moiety or bridge motif, which show a strong dependency of it pK_a on the existence of a double bond.

4.3.2 NH and OH Acidity of (Hetero)cyclic Molecules

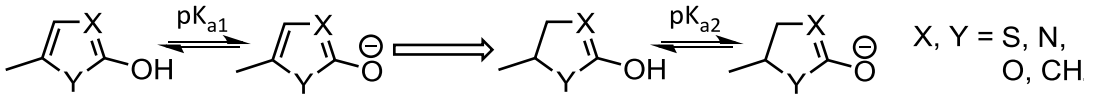

#	Structure	pK$_{a1}$	pK$_{a2}$	#	Structure	pK$_{a1}$	pK$_{a2}$
1	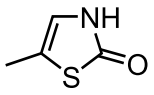	9.49 ± 0.4	12.82 ± 0.4	*11*	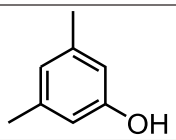	10.19 ± 0.10	-
2	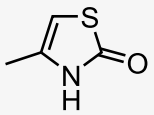	9.51 ± 0.4	12.84 ± 0.4	*12*	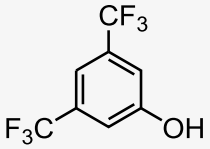	7.69 ± 0.10	-
3	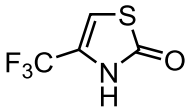	6.99 ± 0.4	10.33 ± 0.4	*13*	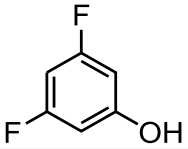	7.97 ± 0.10	-
4	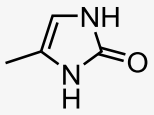	12.54 ± 0.70	14.93 ± 0.4	*14*	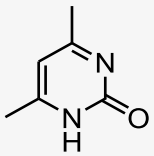	10.34 ± 0.10	-
5	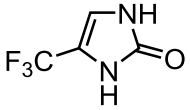	10.05 ± 0.70	12.43 ± 0.4	*15*	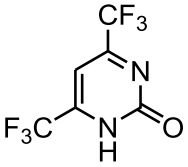	3.74 ± 0.10	-
6	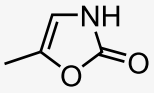	9.07 ± 0.40	12.84 ± 0.40	*16*	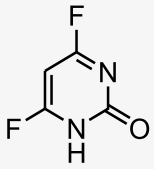	5.52 ± 0.10	-
7	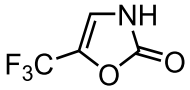	6.56 ± 0.40	10.33 ± 0.40	*17*	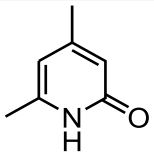	12.15 ± 0.10	-
8	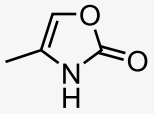	9.05 ± 0.40	12.82 ± 0.40	*18*	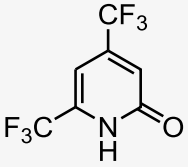	6.77 ± 0.10	-
9	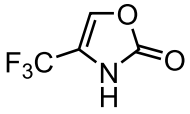	7.38 ± 0.40	11.15 ± 0.40	*19*	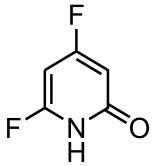	4.94 ± 0.10	-
10	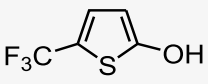	7.03 ± 0.18	-	*20*	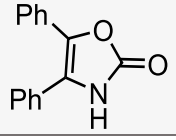	7.79 ± 0.60	-

Figure 4-5 Estimated pK$_a$ changes of five- and six-membered (hetero)cyclic molecules upon saturation.[95]

To access the previously discussed pH-window of around 7.4 the pK_a change achievable with DAEs needs to be estimated. Therefore five- and six-membered aromatic (hetero)cycles will be compared to their dihydro adducts (see Figure 4-5). The pK_{a1} defines the dissociation in an aqueous medium of the aromatic (hetero)cycles and pK_{a2} the one of deprotonation of the dihydro aromatic (hetero)cycles. The five-membered heterocyclic molecules **3** and **7** with an acidic group seem to be the most promising moieties for a use in DAEs, due to the change of dissociation constant over three orders of magnitude. These heterocyclic molecules can be seen either as a hydroxy substituted 3*H*-thiazol-2-one respectively 3*H*-oxazol-2-one or as cyclic (thio)carbamate (Figure 4-6). In fact these two forms are interconnected by a tautomeric equilibrium, first described by Hantzsch in 1927.[96] Due to the low aromatic stabilization energy of thiazole (20 kJ mol^{-1})[97] and the high bond energy of the carbon-oxygen double bond this tautomerism lies on the (thio)carbamate side. For convenience, 3*H*-thiazol-2-one and 3*H*-oxazol-2-one will be shortened to “thiazolone” and “oxazolone” in the following. The acyclic *O*-ethyl carbamate (pK_a 24.6 in DMSO) has a significant lower acidity compared to the cyclic dihydro-oxazolone (pK_a 20.9 in DMSO), shown by Bordwell and co-workers.[98] The fixed anti-conformation in the cyclic molecule is discussed as a reason for this observation, similar to Meldrum’s acid. The acidity increases further in the oxazolone (pK_a 15.0 in DMSO), due to the presence of the carbon-carbon double bond. The negative charge can be stabilized in a [4n+2] π aromatic ring (see Figure 4-6). Therefore the double bond is of great importance for their acidity.[98] The difference between oxazolone and thiazolone is presumably caused by the higher electronegativity of the oxygen compared to the sulfur.

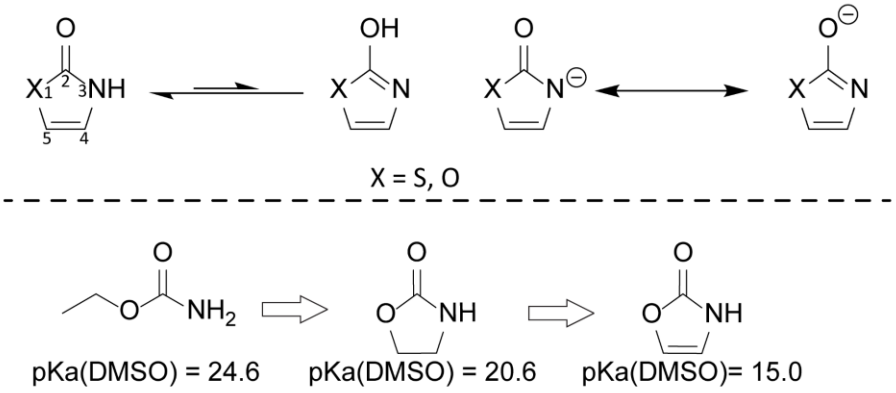

Figure 4-6 Thiazolone and Oxazolone: (a) Tautomeric equilibrium, (b) Delocalization of the negative charge in the deprotonated forms.[96, 98]

Electron-withdrawing groups lead to a stabilization of the negative charge or respectively to a destabilization of a cation. Hence, an acceptor group will lead to an increased acidity, while electron-donating groups will show the opposite effect. Trifluoromethyl-thiazolone (Figure 4-5;

No. 3), the trifluoromethyl-oxazolone (No.7) as well as the hydroxo-trifluoromethyl-thiophene (No.10) are the most promising candidates within the group of the five-membered heterocyclic aromatic compounds to be incorporated into an DAE as an aryl moiety. An oxazolone-bridged DAE could be used, as well, even though the pK_a change is not available by this estimation. 4,5-Diaryloxazol-2-ones are well-established and are known to show a photoreaction.[99]

The pK_a change of the six-membered rings could not be estimated this way, because only the pK_a values of the aromatic compounds were described in the literature. Nevertheless, bis(trifluoromethyl)-pyridone could be an interesting moiety for a DAE, but suffers from fairly limited accessibility.[100]

4.3.3 Synthetic Approach and Use of 3*H*-thiazol-2-one and 3*H*-oxazol-2-one

Hantzsch described the synthesis of 4-methyl-3*H*-thiazol-2-one, for the first time in 1927[96] and used an *α*-halo carbonyl group as starting material (Figure 4-7*a*). The reaction with ammonium thiocarbamate lead directly to thiazolone. Until today, his synthetic approach is one of the two feasibly synthetic concepts to synthesize thiazolones. The second one being nucleophilic substitution of a 2-halo-thiazol. *O*-alkyl-protected thiazolones are available *via* these routes, too.

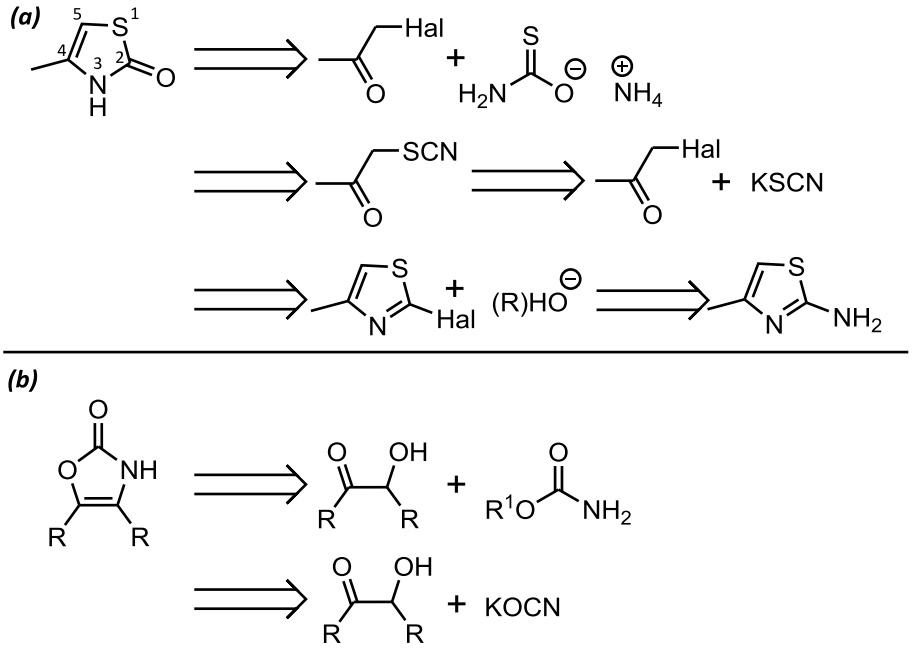

*Figure 4-7 Retrosynthetic approaches to 3H-thiazol-2-one **(a)** and 3H-oxazol-2-one **(b)**.*

Alkoxy-thiazoles are accessible by use of *O*-alkyl thiocarbamates. The deprotection occurs under acidic conditions[101] and other dealkylating reagents.[102] Thiocyanate reacts in a nucleophilic substitution with the *α*-halide and isomerizes afterwards, catalyzed by aqueous acid, to the thiazolone. Unfortunately, a dimerization of thiazolone in strong acidic conditions is reported.[103] 2-Halo thiazole as well as all other 2-halo *N*-heterocyclic aromatic rings can be functionalized by a nucleophilic reaction with hydroxide or alkoxides. More synthetically

challenging strategies have been established *via* cumulenes.[104] The synthetic strategy for the construction of 4-substituted thiazolones is rather simple *via* Hantzsch's approach. The preparation of 5-substituted thiazolone conducted mainly *via* the thiazole route. Even if the synthesis *via* an *α*-halo aldehyde is theoretically feasible,[105] it has not been reported so far. The preparation of 4-trifluoromethyl-thiazolone (Figure 4-5; No. 3) is literature known, while one of its isomer 5-trifluoromethyl-thiazolone is not reported.

Thiazolones act as nucleophiles in reactions. Alkylation occurs mainly on the nitrogen under neutral or basic conditions. Only the use of diazomethane leads to a mixture of *N*- and *O*-methylation.[106] Triflation with triflate anhydride occurs at the *O*-terminus.[107] Under Friedel-Crafts conditions or *via* other electrophilic substitutions, 4-methyl-thiazolone can be substituted at the 5 position.[108] Furthermore, reactions of pyridinium salts with thiazolone at the *C*-terminus have been reported.[109] The nucleophilicity of the 5 position originates from the electron-donating effect of the hydroxy substituent in the thiazole tautomer.[108a]

In general, the synthetic approach towards oxazolone is more laborious than for thiazolone derivatives, unless it is mono-substituted in 4 or disubstituted in the 4 and 5 positions. Unsubstituted oxazolones can be synthesized using 1,3-oxazolidin-2-one derivatives as starting materials.[110] While the functionalization of the nitrogen is widely explored,[111] a substitution at the 4 and 5 positions is not reported. The preparation of 5-methyl-oxazolone was conducted by reaction of *N*-hydroxyacetoacetamide under basic conditions.[112] An efficient approach to diaryloxazolone derivatives is the reaction of *α*-hydroxy-ketones with cyanate under acidic conditions, which is mechanistic similar to the synthesis of thiazolone(Figure 4-7*b*). This synthesis is mainly reported for aryl substituted derivatives.[113] The reaction of urethane with *α*-hydroxy-ketones was used for the preparation, too.[114] Interestingly, a photoreaction of an diphenyloxazolone was already described as early as 1956.[99] The nucleophilic substitution of 2-chloro-oxazole leads to oxazolone.[115] Alkylation under basic conditions occur at the nitrogen.[99b, 116] The use of Meerwein salts furnish *O*-alkylation products.[117] Michael additions as well as Friedel-Crafts acylation in the 5 position are described for mono-substituted reagents.[118][119]

4.4 Results and Discussion

4.4.1 First Generation – Oxazolone-bridged DAEs

4.4.1.1 Target Structure and Physical-organic Considerations

Target structure **4-1oH** is an oxazolone bridged DAE, substituted by a 2-methyl-5-chloro-thien-3-yl and a 3-methyl-benzo[b]thien-2yl rest. This setup, classified as semi-inverse DAE exhibits two different linear conjugation paths between the bridge and the aryl moieties, addressable *via* the light-induced switching of the open form **4-1oH** to the closed form **4-1cH** (Figure 4-8). In both photoisomers, a dissociation equilibrium allows the formation of the charged forms **4-1o** and **4-1c**, determined by the dissociation constants K_A^O and K_A^C. The modulation of the double bond motif should induce a pK_a increase through the ring closure as discussed in chapter 4.3.2. The chlorine attached to the thiophene moiety allows a post-functionalization, e.g. to tune the absorption or polarity, if the target structure fulfills the concept.

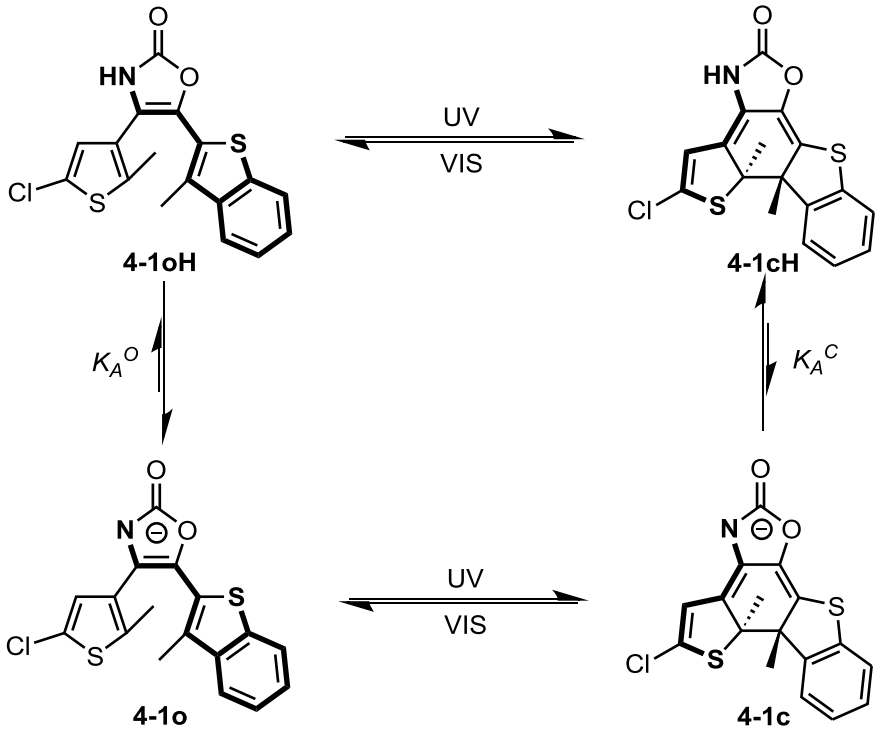

*Figure 4-8 Target structures of the first generation and its four-state reaction cycle, including the photoisomerization **4-1oH** ⇌ **4-1cH** and **4-1o** ⇌ **4-1c** as well as the dissociation equilibria **4-1oH** ⇌ **4-1o** and **4-1cH** ⇌ **4-1c**.*

4.4.1.2 Synthesis

Target molecule **4-1o** was synthesized in three steps (Figure 4-9), starting from the literature known with *α*-dihydroxyketone **4-7**. 3-methylbenzo[b]thiophene **4-8** was substituted *via* an electrophilic substation with **4-7** to give the hydroxyketone **4-9** in good yields. The bridging

oxazolone ring was established by reaction of **4-9** with urethane **4-10** in pyridine. A mixture of two isomers was isolated. The isomers were separated by preparative HPLC and characterized by NMR. The NMR spectra show no change in number and integration of the signals, only differences in the chemical shifts. The UPLC shows similar UV/vis spectra as well as the same mass (m/z) of the desired product **4-1oH**. The pyridine used in the synthesis of **4-1oH** could induce a tautomerization of the hydroxyketone **4-9**, resulting in two regioisomers.

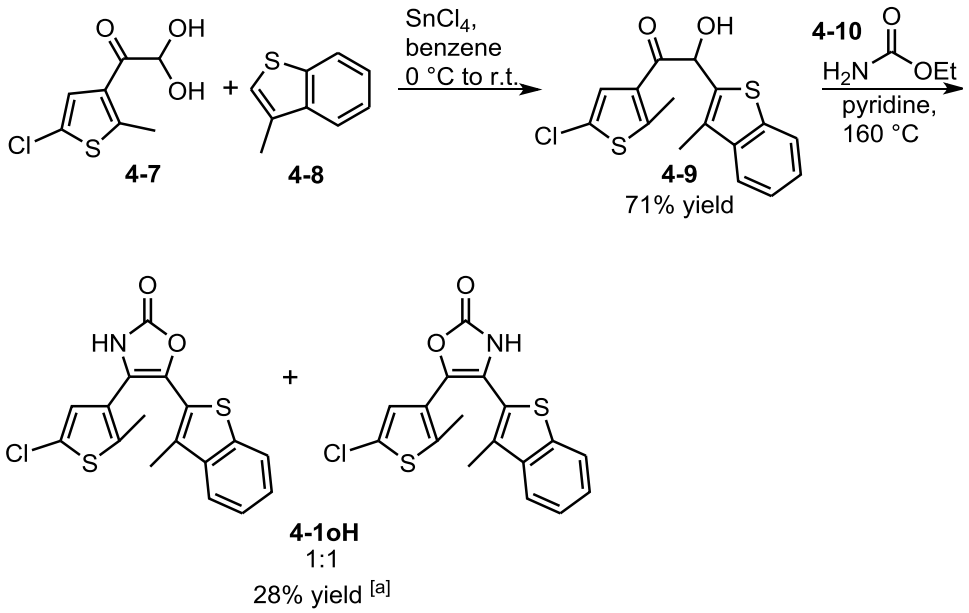

*Figure 4-9 Synthesis of **4-1o**.[a] given yields include both regioisomers.[120]*

So far, no crystals suitable for X-ray analysis could be grown, NOESY experiments did not offer additional information to distinguish the two isomers. For differentiation, the compound with the lower retention time in the preparative HPLC will be called isomer 1 (**iso1**), the other isomer 2 (**iso2**).

4.4.1.3 Photochemical Analysis

The photochemical characterization and titration were conducted in an aqueous 0.15 M potassium chloride solution containing 30 *vol*-% acetonitrile. To obtain complete differentiation between protonated and deprotonated species, a 0.1 M hydrogen chloride or potassium hydroxide solution was used. As titrand, an aqueous 0.7 M hydrogen chloride solution containing 30 *vol*-% acetonitrile was used.

The spectra of all four-states are summarized in Figure 4-10a. The titration of **4-1-iso1** shows a ${}^{S}_{S}pK_a$ change of -0.4 ± 0.4 from 9.0 ± 0.1 in the open form to 8.6 ± 0.3 in the closed isomer (Figure 4-10b) . It is important to point out that the pK_a change is within the uncertainty of the titration method. To decrease the uncertainty, a bigger spectral change is necessary, which could be achieved by isolation of the closed isomer and use of higher concentrations. **4-1oH-iso1** shows the strongest absorption at 230 nm and a second band at 310 nm. The cyclization with 313 nm under

acidic conditions (**4-1oH-Iso1** ⟶ **4-1cH-Iso1**, Figure 4-10c) leads to photocyclization, which is reversible by irradiation with 436 nm (**4-1cH-Iso1** ⟶ **4-1oH-Iso1**, Figure 4-10d), although the initial spectrum is not fully recovered. The irradiation with UV light lead to a decrease of the 310 nm band and a rising band at 420 nm. After cycloreversion a broad band at 450 nm remains, which results from a side reaction. The Mauser diagrams show no linear behavior. The mass spectrometry of the byproduct in the UPLC shows no chlorine isotope pattern. Nevertheless, the molar fraction of the closed isomer after irradiation with 313 nm and 436 nm at PSS was estimated from the UPLC measurement to be 22% after the ring closure and 0% after cycloreversion. Under basic conditions the UV band is bathochromicly shifted to 340 nm. The irradiation with 313 nm under basic conditions (**4-1o-Iso1** ⟶ **4-1c-Iso1**, Figure 4-10e) leads to a similar spectral evolution and a molar fraction of the closed isomer at the PSS of 9%. The irradiation with 436 nm leads to a quantitative reaction (**4-1c-Iso1** ⟶ **4-1o-Iso1**, Figure 4-10f) with a reversed spectral change. The spectral analysis and the UPLC measurements lead to the conclusion that no unimolecular photoreaction proceeds through irradiation.

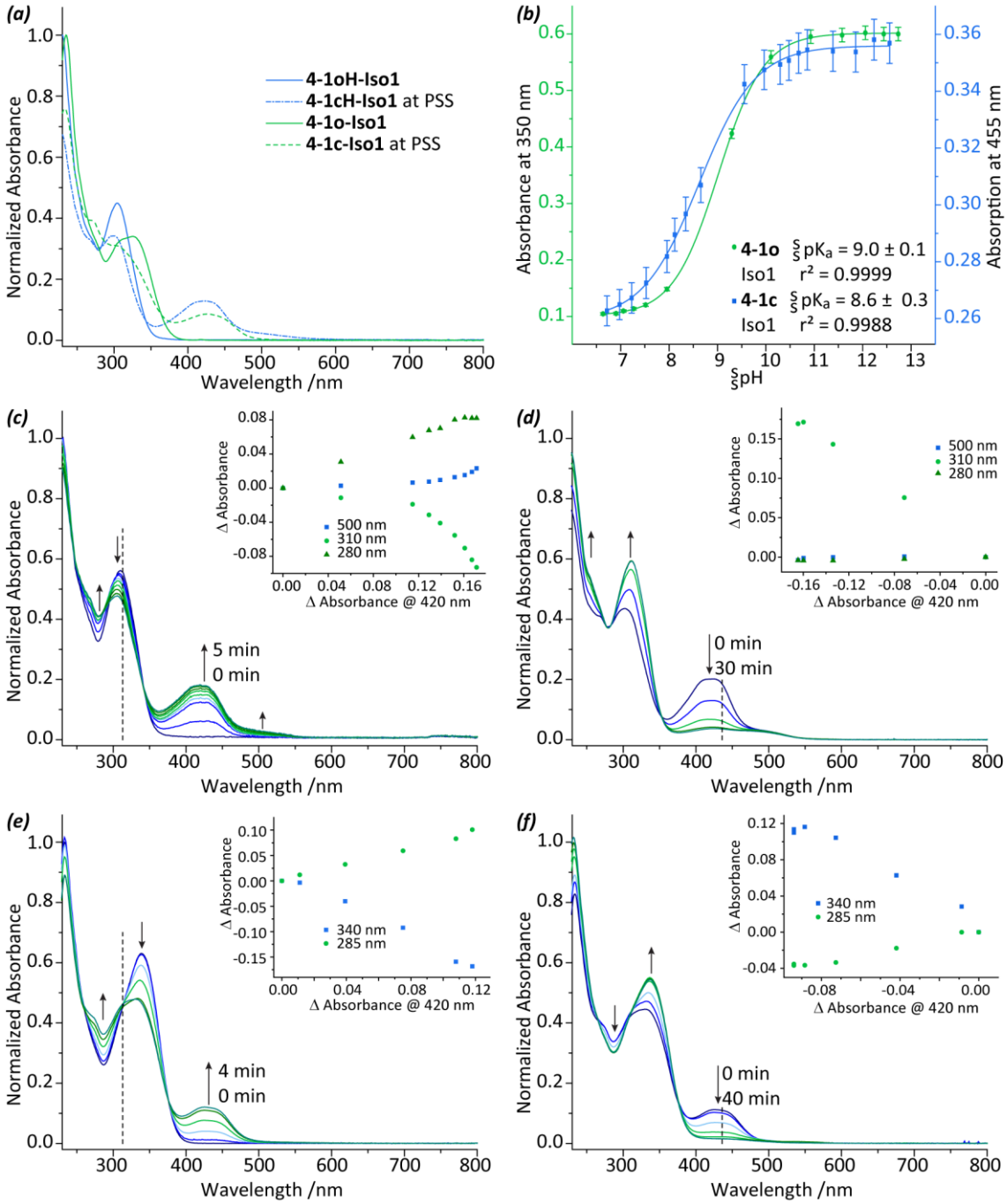

*Figure 4-10 Photochemistry and acid-base equilibrium of **4-1-Iso1** in aqueous 0.15 M potassium chloride solution containing 30 vol.-% acetonitrile, C = 42.5 µM: (a) absorption spectra and extinction coefficient of all four species **4-1oH**, **4-1cH**, **4-1o**, **4-1c**; (b) spectrophotometric titration with aqueous 0.7 M hydrogen chloride solution containing 30 vol.-% acetonitrile and its dose-response sigmoidal fit to determine the ${}^{s}_{s}pK_a$ values (**4-1oH** ⇌ **4-1o**, **4-1cH** ⇌ **4-1c**); (c) spectral analysis of the ring closure with 313 nm under acidic conditions (**4-1oH** ⟶ **4-1cH**) including Mauser diagram (inset); (d) spectral analysis of the ring opening with 546 nm under acidic conditions (**4-1cH** ⟶ **4-1oH**) including Mauser diagram (inset); (e) spectral analysis of the ring closure with 313 nm under acidic conditions (**4-1o** ⟶ **4-1c**) including Mauser diagram (inset); (f) spectral analysis of the ring opening with 546 nm under acidic conditions (**4-1cH** ⟶ **4-1oH**) including Mauser diagram (inset).*

The spectra of all four-states are summarized in Figure 4-11a. The titration of **4-1-iso2** shows a ${}^{s}_{s}pK_a$ change of -0.5 ± 0.7 from 8.9 ± 0.1 in open form to 8.4 ± 0.6 in the closed isomer (Figure 4-11b) . The cyclization with 313 nm under acidic conditions (**4-1oH-Iso2** ⟶ **4-1cH-Iso2**, Figure

4-11c) leads to a decrease of the bands at 230 nm and 305 nm. As in case of isomer 1, a band at 420 nm rises which is reversible *via* irradiation with 436 nm (**4-1cH-Iso2** ⟶ **4-1oH-Iso2**, Figure 4-11d). A similar side reaction as in the case of isomer 1 is observable. Nevertheless, the molar fraction of the closed isomer after irradiation with 313 nm and 436 nm at PSS were estimated from the UPLC measurement to be 31% after the ring closure and 0% after cycloreversion. Under basic conditions the UV band is bathochromicly shifted to 330 nm. The irradiation with 313 nm under basic conditions (**4-1o-Iso2** ⟶ **4-1c-Iso2**, Figure 4-11e) leads to the cyclization, with a molar fraction of the closed isomer at the PSS of 26%. The cycloreversion with 436 nm leads to a quantitative reaction (**4-1c-Iso2** ⟶ **4-1o-Iso2**, Figure 4-11f). For both irradiation experiments, the spectral analysis and the UPLC measurements show no clean photoreaction.

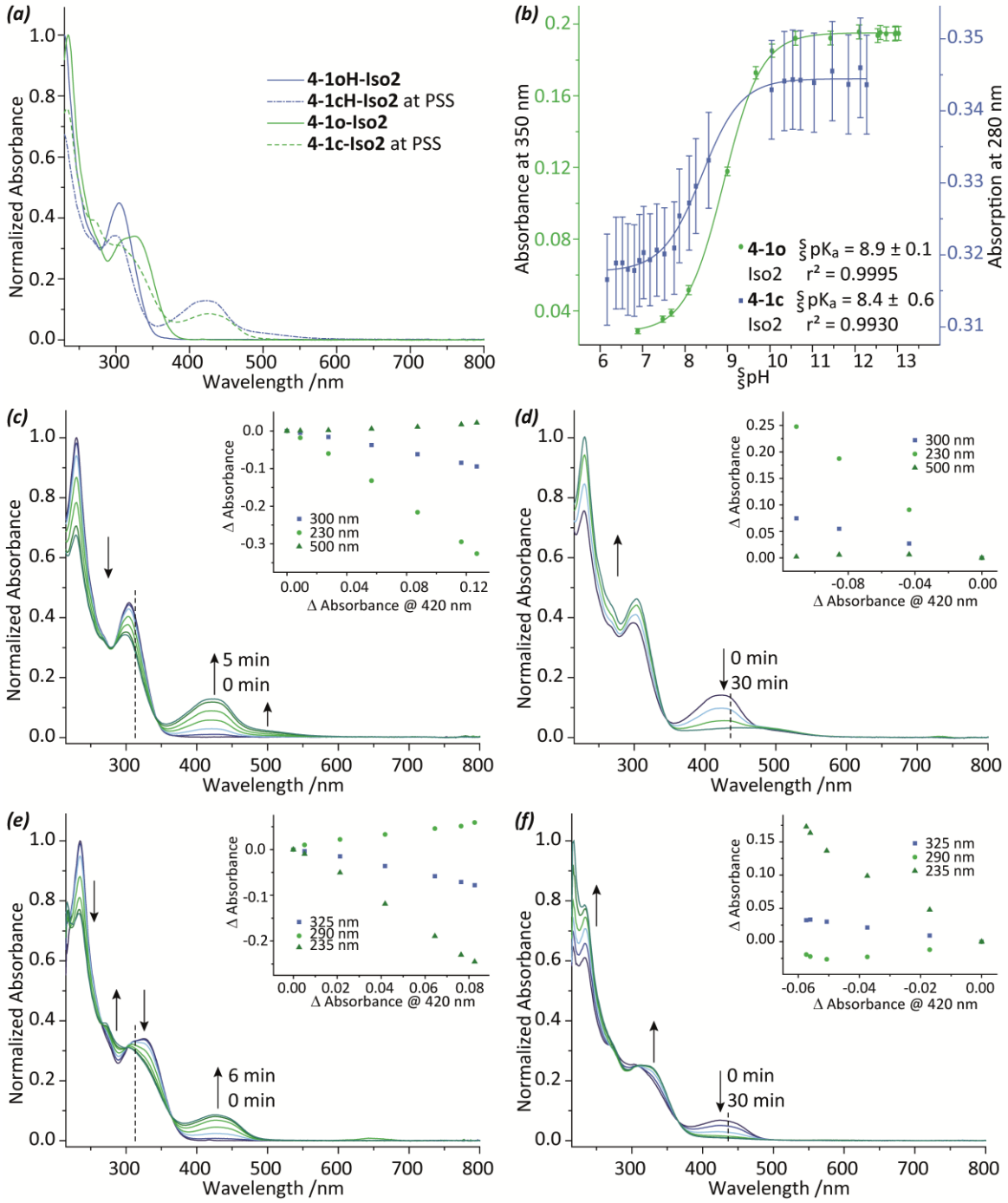

*Figure 4-11 Photochemistry and acid-base equilibrium of **4-1-Iso2** in aqueous 0.15 M potassium chloride solution containing 30 vol.-% acetonitrile, C = 42.5 µM: (a) absorption spectra and extinction coefficient of all four species **4-1oH**, **4-1cH**, **4-1o**, **4-1c**; (b) spectrophotometric titration with aqueous 0.7 M hydrogen chloride solution containing 30 vol.-% acetonitrile and its logistic fit to determine the ${}^{s}_{s}pK_a$ values (**4-1oH** ⇌ **4-1o**, **4-1cH** ⇌ **4-1c**); (c) spectral analysis of the ring closure with 313 nm under acidic conditions (**4-1oH** ⟶ **4-1cH**) including Mauser diagram (inset); (d) spectral analysis of the ring closure with 546 nm under acidic conditions (**4-1cH** ⟶ **4-1oH**) including Mauser diagram (inset); (e) spectral analysis of the ring closure with 313 nm under acidic conditions (**4-1o** ⟶ **4-1c**) including Mauser diagram (inset); (f) spectral analysis of the ring closure with 546 nm under acidic conditions (**4-1cH** ⟶ **4-1oH**) including Mauser diagram (inset).*

The 1th generation exhibits small a change of acidity, which is presumably caused by the extended delocalization of the negative charge in both photoisomers. This apparent drawback could be used to influence the acidity of both photoisomers with the substitution pattern, but

molecule **4-1oH** does not fulfill the aimed molecular concept. Additionally, a side reaction was observed, which avoidable by substitution of the chlorine. For that reasons the molecular design **4-1oH** was not investigated, further.

4.4.2 Second Generation – 3*H*-thiazol-2-on-4-yl DAE

4.4.2.1 Target Structure and Physical-organic Considerations

In the target structure of the second generation, **4-2oH**, is a 5-methyl-thiazol-2-one-4-yl and a 2-methyl-5-(4-methoxyphenyl)-thien-3-yl rest incorporated, bearing a central hexafluoro cyclopentene bridge (Figure 4-12). A common DAE ring closure to **4-2cH** should occur upon UV irradiation. In both photoisomers, a protonation/deprotonation equilibrium allows the formation of the charged forms **4-2o** and **4-2c**, determined by the dissociation constants K_A^O and K_A^C. The estimated pK_a values for both the thiazolone are well within the desired range with a significant change to be expected upon switching. Their reactivity as a nucleophile in organic reactions matches with the common diarylhexafluorocyclohexene syntheses.

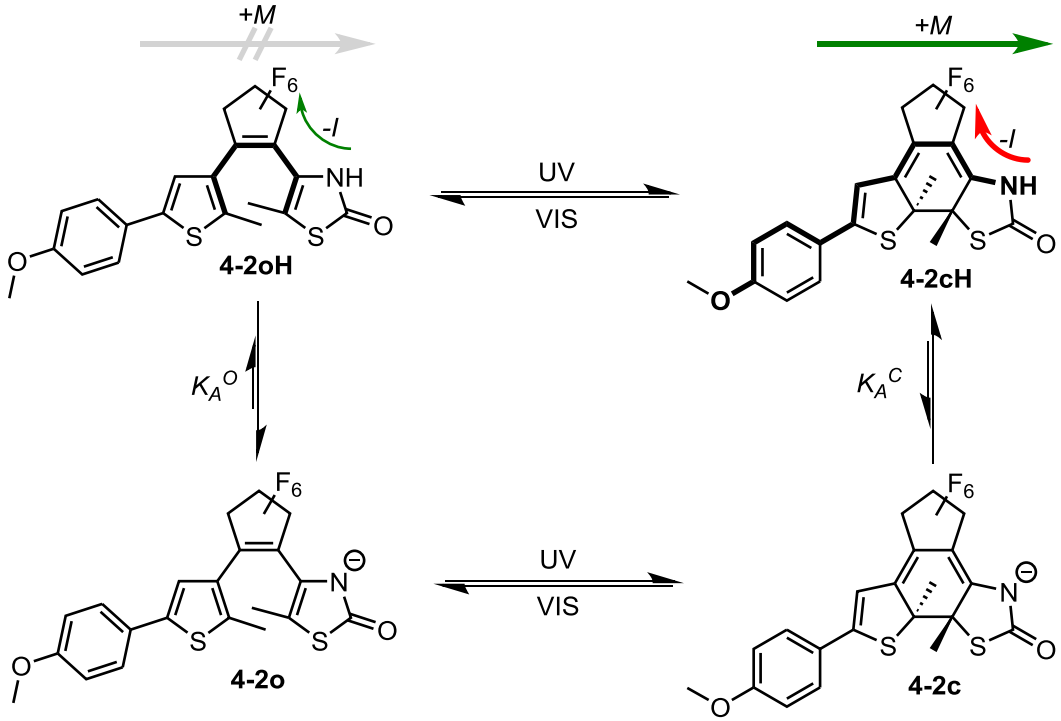

*Figure 4-12 Target structures of the second generation and the four-state reaction cycle, including the photoisomerization **4-2oH** ⇌ **4-2cH** and **4-2o** ⇌ **4-2c** as well as the dissociation equilibria **4-2oH** ⇌ **4-2o** and **4-2cH** ⇌ **4-2c**.; green arrow: desired interaction, red arrow: undesired interaction, gray arrow: no or negligible interaction.*

The first target structure **4-2oH** is designed to combine three different design aspects, which cause the pK_a-change. The main effect is induced by removing the double bond, decreasing the acidity, or rather an increase of the pK_A^O to pK_A^C (see chapter 4.3.2). The 2-(4-methoxyphen-1-yl)-5-methyl-thienyl-4-yl rest should induce an electron donating effect (*+M*) in the closed form **4-2cH** and **4-2c**, decreasing the stability of the negative charge, while being decoupled in the open

forms **4-2oH** and **4-2o**. The perfluorinated bridge exhibits an electron withdrawing effect, which might be counter-productive for the pK_a-change. The electronic effect is presumably less pronounced in the open form **4-2oH** than in the closed isomer **4-2cH**, due to the change from a cross- to a linear-conjugation. However, the effect is limited, due to the rotation around the carbon-carbon single bond in **4-2oH**, while the rotation is not possible in the **4-2cH**. Anticipating chapter 4.4.2.2, the main advantage of molecule **4-2oH** lies in the straightforward synthesis.

4.4.2.2 Synthesis

Compound **4-2oH** was synthesized as shown in Figure 4-13. The synthesis of 2,4-dibromo-5-methylthiazole **4-11** has been conducted as described in the literature, starting from the commercially available 2-amino-5-methylthiazole in two steps,[24] followed by nucleophilic substitution of the bromine in the 2 position to **4-12**. A so far literature known functionalization of a 5-methylthiazolone at the 4 position *via* lithiation was conducted. Therefore **4-12** was deprotonated with sodium hydride, followed by lithium halide exchange with ^{n}butyl lithium. In parallel the DAE precursor **3-2** was synthesized as reported in the literature.[27] The reaction of the lithiated **4-12** with **3-2** leads to the target molecule **4-2o**. Interestingly not only the *C*-terminus, but also the *N*-terminus undergoes the substitution reaction. This leads to byproduct **4-13**, which shows an irreversible photoreaction and was unambiguously identified by NMR and single-crystal X-ray diffraction. (see chapter 5.2 and 5.1.3.2).

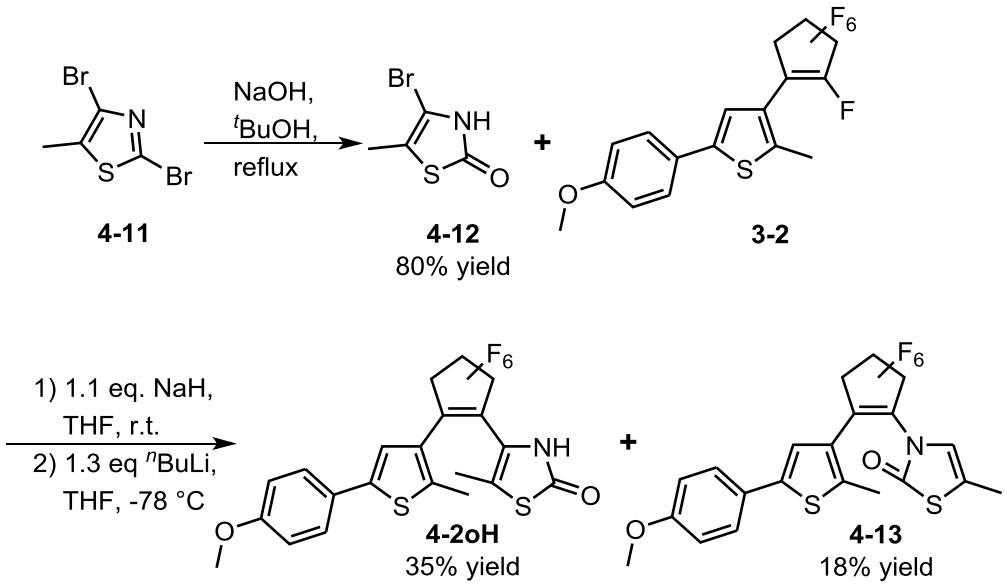

*Figure 4-13 Synthesis of **4-2oH**.*

4.4.2.3 Photochemical Analysis

Compound **4-2oH** has its absorption maximum at 300 nm in acetonitrile (Figure 4-14a) and shows the typical photochromism of DAEs. Upon irradiation with 313 nm light the UV band decreases, and a new band rises at 480 nm, with a sufficient band separation.

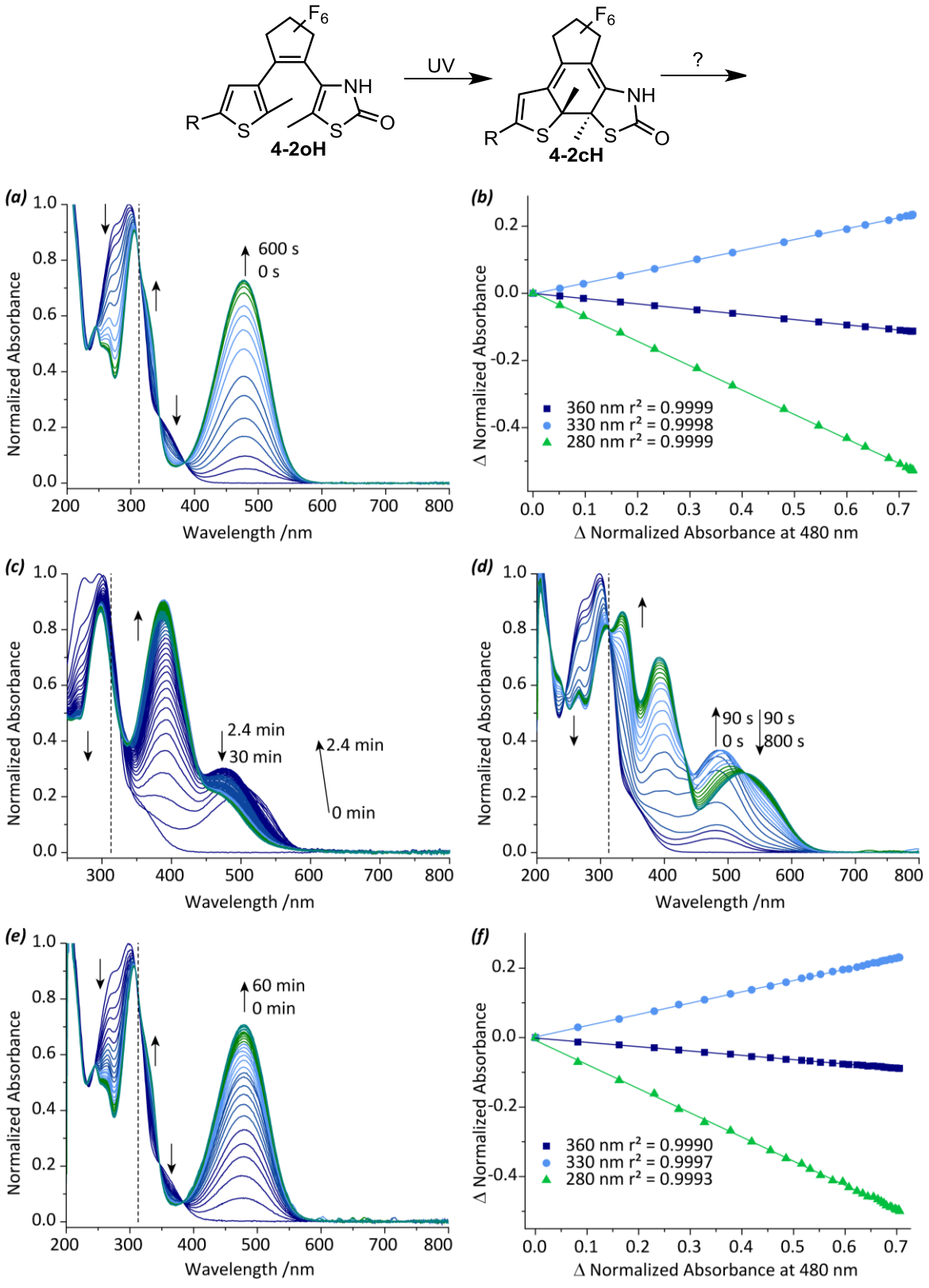

*Figure 4-14 Cyclization of **4-2o** by irradiation with 313 nm in different solvents: (a) acetonitrile; (b) Mauser diagram of irradiation in acetonitrile, C = 39.2 µM; (c) ethanol, C = 30.1 µM; (d) water:acetonitrile 4:6, C = 42.0 µM; (e) water:acetonitrile 4:6, C = 41.9 µM, 0.3 M hydrogen chloride; (f) Mauser diagram of irradiation in water:acetonitrile 4:6, 0.3 M hydrogen chloride.*

Both the observation of isosbestic points as well as the linear Mauser diagram fits indicate a clean photoreaction (Figure 4-14b). The UPLC analysis shows a rising peak of the **4-2cH**, clearly identified

via UV/vis spectra and mass spectrometry (Figure 4-15a). A second product **4-2water** is observed, with a mass (m/z, M-H) of 468.037 Da, compared to **4-2o** decreased by -22.00 Da, which is not photoresponsive. Even though the byproduct is formed either while irradiation in pure acetonitrile or as an artifact under UPLC conditions, the molar fraction of the closed isomer can be approximated to be higher than 87%. The irradiation with 436 nm leads to a reversed spectral development (not shown), but not to a complete regeneration of the initial open isomer spectrum. To analyze the byproduct formation, further irradiation experiments together with parallel UPLC sampling in different solvents were conducted. The irradiation with 313 nm in ethanol (Figure 4-14c) leads to a photoconversion followed by a thermal reaction. Initially, a similar spectral development to that in acetonitrile is observed, which is followed by a hypso- and hypochromic shift of the visible band (λ = 495 nm) by -20 nm. The UPLC measurement shows consumption of the open isomer **4-2oH** and only minuscule amounts of closed isomer **4-2cH** (see Figure 4-15a). The main product **4-2etoh** has a mass (m/z, M-H) of 542.109 Da, compared to **4-2o** increased by +52.07 Da.

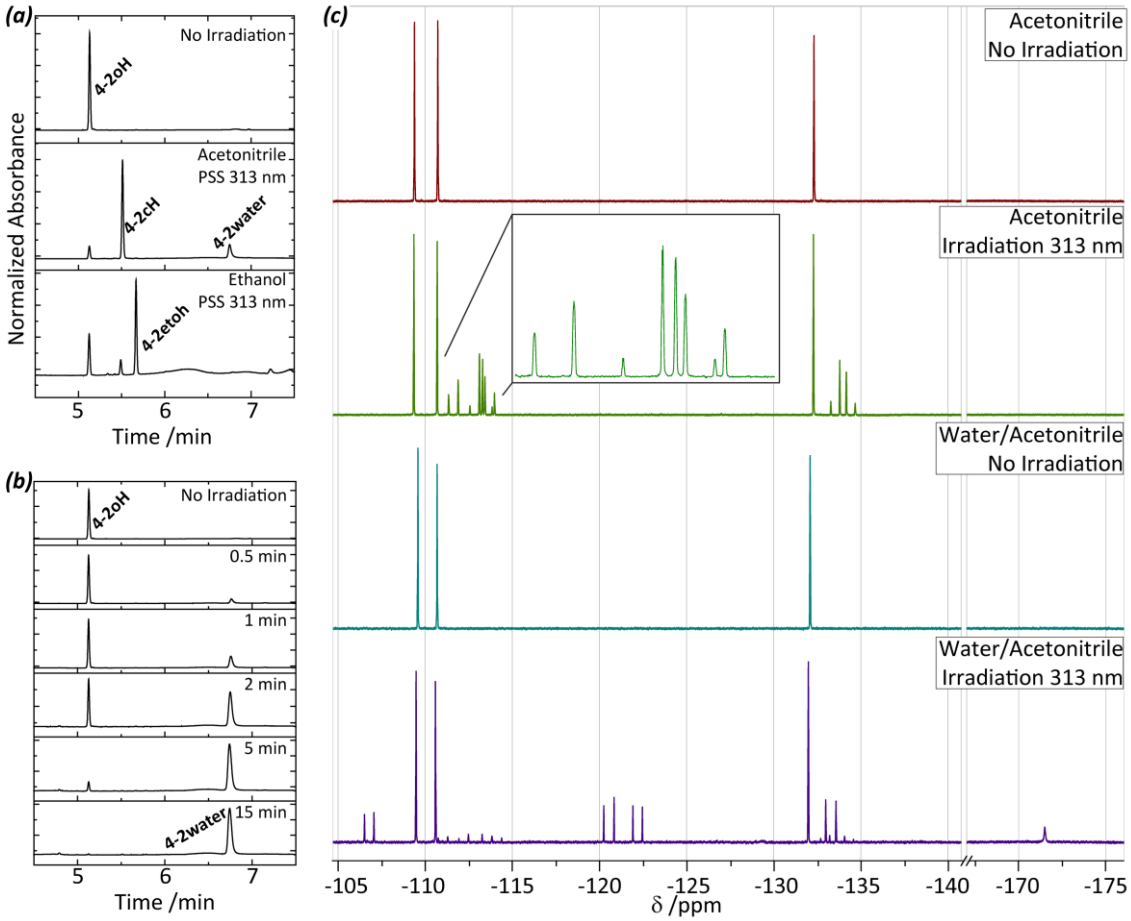

*Figure 4-15 Characterization of the side reaction: (a) UPLC traces of irradiation experiments in acetonitrile and ethanol; (b) UPLC traces of irradiation experiments in water: acetonitrile (4:6); (c) ^{19}F-NMRs in acetonitrile and water: acetonitrile (4:6) before and after irradiation with 313 nm: **4-2oH** ^{19}F NMR (471 MHz, acetonitrile-d) δ/ppm = -104.86 (A, 2F), -106.19 (A, 2F), -127.78 (A, 2F); **4-2cH** ^{19}F NMR (471 MHz, acetonitrile-d) δ/ppm = -111.61, -113.64 (ABq, J/Hz = 256.6, 2F), -112.84, -113.12 (ABq, J/Hz = 257.4, 2F), -133.53, -134.42 (ABq, J/Hz = 239.5, 2F); **4-2water** ^{19}F NMR (471*

MHz, acetonitrile-d) δ/ppm = -106.79, -122.19 (AXq, J/Hz = 255.2, 2F), -120.19, -133.28 (AXq, J/Hz = 277.8, 2F), -171.49 (A, 1F).

The irradiation in a mixture of water: acetonitrile (4:6) follows the same trend (Figure 4-14d). The visible band of the closed isomer (λ = 490 nm) shifts batho- and hypsochromic to 520 nm. UPLC traces show a complete conversion of the closed isomer **4-2cH** to the byproduct (see Figure 4-15b). The occurrence of isosbestic points and linearity of Mauser plots in pure acetonitrile (Figure 4-14a and b) and more important, upon addition of acid to the water-acetonitrile mixture, (Figure 4-14e and f), indicate a clean photoreaction. ^{19}F-NMR experiments in acetonitrile with and without the addition of water prove that the side reaction occurs at the hexafluorocyclopentene bridge (see Figure 4-15c). The ^{19}F-NMR of the open isomer **4-2oH** shows in pure acetonitrile as well as in the mixture three singlets of equal intensity. Upon irradiation, a set of three AB-signals appears. If water is added to the NMR tube, the signals of **4-2cH** disappear while the peaks of **4-2oH** stay constant and two AX-signals arise. A third singlet appears in the higher field. The AX-signals integrate to the same absolute value, which suggests that the side reaction results in loss of two fluorine atoms. Accordingly, the following byproducts and reaction mechanism is proposed, similar to the one published by Kobatake and co-workers:[29]

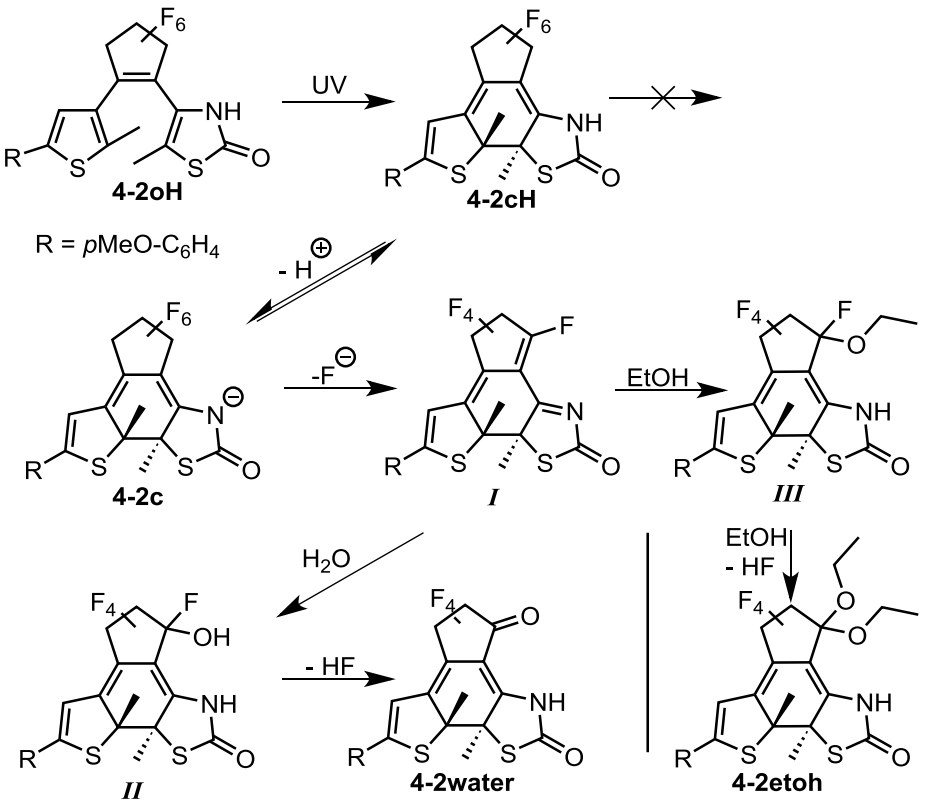

*Figure 4-16 Proposed byproducts **4-2water** and **4-2etoh** and the reaction mechanism of the decomposition of **4-1oH** in protic, nucleophilic solvents.*

The irradiation with UV light results in the known cyclization of DAE **4-2oH**, inducing a change from cross conjugation to linear conjugation between the *NH* and the fluorine substituted bridge. In the presence of acid, neither the deprotonation equilibrium nor the byproduct formation are

persistent. An elimination of fluoride, which is probably stabilized by hydrogen bonding in the protic solvents, leads to intermediate ***I***. In the next step, the addition of the nucleophile leads to either compound ***II*** or ***III*** depending on the used solvent. The absence of water has presumably three effects: First an inhibition of the deprotonation equilibrium, second nonappearance of the stabilization of the fluoride and at last, the absence of a nucleophile. In the case of ***II*** an elimination of hydrogen fluoride results in byproduct **4-2water** (m/z [M-H]: 469.043 Dq) in which two fluorenes are substituted by a carbonyl group, which is in excellent agreement with the obtained ESI-MS data. In the case of ***III***, where ethanol was used as a solvent, a second elimination/addition mechanism will follow to give the byproduct **4-2etoh** (m/z [M-H]: 543.116 Dq), which is also in good agreement with the obtained ESI-MS data. It is worth mentioning that the results discussed contradict the existing literature, claiming that an acceptor facilitates elimination of fluoride from the bridging five-membered ring. In this context it is important to point out, that the previously described molecule **3-1o** shows no decomposition, even though a strong acceptor is attached. Nevertheless, the occurrence of side reactions needs to be taken into account, especially when designing DAE switches for application in biological media.

4.4.3 Third Generation – 3*H*-thiazol-2-on-5-yl DAEs

4.4.3.1 Target Structure and Physical-organic Considerations

The third generation is purposed to avoid the substitution of fluorines in the bridge. Contrary to the second generation, a 4-methyl-thiazol-2-one-***5***-yl or 4-trifluoromethyl-thiazol-2-one-***5***-yl moiety are incorporated into the DAEs **4-3oH** and **4-4oH** (Figure 4-17). Analogously to **4-1cH**, the *+M*-effect of the 2-methyl-5-(4-methoxyphenyl)-thien-3-yl rest is apparent in the closed forms **4-3cH** and **4-4cH**, even though the effect is expected to be smaller, due to the linear conjugation to the sulfur of the thiocarbamate instead to the acidic *NH*. The withdrawing effect of the perfluorinated bridge affects the acidic *NH* directly in the open forms **4-3oH** and **4-4oH** and in the closed isomer **4-3cH** and **4-4cH** *via* the carbonyl motif indirectly. This is the most important difference to the second generation, because it is supposed to suppress the observed fluorine substitution in the bridge. The 4-postion of the thiazol-2-one, substituted with a methyl or trifluoromethyl group changes from a sp^2-hybrid in the open to a sp^3- hybridized orbital in the closed isomer. Hence, the inductive effects of the groups should differ between the photoisomers.

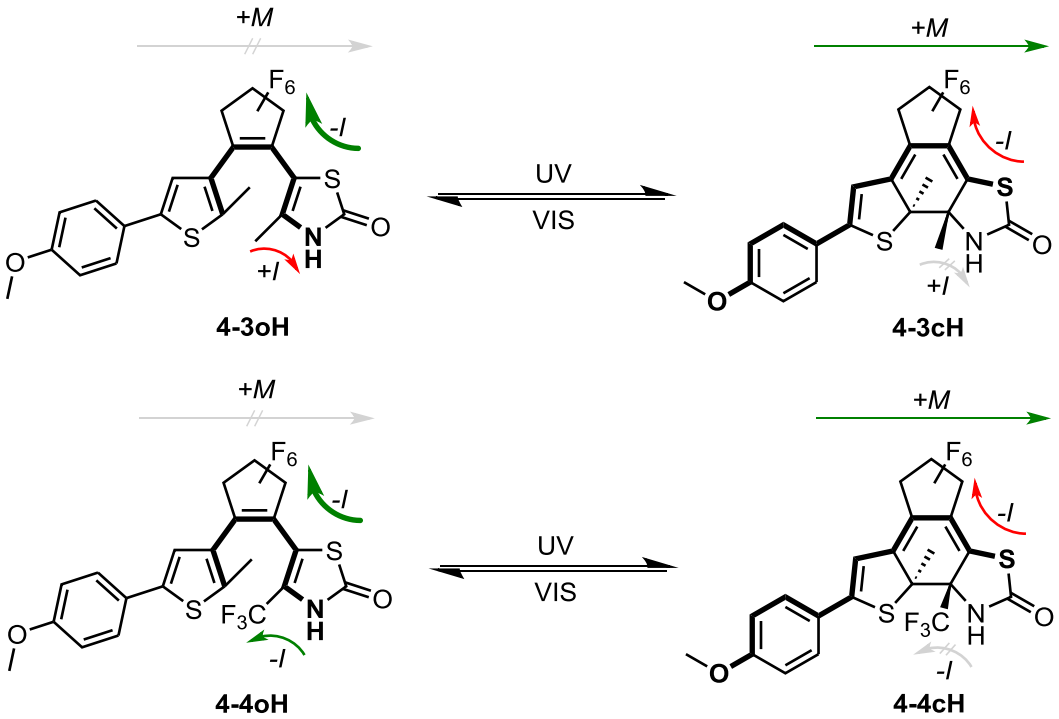

*Figure 4-17 Target structures of the third generation and its photoreactions **4-3oH** ⇌ **4-3cH** as well as **4-4oH** ⇌ **4-4cH**; green arrow: desired interaction, red arrow: undesired interaction, gray arrow: no or negligible interaction.*

4.4.3.2 Synthesis

Compound **4-2oH** and **4-3oH** were synthesized as shown in Figure 4-18. chloroacetone **4-14** and 3-bromo-1,1,1-trifluoroacetone **4-15** were substituted with potassium thiocyanate and isomerized under highly acidic conditions. To accelerate the reaction of chloroacetone **4-14**, a Finkelstein reaction with potassium iodide was used. The compounds **4-16** and **4-17** were deprotonated twice with excess ^{n}butyl lithium. The reaction temperature is important for the success of the lithiation, starting at -78 °C and consequent rising to 0 °C. The substitution of **3-2** with the lithiated compounds leads to **4-3oH** and **4-4oH**. The previously formed byproduct **4-13** was not observed.

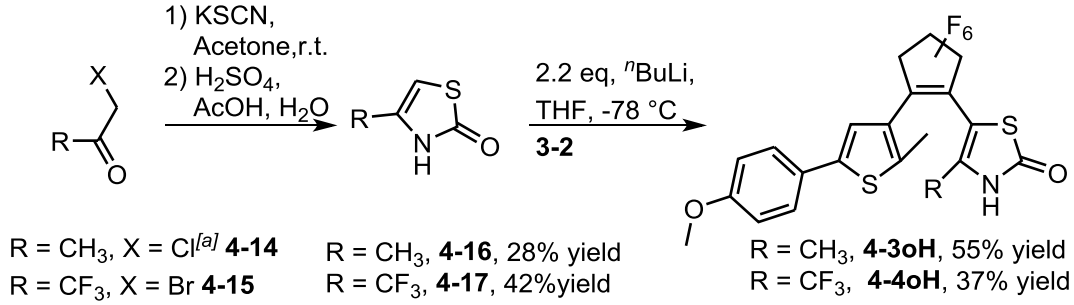

*Figure 4-18 Synthesis of **4-3oH** and **4-4oH**, [a] The reaction of **4-14** to **4-16** was conducted in ethanol with a catalytic amount of potassium iodide.*

4.4.3.3 Photochemical Analysis

The photochemical characterization and titration were conducted in an aqueous 0.15 M potassium chloride solution containing 30 vol.-% acetonitrile. To obtain complete differentiation

between protonated and deprotonated species, a 0.1 M hydrogen chloride or potassium hydroxide solution was used. As titrand, an aqueous 0.7 M hydrogen chloride solution containing 30 vol.-% acetonitrile was used.

Compound **4-16** and **4-17** were titrated and the stability towards water under acidic as well as basic conditions were evaluated. No side reaction was observed and a $^{S}_{S}pK_a$ of 11.2 ± 0.1 for **4-16** and 6.6 ± 0.1 for **4-17** has been determined (Figure 4-19). The second value is in good agreement with the previous done approximation (chapter 4.3.2), while the first shows a significant difference.

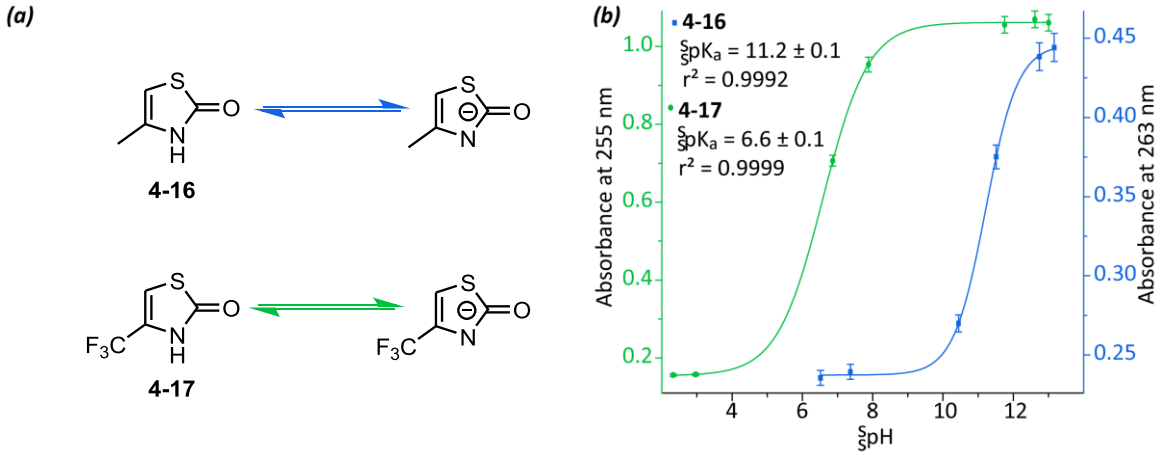

*Figure 4-19 Acid-base equilibria of **4-16** and **4-17**: (a) structure and deprotonation; (b) spectrophotometric titration in aqueous 0.15 M potassium chloride solution containing 30 vol.-% acetonitrile with aqueous 0.7 M hydrogen chloride solution containing 30 vol.-% acetonitrile and its logistic fit.*

The spectra of all four-states are summarized in Figure 4-20a. The titration shows a low $^{S}_{S}pK_a$change of 0.5 ± 0.3 units, with 8.8 ± 0.1 for the $^{S}_{S}pK_a$ of **4-3oH** and a closed $^{S}_{S}pK_a$ **4-3cH** of 9.3 ± 0.2 (Figure 4-20b). **4-3oH** exhibits a strong absorption at 300 nm with a tail until 400 nm. Upon irradiation with 313 nm under acidic conditions (**4-3oH** ⟶ **4-3cH**, Figure 4-20c) the DAE shows the characteristic decrease of the UV band and a rising absorbance at 490 nm appears, caused by the cyclization, resulting in a molar fraction of the closed isomer of 76%. A quantitative cycloreversion occurs by irradiation with 546 nm (**4-3cH** ⟶ **4-3oH**, Figure 4-20d), accompanied with a reversed spectral change. Isosbestic points as well as the Mauser diagrams indicate a clean photoreaction for both cyclization and cycloreversion under acidic conditions. The open isomer under basic conditions shows two maxima at 275 nm and 300 nm with similar absorbance. The previously observed tailing until 400 nm rises to a band with maximum at 370 nm. The spectral evolution and its analysis indicate a clean cyclization upon irradiation with 313 nm under basic conditions (**4-3o** ⟶ **4-3c**, Figure 4-20e), resulting in at least 47% closed isomer. Although a photoreaction can be observed, the initial spectrum corresponding to the open isomer cannot be regained after irradiation with 546 nm (**4-3c** ⟶ **4-3o**, Figure 4-20f). UPLC experiments indicate the

existence of an additional side product, next to the one discussed above, whose structure could not be fully assigned. Compound **4-3oH** was not further investigated due to that side reaction.

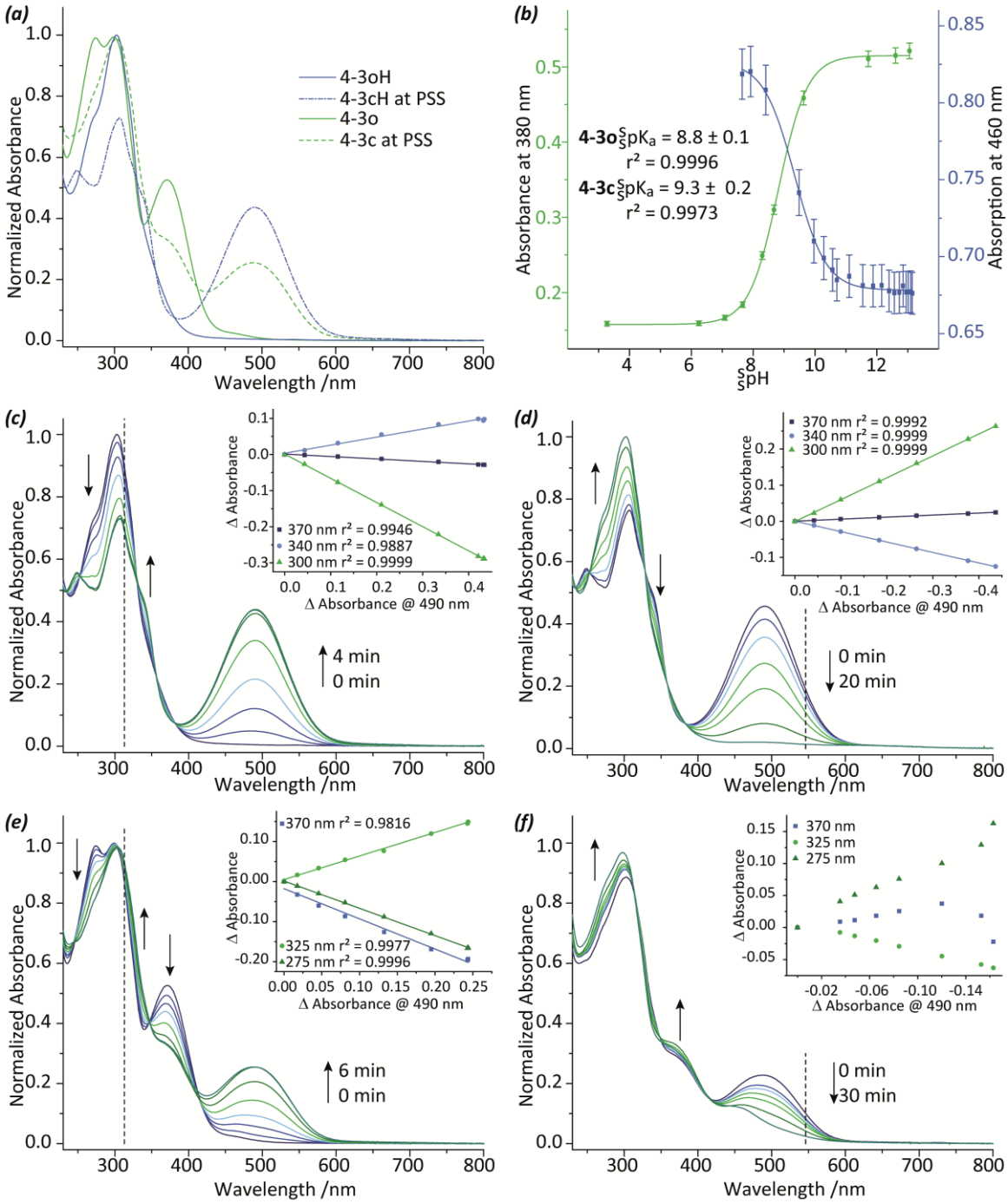

*Figure 4-20 Photochemistry and acid-base equilibrium of **4-3** in aqueous 0.15 M potassium chloride solution containing 30 vol.-% acetonitrile, C = 42.5 µM: (a) absorption spectra and extinction coefficient of all four species **4-3oH**, **4-3cH**, **4-3o**, **4-3c**; (b) spectrophotometric titration with aqueous 0.7 M hydrogen chloride solution containing 30 vol.-% acetonitrile and its dose-response sigmoidal fit to determine the ${}^{s}_{s}pK_a$ values(**4-3oH** ⇌ **4-3o**, **4-3cH** ⇌ **4-3c**); (c) spectral analysis of the ring closure with 313 nm under acidic conditions(**4-3oH** ⟶ **4-3cH**) including Mauser diagram (inset); (d) spectral analysis of the ring opening with 546 nm under acidic conditions(**4-3cH** ⟶ **4-3oH**) including Mauser diagram (inset); (e) spectral analysis of the ring closure with 313 nm under acidic conditions(**4-3o** ⟶ **4-3c**) including Mauser diagram (inset); (f) spectral analysis of the ring opening with 546 nm under acidic conditions(**4-3cH** ⟶ **4-3oH**) including Mauser diagram (inset).*

Target molecule **4-4oH** is involved in a four-state cycle, interconnecting the acid-base equilibrium (**4-4oH** ⇌ **4-4o** and **4-4cH** ⇌ **4-4c**) with the photochemical reaction (**4-4oH** ⇌ **4-4cH** and **4-4o** ⇌ **4-4c**, Figure 4-21).

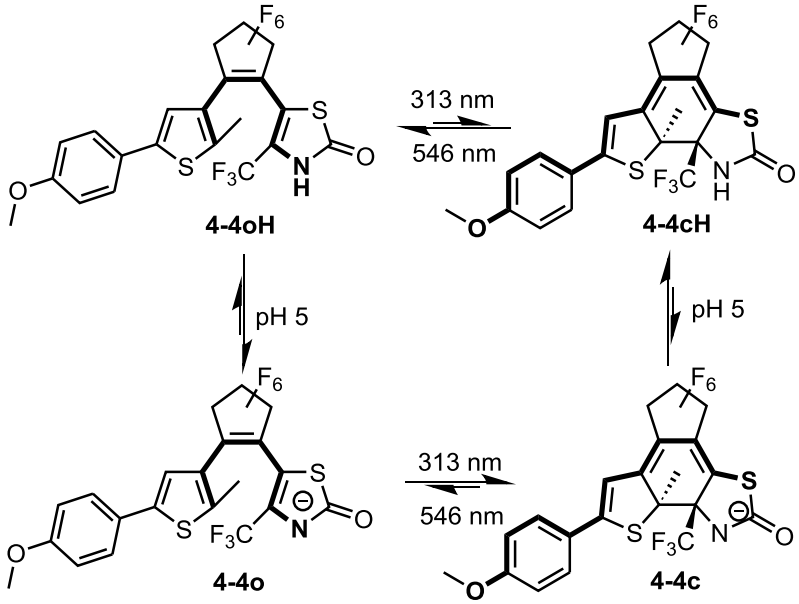

*Figure 4-21 Four-state reaction cycle of molecule **4-4**, including the photoisomerization **4-4oH** ⇌ **4-4cH** and **4-4o** ⇌ **4-4c** as well as the dissociation equilibria **4-4oH** ⇌ **4-4o** and **4-4cH** ⇌ **4-4c**.*

The spectra of all four-states are summarized in Figure 4-22a. The titration of **4-4o** gives a ${}^{S}_{S}pK_a$ of 4.0 ± 0.1 ($\Delta G_a{}^{O}$ = 22.8 kJ mol^{-1}) while the titration of **4-4c** gives a ${}^{S}_{S}pK_a$ of 6.8 ± 0.1 ($\Delta G_a{}^{C}$ = 38.8 kJ mol^{-1}, Figure 4-22b), which results in a significant ${}^{S}_{S}pK_a$ change of 2.8 ± 0.2 units. The open isomers (**4-4oH** & **4-4o**) show a strong absorption in the UV region until 330 nm, which is probably caused by the $S_0 \rightarrow S_2$ transition (Figure 4-22a). The deprotonated form **4-4o** shows a band at 360 nm, while the protonated form **4-4oH** exhibits a tail until 420 nm, dedicated to the $S_0 \rightarrow S_1$ transition. Irradiation with 313 nm UV light leads to a rise of an intense band at 500 nm in the protonated form **4-4cH**, as well as in the deprotonated compound **4-4c**.

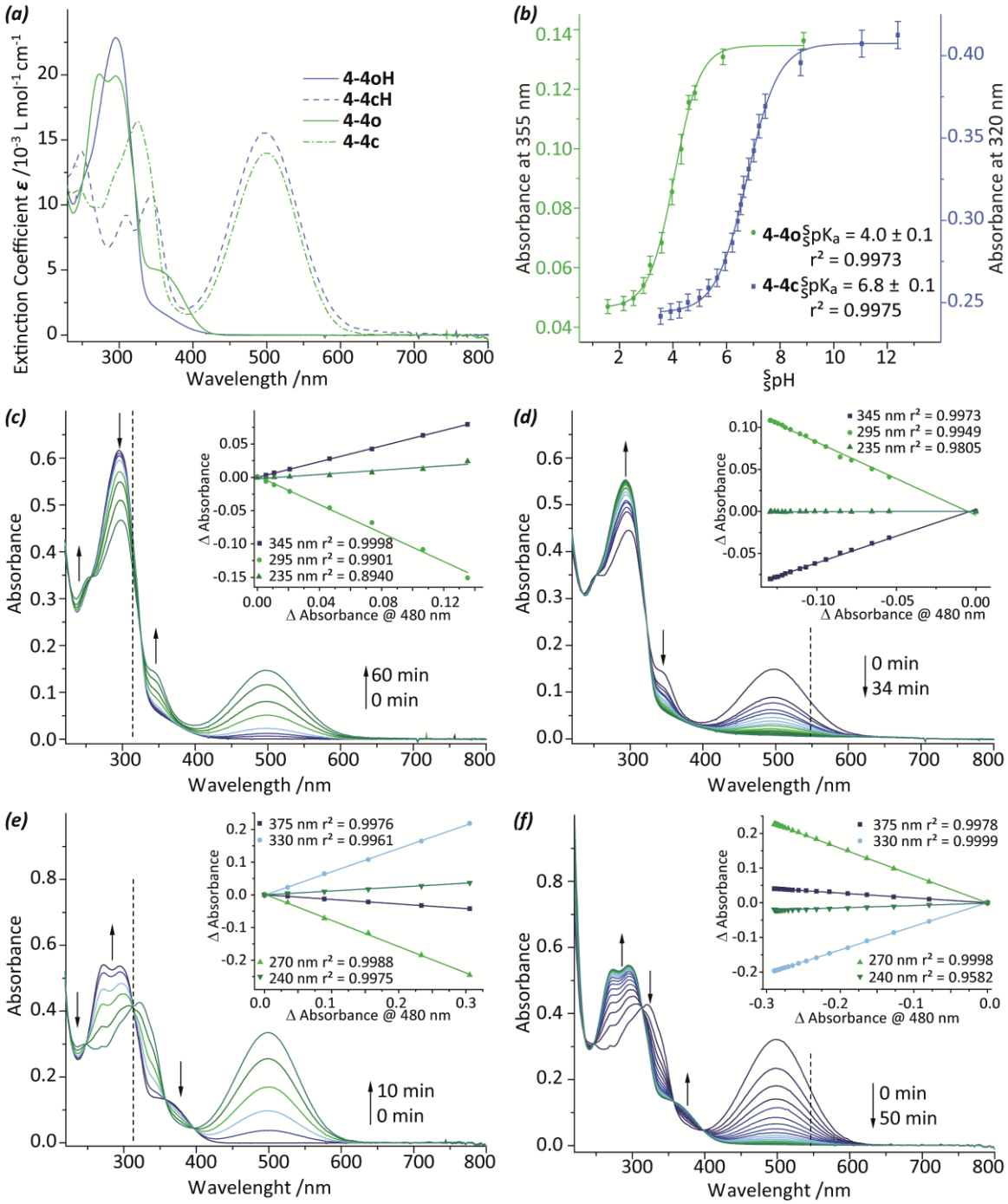

*Figure 4-22 Photochemistry and acid-base equilibrium of **4-4oH** in aqueous 0.15 M potassium chloride solution containing 30 vol.-% acetonitrile, C = 26.6 µM: (a) absorption spectra and extinction coefficient of all four species **4-4oH**, **4-4cH**, **4-4o**, **4-4c**; (b) spectrophotometric titration with aqueous 0.7 M hydrogen chloride solution containing 30 vol.-% acetonitrile and its dose-response sigmoidal fit to determine the ${}^{s}_{s}pK_a$ values (**4-4oH** ⇌ **4-4o**, **4-4cH** ⇌ **4-4c**); (c) spectral analysis of the ring closure with 313 nm under acidic conditions(**4-4oH** ⟶ **4-4cH**) including Mauser diagram (inset); (d) spectral analysis of the ring opening with 546 nm under acidic conditions(**4-4cH** ⟶ **4-4oH**) including Mauser diagram (inset); (e) spectral analysis of the ring closure with 313 nm under acidic conditions(**4-4o** ⟶ **4-4c**) including Mauser diagram (inset); (f) spectral analysis of the ring opening with 546 nm under acidic conditions(**4-4cH** ⟶ **4-4oH**) including Mauser diagram (inset).*

Irradiation with green light (546 nm) leads to complete cycloreversion. Spectral analysis of both cyclization and cycloreversion show clean photoreactions, in the protonated cases (Figure 4-22c and d) as well as in the deprotonated one (Figure 4-22f and e), proven by the isosbestic points and

Mauser diagrams. Photokinetic analysis of the ring closure and ring opening show a strong dependence of rate and conversion of the photoreaction on the protonation state. While the protonated forms show a low conversion to the closed isomer (Table 4-1 and Figure 4-23a) and a lower rate of conversion, the deprotonated forms shows a much higher conversion and faster rate of reaction.

Table 4-1 Spectroscopic and photochemical data in dependence of the pH in aqueous 0.15 M KCl solution (30 vol-% MeCN); [a] monochromator bandwidth [b] effective quantum yield.

	$^{s}_{s}pH$	λ_{max} /nm	λ_{irrad} /nm	ε_{max} / l·mol^{-1}·cm^{-1}	ε_{313nm} / l·mol^{-1}·cm^{-1}	ε_{546nm} / l·mol^{-1}·cm^{-1}	x_C^{PSS}	φ
4-4oH	1.3	295 ± 1	313 ± 6[a]	22900 ± 500	16900 ± 400		0.35 ± 0.05	0.021 ± 0.002
4-4cH	1.3	497 ± 1	546 ± 6[a]	15600 ± 800	9000 ± 500	8600 ± 400	0.03 ± 0.05	0.036 ± 0.004
4-4o	9.0	295 ± 1	313 ± 6[a]	19900 ± 400	15600 ± 300		0.85 ± 0.05	0.47 ± 0.05
4-4c	9.0	500 ± 1	546 ± 6[a]	14000 ± 700	15200 ± 800	7500 ± 400	0.0 ± 0.05	0.096 ± 0.01
	5.0		313 ± 6[a]				1.0 ± 0.05	0.34 ± 0.03 [b]
	5.0		546 ± 6[a]				0.0 ± 0.05	0.040 ± 0.004 [b]

The cycloreversion is in both cases complete, but the rates of the photoreaction show the same behavior as the cyclization; (deprotonated is faster than protonated). Analysis of the photokinetic data shows that the quantum yields differ significantly by an order of magnitude between the cyclization of the deprotonated (**4-4o** ⟶ **4-4c**) and protonated form (**4-4oH** ⟶ **4-4cH**). A slow side reaction of closed, deprotonated compounds **4-4c** and an even slower side reaction of **4-4cH** with water at 25 °C can be observed (Figure 4-23b).[27-28] UPLC analysis show m/z counts similar to the ones obtained for molecule **4-4water**. Nevertheless, the design change from **4-2** to **4-4** was successful, due to the drastic gain of stability towards water. It is noteworthy to point out that no thermal ring opening has been observed, neither in the protonated nor in the deprotonated forms.

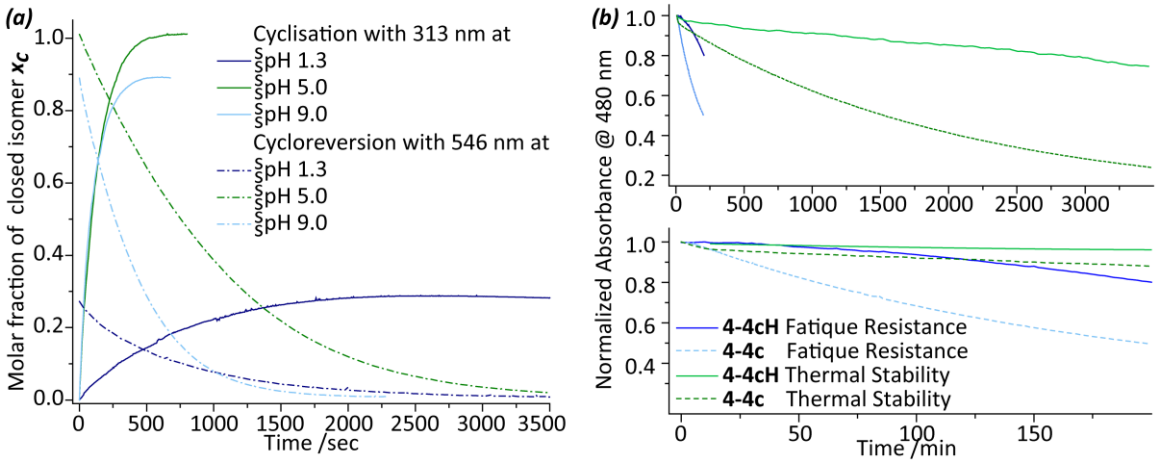

*Figure 4-23 Kinetic analysis of **4-4oH**: (a) photokinetic of cyclization and cycloreversion in dependence of the pH; (b) thermal stability and fatigue resistance in dependence of the protonation state, TOP long time scale and BOTTOM short time scale of the same experiments.*

Besides the thermal stability, the photochemical fatigue was investigated, as well. (Figure 4-23b) Under harsh basic conditions a decomposition upon irradiation with 313 nm has been observed, while an acidic milieu leads to only marginal fatigue.

If the pH is adjusted to 5, within the range of pK_a modulation, a *catalytic-cooperative interconnection* between all involved equilibria is observable. The performance of the photoisomerization is significantly enhanced by coupling to a thermal equilibrium. Irradiation of the solution with UV light (313 nm) leads to a complete conversion, with a similar reaction speed for the ring closure of the deprotonated forms (**4-4o** ⟶ **4-4c**, Table 4-1 and Figure 4-23a). The cycloreversion occurs with the rate of the protonated species (**4-4cH** ⟶ **4-4cH**). The calculation of an effective quantum yield confirms this statement, which were calculated from the photokinetic traces at pH 5, assuming the presence of **4-4o** and **4-4cH**. The four-states of the system are connected by a catalytic cycle, where a base (*e.g.* hydroxide in aqueous environment), acts as catalyst while being orders of magnitude lower in concentration at pH 5 in comparisons to compound **4-4**.

Analyzing and comparing the molecules of the second generation it can be concluded that the trifluoromethyl group attached to the thiazolone seems to be an integral part for a good switching performance and the significant $^{S}_{S}pK_a$ change. The design changes from 2st to 3nd generation fulfil their purpose, resulting in a decrease of side reactions, even though they are not inhibited completely. The initial assumption for the pK_a modulation fits pretty well for **4-4oH**, even though the electron accepting effect of the perfluorinated bridge was underestimated. Therefore, the aimed pK_a window around pH = 7.4 is missed. The done assumption failed for compound **4-3oH** including the pK_a prediction of the 5-methyl-thiazol-2-one. It is not clear why the pK_a changes differs that much. The described four-state system (**4-4oH**, **4-4o**, **4-4c** & **4-4cH**) might be regarded from two interconnected perceptions; the modulation of the acidity by light, and the modulation of a photoreaction with the pH. On the one hand, we were able to establish a light induced pKa modulation of $\Delta^{S}_{S}pK_a = 2.8 \pm 0.2$ units between two distinct states where no thermal interconversion was observed. Our molecular design marks an important milestone in photoacid research. On the other hand, molecule 1oH exhibits unique catalytic-cooperative interconnection of a thermal with a photochemical equilibrium, and is strongly connected to pH gated photochromism. This concept realizes the coupling of a thermodynamically controlled acid-base reaction with a light-driven isomerization reaction.

4.4.3.4 Ground- and Excited-state Potential Energy Surface[4]

The reaction cycle of **4-4oH** was investigated by UV/vis experiment, transient absorption measurements in acetonitrile as well as static calculations on the ground- and excited-state energy hypersurface, to give further insight into the energetics and photochemical behavior. The transformation between closed and open forms in the ground state is prevented by existence of large barrier: $\Delta G^{\neq}$ = 173.6 kJ mol^{-1} for neutral molecule (**4-4cH** → **4-4oH**) and an even larger value of 196.2 kJ mol^{-1} is found for the deprotonated switch (**4-4c** → **4-4o**). In both cases, the open form is thermodynamically preferred: neutral ΔG_r = - 28.9 kJmol^{-1} (**4-4cH** ⇌ **4-4oH**), deprotonated ΔG_r = - 41.8 kJ mol^{-1} (**4-4c** ⇌ **4-4o**). It should be noted that the photochromism shows the same trends in pure acetonitrile as in previously used acetonitrile-water mixtures (see appendix 7.2). The protonated forms **4-4oH** and **4-4cH** as well as the closed, deprotonated form (**4-4c**) show an excited-state energy diagram and reaction dynamic similar to already characterized DAEs. The irradiation of the open, protonated isomer **4-4oH** results in extinction to the S_2 state, which decay to S_1 (τ = 50 fs). This excited state has very low oscillator strength and thus is, most probably, populated indirectly *via* internal conversion. The system relaxes towards a conical intersection, in a barrier less fashion (τ = 300 fs) followed by the crossing of the intersection and cooling of the resulting hot ground state towards the open or closed isomer (τ = 31 ps). The extinction of **4-4cH** and **4-4c** results in the S_1 state followed by a Franck-Condon relaxation towards local minima (τ(**4-4cH**) = 50 fs, τ(**4-4c**) = 100 fs). As already known for DAEs, small barriers of approximately 4.2 kJ mol^{-1} were found on the excited reaction path of the cycloreversion. Relaxation to the hot ground-states were observed (τ(**4-4cH**) = 300 fs, τ(**4-4c**) = 500 fs) and afterwards their cooling (τ(**4-4cH**) = 8.4 ps, τ(**4-4c**) = 7.2 ps). The excited-state energy hypersurface of the deprotonated cyclisation differs from other DAEs, by an additional local minimum separated through a small barrier, which is counterintuitive to the observed, high quantum yield. The reaction dynamic is not less complex, and therefore not fully understood, yet. Anyways, the extinction of **1o** results in the S_1 state, which exhibits a far higher oscillator strength. An ultra-fast relaxation to the closed ground-state was observed (τ= 60 fs). Besides this a population of an unknown state X was found, which cannot be pictured by calculation. From there further spectral changes were observed (details see SI). Further investigation needed to be done, take dynamic effects into account.

[4] Conducted by Dr. Martin Quick, Dr. Sergai Kovalenko, Dr. Simon Budzak and Prof. Denis Jacquemin.

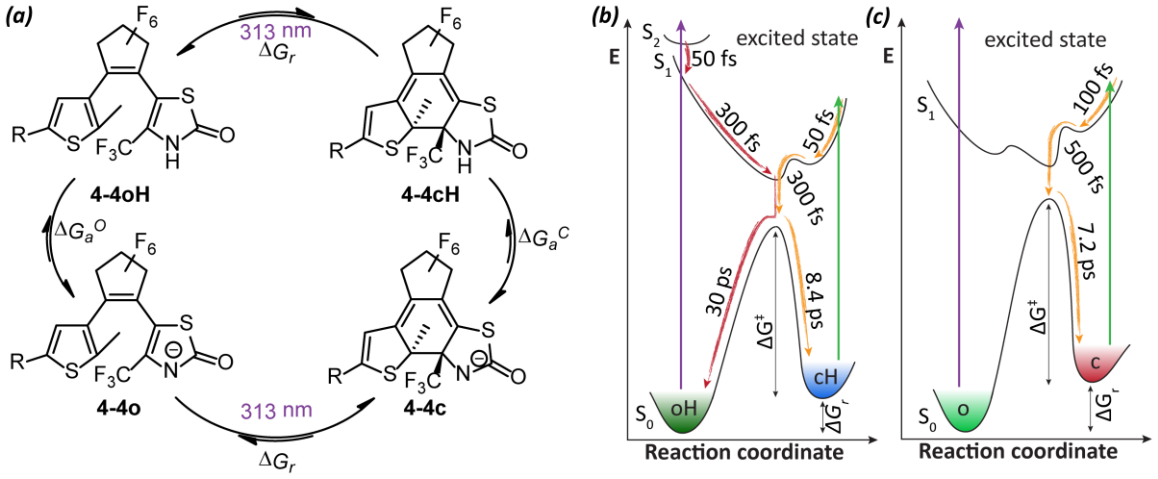

Figure 4-24 Potential energy diagram and excited state kinetics; ***(a)*** *four state reaction cycle of* ***4-4oH,*** ΔG_a^O = 22.8 kJ mol^{-1} (***4-4oH*** + H_2O → ***4-4o*** + H_3O^+), ΔG_a^C = 38.8 kJ mol^{-1} (***1cH*** + H_2O → ***1c*** + H_3O^+); ***(b)*** *protonated forms* ***4-4oH*** *and* ***4-4cH,*** $\Delta G^{\neq}$ = 173.6 kJ mol^{-1}, ΔG_r = -28.8 kJ mol^{-1} (***4-4cH*** → ***4-4oH***); ***(c)*** *deprotonated forms* ***4-4o*** *and* ***4-4c,*** $\Delta G^{\neq}$ = 196.2 kJ mol^{-1}, ΔG_r = -41.8 kJ mol^{-1} (***4-4c*** → ***4-4o***).

4.4.4 Fourth Generation – 3*H*-thiazol-2-on-5-yl Terarylene

4.4.4.1 Target Structure and Physical-organic Considerations

The fourth structural design, **4-5oH** differs from the classic DAE and resembles terarylenes. The bridge is exchanged for a five-membered aromatic heterocycle, in this case thiazole. The purpose of this substitution is a further improvement of the stability of the closed isomer in water and the shift of the previously observed pK$_a$ shift to the desired pK$_a$ window, around pH = 7.4. The light absorbing unit is attached to the bridge, while the thienyl moiety is substituted with a chlorine, usable for post-functionalizations. The linear conjugation in the open isomer **4-5oH** between the acidic *NH* and the bridge may be used to modulate the pK$_a$ further. Structure **4-6oH** is the regioisomer of **4-5oH**. In the open isomer, the acidic nitrogen is not linearly conjugated to the bridge, prohibiting the tuning of the acidity *via* substitution of the latter.

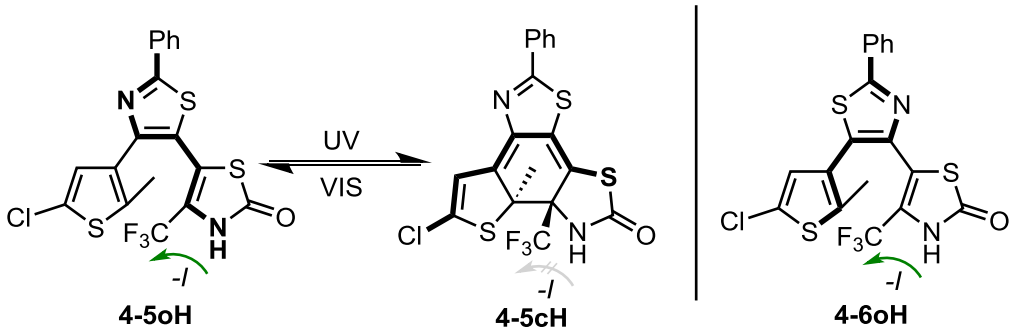

Figure 4-25 Target structures of the fourth generation and its photoreaction; green arrow: desired interaction, gray arrow: no or negligible interaction.

4.4.4.2 Synthesis

The aim in the synthesis of target molecule **4-5oH** and **4-6oH** was the direct functionalization of the thiazolone, without protecting groups or the use of precursor structures. Therefore, the first approach was the connection of the aryl moieties *via* the *α*-hydroxyketone **4-18** and **4-19**, followed by the build-up of the heteroaromatic bridge. Electrophilic substitution in 4 position of the thiazolones were reported, as it is discussed in chapter 4.3.3.

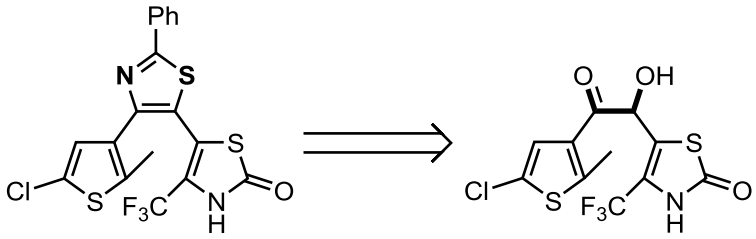

4-5oH **4-18**

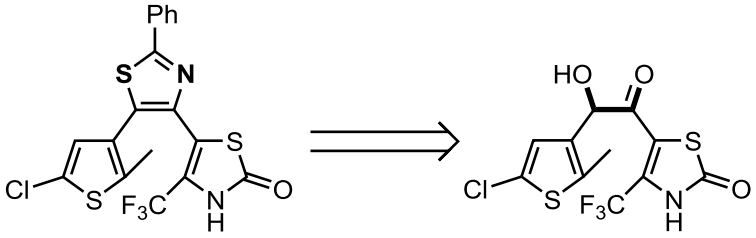

4-6oH **4-19**

The glyoxal **4-20** was synthesized *via* dehydration reaction, starting from the literature known dihydroxyketone **4-7**, which was already used in the previous synthesis. The direct electrophilic addition of **4-17** at **4-20** under Friedel-Crafts conditions as well as an *umpolung* by lithiation lead to either no reaction or decomposition (Figure 4-26a). The classic construction of *α*-hydroxyketone *via* Corry-Seebach reaction or benzoin condensation was attempted as well, without success (Figure 4-26b). The required aldehydes **4-22** and **4-24** were achieved *via* a Bouveault aldehyde synthesis, starting from **4-21** and **4-17**. The synthesis of the thioacetals **4-25** was successful, while its counterpart **4-23** could not be isolated. Lewis-acidic conditions did not furnish the desired product, instead desilylation of **4-22** was observed in the UPLC. The *umpolung* by lithiation leads to decomposition of thiazolone **4-25**. Different benzoin condensation and Stetter reaction conditions were screened (Figure 4-26c), but either no conversion of starting materials **4-22** and **4-24** was observed, or an undefined decomposition occurred. The synthesis of the glyoxal group at the thiazolone **4-26** was approached *via* acetylation of **4-17** (Figure 4-26d), but neither a Friedel-Crafts reaction nor the reaction of the lithiated species of **4-17** with dimethylacrylamide gave the desired product **4-25**. Also, the direct preparation of **4-25** *via* a bromination followed by a Hantzsch thiazole syntheses, starting with 1,1,1-trifluoroacetylacetate **4-27** was not successful. A

mixture of different products was isolated, presumably caused through multiple bromine substitutions.

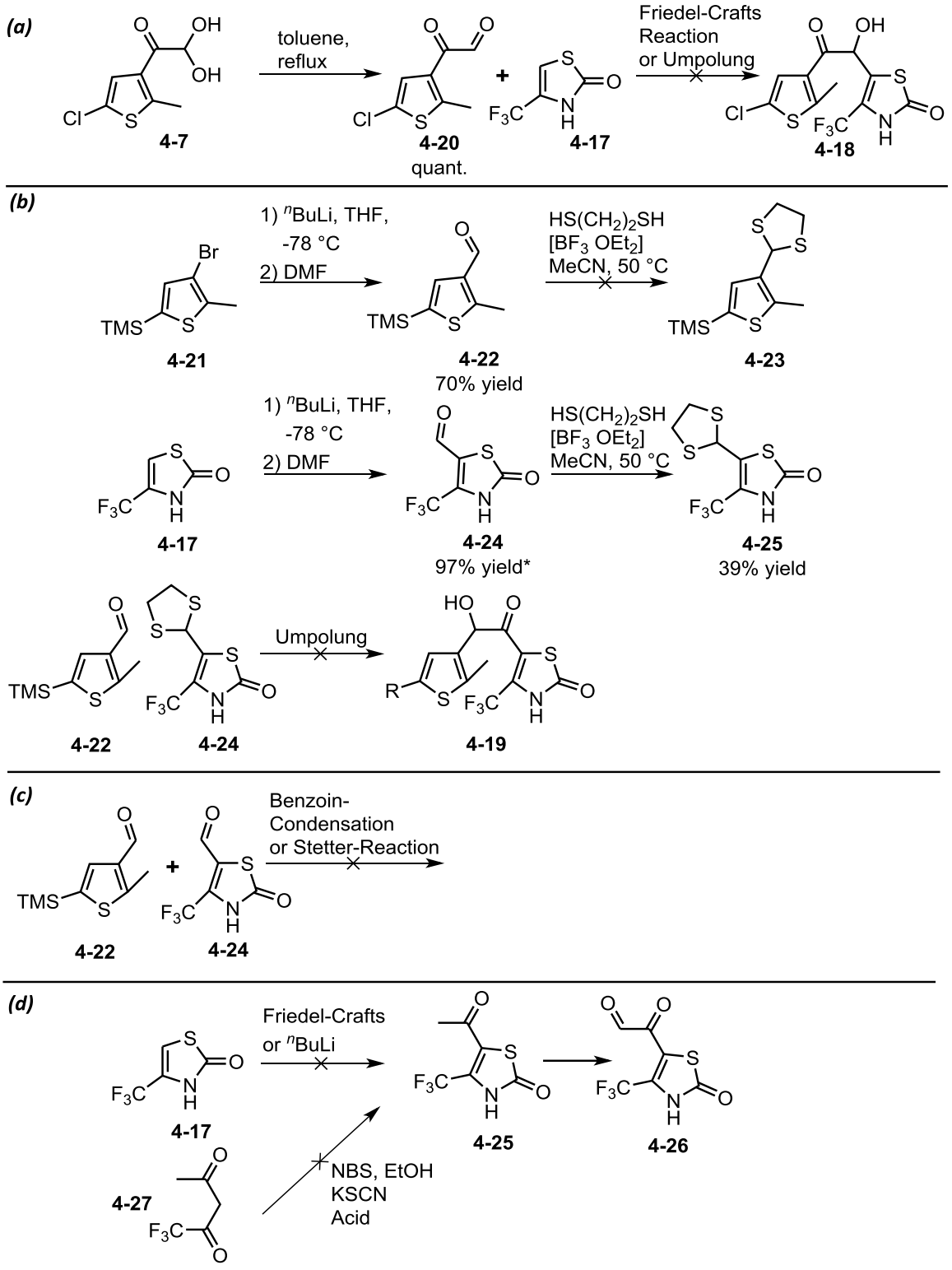

Figure 4-26 Attempted synthesis of the fourth generation of pK_a switches via diaryl-α-hydroxyketones; ***(a)*** *using glyoxal* ***4-20*** *as key intermediate;* ***(b)*** *using Corey-Seebach reaction; (c) using Benzoin condensations and Stetter reaction conditions;* ***(d)*** *using glyoxal* ***4-25*** *as key intermediate.*

In second strategy target molecule **4-5oH** was approached *via* linear synthesis, building the hexatriene backbone first (Figure 4-27). For this approach the glyoxal **4-20** was connected to 1,1,1-trifluoroacetone *via* a Knoevenagel condensation to give **4-28**. The heterocyclic DAE bridge was established by a Michael addition of benzothioamide **4-29** at **4-28**, followed by a condensation to give **4-30**. The 1,4-addition is directed by the strong electron withdrawing effect of the trifluoroacetyl group. The identity of **4-30** was proven by ^{19}F-^{13}C coupling, where the signal of the carbonyl carbon was observed as a quadruplet with a coupling constant of 35.9 Hz, similar to the pattern of compound **4-28**. This implies that the carbonyl carbon is still connected to the trifluoromethyl group. Compound **4-30** was treated with bromine in methylene dichloride, which results in bromine pattern in the mass spectrum of the crude intermediate **4-32**. Nevertheless, the desired product **4-30** were isolated, due to hydrolyzation during aqueous work up, giving presumably **4-34**. An *in-situ* treatment with potassium thiocyanate under anhydrous conditions followed by heating under aqueous acid conditions was not successful and results in the same hydrolyzed product **4-34**, according to the UPLC. Because the targeted compound was difficult to access, changes in the design are possible. The oxazolone would fulfill the concept as well and should be considered in future approaches.

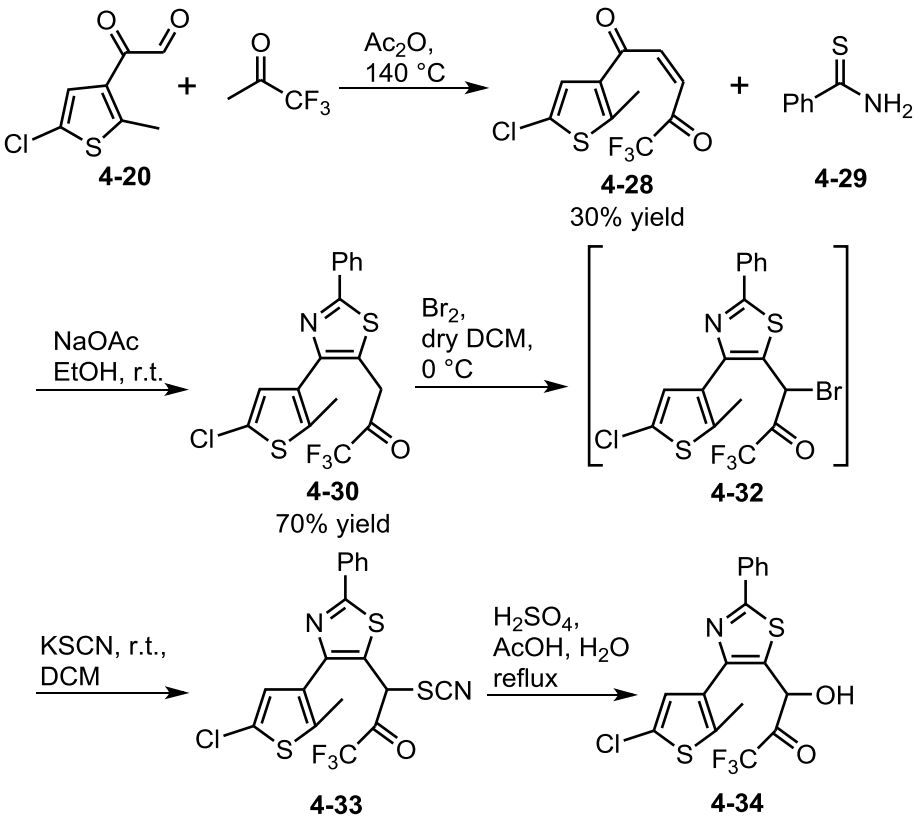

Figure 4-27 Preparative approached towards the fourth generation via a linear synthesis route avoiding cross-coupling.

To rapidly attain compounds, cross-coupling reaction conditions were tested as well (Figure 4-28). The iodide **4-35** was synthesized *via* lithiation of **4-12**. Chloro-methylthiophene **4-36** was substituted with a chloroacetyl group, giving **4-37** as a mixture of regioisomers in a ratio of approximately one to one. The isomers were not separated, and the mixture was used for further reactions. The bridging thiazole **4-38** was synthesized *via* the previously described Hantzsch's thiazole synthesis and borylated *via* lithiation with lithium diisopropylamine (LDA). To evaluate reaction conditions and the general feasibility for direct coupling of thiazolones, test reactions with different phenyl species were conducted and analyzed by TLC and UPLC (more details see chapter 5.1.3.19). Different catalysts, bases and solvents were tested and the most promising were applied on the coupling of **4-35** with **4-39**, without success.

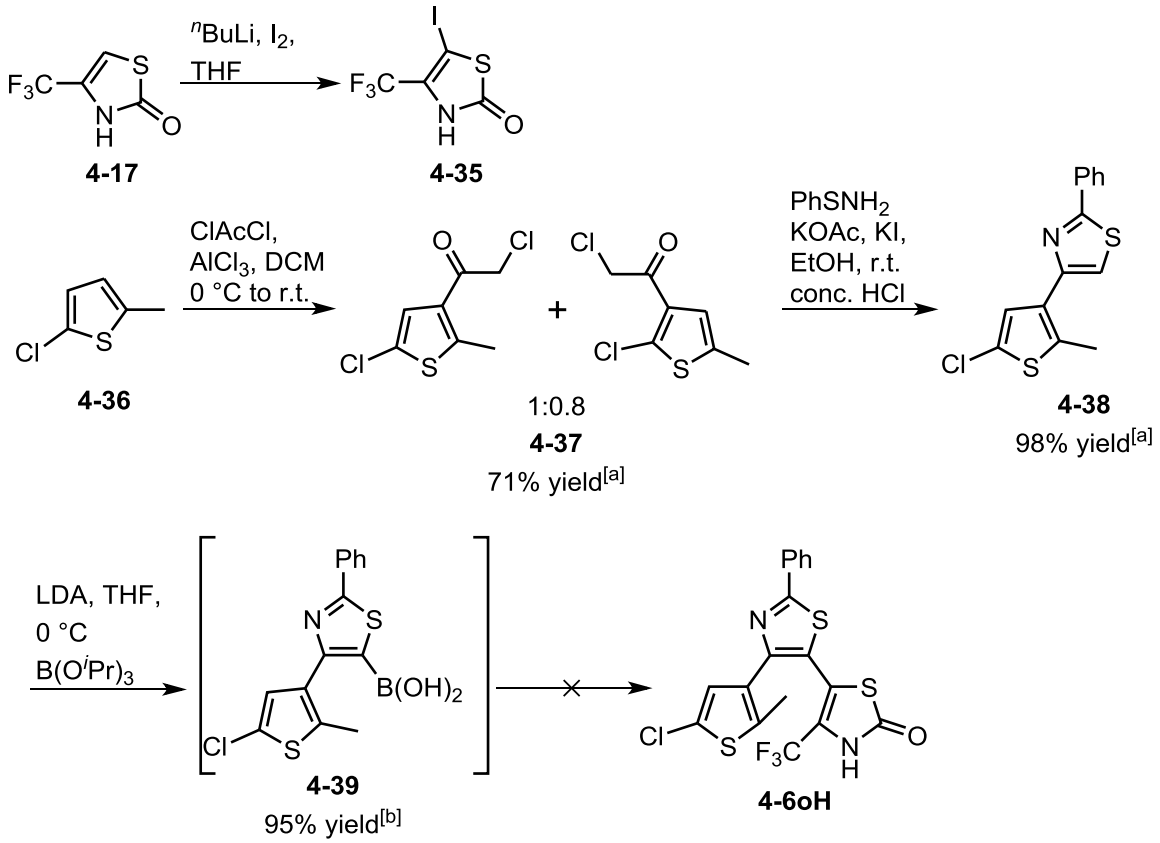

Figure 4-28 Preparative approached towards the fourth generation via cross-coupling.

No synthetic approach was found leading to target compound **4-5oH** or **4-5oH**. However, a novel direct coupling condition for unprotected thiazolone was successfully established.

4.5 Conclusion and Outlook

By incorporating a trifluoromethyl-thiazolone into DAE photoswitch, as presented for compound **4-4oH** a potent light-induced pK_a modulation was achieved with a change of 2.8 ± 0.2 units, from an acidic pK_a to a neutral. Most importantly, no thermal interconversion between the

two thermal equilibria was observed. A significant change of the photochemical performance between the protonated and deprotonated forms was observed. Compound **4-4oH** is a good example how a photochemical and a thermal reaction can influence each other. The photoreaction separates two dissociation equilibria, which leads to the observed pK_a change, while the pH determines the ratio of the acids and their corresponding bases. The introduced system shows a change of the excited-state energy hypersurface induced by the deprotonation. The way how this affects the performance of the photoreaction, in particular for the deprotonated cyclization, is not clear. The energetics of the four-state reaction cycle was investigated and used to enhance the photocyclization reaction by applying pH as a catalytic trigger. As a result, complete photoconversion for both cyclization and cycloreversion was achieved and the intrinsic photochemical performance parameters, e.g. absorption and quantum yield, were gated, to gain the worst or best possible photoconversion. Nevertheless, a slow, pH dependent, thermal side reaction still limits the system to non-aqueous application. It is important to point out, that this side reaction does not occur in other nucleophilic solvents, e.g. ethanol. Even though, a significant pK_a was achieved, the aimed pH-window remains out of reach.

Compound **4-5oH** is a good candidate to achieve this goal. It is a pleasure for me to report at this point, that while writing this thesis, compound **4-5oH** could successfully be synthesized by Florian Römpp. The ${}^{S}_{S}pK_a$ change lies with 2.5 units in the same dimension as **4-4oH** and most importantly the pK_a window extends from 5.2 in the open form to 7.7 in the closed isomer. No thermal side reaction was observed so far. This opens the initially mentioned possibilities to apply pK_a switches in life science, biology and material science as well as in catalysis (Figure 4-29).

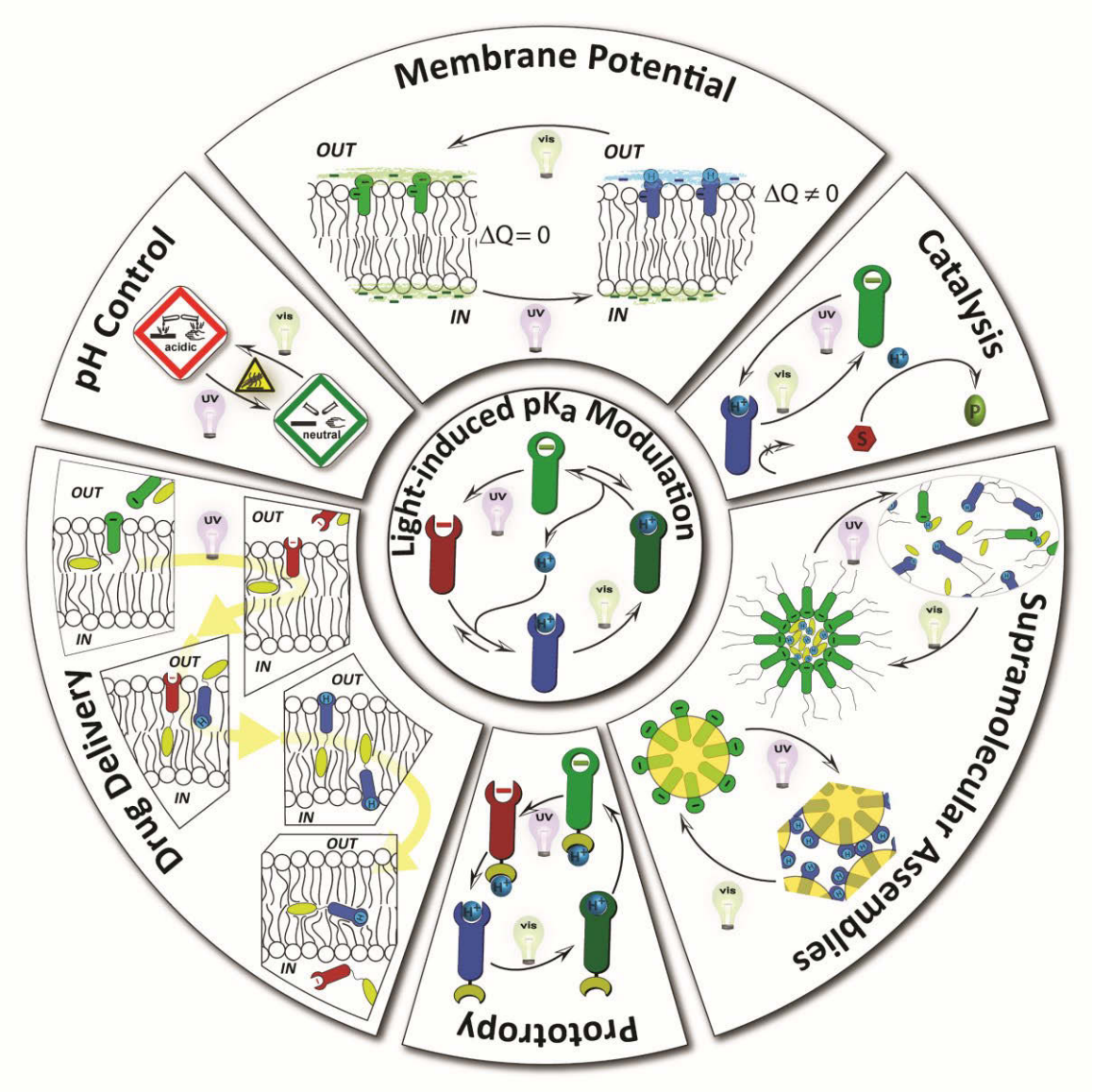

Figure 4-29 Outlook: Concepts towards the application of pK_a photoswitches.

5 EXPERIMENTAL PART

5.1 SYNTHESES

5.1.1 Materials, Analytic and Preparative Instrumentation

Chemicals and solvents were purchased from ABCR, Alfa-Aesar, Sigma-Aldrich, Fisher Scientific as well as TCI and used as received, including **4-8**, **4-10, 4-14**, **4-15**, **4-27, 4-36**. Bulk chemicals were purchased from Grüssing. Celite®545 (treated with sodium carbonate, flux-calcined) purchased from Sigma-Aldrich was used as filter aid.

Compounds **3-2**[64a], **3-3**[45], **3-6**[69], **4-7**[121], **4-11**[24] and **4-21**[122] have been synthesized according to literature procedures.

Solvents were dried using a Pure Solv Micro Solvent Purification System from Innovative Technologies. The water was deionized by a SG – LaboStar™ 1-UV Reinstwassersystem. Weighing of small quantities was performed on a Sartorius ME5 analytical microbalance. TLC plates are coated with SiO_2-60 UV_{254} and were purchased from Merck. Flash chromatography was performed by a Teledyne ISCO Combi Flash Rf 300 system. Recycling gel permeation chromatography (GPC) was performed with a JAI LC-9210NEXT using dichloromethane as the eluent. HPLC was performed on a Waters 600 connected to a Waters 996 Diode Array Detector and a Waters Fraction Collector III equipped with a Luna Phenyl-Hexyl column (250 x 21 mm, 10 μm particle size). The solvents were of HPLC grade and degassed with helium prior to use.

NMR spectra were recorded on a Bruker Avance II 300 (300.13 MHz for ^{1}H and 75.47 MHz for ^{13}C) and a Bruker Avance II 500 (500.13 MHz for ^{1}H and 125.76 MHz for ^{13}C) at room temperature. Spectra were referenced to the residual solvent signal. Deuterated solvents were purchased from EurisoTOP and used without further purification. Multiplicities are abbreviated as follows: singlet (s), doublet (d), triplet (t), doublet of doublets (dd), quintet (q) and multiplet (m). Coupling constants (J) are given in Hz. Chemical shifts (δ) are given in ppm.

Ultraperformance liquid chromatography coupled to mass spectrometry detection (UPLC-TOF) was performed with a Waters Alliance system (gradient mixture of acetonitrile/water) equipped with Acquity UPLC column chromatographys. The Waters system consisted of a Waters Separations Module 2695, a Waters Diode Array Detector 996, a LCT Premier XE mass spectrometer, and a Waters Mass Detector ZQ 2000.

5.1.2 Acid-catalyzed Cycloreversion

5.1.2.1 Synthesis of Target Molecule 3-1o

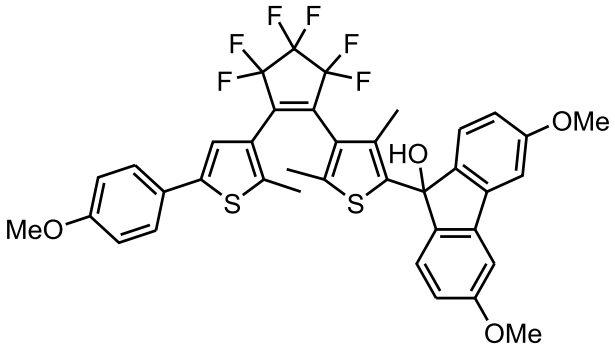

In a dried 10 mL Schlenk tube **3-5** (85 mg, 0.15 mmol, 1 eq.) was dissolved in 1.5 mL of dry THF under argon and cooled to -78 °C. First, 0.09 mL of n-butyl lithium (2.3 M solution in cyclohexane, 0.2 mmol, 1.3 eq.) was added and the reaction mixture stirred for 2 h at -78 °C. Compound **3-6** (60 mg, 0.15 mmol, 1 eq.) was added slowly at -78 °C to the previously prepared reaction mixture and allowed to warm to room temperature and stirred for 12 h. The reaction was quenched with a 1 M sodium hydroxide solution, extracted three times with diethyl ether and washed with water and brine. The organic phase was dried over magnesium sulfate and filtered. The solvent was removed under reduced pressure and the crude product was purified by column chromatography (methylene chloride: petroleum ether), followed by a recycling gel permeation chromatography. Compound **3-1o** (44 mg, 0.060 mmol, 40% yield) was isolated as a white solid. ^{1}H NMR (500 MHz, chloroform-*d*) δ = 7.39 – 7.35 (m, 2H), 7.26 (d, *J* = 8.3 Hz, 1H), 7.11 (d,^{2}*J* = 2.4 Hz, 1H), 7.08 (d, *J* = 2.3 Hz, 1H), 7.00 (d, *J* = 8.3 Hz, 1H), 6.93 – 6.89 (m, 2H), 6.86 (s, 1H), 6.79 (dd, *J* = 8.3, 2.3 Hz, 1H), 6.62 (dd, *J* = 8.3, 2.3 Hz, 1H), 3.84 (s, 3H), 3.83 (s, 3H), 3.76 (s, 3H), 2.65 (s, 1H), 2.27 (d, *J* = 1.5 Hz, 3H), 1.96 (s, 3H), 0.98 (d, *J* = 1.5 Hz, 3H). ^{13}C NMR (126 MHz, chloroform-*d*) δ = 161.7, 161.5, 160.1, 141.9, 141.3, 140.1, 137.3, 131.0, 128.9, 127.6, 127.4, 126.6, 125.8, 125.5, 122.1, 114.8, 114.6, 106.2, 106.1, 81.4, 56.1, 56.0, 55.9, 14.7, 13.0, 12.9. ^{19}F NMR (471 MHz, chloroform-*d*) δ = -109.89 (d, *J* = 262.4 Hz, 1F), -110.85 (d, *J* = 265.2 Hz, 2F), -111.50 (d, *J* = 262.2 Hz, 1F), -112.00 (d, *J* = 263.4 Hz, 2F), -133.76 (s, 2F). UPLC-TOF-ES^{+}: m/z = 711.145 [M-H_2O] (calc.: 711.146 for [$C_{38}H_{29}F_6O_3S_2$]$^{+}$)

5.1.2.2 Synthesis of compound 3-4

The synthesis was conducted similar to reported protocols.[123]

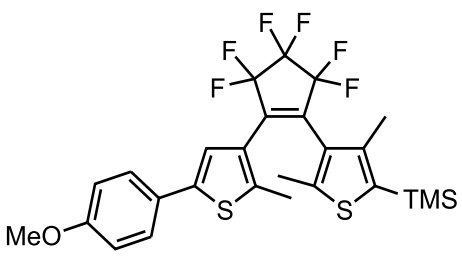

In a dried 60 mL Schlenk tube **3-3** (0.84 g, 4 mmol, 1 eq.) was dissolved in 20 mL of dry tetrahydrofuran (THF) under argon and cooled to -78 °C. 2 mL of n-butyl lithium (2.3 M solution in cyclohexane, 4.4 mmol, 1.1 eq.) was added slowly and the reaction mixture was stirred for 1 h at -78 °C. Then, compound **3-2** (1.11 g, 2.8 mmol, 0.7 eq.) was dissolved in 5 mL of dry THF and added slowly. The reaction mixture was allowed to warm to room temperature and stirred for 12 h. The reaction was quenched with a solution of saturated aqueous ammonium chloride, extracted three times with ethyl acetate and washed with water, and brine. The organic phase was dried over magnesium sulfate and filtered. The solvent was removed under reduced pressure and the crude product was purified by column chromatography (methylene chloride: petroleum ether). Compound **3-4** (1.00 g, 1.79 mmol, 64% yield) was isolated as a white solid. ^{1}H NMR (500 MHz, chloroform-*d*) δ = 7.40 – 7.36 (m, 2H), 6.95 (s, 1H), 6.91 – 6.87 (m, 2H), 3.81 (s, 3H), 2.23 (d, *J* = 1.1 Hz, 3H), 2.11 (s, 3H), 2.10 (d, *J* = 1.8 Hz, 3H), 0.30 (s, 9H). ^{13}C NMR (126 MHz, chloroform-*d*) δ = 160.1, 145.2, 143.7, 142.0, 141.4, 132.9, 128.9, 128.8, 127.3, 126.6, 125.6, 122.3, 114.9, 55.9, 16.5, 16.4, 14.8, 0.0. ^{19}F NMR (471 MHz, chloroform-*d*) δ = -109.81 (dd, J = 263.40, 10.52 Hz, 1F),-109.89 (dd, J = 262.44, 8.36 Hz, 1F), -111.94 (dd, J = 262.56, 8.46 Hz, 1F), -112.17 (dd, J = 263.22, 10.09 Hz, 1F) -133.12 (dt, *J* = 240.01, 10.05 Hz, 1F), -134.32 (dt, *J* = 239.89, 9.91 Hz, 1F). UPLC-TOF-ES+: m/z = 561.114 [M+H] (calc.: 561.117 $[C_{26}H_{27}F_6OS_2Si]^+$)

5.1.2.3 Synthesis of compound 3-5[124]

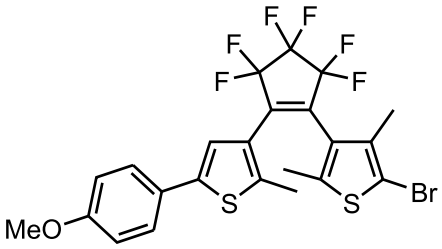

Compound **3-4** (1.00 g, 1.79 mmol, 1 eq.) was dissolved in 15 mL of THF and cooled to 0 °C, after which *N*-bromosuccinimide (0.38 g, 2.15 mmol, 1.2 eq.) was added. The reaction mixture was stirred for 3 h at 0 °C and quenched afterwards with water, extracted with diethyl ether and washed with water, and brine. The organic phase was dried over magnesium sulfate and filtered. The solvent was removed under reduced pressure and the crude product was purified by recrystallization from ethanol to give compound **3-5** (1.01 g, 1.78 mmol, 99% yield) as a white solid. ^{1}H NMR (500 MHz, chloroform-*d*) δ = 7.43 – 7.38 (m, 2H), 6.99 (s, 1H), 6.93 – 6.89 (m, 2H), 3.83 (s, 3H), 2.21 (d, *J* = 1.2 Hz, 3H), 2.11 (s, 3H), 1.95 (d, *J* = 1.6 Hz, 3H). ^{13}C NMR (126 MHz, chloroform-*d*) δ = 159.7, 142.1, 140.7, 140.4, 136.2, 127.1, 126.2, 125.8, 124.9, 121.5, 114.5, 107.4, 55.5, 14.9, 14.7, 14.6. ^{19}F NMR (471 MHz, Chloroform-*d*) δ -110.04 (d, *J* = 263.8 Hz, 1F), -110.96 (s, 2F), -111.00 (d, *J* = 263.7 Hz, 1F), -133.27 (p, *J* = 5.5 Hz, 2F).

UPLC-TOF-ES+: m/z = 566,985 [M+H] (calc.: 566.988 $[C_{23}H_{18}BrF_6OS_2]^+$)

5.1.3 Light-induced pK_a Modulation

5.1.3.1 Synthesis of target molecule 4-1oH[5]

The synthesis was conducted similar to reported protocols.[99b]

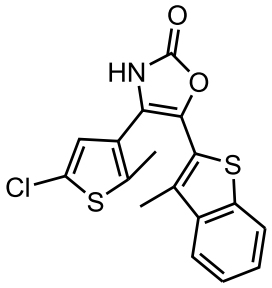

Compound **4-9** (1.011 g, 3.00 mmol, 1 eq.) and urethane (0.67 g, 7.50 mmol, 2.5 eq.) were degassed in a sealed pressure tube by several cycles of evacuation and backfilling with Argon and dissolved in 5 mL pyridine. The reaction mixture was heated to 150 °C for 18 h. The mixture was allowed to cool to room temperature and was suspended in petroleum ether: diethyl ether, filtered and the precipitate was washed with petroleum ether. The crude product was purified by column chromatography (methylene chloride: methyl alcohol: triethylamine). Compound **4-1** (0.31 g, 0.83 mmol, 28% yield) was isolated as a mixture of two isomers.

Isomer-1: ^{1}H NMR (500 MHz, chloroform-*d*) δ = 9.9 (s, 1H), 7.8 (dd, *J*=6.93, 1.51, 1H), 7.7 (dd, *J*=6.98, 1.58, 1H), 7.4 (pd, *J*=7.12, 1.34, 2H), 6.8 (s, 1H), 2.3 – 2.3 (m, 6H), 2.2 (s, 3H). ^{13}C NMR (126 MHz, Chloroform-*d*) δ = 156.2, 139.9, 139.7, 139.0, 132.4, 132.0, 127.9, 126.1, 125.6, 124.6, 123.0, 123.0, 122.6, 122.5, 118.8, 14.3, 13.1.

^{1}H NMR (500 MHz, Methylene Chloride-d_2) δ = 9.17 (s, 1H), 7.79 – 7.77 (m, 1H), 7.72 – 7.69 (m, 1H), 7.42 – 7.35 (m, 2H), 6.83 (s, 1H), 2.23 (s, 3H), 2.12 (s, 3H).

Isomer-2**:** ^{1}H NMR (500 MHz, Methylene Chloride-d_2) δ = 7.86 – 7.83 (m, 1H), 7.76 – 7.73 (m, 1H), 7.47 – 7.41 (m, 2H), 6.72 (s, 1H), 2.21 (s, 3H), 2.20 (s, 3H).

UPLC-TOF-ESI$^-$-MS m/z: 359.994 [M-H] (calc.: 359.993 $[C_{17}H_{11}ClNO_2S_2]^-$).

5.1.3.2 Synthesis of Target Molecule 4-2o

The synthesis was conducted similar to reported protocols.[123]

[5] Conducted by Jutta Schwarz

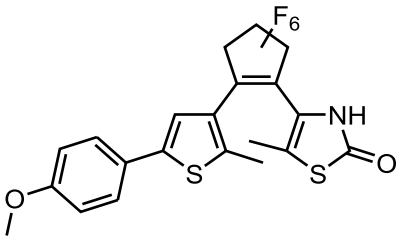

In a dried 20 mL Schlenk tube thiazolone **4-16** (0.58 g, 3.00 mmol, 1 eq.) was dissolved in 10 mL of dry tetrahydrofuran under argon. First, sodium hydride (0.132 g, 3.3 mmol, 1.1 eq.) was added and the reaction mixture was stirred until the gas formation stopped. Afterwards, the mixture was cooled to -78 °C and 1.67 mL of n-butyl lithium (2.3 M solution in cyclohexane, 3.9 mmol, 1.3 eq.) was added slowly. The reaction mixture was stirred for 1 h at -78 °C. Compound **3-2** (1.07 g, 2.70 mmol, 0.9 eq.) in 2 mL of dry tetrahydrofuran was added to the previously prepared reaction mixture and stirred for 10 min at -78°C and afterwards 18 h at room temperature. The reaction was quenched with a 1 M hydrochloric acid, extracted three times with ethyl acetate and washed with an aqueous hydrochloric acid-sodium chloride solution. The organic phase was dried over magnesium sulfate and filtered. The solvent was removed under reduced pressure and the crude product was purified by column chromatography (cyclohexane: ethyl acetate), followed by a recycling gel permeation chromatography. Compound **4-2o** (0.52 g, 1.06 mmol, 35% yield) was isolated as a white solid.

^{1}H NMR (500 MHz, chloroform-*d*) δ = 8.84 (s, 1H), 7.46 (d, *J* = 8.86 Hz, 2H), 7.13 (s, 1H), 6.92 (d, *J* = 8.86 Hz, 2H), 3.83 (s, 3H), 2.18 (s, 3H), 1.75 (s, 3H). ^{13}C NMR (126 MHz, chloroform-*d*) δ = 171.7, 171.4, 159.9, 143.2, 141.6, 127.2, 125.8, 124.9, 122.1, 120.9, 117.2, 114.6, 55.5, 14.7, 13.6. ^{19}F NMR (471 MHz, methylene Chloride-d_2) δ = -109.0, -110.6, -132.2. UPLC-TOF-ESI$^-$-MS m/z: 490.040 (calc.: 490.038).

The byproduct **4-13** (0.26 g, 0.53 mmol, 18% yield) could be isolated from the reaction mixture as well.

^{1}H NMR (500 MHz, chloroform-*d*) δ = 7.47 (d, *J*=8.7, 2H), 7.13 (s, 1H), 6.90 (d, *J*=8.7, 2H), 6.38 (d, *J*=1.8, 1H), 3.83 (s, 3H), 2.19 (s, 3H), 2.17 (d, *J*=1.5, 3H). ^{19}F NMR (471 MHz, chloroform-*d*) δ = -109.78, -111.61, -131.42.

5.1.3.3 Synthesis of target molecule 4-3o

The synthesis was conducted similar to reported protocols.[123]

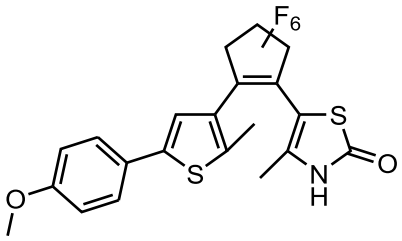

In a dried 10 mL Schlenk tube thiazolone **4-17** (0.127 g, 0.75 mmol, 1 eq.) was dissolved in 7 mL of dry tetrahydrofuran under argon and cooled to -78 °C. First 0.82 mL of n-butyl lithium (2.3 M solution in cyclohexane, 1.88 mmol, 2.5 eq.) was added slowly at -78 °C and the reaction mixture stirred for 30 min at 0 °C. Compound **3-2** (0.298 g, 0.75 mmol, 1 eq.) in 3 mL of dry tetrahydrofuran was added to the previously prepared reaction mixture and stirred for 3 h at 0 °C. The reaction was quenched with a 1 M hydrochloric acid solution, extracted three times with ethyl acetate and washed with a solution of aqueous hydrochloric acid & sodium chloride. The organic phase was dried over magnesium sulfate and filtered. The solvent was removed under reduced pressure and the crude product was purified by column chromatography (cyclohexane: ethyl acetate: acetic acid), followed by a recycling gel permeation chromatography. Compound **4-3o** (0.15 g, 0.28 mmol, 37% yield) was isolated as a white solid. ^{1}H NMR (500 MHz, chloroform-*d*) δ = 10.41 (s, 1H), 7.43 (d, *J* = 8.75 Hz, 2H), 6.95 (s, 1H), 6.91 (d, *J* = 8.74 Hz, 2H), 3.84 (s, 3H), 2.32 (s, 3H). ^{13}C NMR (126 MHz, chloroform-*d*) δ= 171.4, 159.8, 143.0, 141.2, 127.2, 125.9, 123.5, 121.7, 119.1, 114.6, 108.9, 55.5, 14.9. ^{19}F NMR (471 MHz, chloroform-*d*) δ = -63.1, -110.8, -111.8, -132.3. UPLC-TOF-ESI^{-}-MS m/z: 544.007 (calc.: 544.009).

5.1.3.4 Synthesis of target molecule 4-4oH

The synthesis was conducted similar to reported protocols.[123]

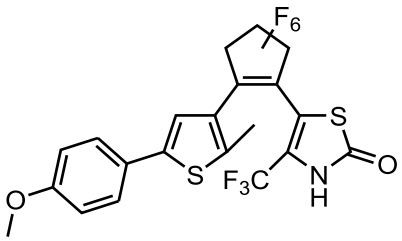

In a dried 20 mL Schlenk tube thiazolone **4-13** (0.05 g, 0.45 mmol, 1 eq.) was dissolved in 4 mL of dry tetrahydrofuran under argon and cooled to -78 °C. First 0.49 mL of n-butyl lithium (2.3 M solution in cyclohexane, 1.25 mmol, 2.5 eq.) was added slowly at -78 °C and the reaction mixture stirred for 30 min at 0 °C. Compound **3-2** (0.298 g, 0.75 mmol, 1 eq.) in 0.8 mL of dry tetrahydrofuran was added to the previously prepared reaction mixture and stirred for 3 h at 0°C. The reaction was quenched with a 1 M hydrochloric acid solution, extracted three times with ethyl

acetate and washed with an aqueous hydrochloric acid & sodium chloride solution. The organic phase was dried over magnesium sulfate and filtered. The solvent was removed under reduced pressure and the crude product was purified by column chromatography (cyclohexane: ethyl acetate: acidic acid), followed by a recycling gel permeation chromatography. Compound **4-4oH** (0.122 g, 0.25 mmol, 55% yield) was isolated as a white solid.

^{1}H NMR (500 MHz, chloroform-*d*) δ = 10.52 (s, 1H), 7.46 (d, *J* = 8.84 Hz, 2H), 7.05 (s, 1H), 6.92 (d, *J* = 8.75 Hz, 2H), 3.84 (s, 3H), 2.21 (s, 3H), 1.90 (s, 3H). ^{13}C NMR (126 MHz, chloroform-*d*) δ = 174.4, 159.7, 143.0, 140.9, 135.2, 127.1, 126.1, 125.0, 121.4, 114.5, 101.7, 55.5, 14.7, 14.0. ^{19}F NMR (471 MHz, chloroform-*d*) δ = -108.9, -110.3, -131.8. UPLC-TOF-ESI$^-$-MS m/z: 490.034 (calc.: 490.038).

5.1.3.5 Synthesis of compound 4-9[6]

The synthesis was conducted similar to reported protocols.[121]

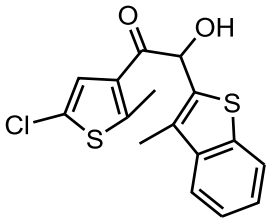

Glyoxal **4-20** (2.07 g, 10.0 mmol, 1 eq.) was dissolved in 37 mL dry benzene under argon. 3-Methylbenzothiophene **4-8** (1.39 mL, 10.6 mmol, 1.06 eq.) was added and cooled to 0°C. Tin tetrachloride (1.17 mL, 10.0 mmol, 1.0 eq.) was added dropwise at 0 °C, the reaction mixture was stirred at room temperature for 5 hours, poured into ice cooled water and extracted three times with ethyl acetate. The combined organic phases were washed with water, saturated aqueous sodium bicarbonate solution, and brine, dried over magnesium sulfate and filtered. The solvent was removed under reduced pressure and the crude product was suspended in petroleum ether and filtered. Compound **4-9** (2.40 g, 7.12 mmol, 71% yield) was used without further purification for the next step.

UPLC-TOF-ESI$^-$-MS m/z: 334.997 [M-H] (calc.: 334.997 [$C_{16}H_{12}ClO_2S_2$]$^-$).

5.1.3.6 Compound 4-12

The synthesis was conducted similar to reported protocols.[125]

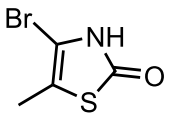

[6] Conducted by Jutta Schwarz

2,3-Dibromo-5-methylthiazol **4-11** (3.82 g, 15 mmol, 1 eq.) and fresh powdered sodium hydroxide (3.75 g, 45 mmol, 3 eq.) were dissolved in 15 mL tert-butyl alcohol and refluxed for 18 h. The reaction was quenched by addition of 30 mL of a 1 M aqueous hydrochloric acid solution. The aqueous phase was extracted three times with ethyl acetate. The combined organic phases were washed with brine and dried over magnesium sulfate. The solvent was removed under reduced pressure and the crude product was purified by column chromatography (cyclohexane: ethyl acetate). Compound **4-12** (2.34 g, 12.06 mmol, 80% yield) was isolated as a white powder. ^{1}H NMR (500 MHz, chloroform-*d*) δ = 10.37 (s, 1H), 2.10 (s, 3H). ^{13}C NMR (126 MHz, Chloroform-*d*) δ = 173.6, 112.5, 97.6, 13.6. UPLC-TOF-ESI^{-}-MS m/z: 193.928 [M+H] (calc.: 193.927 [$C_4H_3BrNOS]^+$).

5.1.3.7 Synthesis of compound 4-16

The synthesis was conducted similar to reported protocols.[126]

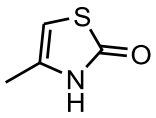

3-Chloroacetone **4-14** (16.01 mL, 200.0 mmol, 1 eq.) was added to a suspension of potassium thiocyanate (23.32 g, 240 mmol, 1.2 eq.) and potassium iodide (1.99 g, 12 mmol, 0.06 eq.) in 200 mL ethanol, and the mixture was stirred at room temperature for 60 h. The precipitate was filtered off, washed with ethanol, and the filtrate was evaporated to remove all ethanol. MTBE was added and the white precipitate was filtered off using celite. This procedure of concentration, precipitation with MTBE and filtration over celite was repeated three times in total. After the evaporation of MTBE the crude intermediate product (20.90 g, 181.5 mmol, 91% yield) isolated as brownish liquid. The thiocyanato-propane-2-one (5.07 g, 44.0 mmol, 1 eq.) was dissolved without further purification in 100 mL water, and 2.5 mL concentrated aqueous hydrochloric acid was added. The mixture was stirred for 3h at 90 °C. The reaction mixture was allowed to cool to room temperature. It was extracted six times with methylene chloride. The combined organic phases were dried over magnesium sulfate. The solvent was removed under reduced pressure and the crude product was purified by column chromatography (methylene chloride: ethyl acetate). Compound **4-16** (0.47 g, 4.08 mmol, 9% yield) was isolated as a white solid. ^{1}H NMR (500 MHz, chloroform-*d*) δ = 10.64 (s, 1H), 5.67 (p, *J*=1.34, 1H), 2.09 (d, *J*=1.32, 3H). ^{13}C NMR (126 MHz, chloroform-*d*) δ = 176.8, 131.2, 97.6, 14.5. UPLC-TOF-ESI^{+}-MS m/z: 116.017 [M-H] (calc.: 116.016 [$C_4H_4NOS]^-$).

5.1.3.8 Synthesis of compound 4-17

The synthesis was conducted similar to reported protocols.[127]

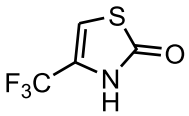

3-Bromo-1,1,1-trifluoroacetone **4-15** (3.22 mL, 31.0 mmol, 1 eq.) was added to a suspension of potassium thiocyanate (12.05 g, 124.0 mmol, 4 eq.) in 120 mL acetone, and the mixture was stirred at room temperature for 30 min. After filtration over celite, the mixture was concentrated in vacuo, and MTBE was added. The white precipitate was filtered off using celite. This procedure of concentration, precipitation with MTBE and filtration over celite was repeated three times in total. After evaporation of MTBE, the crude intermediate product was dissolved in 200 mL acetic acid, and 20 mL of a 50% sulfuric acid was added. The mixture was refluxed for 3 hours, quenched with ice-water and filtered. The acetic acid was removed under reduced pressure. The remaining aqueous phase was extracted three times with ethyl acetate. The combined organic phase was dried over magnesium sulfate. The solvent was removed under reduced pressure and the crude product was purified by column chromatography (methylene chloride: ethyl acetate). Compound **4-17** (2.18 g, 12.88 mmol, 42% yield) was isolated as a white solid. ^{1}H NMR (500 MHz, Chloroform-*d*) δ = 11.20 (s, 1H), 6.71 (q, *J*=1.44, 1H). ^{13}C NMR (126 MHz, chloroform-*d*) δ = 174.9(s), 123.7 (q, *J*=40.3), 118.3 (q, *J*=270.4), 107.2 (q, *J*=4.6). ^{19}F NMR (471 MHz, chloroform-*d*) δ = -65.4. UPLC-TOF-ESI^{+}-MS m/z: 169.987 [M-H] (calc.: 169.988 $[C_4HF_3NOS]^-$).

5.1.3.9 Synthesis of compound 4-20[7]

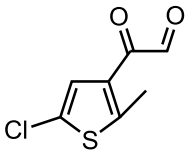

Thienylglyoxal monohydrate **4-7** was synthesized as reported and was converted to the glyoxal **4-20** by heating in toluene with a Dean-Stark trap.

^{1}H NMR (300 MHz, chloroform-*d*) δ = 9.46 (s, 1H), 7.67 (s, 1H), 2.74 (s, 3H). UPLC-TOF-ESI^{+}-MS m/z: 186.962 [M+H] (calc.: 186.963 $[C_7H_6ClO_2S]^+$).

5.1.3.10 Synthesis of compound 4-22

The synthesis was conducted similar to reported protocols.[128]

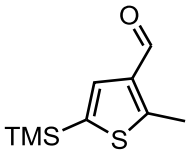

[7] Conducted by Jutta Schwarz

In a dried 100 mL Schlenk tube thiophene **4-21** (2.50 g, 10.03 mmol, 1 eq.) was dissolved in 50 mL of dry tetrahydrofuran under argon and cooled to -78 °C. First 4.80 mL of n-butyl lithium (2.3 M solution in cyclohexane, 11.03 mmol, 1.1 eq.) was added slowly at -78 °C and the reaction mixture stirred for 60 min. Dimethylformamide (0.854 mL, 11.03 mmol, 1.1 eq.) was added to the previously prepared reaction mixture, stirred for 15 min at -78 °C and was then allowed to warm to room temperature. The reaction was quenched with water, extracted three times with ethyl acetate and washed with brine. The organic phase was dried over magnesium sulfate and filtered. The solvent was removed under reduced pressure and the crude product was purified by column chromatography (petrol ether: ethyl acetate). Compound **4-22** (1.40 g, 7.06 mmol, 70% yield) was isolated. ^{1}H NMR (300 MHz, chloroform-*d*) δ = 10.03 (s, 1H), 7.50 (s, 1H), 2.78 (s, 3H), 0.30 (s, 9H).

GC-EI-QMS m/z: 198.2 [M+e$^-$] (calc.: 198.4 [$C_9H_{14}OSSi]^-$).

5.1.3.11 Synthesis of compound 4-24

The synthesis was conducted similar to reported protocols.[128]

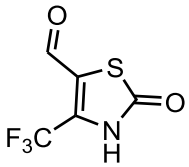

In a dried 60 mL Schlenk tube thiazolone **4-17** (1.02 g, 6.00 mmol, 1 eq.) was dissolved in 20 mL of dry tetrahydrofuran under argon and cooled to -78 °C. First 6.00 mL of n-butyl lithium (2.3 M solution in cyclohexane, 13.80 mmol, 2.3 eq.) was added slowly at -78 °C and the reaction mixture stirred for 30 min at 0 °C. Dimethylformamide (1,77 mL, 24.00 mmol, 4.0 eq.) was added to the previously prepared reaction mixture and stirred for 3 h at room temperature. The reaction was quenched with a 1 M hydrochloric acid solution, extracted three times with ethyl acetate and washed with an aqueous hydrochloric acid & sodium chloride solution. The organic phase was dried over magnesium sulfate and filtered. The solvent was removed under reduced pressure and the product was used without further purification. Compound **4-24** (1.18 g, 5.82 mmol, 97% yield) was isolated. ^{1}H NMR (500 MHz, chloroform-*d*) δ = 9.91 (s, 1H), 9.80 (s, 1H). ^{19}F NMR (471 MHz, chloroform-*d*) δ = -59.3. UPLC-TOF-ESI$^-$-MS m/z: 195.967 [M-H] (calc.: 195.969 [$C_5HF_3NO_2S]^-$).

5.1.3.12 Synthesis of compound 4-25

The synthesis was conducted similar to reported protocols.[129]

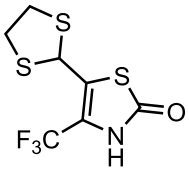

In a dried 60 mL Schlenk tube thiazolone **4-24** (1.18 g, 6.00 mmol, 1 eq.) and 1,2-ethandithiole (3.02 mL, 36.00 mmol, 6.0 eq.) was dissolved in 25 mL of dry acetonitrile under argon. Boron trifluoride diethyl ether complex (0.38 mL, 3.00 mmol, 0.5 eq.) was added and the reaction mixture stirred for 4 h at 50 °C. The reaction was quenched with water, extracted three times with ethyl acetate and washed with brine. The organic phase was dried over magnesium sulfate and filtered. The solvent was removed under reduced pressure at 25 °C and the product was precipitated from methylene chloride. The solid was washed with cold methylene chloride to give compound **4-25** (0.64 g, 2.34 mmol, 39% yield) was isolated.

^{1}H NMR (500 MHz, acetonitrile-d_3) δ = 9.52 (s, 1H), 5.91 (s, 1H), 3.49 – 3.31 (m, 5H). ^{13}C NMR (126 MHz, acetonitrile-d_3) δ = 169.6, 129.7 (q, *J*=3.35), 121.3, 47.3, 41.4. ^{19}F NMR (471 MHz, acetonitrile-d_3) δ = -59.9. UPLC-TOF-ESI$^-$-MS m/z: 271.948 [M-H] (calc.: 271.949 [$C_7H_5F_3NOS_3$]$^-$).

5.1.3.13 Synthesis of compound 4-28

The synthesis was conducted similar to reported protocols.[130]

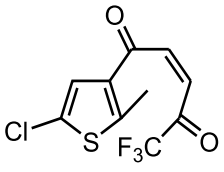

Glyoxal **4-20** (1.00 g, 5.30 mmol, 1 eq.) was dissolved in 20 mL acetic anhydride under argon, and cooled to 0 °C. 1,1,1-Trifluoroacetone (7.12 mL, 79.50 mmol, 15 eq.) was added, the reaction flask was sealed and stirred for 24 h at 140 °C. The reaction mixture was allowed to cool to room temperature and poured in to an ice cooled saturated aqueous sodium bicarbonate solution and MTBE. Under vigorous stirring, small portions of solid sodium bicarbonate were added until gas formation stopped. The phases were separated and the aqueous phase was extracted three times with MTBE. The combined organic phases were washed with saturated sodium carbonated solution, and brine, dried over magnesium sulfate and filtered. The solvent was removed under reduced pressure and the crude product was purified by column chromatography (cyclohexane: ethyl acetate). Compound **4-28** (0.41 g, 1.45 mmol, 27% yield) was isolated as a yellow solid. ^{1}H NMR (500 MHz, chloroform-*d*) δ = 7.78 (d, *J*=15.53, 1H), 7.32 (dq, *J*=15.52, 0.87, 1H), 7.22 (s, 1H), 2.72 (s, 3H). ^{13}C NMR (126 MHz, chloroform-*d*) δ = 182.4, 180.5 (q, *J*=37.5), 151.4, 141.6, 134.5, 129.0, 126.7, 126.5, 115.9 (q, *J*=289.9), 16.4. ^{19}F NMR (471 MHz, Chloroform-*d*) δ = -78.1. UPLC-TOF-ESI$^-$-MS m/z: 280.969 [M-H] (calc.: 280.966 [$C_{10}H_5ClF_3O_2S$]$^-$).

5.1.3.14 Synthesis of compound 4-30

The synthesis was conducted similar to reported protocols.[126, 130-131]

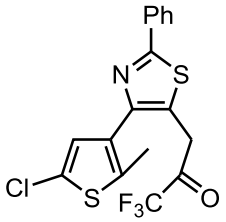

Compound **4-28** (0.25 g, 0.90 mmol, 1 eq.) and thiobenzamide **4-29** (0.19 g, 1.35 mmol, 1.5 eq.) was dissolved in 2 mL ethanol. Sodium acetate (0.37 g, 4.5 mmol, 5 eq.) was added and the reaction mixture was stirred at room temperature for 2 h. Concentrated hydrochloric acid (0.75 mL, 9.00 mmol, 10.0 eq.) was added and the reaction was stirred for 45 min. Water was added to the reaction and the mixture was extracted three times with ethyl acetate. The combined organic phases were washed with saturated aqueous sodium bicarbonate solution, and brine, dried over magnesium sulfate and filtered. The solvent was removed under reduced pressure and the crude product was purified by column chromatography (cyclohexane: ethyl acetate). Compound **4-30** (0.22 g, 0.55 mmol, 62% yield) was isolated. ^{1}H NMR (500 MHz, chloroform-*d*) δ = 7.99 – 7.93 (m, 2H), 7.48 – 7.42 (m, 3H), 6.78 (s, 1H), 4.20 (s, 2H), 2.34 (s, 3H). ^{13}C NMR (126 MHz, chloroform-*d*) δ = 187.4 (q, *J*=35.9), 167.8, 150.0, 137.8, 133.2, 130.7, 130.2, 129.2, 127.2, 127.0, 126.7, 122.0, 115.7 (q, *J*=292.6), 34.9, 14.2. ^{19}F NMR (471 MHz, chloroform-*d*) δ = -78.5.

UPLC-TOF-ESI^{-}-MS m/z: 399.985 [M-H] (calc.: 399.986 [$C_{17}H_{10}ClF_3NOS_2$]$^{-}$).

5.1.3.15 Synthesis of compound 4-35

The synthesis was conducted similar to reported protocols.[132]

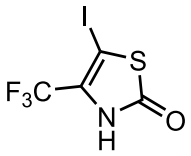

In a dried 50 mL Schlenk tube thiazolone **4-17** (0.61 g, 3.00 mmol, 1 eq.) was dissolved in 10 mL of dry tetrahydrofuran under argon and cooled to -78 °C. First, 3.6 mL of n-butyl lithium (2.3 M solution in cyclohexane, 8.28 mmol, 2.3 eq.) was added slowly at -78 °C and upon finished addition, the reaction mixture stirred for 30 min at 0 °C. Iodine (1.77 mL, 24.00 mmol, 4.0 eq.) dissolved in 5 mL of dry tetrahydrofuran was added to the previously prepared reaction mixture and stirred for 1 h at 0 °C. The reaction was quenched with water and adjusted with 1 M hydrochloric acid to pH 1-2, extracted three times with ethyl acetate and washed with an aqueous hydrochloric acid and sodium chloride solution. The organic phase was dried over magnesium sulfate and filtered. The solvent was removed under reduced pressure and the crude product was purified by column chromatography (cyclohexane: ethyl acetate). Compound **4-35** (1.18 g, 5.82 mmol, 92% yield) was isolated, containing 5% of the substrate. 1H NMR (500 MHz,

chloroform-d) δ = 10.64 (s, 1H). 13C NMR (126 MHz, chloroform-d) δ = 175.0, 126.0 (q, J=37.9), 118.5 (q, J=272.9), 54.8 (q, J=4.5). 19F NMR (471 MHz, Chloroform-d) δ = -61.75. UPLC-TOF-ESI$^-$-MS m/z: 293.871 [M-H] (calc.: 293.870 [C4F3INOS]$^-$).

5.1.3.16 Synthesis of compound 4-37

The synthesis was conducted similar to reported protocols.[133]

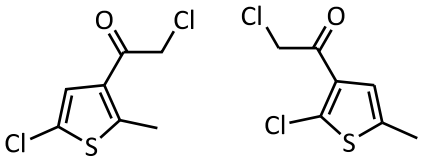

Isomer 1 Isomer 2

Chloroacetyl chloride (1.59 mL, 20 mmol, 1 eq.) and aluminium trichloride (3.33 g, 25 mmol, 1.25 eq.) were dissolved at 0 °C in 50 mL of dry methylene chloride and stirred for 30 min at 0 °C. 5-Chloro-2-methylthiophene **4-36**, (2.18 mL, 20 mmol, 1.0 eq.) dissolved in 25 ml of dry methylene chloride was added slowly over 4 h to the previously prepared mixture at 0 °C. The reaction mixture was stirred for 5h and the reaction temperature was allowed to rise to room temperature. 100 mL of ice-cooled water was added, the phases were separated and the organic layer was washed with saturated aqueous sodium bicarbonate solution. After drying over magnesium sulfate and filtration, the solvent was removed under reduced pressure and the crude product was purified by column chromatography (cyclohexane: methylene chloride). Compound **4-37** (2.97 g, 14.19 mmol, 71% yield) was isolated as a mixture of two isomers 1/0.8 and used without further purification.

Isomer 1: ^{1}H NMR (300 MHz, chloroform-*d*) δ = 7.15 (s, 1H), 4.44 (s, 2H), 2.67 (s, 3H).

Isomer 2: ^{1}H NMR (300 MHz, chloroform-*d*) δ = 7.03 (q, *J*=1.1, 1H), 4.64 (s, 2H), 2.39 (d, *J*=1.2, 2H).

GC-EI-QMS m/z: 208.1 [M+e$^-$] (calc.: 208.0 [$C_7H_6Cl_2OS$]$^-$); 159.1 [M-CH_2Cl+e$^-$] (calc.: 159.0 [C_6H_4ClOS]$^-$).

5.1.3.17 Synthesis of compound 4-38

The synthesis was conducted similar to reported protocols.[126, 131]

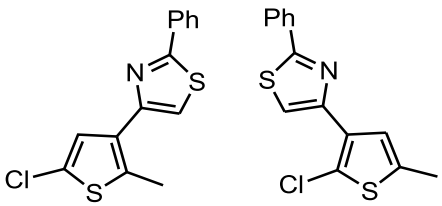

Isomer 1 Isomer 2

Compound **4-37** (0.84 g, 4.0 mmol, 1 eq.), thiobenzamide (0.82 g, 6.00 mmol, 1.5 eq.), potassium acetate (1.96 g, 20.0 mmol, 5.0 eq.) and a catalytic amount of potassium iodide were dissolved in 10 mL ethyl alcohol and stirred at room temperature for 18 h. Concentrated hydrochloric acid (3.33 mL, 40 mmol, 10.0 eq.) was added and the reaction mixture was stirred for 30 min at room temperature. Water was added and the solution was extracted three times with ethyl acetate. The combined organic phases were washed with 1 M aqueous sodium hydroxide solution, dried over magnesium sulfate and filtration. The solvent was removed under reduced pressure and the crude product was purified by column chromatography (cyclohexane: ethyl acetate). Compound **4-38** (1.04 g, 3.56 mmol, 89% yield) was isolated as a mixture of two isomers and used for the next step without further purification.

Isomer 1: ^{1}H NMR (500 MHz, chloroform-*d*) δ = 8.06 – 7.93 (m, 2H), 7.50 – 7.41 (m, 2H), 7.24 (s, 1H), 7.18 (s, 1H), 2.67 (s, 3H).

Isomer 2: ^{1}H NMR (500 MHz, chloroform-*d*) δ = 8.06 – 7.98 (m, 3H), 7.79 (s, 1H), 7.54 – 7.43 (m, 3H), 7.34 (q, *J*=1.2, 1H), 2.46 (d, *J*=1.2, 3H).

UPLC-TOF-ESI^{+}-MS m/z: 292.002 [M+H] (calc.: 292.002 $[C_{14}H_{11}ClNS_2]^{+}$).

5.1.3.18 Synthesis of compound 4-39

Diisopropylamine (0.17 g, 1.2 mmol, 1.0 eq.) was dissolved in 5 mL of dry tetrahydrofuran under argon and cooled to -78°C. First 0.52 mL of n-butyl lithium (2.3 M solution in cyclohexane, 1.20 mmol, 1.2 eq.) was added slowly at -78 °C and the reaction mixture was allowed to warm to room temperature. After cooling to -78 °C, **4-38** (0.29 g, 1.00 mmol, 1.0 eq.) dissolved in 2 mL of dry tetrahydrofuran, was added to the previously prepared solution. The reaction mixture was allowed to warm to 0 °C and stirred for 1 hour. The reaction was quenched with 1 M aqueous hydrochloric acid solution and was extracted three times with MTBE. The combined organic phases were washed with 1 M aqueous hydrochloric acid solution, dried over magnesium sulfate and filtered. The solvent was removed under reduced pressure compound **4-39** (0.33 g, 0.95 mmol, 95% yield) was used without further purification.

5.1.3.19 Coupling of 4-35 to a Phenyl Rest

Compound **4-35** (15 mg, 50 µmol, 1 eq.), phenyl species (1 eq.), base (3 eq.) and catalyst (0.1 eq.) were evacuated and flushed with argon. The solvent (1 mL) was added and degassed. The flask was sealed and the reaction mixture was refluxed at 110 °C for 18 h. The reaction was allowed to cool to room temperature and water was added. The mixture was extracted with ethyl acetate, filtered over celite and the solvent was removed under reduced pressure. The crude product was analyzed *via* UPLC.

UPLC-TOF-ESI$^-$-MS m/z: 244.006 [M-H] (calc.: 244.005 $[C_{10}H_5F_3OS]^-$).

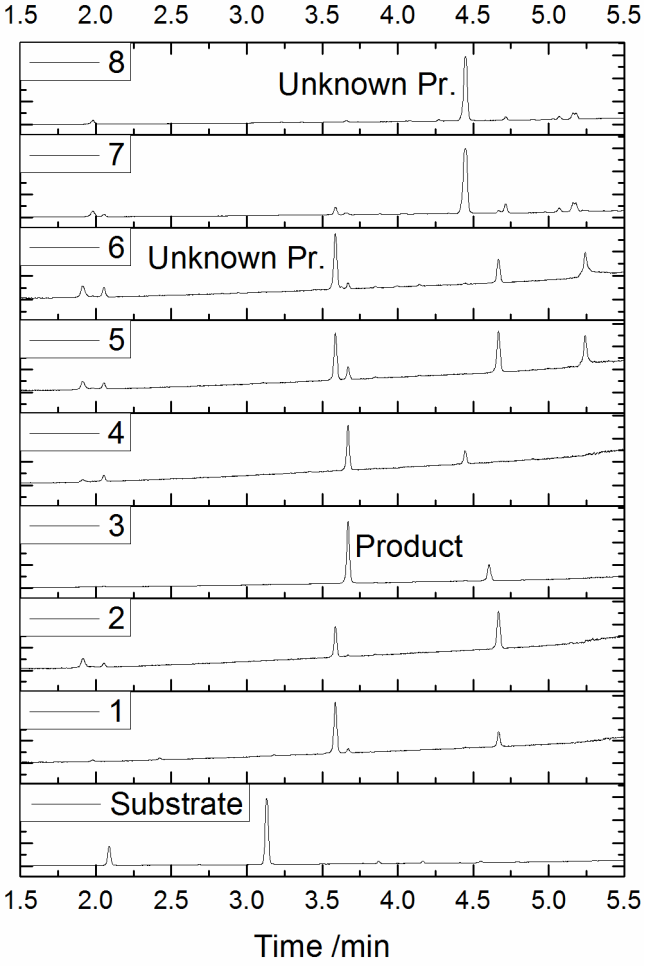

*Figure 5-1 UPLC analysis of coupling **4-35** to a phenyl substituent.*

*Table 5-1 Coupling of phenyl with thiazolone **4-35** with different phenyl species and under various reaction. conditions.*

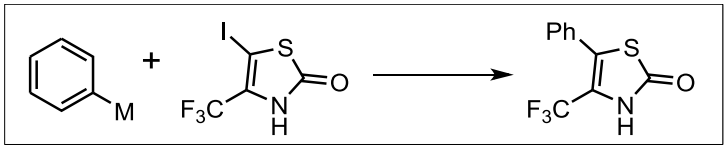

#	Rest M	Catalyst	Base	Ligand	Solvent	Result
1	$B(OH)_2$	$[Pd(PPh_3)_4]$	Cs_2CO_3	-	toluene/ water/ethanol	traces product and unknown product
2	$B(OH)_2$	$[Pd(PPh_3)_4]$	Cs_2CO_3	-	dioxane/water	unknown product
3	$B(OH)_2$	$Pd(OAc)_2$	Cs_2CO_3	Sphos	dioxane/water	significant amount of product and traces of dehalogenation
4	$B(OH)_2$	$[Pd(dppf)Cl_2DCM]$	Cs_2CO_3	-	dioxane/water	significant amount of product and traces of dehalogenation
5	$B(OH)_2$	$[Pd(PPh_3)_4]$	K_3PO_4	-	dioxane/water	unknown product
6	$B(OH)_2$	$[Pd(PPh_3)_4]$	Cs_2CO_3	-	dioxane/water	unknown product
7	MgBr	$[Pd(PPh_3)_4]$	-	-	CPME	unknown product
8	MgBr	$[Ni(dppp)Cl_2]$	-	-	CPME	unknown product

5.2 Crystallographic Details[8]

Colorless crystals of **4-4oH**, **4-13** and **4-17,** suitable for X-ray diffraction were mounted using a microfabricated polymer film crystal-mounting tool (dual-thickness MicroMount, MiTeGen) using low viscosity oil (perfluoropolyalkylether; viscosity 1800 cSt, ABCR) to reduce the X-ray absorption and scattering. A Bruker D8 Venture single-crystal X-ray diffractometer with area detector using Mo-K_α (λ = 0.71073 Å) radiation was used for data collection at -173 °C. Multiscan absorption corrections implemented in SADABS[134] were applied to the data. The structures were solved by intrinsic phasing (SHELXT-2013)[135] and refined by full-matrix least-squares methods on F^2 (SHELXL-2014).[136] The hydrogen atoms were placed at calculated positions and refined by using a riding model. CCDC XXXXXXX (**4-4oH**), CCDC XXXXXXX (**4-13**), and XXXXXXX (**4-17**) contain the supplementary crystallographic data for this paper. These data can be obtained free of charge from The Cambridge Crystallographic Data Centre.

[8] Conducted by Dr. Bernd M. Schmidt (**4-4oH** & **4-17**) and Dr. Beatrice Braun-Cula (**4-13**)

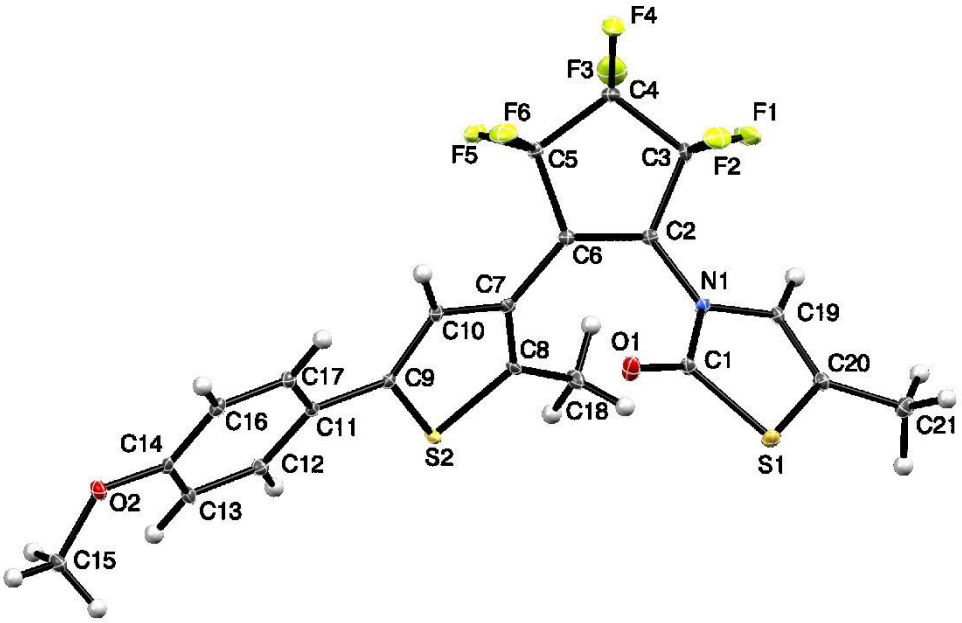

*Figure 5-2 Asymmetric unit of **4-13**. Ring-closing carbons distance C1–C8 3.529(4), N1–C1 1.394(4), C1–O1 1.203(4), S1–C1 1.775(3), S1–C20 1.751(3), S2–C8 1.721(3), S2–C9 1.735(2). The structure was solved in the monoclinic space group $P2_1/c$ with $R_{int} = 0.071$, $R[F^2 > 2\sigma(F^2)] = 0.047$, $wR(F^2) = 0.114$ and S = 1.00.*

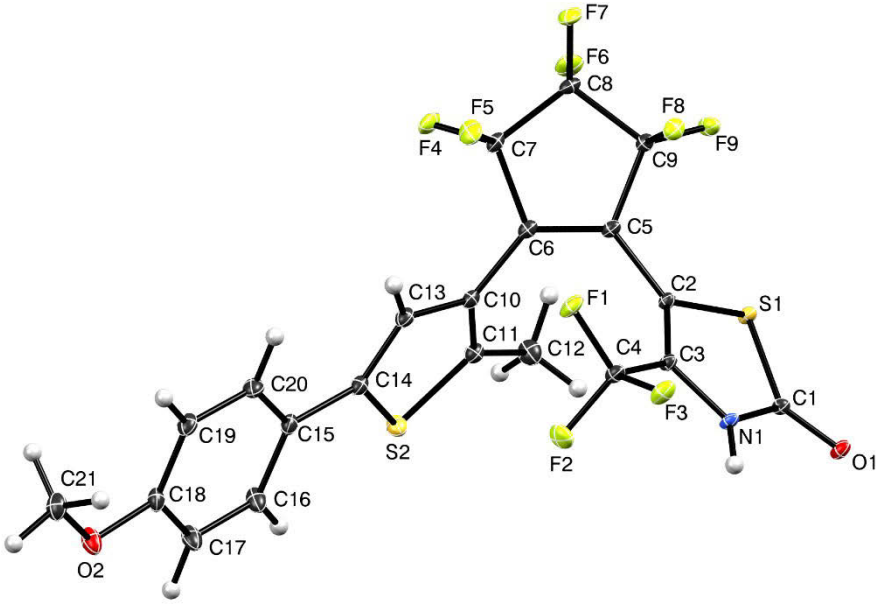

*Figure 5-3 Asymmetric unit of **4-4oH**. Selected bond lengths [Å]: Ring-closing carbons distance C3–C11 3.866(2), N1–C1 1.360(2), C1–O1 1.227(2), S1–C1 1.774(1), S1–C2 1.757(1), S2–C11 1.702(1), S2–C14 1.737(1). The structure of **4-4oH** was solved in the monoclinic space group $P2_1/c$ with $R_{int} = 0.032$, $R[F^2 > 2\sigma(F^2)] = 0.029$, $wR(F^2) = 0.074$ and S = 1.04.*

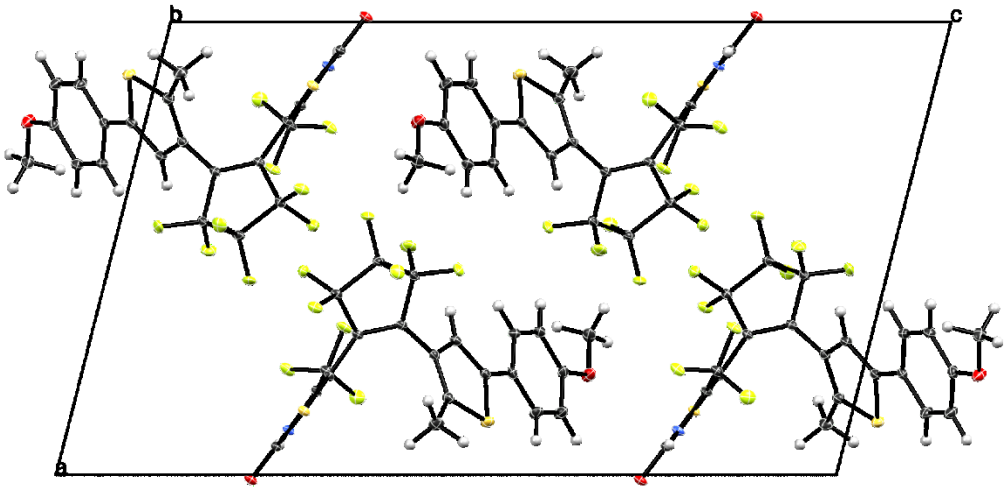

*Figure 5-4 View of the unit cell along the crystallographic b axis of **4-4oH**.*

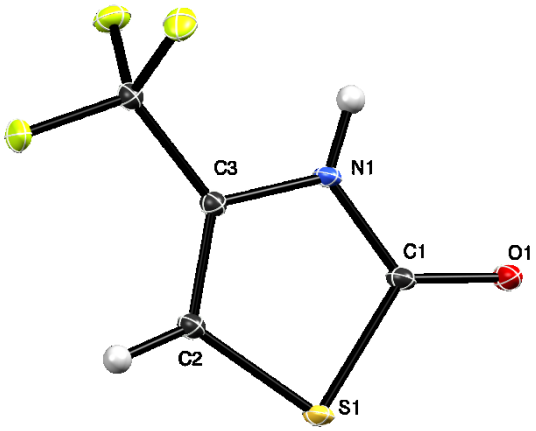

*Figure 5-5 Asymmetric unit of **4-17**. Selected bond lengths [Å]: S1–C1 1.773(1), S1–C2 1.738(1), C1–N1 1.361(1), C1–O1 1.229(1). The structure of **4-17** was solved in the monoclinic space group $P2_1/c$ with $R_{int} = 0.022$, $R[F^2 > 2\sigma(F^2)] = 0.022$, $wR(F^2) = 0.064$ and $S = 1.04$*

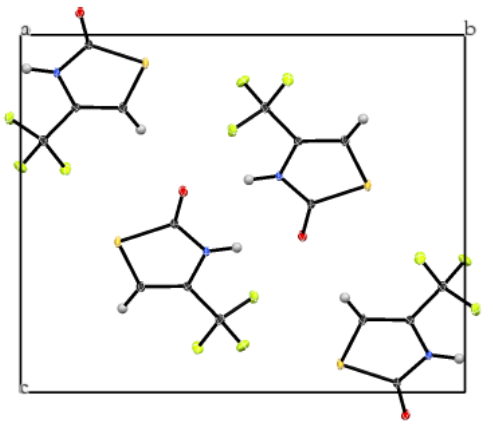

*Figure 5-6 Figure 5-7 View of the unit cell of **4-17** along the crystallographic an axis.*

5.3 PHOTOCHEMICAL EXPERIMENTS

5.3.1 Determination of the Photostationary State Composition and the Extinction Coefficients[19b, 24]

The ratio of open to closed isomer after several irradiation cycles and in the photostationary state (PSS) was determined by injection of irradiated samples into a UPLC and detection by the UV/vis diode array, integrated at the isosbestic point of the corresponding irradiation spectrum. The different ratios of water and acetonitrile caused by the gradient in the UPLC were neglected, as no significant shift of the spectra compared to pure acetonitrile solutions was observed.

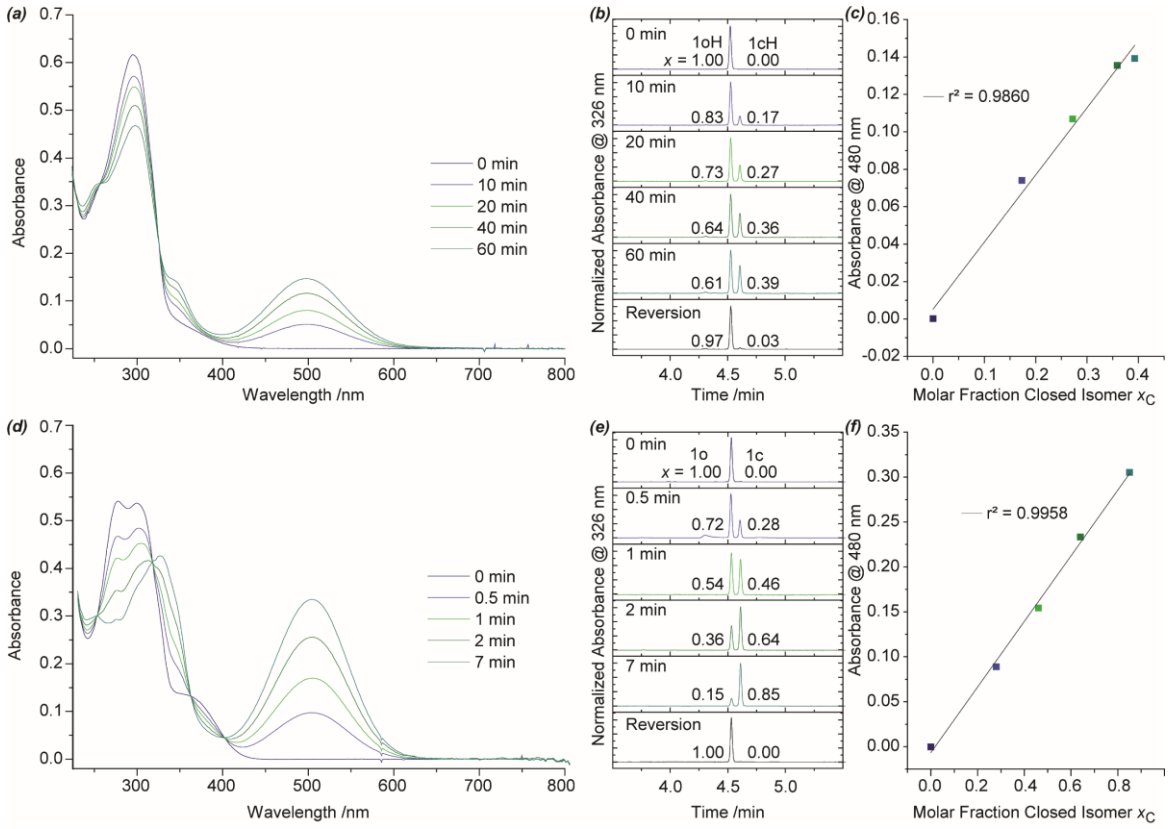

Figure 5-8 Determination of the extinction coefficient in aqueous 0.15 M potassium chloride solution containing 30 vol-% acetonitrile at 25 °C under acidic conditions (pH 2, a-c) or basic conditions (pH 13, d-f): (a+d) UV/vis spectra after different irradiation times with 313 nm light of a 2.66 · 10-5 M 4-2oH or 4-2o solution; (b+e) UPLC traces observed at 326 nm after different irradiation times with 313 nm light and the molar fraction of open and closed isomer determined by integration of the peaks; (c+f) Plot of the absorbance at 480 nm vs. the molar fraction of the closed isomer giving a linear behavior.

5.3.2 Determination of Quantum Yields and Actinometry[19b, 24]

The extinction coefficients of the open diarylethene isomers were determined upon precise preparation of stock solutions with defined concentrations and subsequent measurement of the absorption spectra. The molar absorptivity of the closed form was determined equally with respect to the ratio of isomers in the photo stationary state *via* UPLC-UV/vis-detector.

The light intensity at 313 nm was determined by using ferrioxalate actinometry.[137] Therefore 3 mL of a 0.006 M solution of ferrioxalate in 0.05 M H_2SO_4 was irradiated and 0.5 mL of phenanthroline (0.1 wt% in 0.5 M H_2SO_4/1.6 M NaOAc) were added subsequently. The resulting absorbance at 510 nm was used to calculate the light intensity *via* formula S 1.

$$I_0 = \frac{\Delta A_{510nm}}{\Delta t * \varepsilon_{510nm} * \Phi_{\mathrm{irr}} * 1000} * \frac{3.5mL}{3mL} \qquad \textbf{(E6-1)}$$

Thereby ΔA_{510nm} is the difference of the absorption at 510 nm for an irradiated versus a non-irradiated solution, Δt is the irradiation time, ε_{510nm} is 11100 M^{-1} cm^{-1} and Φ_{irr} is the quantum yield at the used irradiation wavelength (1.24 for 302 nm and 1.14 for 546 nm).

For the ring-opening a wavelength was needed that exceeds the range for ferrioxalate actinometry. Therefore, actinometry *via* 1,2-bis(2,4-dimethyl-5-phenyl-3-thienyl)-3,3,4,4,5,5-hexafluoro-1-cyclopentene was performed.[138] A solution of the switch in *n*-hexane was irradiated at 22 °C approximately for 5 min at 313 nm. The concentration of the closed form in the solution was then determined from the absorbance at 546 nm and the extinction coefficient can be calculated at the given irradiation wavelength. The quantum yield for the ring opening reaction was determined at the selected wavelength in time intervals of 30 s or 60 s. The absorbance at the irradiation wavelength was insterted in the following equation:

$$\log\left(10^{Abs'(t)} - 1\right) - \log\left(10^{Abs'(t=0)} - 1\right) = 1000 * \varepsilon * I_0 * l * \Phi_{cl\rightarrow op} * t \qquad \textbf{(E6-2)}$$

Since the quantum yield for the ring opening is given for the wavelength, I_0 can be calculated from the slope.

For the determination of the quantum yield formula **E6-3** was used:

$$\Phi = \frac{\Delta A/\Delta t}{(1-10^{-A'})*\varepsilon*I_0*1000} \qquad \textbf{(E6-3)}$$

ΔA/Δt describes the change of absorbance at a wavelength, which varies during irradiation over time. $1 - 10^{-A'}$ is the percentage of the absorbed photons of the solution at the given irradiation wavelength, ε is the extinction coefficient for the observed wavelength and I0 is the light intensity. This method of calculating the quantum yield was appliedto only the initial 5% of photochemical conversion. Alternatively, the complete kinetic profile was fitted with the Runge-Kuttar algorithm, using the rate equations of the photoreactions E6-4 and E6-5.

$$\frac{dc}{dt} = 1000 I_0 F(t) l\left(-\varepsilon_o^{irrad}\,\phi_{op\rightarrow cl} \pm \varepsilon_c^{irrad}\,\phi_{cl\rightarrow op}\right) \qquad \textbf{(E6-4)}$$

$$F(t) = \frac{1-10^{-Abs'(t)}}{Abs'(t)} \qquad \textbf{(E6-5)}$$

5.3.3 Spectrophotometric Titration in Water/Acetonitrile

The spectrophotometric titrations were conducted in an aqueous, buffered solution containing 30 vol-% acetonitrile. As titrant a 0.7 M hydrochloric acid solution containing 30 vol-% acetonitrile

was used, prepared from a 1 M aqueous standard solution purchased from Acros Organics. The ion strength of the titrand was adjusted with potassium chloride to 0.15 M. To determine the ${}^{s}_{s}pK_a$ (pK_a determined in acetonitrile/water with electrodes calibrated in the same acetonitrile/water mixture) of the open isomer (**4-4oH** ⇌ **4-4o**) as titrand a solution containing $2.66 \cdot 10^{-5}$ M of **4-4oH** buffered by 0.01 M potassium hydroxide and 0.01 M dipotassium citrate was used. The titration was followed by monitoring the 355 nm band. For the determination of closed ${}^{s}_{s}pK_a$ (**4-4cH** ⇌ **4-4c**), a solution containing $2.66 \cdot 10^{-5}$ M of **4-4oH** buffered with 0.02 M potassium hydroxide, 0.01 M dipotassium citrate and 0.01 M dipotassium carbonate was irradiated with 300 nm light, which results in almost complete conversion to the closed isomer. The titration was observed at 320 nm (the isosbestic point of the dissociation reaction of the open isomer). To convert the resulting ${}^{s}_{w}pH$ scale (pH determined in acetonitrile/water with electrodes calibrated in the same water) to a ${}^{s}_{s}pH$ (pH determined in acetonitrile/water with electrodes calibrated in the same acetonitrile/water mixture) the conversion parameter published by Bosch *et. al* was used.[139]

5.4 Computational Methods — Acid-catalyzed Cycloreversion

The molecular structures (**3-1o**, **3-1c**, **3-1o**$^{+}$, **3-1c**$^{+}$, details see appendix 7.4.1) were generated and pre-optimized by MM2 with PerkinElmer CambridgeSoft Chem3D Ultra 10.0. Complete geometry optimizations and harmonic frequency calculations of the reactants, products, and transition states were performed using Gaussian 09 Rev. C.01 program package.[140] Transition states were computed with the help of Opt=TS keyword using Berny algorithm to optimize to a transition state rather than a local minimum.[46] Each stationary point was characterized by the number of imaginary frequencies (NImag = 1 for transition state and NImag = 0 for the local minimum) and by total electronic energies and thermal correction to the Gibbs free energy. To follow unrestricted Kohn-Sham solution, the broken-symmetry guess was generated and followed using keyword Guess (mix, always). The B3LYP level of density functional theory (DFT) was used in combination with a 6-31G* basis set. Due to C_1 symmetry the nosymm keyword was used. The stability of the Kohn-Sham orbitals were tested before and after geometry optimization, using the keyword Stable=Opt. In cases where instability was found, the geometry optimization was repeated with the stable set of orbitals used for the initial guess.

Solvation by acetonitrile/water was calculated by using the scrf=(smd,solvent=acetonitrile) keyword. The static dielectric constant and dynamic dielectric constant was modified to simulate an acetonitrile:water (90:10) mixture, which is literature known.[139] The dynamic dielectric constant was calculated by the Lorentz-Lorenz equation and the Maxwell equation.

In analogy to the proton exchange method for calculation of the pK_a of organic compounds, a reference was used to compute the Gibbs free energy of the dehydration, to avoid the calculation of water, a proton or a hydroxide anion.[141] The equilibrium constant of the dehydration of triphenylmethanol in acetonitrile:water (90:10) is literature known.[142]

6 LITERATURE

[1] J. Gurke, M. Quick, N. P. Ernsting, S. Hecht, *Chem. Commun.* **2017**, *53*, 2150-2153.

[2] J. Gurke, M. Quick, S. Kovalenko, B. Simon, B. M. Schmidt, D. Jacquemin, S. Hecht, *submitted*.

[3] P. Muller, *Pure Appl. Chem.* **2009**, *66*, 1077-1184.

[4] G. N. Lewis, *Valence and the Structure of Atoms and Molecules*, Chemical Catalog Company, Incorporated, **1923**.

[5] J. N. Turro, V. Ramamurthy, J. C. Scaiano, *Modern Molecular Photochemistry of Organic Molecules*, University Science Book, Sausalito, California, **2010**.

[6] a) H. Bouas-Laurent, H. Dürr, in *Pure Appl. Chem., Vol. 73*, **2001**, p. 639; b) X. D. Sun, M. G. Fan, X. J. Meng, E. T. Knobbe, *J. Photochem. Photobiol., A* **1997**, *102*, 213-216.

[7] J. F. Ireland, P. A. H. Wyatt, *Adv. Phys. Org. Chem.* **1976**, *12*, 131-221.

[8] a) M. Kathan, S. Hecht, *Chem. Soc. Rev.* **2017**; b) R. Gostl, A. Senf, S. Hecht, *Chem. Soc. Rev.* **2014**, *43*, 1982-1996.

[9] K. A. Muszkat, E. Fischer, *J. Chem. Soc. B* **1967**, 662-678.

[10] R. B. Woodward, R. Hoffmann, *J. Am. Chem. Soc.* **1965**, *87*, 395-397.

[11] R. B. Woodward, R. Hoffmann, *Angew. Chem. Int. Ed.* **1969**, *8*, 781-853.

[12] a) M. Irie, M. Mohri, *J. Org. Chem.* **1988**, *53*, 803; b) M. Irie, S. Nakamura, *J. Org. Chem.* **1988**, *53*, 6136.

[13] M. Irie, T. Fukaminato, K. Matsuda, S. Kobatake, *Chem. Rev.* **2014**, *114*, 12174-12277.

[14] M. Kathan, P. Kovaříček, C. Jurissek, A. Senf, A. Dallmann, A. F. Thünemann, S. Hecht, *Angew. Chem. Int. Ed.* **2016**, *55*, 13882.

[15] a) M. Irie, S. Nakamura, *J. Org. Chem.* **1988**, *53*, 6136; b) M. Irie, M. Mohri, *J. Org. Chem.* **1988**, *53*, 803.

[16] a) V. A. Barachevsky, *Review Journal of Chemistry* **2017**, *7*, 334-371; b) T. Fukaminato, T. Doi, M. Tanaka, M. Irie, *J. Phys. Chem. C* **2009**, *113*, 11623-11627.

[17] M. Boggio-Pasqua, M. Ravaglia, M. J. Bearpark, M. Garavelli, M. A. Robb, *J. Phys. Chem. A* **2003**, *107*, 11139-11152.

[18] K. Fukui, T. Yonezawa, H. Shingu, *J. Chem. Phys.* **1952**, *20*, 722-725.

[19] a) M. Irie, T. Fukaminato, K. Matsuda, S. Kobatake, *Chemical Reviews* **2014**, *114*, 12174; b) M. Herder, Humboldt-Universität zu Berlin, Mathematisch-Naturwissenschaftliche Fakultät **2015**.

[20] T. Nakashima, K. Tsuchie, R. Kanazawa, R. Li, S. Iijima, O. Galangau, H. Nakagawa, K. Mutoh, Y. Kobayashi, J. Abe, T. Kawai, *J. Am. Chem. Soc.* **2015**, *137*, 7023-7026.

[21] a) K. Daichi, K. Seiya, *Chem. Lett.* **2011**, *40*, 93-95; b) A. G. Lvov, V. Z. Shirinian, V. V. Kachala, A. M. Kavun, I. V. Zavarzin, M. M. Krayushkin, *Org. Lett.* **2014**, *16*, 4532-4535; c) V. Valderrey, A. Bonasera, S. Fredrich, S. Hecht, *Angew. Chem. Int. Ed.* **2017**, *56*, 1914-1918.

[22] S. Delbaere, J. Berthet, T. Shiozawa, Y. Yokoyama, *J. Org. Chem.* **2012**, *77*, 1853-1859.

[23] H. Kenji, M. Kenji, K. Seiya, Y. Taro, K. Tsuyoshi, I. Masahiro, *Bull. Chem. Soc. Jpn.* **2000**, *73*, 2389-2394.

[24] M. Herder, B. M. Schmidt, L. Grubert, M. Pätzel, J. Schwarz, S. Hecht, *Journal of the American Chemical Society* **2015**, *137*, 2738-2747.

[25] H. Kenji, M. Kenji, Y. Taro, K. Tsuyoshi, I. Masahiro, *Chem. Lett.* **2000**, *29*, 1358-1359.

[26] a) H.-h. Liu, Y. Chen, *New J. Chem.* **2012**, *36*, 2223-2227; b) O. Galangau, T. Nakashima, F. Maurel, T. Kawai, *Chem. Eur. J.* **2015**, *21*, 8471-8482; c) R. Kodama, K. Sumaru, K. Morishita, T. Kanamori, K. Hyodo, T. Kamitanaka, M. Morimoto, S. Yokojima, S. Nakamura, K. Uchida, *Chem. Commun.* **2015**, *51*, 1736-1738; d) S. Protti, V. Dichiarante, D. Dondi, M. Fagnoni, A. Albini, *Chem. Sci.* **2012**, *3*, 1330-1337; e) R. Zhu, M.-d. Li, L. Du, D. L. Phillips, *J. Phys. Chem. B* **2017**, *121*, 2712-2720.

[27] S. H. Kawai, S. L. Gilat, J.-M. Lehn, *Eur. J. Org. Chem.* **1999**, *1999*, 2359-2366.

[28] Y. Tadatsugu, K. Yusuke, O. Toru, U. Ayaka, K. Jun-ichiro, K. Megumi, S. Kimio, K. Yoshiro, Y. Satoshi, N. Shinichiro, M. Masakazu, U. Kingo, *Bull. Chem. Soc. Jpn.* **2014**, *87*, 528-538.

[29] S. Kobatake, S. Imao, Y. Yamashiro, Y. Terakawa, *Tetrahedron Lett.* **2011**, *52*, 1905-1908.

[30] S. Kobatake, H. Imagawa, H. Nakatani, S. Nakashima, *New J. Chem.* **2009**, *33*, 1362-1367.

[31] a) L. N. Lucas, J. van Esch, R. M. Kellogg, B. L. Feringa, *Tetrahedron Lett.* **1999**, *40*, 1775-1778; b) K. Beydoun, J. Roger, J. Boixel, H. L. Bozec, V. Guerchais, H. Doucet, *Chem. Commun.* **2012**, *48*, 11951-11953.

[32] M. Singer, A. Jäschke, *J. Am. Chem. Soc.* **2010**, *132*, 8372-8377.

[33] a) A. Alex, *Curr. Top. Med. Chem.* **2001**, *1*, 277-351; b) D. T. Manallack, R. J. Prankerd, E. Yuriev, T. I. Oprea, D. K. Chalmers, *Chem. Soc. Rev.* **2013**, *42*, 485-496; c) S. Babić, A. J. M. Horvat, D. Mutavdžić Pavlović, M. Kaštelan-Macan, *TrAC, Trends Anal. Chem.* **2007**, *26*, 1043-1061.

[34] R. F. Cookson, *Chem. Rev.* **1974**, *74*, 5-28.

[35] a) M. Roses, C. Rafols, E. Bosch, *Anal. Chem.* **1993**, *65*, 2294-2299; b) S. Rondinini, P. Longhi, P. R. Mussini, T. Mussini, in *Pure Appl. Chem., Vol. 59*, **1987**, p. 1693; c) G. Akerlof, *J. Am. Chem. Soc.* **1932**, *54*, 4125-4139.

[36] a) A. Avdeef, J. E. A. Comer, S. J. Thomson, *Anal. Chem.* **1993**, *65*, 42-49; b) A. Avdeef, J. J. Bucher, *Anal. Chem.* **1978**, *50*, 2137-2142.

[37] T. Mussini, A. K. Covington, P. Longhi, S. Rondinini, in *Pure Appl. Chem., Vol. 57*, **1985**, p. 865.

[38] Y. Motoo, *Bull. Chem. Soc. Jpn.* **1959**, *32*, 429-432.

[39] a) P. Bruttel, *Nichtwässrige Titrationen von Säuren und Basen mit potentiometrischer Endpunktindikation*, Metrohm AG, Herisau, Schweiz; b) A. Kütt, I. Leito, I. Kaljurand, L. Sooväli, V. M. Vlasov, L. M. Yagupolskii, I. A. Koppel, *J. Org. Chem.* **2006**, *71*, 2829-2838; c) M. Lõkov, S. Tshepelevitsh, A. Heering, P. G. Plieger, R. Vianello, I. Leito, *Eur. J. Org. Chem.* **2017**, *2017*, 4475-4489.

[40] a) D. Dohoda, K. Tsinman, O. Tsinman, H. Wang, K. Y. Tam, *J. Pharm. Biomed. Anal.* **2015**, *114*, 88-96; b) R. I. Allen, K. J. Box, J. E. A. Comer, C. Peake, K. Y. Tam, *J. Pharm. Biomed. Anal.* **1998**, *17*, 699-712; c) R. C. Mitchell, C. J. Salter, K. Y. Tam, *J. Pharm. Biomed. Anal.* **1999**, *20*, 289-295; d) K. Takács-Novák, K. Y. Tam, *J. Pharm. Biomed. Anal.* **2000**, *21*, 1171-1182; e) K. Y. Tarn, K. Takács-Novák, *Pharm. Res.* **1999**, *16*, 374-381.

[41] J. Reijenga, A. van Hoof, A. van Loon, B. Teunissen, *Anal. Chem. Insights* **2013**, *8*, 53-71.

[42] Sigmoidal Fitting/Dose Response Curves, http://www.originlab.com/index.aspx?go=Solutions%2fCaseStudies&pid=106, 28.10. 2017

[43] T. J. Kucharski, Y. Tian, S. Akbulatov, R. Boulatov, *Energy Environ. Sci.* **2011**, *4*, 4449.

[44] a) K. Moth-Poulsen, D. Coso, K. Borjesson, N. Vinokurov, S. K. Meier, A. Majumdar, K. P. C. Vollhardt, R. A. Segalman, *Energy Environ. Sci.* **2012**, *5*, 8534; b) K. Börjesson, A. Lennartson, K. Moth-Poulsen, *ACS Sustainable Chem. & Eng.* **2013**, *1*, 585; c) V. Gray, A. Lennartson, P. Ratanalert, K. Borjesson, K. Moth-Poulsen, *Chem. Commun.* **2014**, *50*, 5330; d) A. Lennartson, A. Roffey, K. Moth-Poulsen, *Tetrahedron Lett.* **2015**, *56*, 1457; e) M. Quant, A. Lennartson, A. Dreos, M. Kuisma, P. Erhart, K. Börjesson, K. Moth-Poulsen, *Chem. Eur. J.* **2016**, *22*, 13265.

[45] M. Irie, T. Fukaminato, K. Matsuda, S. Kobatake, *Chem. Rev.* **2014**, *114*, 12174.

[46] P. D. Patel, A. E. Masunov, *J. Phys. Chem. C* **2011**, *115*, 10292.

[47] T. Nakashima, K. Atsumi, S. Kawai, T. Nakagawa, Y. Hasegawa, T. Kawai, *Eur. J. Org. Chem.* **2007**, *2007*, 3212.

[48] S. L. Gilat, S. H. Kawai, J.-M. Lehn, *Chem. Eur. J.* **1995**, *1*, 275.

[49] a) S. Kobatake, Y. Terakawa, *Chem. Commun.* **2007**, 1698; b) C. Coudret, T. Nakagawa, T. Kawai, J.-C. Micheau, *New J. Chem.* **2009**, *33*, 1386; c) T. Nagakawa, C. L. Serpentini, C. Coudret, J. C. Micheau, T. Kawai, *Dyes Pigment.* **2011**, *89*, 271; d) Y. Kutsunugi, C. Coudret, J. C. Micheau, T. Kawai, *Dyes Pigment.* **2012**, *92*, 838-846; e) E. Griese, Humboldt-Universität zu Berlin (Berlin), **2017**.

[50] D. Kitagawa, K. Sasaki, S. Kobatake, *Bull. Chem. Soc. Jpn.* **2011**, *84*, 141-147.

[51] J. Zhang, Q. Zou, H. Tian, *Adv. Mater.* **2013**, *25*, 378-399.

[52] a) S. H. Kawai, S. L. Gilat, R. Ponsinet, J.-M. Lehn, *Chem. Eur. J.* **1995**, *1*, 285; b) V. Lemieux, N. R. Branda, *Org. Lett.* **2005**, *7*, 2969-2972; c) V. Lemieux, S. Gauthier, N. R. Branda, *Angew. Chem. Int. Ed.* **2006**, *45*, 6820-6824; d) T. Wu, H. Tang, C. Bohne, N. R. Branda, *Angew. Chem. Int. Ed.* **2012**, *51*, 2741-2744.

[53] a) A. Perrier, F. Maurel, J. Aubard, *J. Photochem. Photobiol., A* **2007**, *189*, 167-176; b) C.-T. Poon, W. H. Lam, V. W.-W. Yam, *J. Am. Chem. Soc.* **2011**, *133*, 19622.

[54] A. Perrier, F. Maurel, D. Jacquemin, *Acc. Chem. Res.* **2012**, *45*, 1173-1182.

[55] Q. Zou, X. Li, H. Ågren, *Dyes Pigment.* **2014**, *111*, 1-7.

[56] X. Li, Y. Ma, B. Wang, G. Li, *Org. Lett.* **2008**, *10*, 3639-3642.

[57] a) M. Irie, O. Miyatake, K. Uchida, *J. Am. Chem. Soc.* **1992**, *114*, 8715-8716; b) M. Irie, O. Miyatake, R. Sumiya, M. Hanazawa, Y. Horikawa, K. Uchida, *Molecular Crystals and Liquid Crystals Science and Technology. Section A. Molecular Crystals and Liquid Crystals* **1994**, *246*, 155-158; c) J. Massaad, J.-C. Micheau, C. Coudret, R. Sanchez, G. Guirado, S. Delbaere, *Chem. Eur. J.* **2012**, *18*, 6568-6575; d) H. Lan, G. Lv, Y. Wen, Y. Mao, C. Huang, T. Yi, *Dyes Pigment.* **2016**, *131*, 18-23.

[58] a) Y. Wu, S. Chen, Y. Yang, Q. Zhang, Y. Xie, H. Tian, W. Zhu, *Chem. Commun.* **2012**, *48*, 528-530; b) Y. Wu, W. Zhu, W. Wan, Y. Xie, H. Tian, A. D. Q. Li, *Chem. Commun.* **2014**, *50*, 14205-14208; c) K. Liu, Y. Wen, T. Shi, Y. Li, F. Li, Y.-l. Zhao, C. Huang, T. Yi, *Chem. Commun.* **2014**, *50*, 9141-9144; d) Y. Mao, K. Liu, G. Lv, Y. Wen, X. Zhu, H. Lan, T. Yi, *Chem. Commun.* **2015**, *51*, 6667-6670.

[59] Y. Cai, Y. Gao, Q. Luo, M. Li, J. Zhang, H. Tian, W.-H. Zhu, *Adv. Opt. Mater.* **2016**, *4*, 1410-1416.

[60] Z. Chen, S. Zhao, Z. Li, Z. Zhang, F. Zhang, *Science in China Series B: Chemistry* **2007**, *50*, 581-586.

[61] a) M. Ohsumi, T. Fukaminato, M. Irie, *Chem. Commun.* **2005**, 3921-3923; b) F.

Nourmohammadian, T. Wu, N. R. Branda, *Chem. Commun.* **2011**, *47*, 10954-10956.
[62] S. Fredrich, R. Göstl, M. Herder, L. Grubert, S. Hecht, *Angewandte Chemie International Edition* **2016**, *55*, 1208-1212.
[63] a) H. Miyasaka, M. Murakami, A. Itaya, D. Guillaumont, S. Nakamura, M. Irie, *J. Am. Chem. Soc.* **2001**, *123*, 753-754; b) Y. Ishibashi, M. Murakami, H. Miyasaka, S. Kobatake, M. Irie, Y. Yokoyama, *J. Phys. Chem. C* **2007**, *111*, 2730-2737; c) M. Murakami, H. Miyasaka, T. Okada, S. Kobatake, M. Irie, *J. Am. Chem. Soc.* **2004**, *126*, 14764-14772; d) D. Dulić, T. Kudernac, A. Pužys, B. L. Feringa, B. J. vanWees, *Adv. Mater.* **2007**, *19*, 2898-2902; e) J. Piard, Y. Ishibashi, H. Saito, R. Métivier, K. Nakatani, G. Gavrel, P. Yu, H. Miyasaka, *J. Photochem. Photobiol., A* **2012**, *234*, 57-65; f) K. Mutoh, Y. Kobayashi, T. Yamane, T. Ikezawa, J. Abe, *J. Am. Chem. Soc.* **2017**, *139*, 4452-4461.
[64] a) S. H. Kawai, S. L. Gilat, J.-M. Lehn, *Eur. J. Org. Chem.* **1999**; b) B. Song, H. Li, L. Yang, F. Zhang, J. Xiang, *Chin. J. Chem .* **2012**, *30*, 1393-1398; c) J. Wolf, T. Huhn, U. E. Steiner, *PCCP* **2015**, *17*, 6066-6075; d) J. Kühni, P. Belser, *Org. Lett.* **2007**, *9*, 1915-1918; e) R. Wang, N. Wang, S. Pu, X. Zhang, G. Liu, Y. Dai, *Dyes Pigment.* **2017**, *146*, 445-454.
[65] a) M. Yamamura, Y. Okazaki, T. Nabeshima, *Chem. Commun.* **2012**, *48*, 5724-5726; b) M. Yamamura, K. Yamakawa, Y. Okazaki, T. Nabeshima*Chem. Eur. J.* **2014**, *20*, 16258-16265; c) M. Lohse, K. Nowosinski, N. L. Traulsen, A. J. Achazi, L. K. S. von Krbek, B. Paulus, C. A. Schalley, S. Hecht, *Chem. Commun.* **2015**, *51*, 9777-9780.
[66] S. H. Kawai, S. L. Gilat, R. Ponsinet, J.-M. Lehn, *Chemistry – A European Journal* **1995**, *1*, 285-293.
[67] J. Gurke, Humboldt-Universität zu Berlin (Berlin), **2013**.
[68] S. Garg, B. Twamley, Z. Zeng, J. n. M. Shreeve, *Chem. Eur. J.* **2009**, *15*, 10554-10562.
[69] P. Gandeepan, C.-H. Hung, C.-H. Cheng, *Chem. Commun.* **2012**, *48*, 9379-9381.
[70] M. Herder, B. M. Schmidt, L. Grubert, M. Pätzel, J. Schwarz, S. Hecht, *J. Am. Chem. Soc.* **2015**, *137*, 2738.
[71] H. Mauser, *Formale Kinetik*, Bertelsmann-Universitätsverlag, **1974**.
[72] a) P. D. Patel, A. E. Masunov, *J. Phys. Chem. C* **2011**, *115*, 10292; b) A. V. Marenich, C. J. Cramer, D. G. Truhlar, *J. Phys. Chem. B* **2009**, *113*, 6378; c) N. Cindro, I. Antol, K. Mlinarić-Majerski, I. Halasz, P. Wan, N. Basarić, *J.Org. Chem.* **2015**, *80*, 12420.
[73] a) C. M. Breneman, K. B. Wiberg, *J. Comput. Chem.* **1990**, *11*, 361; b) J. Cioslowski, *J. Am. Chem. Soc.* **1989**, *111*, 8333.
[74] a) K. Boguslawski, C. R. Jacob, M. Reiher, *J. Chem. Theory Comput.* **2011**, *7*, 2740; b) K. Boguslawski, K. H. Marti, Ö. Legeza, M. Reiher, *J. Chem. Theory Comput.* **2012**, *8*, 1970.
[75] W. A. Velema, W. Szymanski, B. L. Feringa, *J. Am. Chem. Soc.* **2014**, *136*, 2178-2191.
[76] X. Xie, G. A. Crespo, G. Mistlberger, E. Bakker, *Nat. Chem.* **2014**, *6*, 202-207.
[77] J. A. Kellum, *Critical Care* **2000**, *4*, 6-14.
[78] B. K. Siesjö, *Kidney International* **1972**, *1*, 360-374.
[79] A. Roos, W. F. Boron, *Physiological Reviews* **1981**, *61*, 296-434.
[80] C. H. Desch, *Obituary Notices of Fellows of the Royal Society* **1936**, *2*, 250-259.
[81] R. Göstl, S. Hecht, *Angew. Chem. Int. Ed.* **2014**, *53*, 8784-8787.
[82] D. Wilson, N. R. Branda, *Angew. Chem. Int. Ed.* **2012**, *51*, 5431-5434.
[83] M. Kathan, P. Kovaříček, C. Jurissek, A. Senf, A. Dallmann, A. F. Thünemann, S. Hecht, *Angew. Chem. Int. Ed.* **2016**, *55*, 13882-13886.
[84] V. Lemieux, M. D. Spantulescu, K. K. Baldridge, N. R. Branda, *Angew. Chem. Int. Ed.* **2008**, *47*, 5034-5037.
[85] G. Duan, N. Zhu, V. W.-W. Yam, *Chem. Eur. J.* **2010**, *16*, 13199-13209.
[86] T. Nakashima, K. Miyamura, T. Sakai, T. Kawai, *Chem. Eur. J.* **2009**, *15*, 1977-1984.
[87] B. M. Neilson, C. W. Bielawski, *J. Am. Chem. Soc.* **2012**, *134*, 12693-12699.
[88] S. Yagai, K. Iwai, M. Yamauchi, T. Karatsu, A. Kitamura, S. Uemura, M. Morimoto, H. Wang, F. Würthner, *Angew. Chem. Int. Ed.* **2014**, *53*, 2602-2606.
[89] P. Wan, D. Shukla, *Chem. Rev.* **1993**, *93*, 571-584.
[90] Y. Odo, K. Matsuda, M. Irie, *Chem. Eur. J.* **2006**, *12*, 4283-4288.
[91] M. V. Peters, R. S. Stoll, A. Kühn, S. Hecht, *Angew. Chem. Int. Ed.* **2008**, *47*, 5968-5972.
[92] C. E. Weston, R. D. Richardson, M. J. Fuchter, *Chem. Commun.* **2016**, *52*, 4521-4524.
[93] M. Hammarson, J. R. Nilsson, S. Li, T. Beke-Somfai, J. Andréasson, *J. Phys. Chem. B* **2013**, *117*, 13561-13571.
[94] G. Mistlberger, G. A. Crespo, X. Xie, E. Bakker, *Chem. Commun.* **2012**, *48*, 5662-5664.
[95] The pKa-valuse has been used as listed on https://scifinder.cas.org; 21.04.2017, 10:50. The pKa-values has been calculated using Advanced Chemistry Development (ACD/Labs) Software V11.02 (© 1994-2017 ACD/Labs). For further details: http://www.acdlabs.com/products/percepta/predictors/pka/ ; 21.04.2017, 12:56.
[96] A. Hantzsch, *Berichte der deutschen chemischen Gesellschaft (A and B Series)* **1927**, *60*, 2537-2545.
[97] M. Irie, *Chem. Rev.* **2000**, *100*, 1685-1716.
[98] X.-M. Zhang, F. G. Bordwell, *J. Org. Chem.* **1994**, *59*, 6456-6458.
[99] a) R. Gompper, *Chem. Ber.* **1956**, *89*, 1762-1768; b) G. H. Hakimelahi, C. B. Boyce, H. S. Kasmai, *Helv. Chim. Acta* **1977**, *60*, 342-347.
[100] Y. Tanabe, N. Matsuo, N. Ohno, *J. Org. Chem.* **1988**, *53*, 4582-4585.

[101] A. Hantzsch, *Berichte der deutschen chemischen Gesellschaft (A and B Series)* **1928**, *61*, 1776-1788.

[102] A. Ané, G. Prestat, M. Thiam, S. Josse, M. Pipelier, J. P. Pradère, D. Dubreuil, *Nucleosides, Nucleotides and Nucleic Acids* **2002**, *21*, 335-360.

[103] R. Dahlbom, S. Gronowitz, B. Mathiasson, *Acta Chem. Scand.* **1963**, *17*, 2479-2486.

[104] B. Jawabrah Al-Hourani, F. Richter, K. Vrobel, K. Banert, M. Korb, T. Rüffer, B. Walfort, H. Lang, *Eur. J. Org. Chem.* **2014**, *2014*, 2899-2906.

[105] Patent: Sumitomo Chemical Co.; Y. Yuya, T. Teruki, O. Daisuke, A. Shuhe; WO2013JP62982 20130426; 2013.

[106] a) S. P. Cornwell, P. T. Kaye, A. G. Kent, G. D. Meakins, *J. Chem. Soc., Perkin Trans. 1* **1981**, 2340-2343; b) K. Banert, B. J. Al-Hourani, S. Groth, K. Vrobel, *Synthesis* **2005**, *2005*, 2920-2926.

[107] N. F. Langille, L. A. Dakin, J. S. Panek, *Org. Lett.* **2002**, *4*, 2485-2488.

[108] a) E. Ochiai, F. Nagasawa, *Berichte der deutschen chemischen Gesellschaft (A and B Series)* **1939**, *72*, 1470-1476; b) G. Swain, *J. Chem. Soc. Pak.* **1949**, 2898-2901; c) T. Sasaki, A. Nakanishi, M. Ohno, *Chem. Pharm. Bull.* **1982**, *30*, 2051-2060; d) T. P. Bochkareva, B. V. Passet, K. R. Popov, N. V. Platonova, T. I. Koval'chuk, *Chemistry of Heterocyclic Compounds* **1987**, *23*, 1084-1089.

[109] H. Yamazaki, H. Harada, K. Matsuzaki, K. Yoshioka, M. Takase, E. Ohki, *Chem. Pharm. Bull.* **1990**, *38*, 45-48.

[110] a) D. Tavernier, S. van Damme, P. Ricquier, M. J. O. Anteunis, *Bull. Soc. Chim. Belg.* **1988**, *97*, 859-866; b) F. C. Gaenzler, M. B. Smith, *Synlett* **2007**, *2007*, 1299-1301.

[111] a) T. Nagamatsu, T. Kunieda, *Tetrahedron Lett.* **1987**, *28*, 2375-2378; b) F. C. Gaenzler, C. Guo, Y.-W. Zhang, M. E. Azab, M. A. I. Salem, D. P. Fan, M. B. Smith, *Tetrahedron* **2009**, *65*, 8781-8785; c) I. I. F. Boogaerts, G. C. Fortman, M. R. L. Furst, C. S. J. Cazin, S. P. Nolan, *Angew. Chem. Int. Ed.* **2010**, *49*, 8674-8677.

[112] H. Fukumi, K. Oohata, K. Takada, *Heterocycles* **1979**, *12*, 1297-1299.

[113] Q. Wang, X. Tan, Z. Zhu, X.-Q. Dong, X. Zhang, *Tetrahedron Lett.* **2016**, *57*, 658-662.

[114] H. Greenberg, T. Van Es, O. G. Backeberg, *J. Org. Chem.* **1967**, *32*, 2964-2966.

[115] R. Gompper, F. Effenberger, *Chem. Ber.* **1959**, *92*, 1928-1934.

[116] A. Padwa, L. A. Cohen, *J. Org. Chem.* **1984**, *49*, 399-406.

[117] S. E. Whitney, B. Rickborn, *J. Org. Chem.* **1991**, *56*, 3058-3063.

[118] Takeda Chemical Industries, Ltd. Patent: EP1219610 A1, 2002

[119] Merrell Dow Pharmaceuticals Inc. Patent: US4866182 A1, 1989.

[120] Synthesis and experimental protocols were planned by me and conducted by J. Schwarz.

[121] M. Y. Belikov, M. Y. Ievlev, I. V. Belikova, O. V. Ershov, V. A. Tafeenko, M. D. Surazhskaya, *Chemistry of Heterocyclic Compounds* **2015**, *51*, 518-525.

[122] Y. Seigo, K. Hiroaki, S. Tetsuyuki, K. Shigeo, *Chem. Lett.* **1996**, *25*, 139-140.

[123] S. Iwata, Y. Ishihara, C. P. Qian, K. Tanaka, *J. Org. Chem.* **1992**, *57*, 3726-3727.

[124] A. H. Mustafa, M. K. Shepherd, *Chem. Commun.* **1998**, 2743-2744.

[125] E. Vicente-García, R. Ramón, R. Lavilla, *Synthesis* **2011**, *2011*, 2237-2246.

[126] A. Hantzsch, J. H. Weber, *Berichte der deutschen chemischen Gesellschaft* **1887**, *20*, 3118-3132.

[127] Y. Yoshimoto, T. Takahashi, D. Oohira, S. Azuma, C07D 413/12 ed., Sumitomo Chemical Company, **2013**.

[128] L. I. Smith, J. Nichols, *J. Org. Chem.* **1941**, *06*, 489-506.

[129] E. Hiroshi, K. Kenji, K. Kazuhiro, Y. Minoru, M. Masaaki, I. Takaaki, I. Noriko, (Ed.: S. P. C. Ltd.), Japan, **2009**.

[130] T. I. Crowell, G. C. Helsley, R. E. Lutz, W. L. Scott, *J. Am. Chem. Soc.* **1963**, *85*, 443-446.

[131] A. Hantzsch, *Liebigs Ann.* **1889**, *250*, 257-273.

[132] H. Gilman, L. Summers, *J. Am. Chem. Soc.* **1950**, *72*, 2767-2768.

[133] Y. Chen, D. X. Zeng, M. G. Fan, *Org. Lett.* **2003**, *5*, 1435-1437.

[134] G. M. Sheldrick, SADABS, program for empirical absorption correction of area detector data, University of Göttingen, Göttingen, 1996.

[135] G. M. Sheldrick, SHELXT-2013, Program for Crystal Structure Solution, University of Göttingen, Göttingen, 2013.

[136] G. M. Sheldrick, SHELXL-2014, Program for Crystal Structure Refinement, University of Göttingen, Göttingen, 2014.

[137] a) C. Hatchard, C. Parker, *Proceedings of the Royal Society of London. Series A. Mathematical and Physical Sciences* **1956**, *235*, 518; b) M. Montalti, A. Credi, L. Prodi, M. T. Gandolfi, *Handbook of Photochemistry, Third Edition*, CRC Press, Boca Raton, **2006**.

[138] T. Sumi, Y. Takagi, A. Yagi, M. Morimoto, M. Irie, *Chem. Commun.* **2014**, *50*, 3928-3930.

[139] L. G. Gagliardi, C. B. Castells, C. Ràfols, M. Rosés, E. Bosch, *Journal of Chemical & Engineering Data* **2007**, *52*, 1103-1107.

[140] M. J. Frisch, G. W. Trucks, H. B. Schlegel, G. E. Scuseria, M. A. Robb, J. R. Cheeseman, G. Scalmani, V. Barone, B. Mennucci, G. A. Petersson, Gaussian, Inc., Wallingford CT, **2009**.

[141] J. Ho, M. L. Coote, *Theor. Chem. Acc.* **2009**, *125*, 3.

[142] N. Mathivanan, R. A. McClelland, S. Steenken, *J. Am. Chem. Soc.* **1990**, *112*, 8454-8457.

[143] a) S. A. Kovalenko, A. L. Dobryakov, J. Ruthmann, N. P. Ernsting, *Physical Review A* **1999**, *59*, 2369-2384; b) A. L. Dobryakov, S. A. Kovalenko, A. Weigel, J. L. Pérez-Lustres, J. Lange, A. Müller, N. P. Ernsting, *Rev. Sci. Instrum.* **2010**, *81*, 113106.

7 APPENDIX

7.1 LIST OF ABBREVIATIONS (ALPHABETIC)

$CHCl_3$	Chloroform
EI	Electron Impact Ionization
ESI	Electrospray ionization
eq.	Equivalents
DAE	Diarylethene
DCM	Dichloromethane
DTE	Dithienylethene
GC	Gas Chromatography
HOMO	Highest Occupied Molecular Orbital
LUMO	Lowest Unoccupied Molecular Orbital
NMR	Nuclear magnetic resonance spectroscopy
MS	Mass spectrometry
Oxazolone	3*H*-oxazol-2-one
PES	Potential energy surface
PSS	Photo stationary state similar
r.t.	room temperature
TA	Transient absorption
TfOH	Trifluoromethanesulfonic acid
Thiazolone	3*H*-thiazol-2-one
TLC	Thin layer chromatography
TOF	Time-of-flight
UPLC	Ultra Preformation Liquid Chromatography
QMS	Quadrupole Mass Spectrometer

7.2 Further Spectroscopic Details

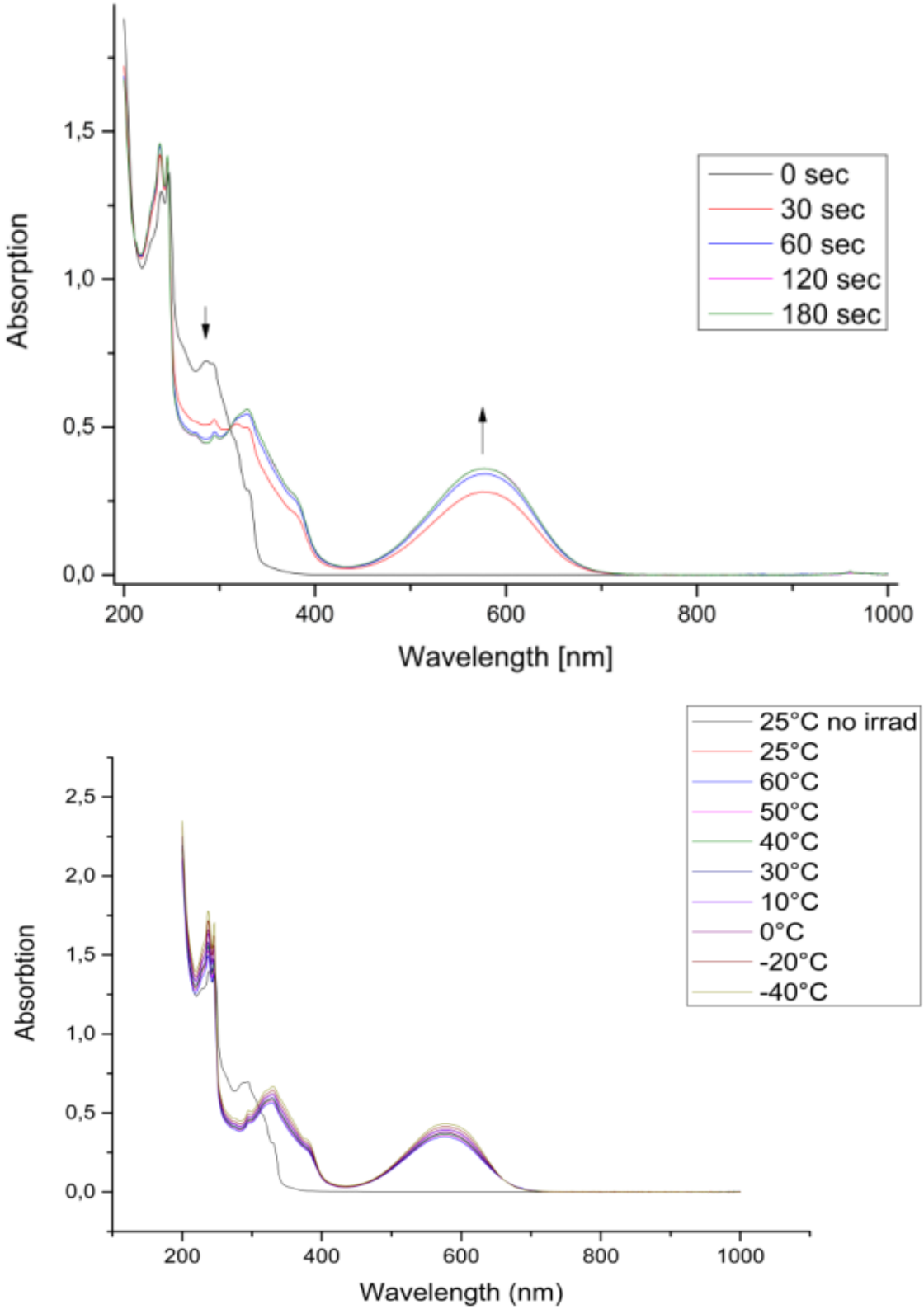

*Figure 7-1 Spectroscopic analysis of **3-1c** in acetonitrile: Right: Temperature dependence absorption spectrum; UV/vis trace shows the evolution of the closed isomer upon light irradiation of a $1.88 \cdot 10^{-5}$M solution (acetonitrile 1 vol% water) 1o with 302 nm light in a 1 cm cuvette after 0 sec, 30 sec, 60 sec, 120 sec and 180 sec.*

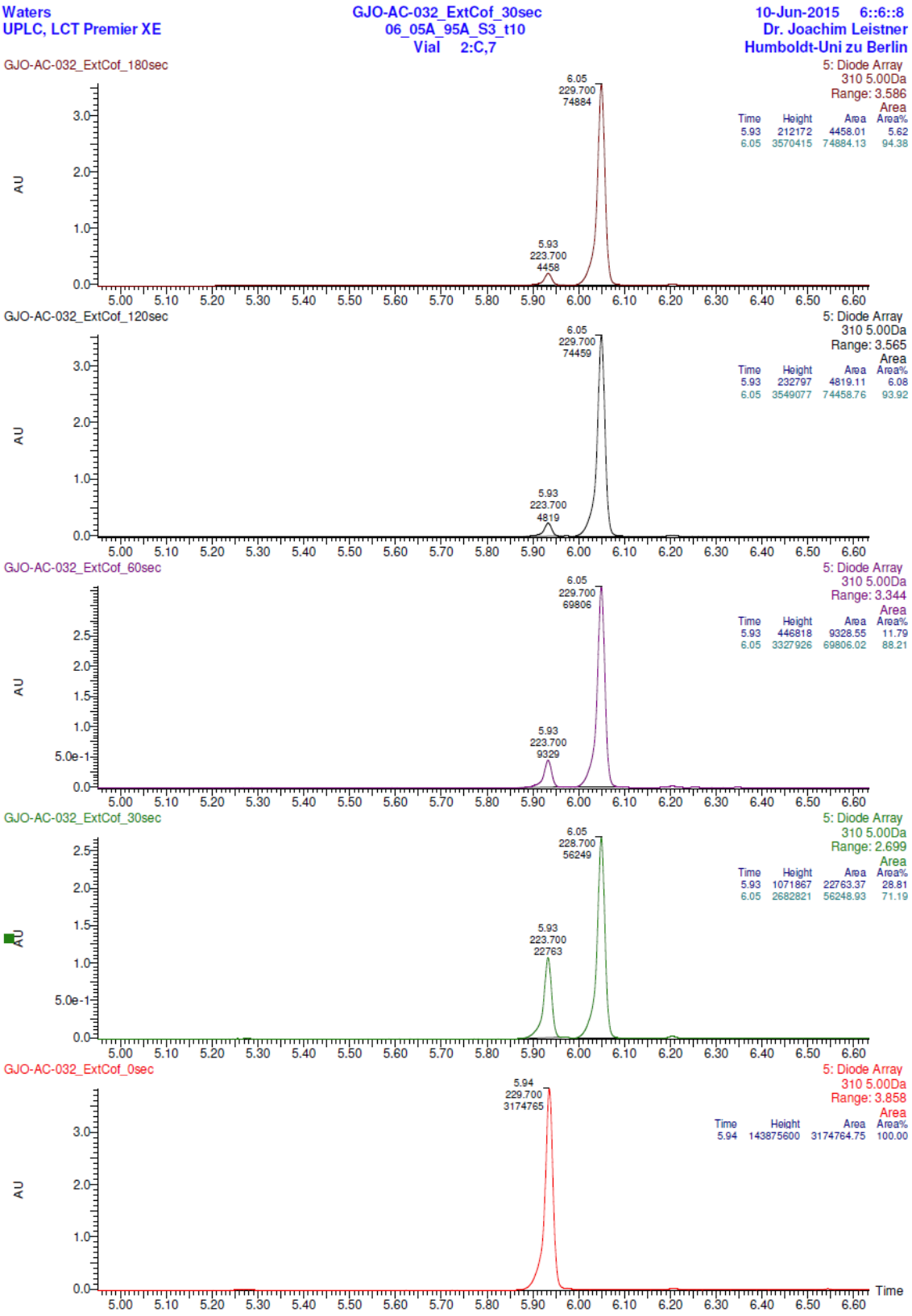

Figure 7-2 UPLC separation of the irradiated solutions shown in Figure 7-1 detected at 310 nm and integrated to determine the ratio of the open to the closed isomer; from 0 sec (bottom) to 180 sec (top) irradiation time.

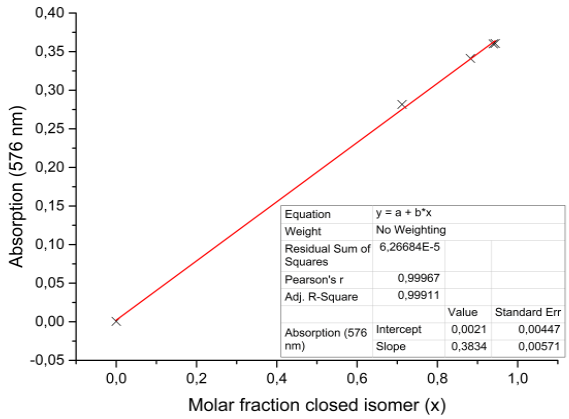

Figure 7-3 Linear Plot of the conversion measured in Figure 7-2 vs. absorption at 576 nm from Figure 7-1.

*Table 7-1 Temperature dependence absorption spectrum of the **3-1c**.*

TEMPERATURE /°C	***ABSORPTION (576 NM)***	***ε /L CM^{-1} MOL^{-1}***
25	0.375 ± 0.004	20565 ± 350
60	0.349 ± 0.003	19124 ± 710
50	0.357 ± 0.004	19600 ± 720
40	0.366 ± 0.004	20075 ± 740
30	0.373 ± 0.004	20467 ± 760
10	0.389 ± 0.004	21350 ± 790
0	0.397 ± 0.004	21770 ± 800
-20	0.413 ± 0.004	22654 ± 840
-40	0.431 ± 0.004	23648 ± 870

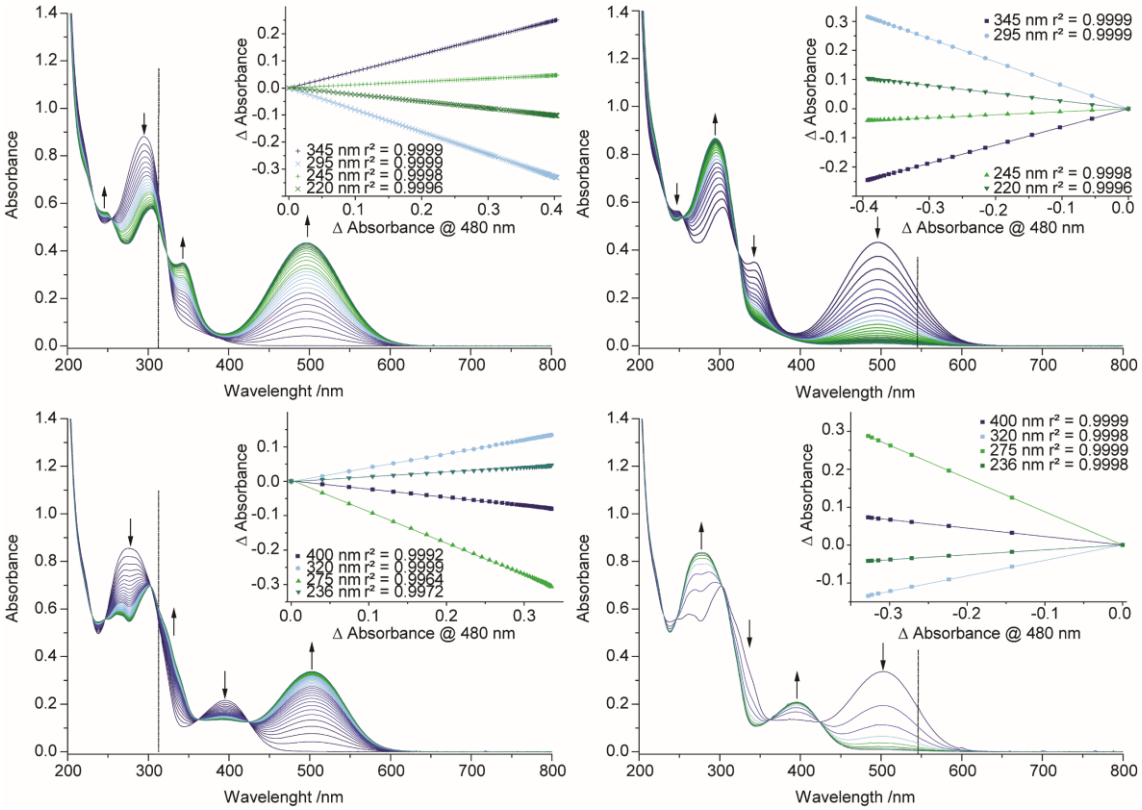

*Figure 7-4 UV/vis spectra describing the photochemical behavior of the **4-4** in acetonitrile (C ≈ 10-5 M) and evaluation of its quality at 25 °C under acidic conditions, by storage over acidic cation exchanger (a-b) or after treatment of the solution with an excess of washed sodium hydride(c-d): inserts show the Mauser diagram with linear fit: (a+c) irradiation with 313 nm; (b+d) irradiation with 546 nm.*

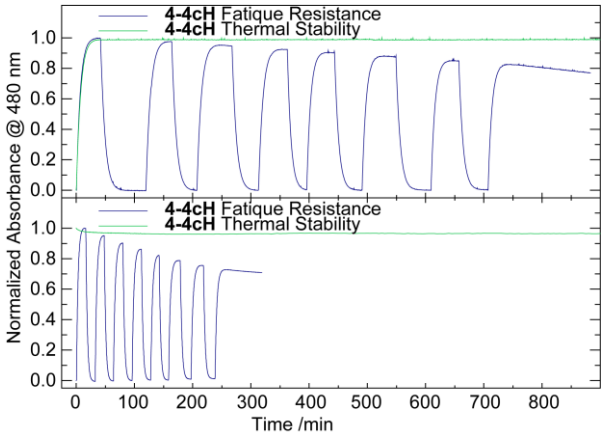

*Figure 7-5 Fatigue and thermal stability of **4-4cH** and **4-4c** at 25°C in acetonitrile.*

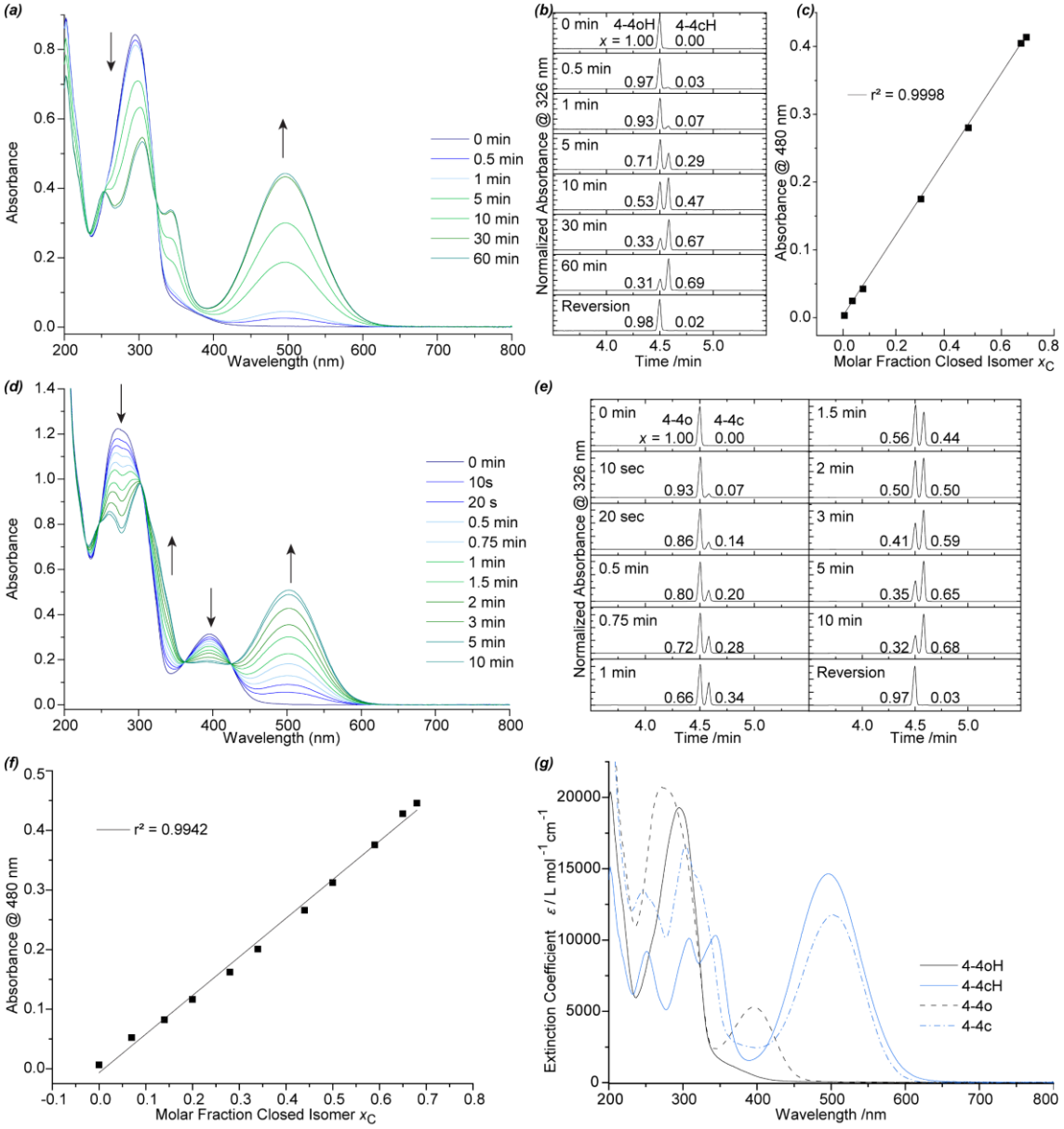

*Figure 7-6 Determination of the extinction coefficient of **4-4**, in acetonitrile at 25 °C under acidic conditions (storage over acidic cation exchanger) (a-c) or after treatment of the solution with an excess of washed sodium hydride (d-f): (a+d) UV/vis spectra after different irradiation times with 313 nm light of a 5.90 · 10^{-5} M 1oH or 1o solution; (b+e) UPLC traces observed at 326 nm after irradiation times as described with 313 nm light and the molar fraction of open and closed isomer determined by integration of the peaks; (c+f) Plot of the absorbance at 480 nm vs. the molar fraction of the closed isomer giving a linear behavior; (g) resulting extinction coefficient of all four species in acetonitrile (**4-4oH**, **4-4o**, **4-4cH** & **4-4c**).*

Table 7-2 Spectroscopic and photochemical data in dependence of the protonation state in acetonitrile; [a] monochromator bandwidth.

	λ_{max} /nm	λ_{irrad} /nm	ε_{max} / l·mol^{-1}·cm^{-1}	ε_{313nm} / l·mol^{-1}·cm^{-1}	ε_{546nm} / l·mol^{-1}·cm^{-1}	x_C^{PSS}	φ
4-4oH	295 ± 1	313 ± 6[a]	19300	14200		0.60	0.056
4-4cH	495 ± 1	546 ± 6[a]	14600	9600	7600	0.02	0.053
4-4o	273 ± 1	313 ± 6[a]	20700	12900		0.67	0.41
4-4c	303 ± 1	546 ± 6[a]	16600	14900	6400	0.03	0.17

7.3 NMRs of the Target Molecules

hefe0301-500.10.1.1r
Gurke GJO-AC-032-3

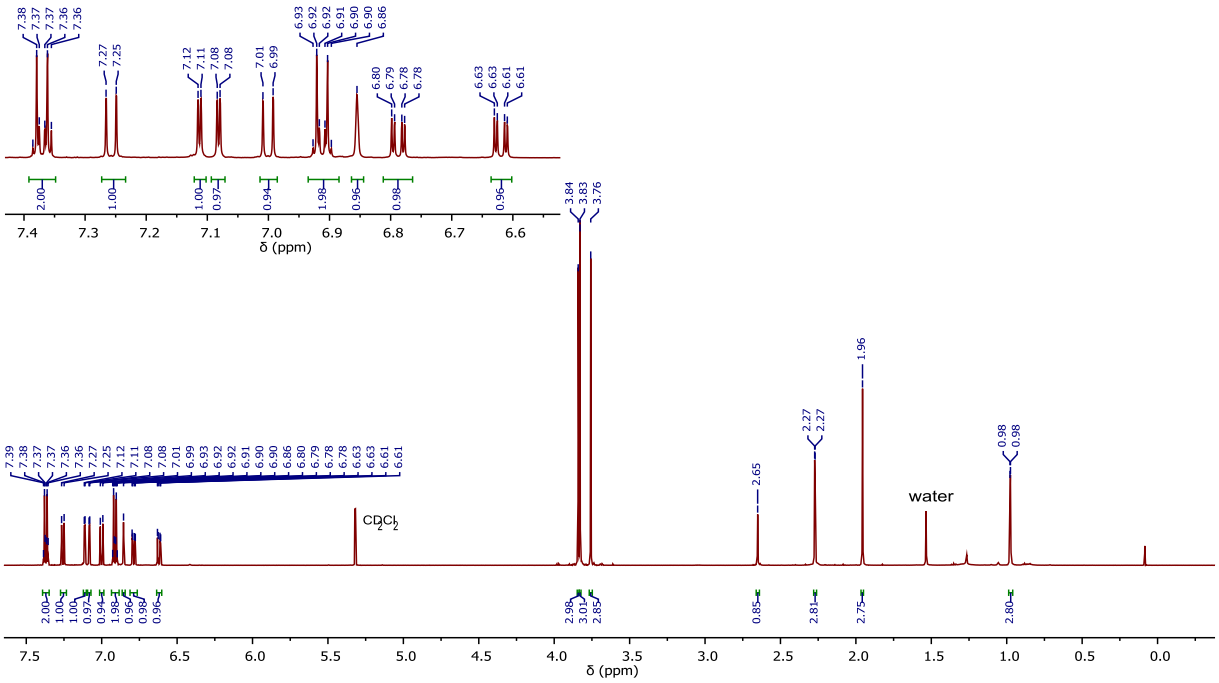

*Figure 7-7 ^{1}H-NMR spectrum of compound **3-1o** in deuterated DCM (25 °C).*

hefe0301-500.11.1.1r
Gurke GJO-AC-032-3

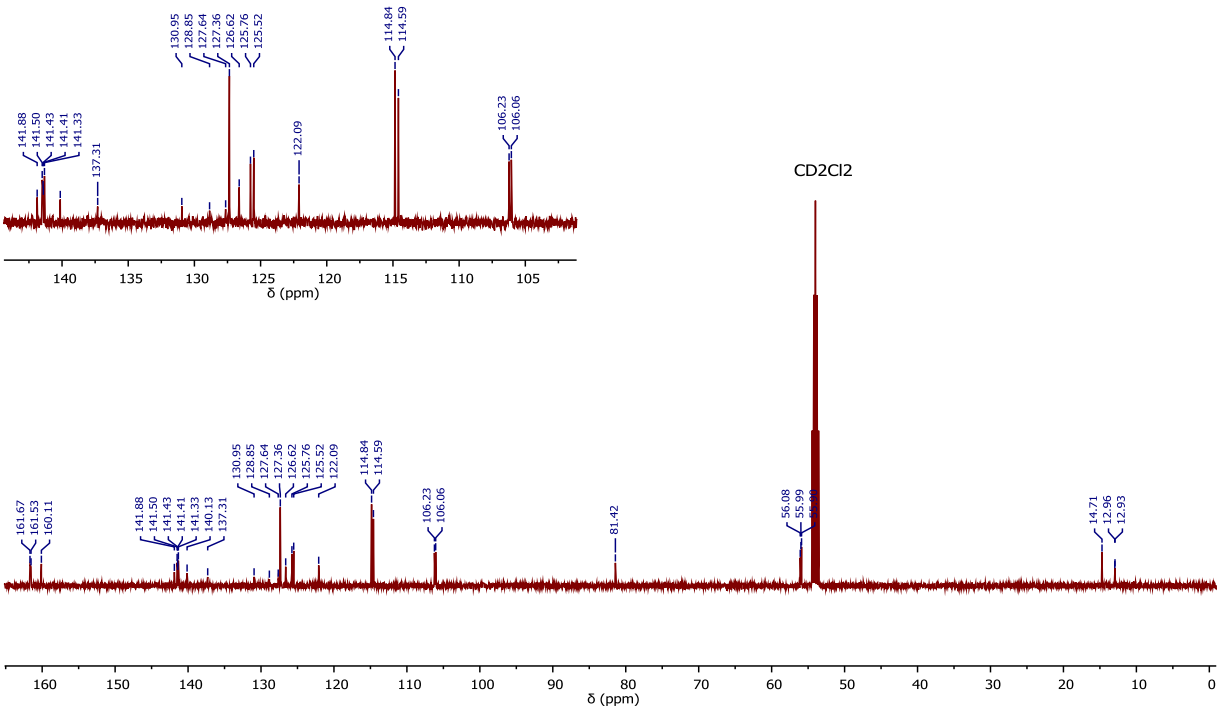

*Figure 7-8 ^{13}C-NMR spectrum of compound **3-1o** in deuterated DCM (25 °C).*

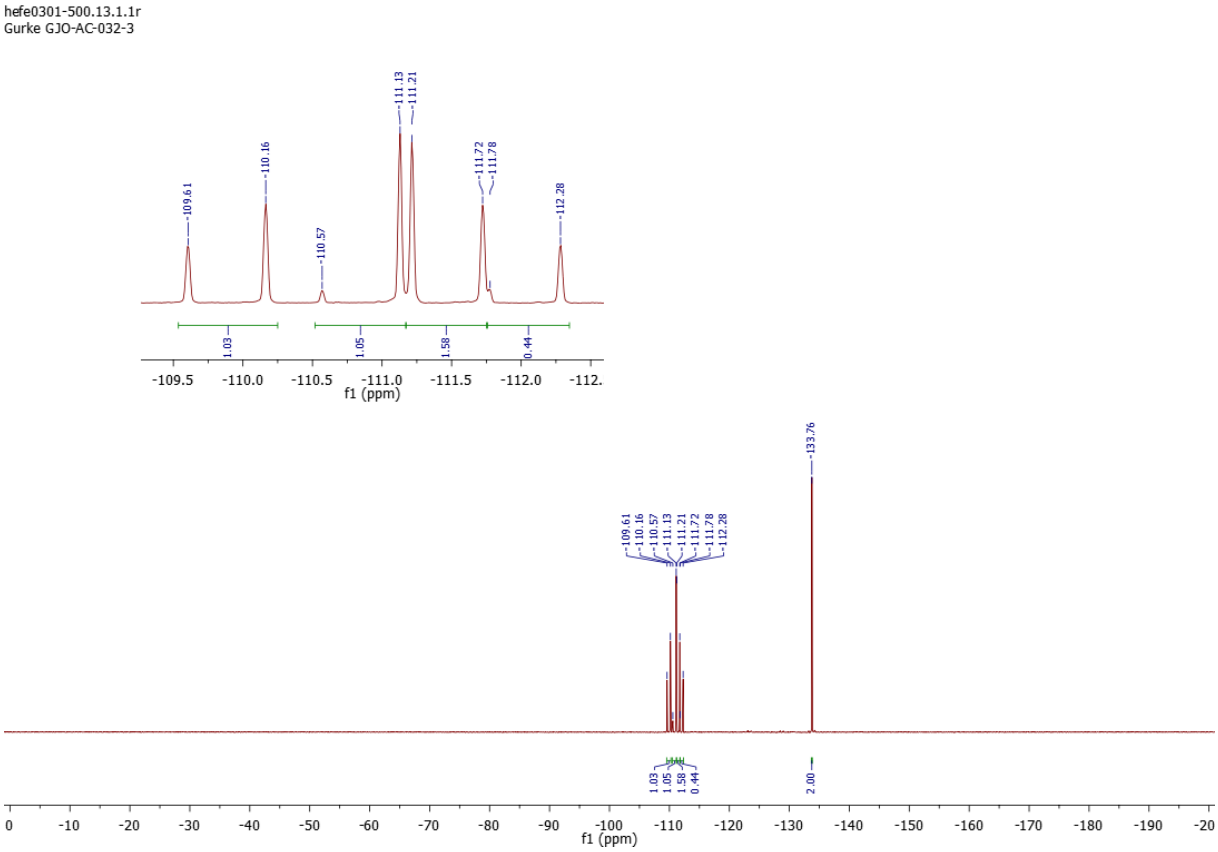

*Figure 7-9 [19]F-NMR spectrum of compound **3-1o** in deuterated DCM (25 °C).*

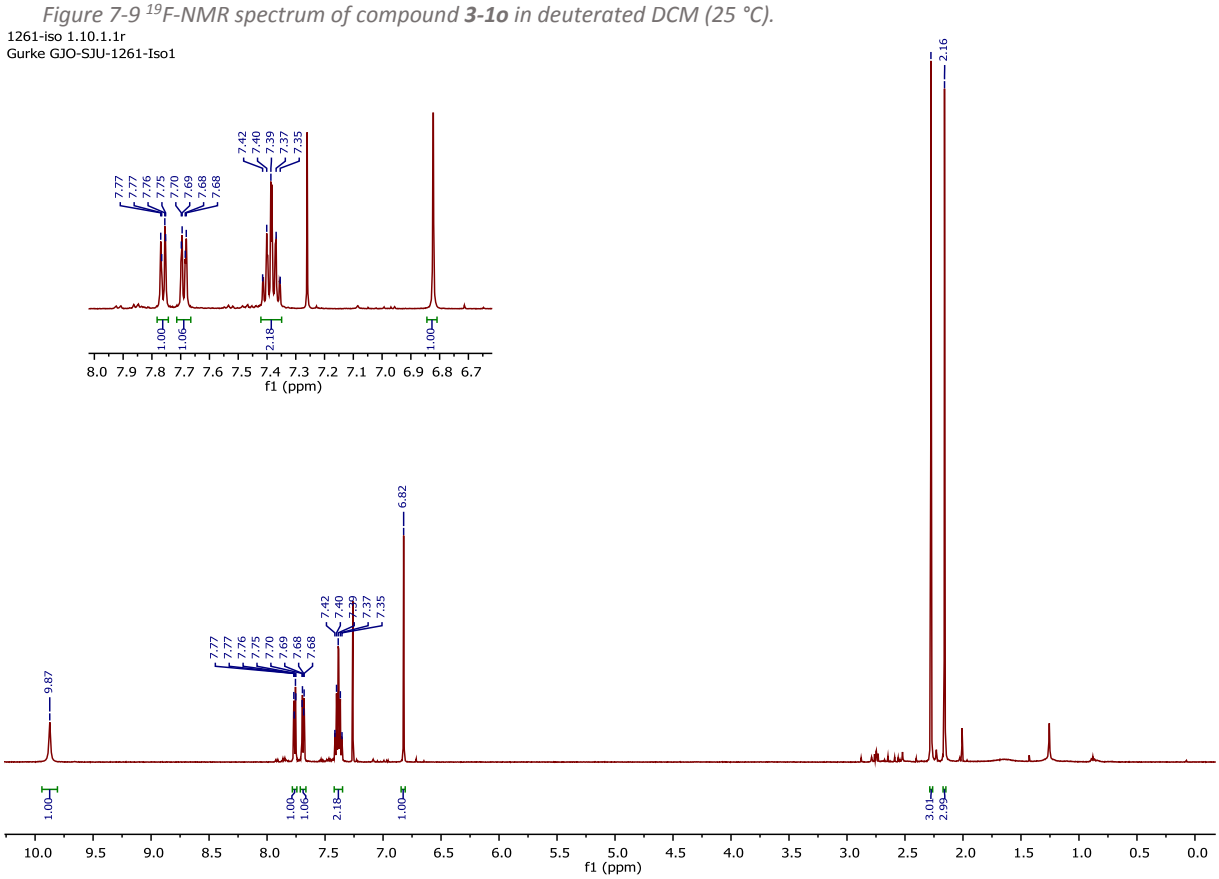

*Figure 7-10 [1]H-NMR spectrum of compound **4-1** Isomer 1 in deuterated chloroform (25 °C).*

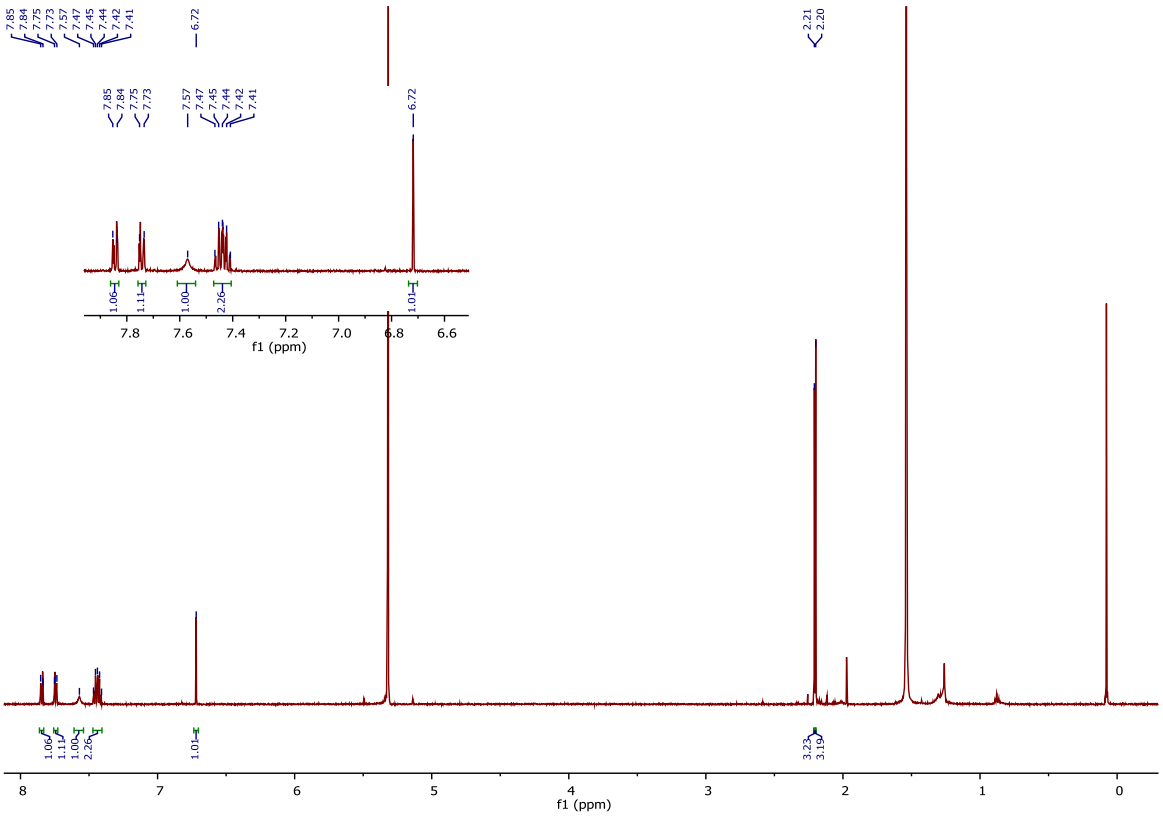

*Figure 7-11 [1]H-NMR spectrum of compound **4-1** Isomer 2 in deuterated DCM (25 °C).*

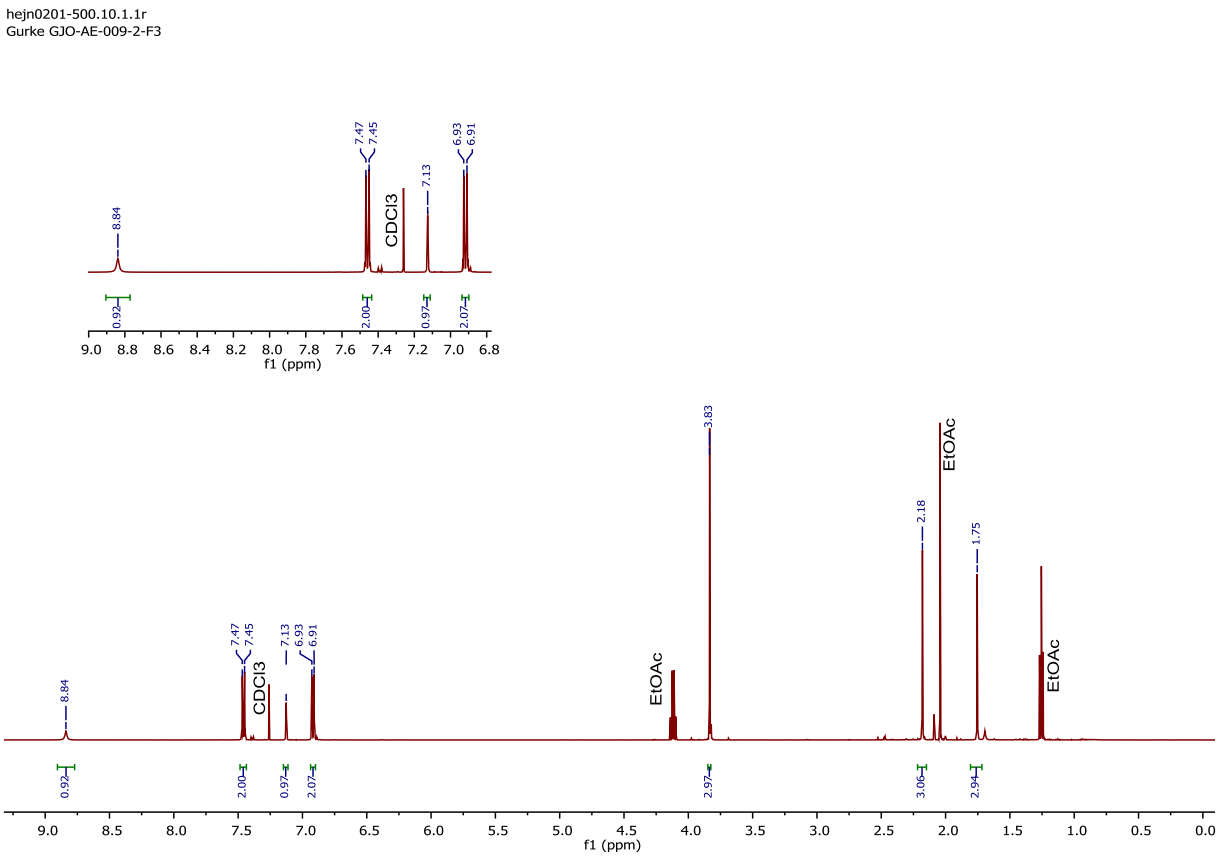

*Figure 7-12 [1]H-NMR spectrum of compound **4-2oH** in deuterated chloroform (25 °C).*

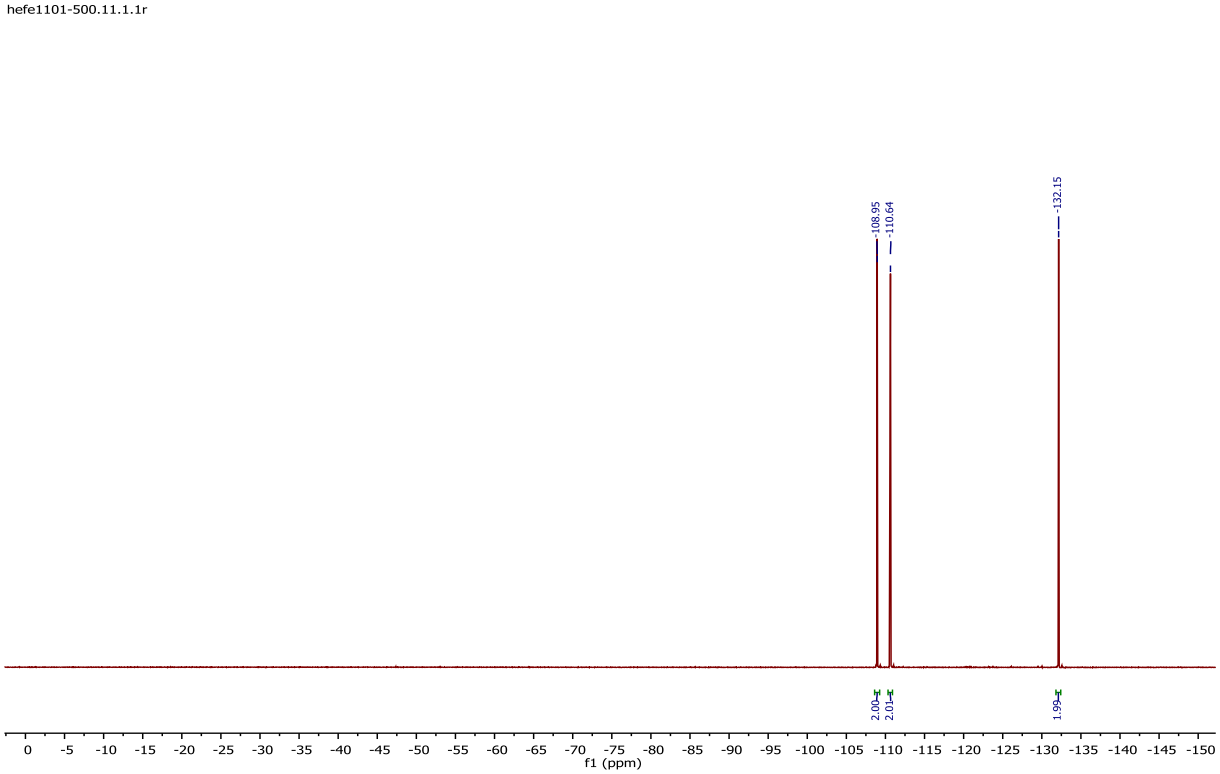

*Figure 7-13 19F-NMR spectrum of compound **4-2oH** in deuterated chloroform (25 °C).*

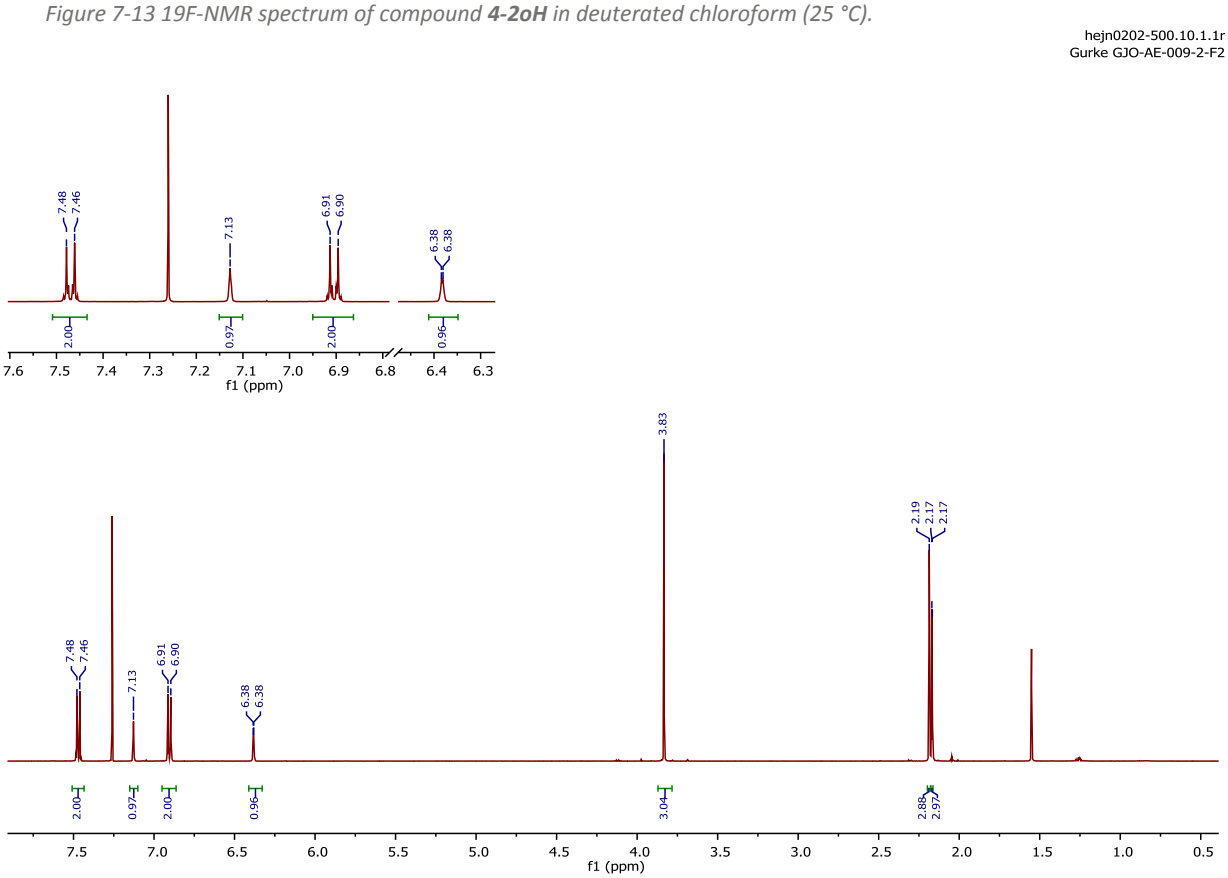

*Figure 7-14 ^{1}H-NMR spectrum of compound **4-2oH** in deuterated chloroform (25 °C).*

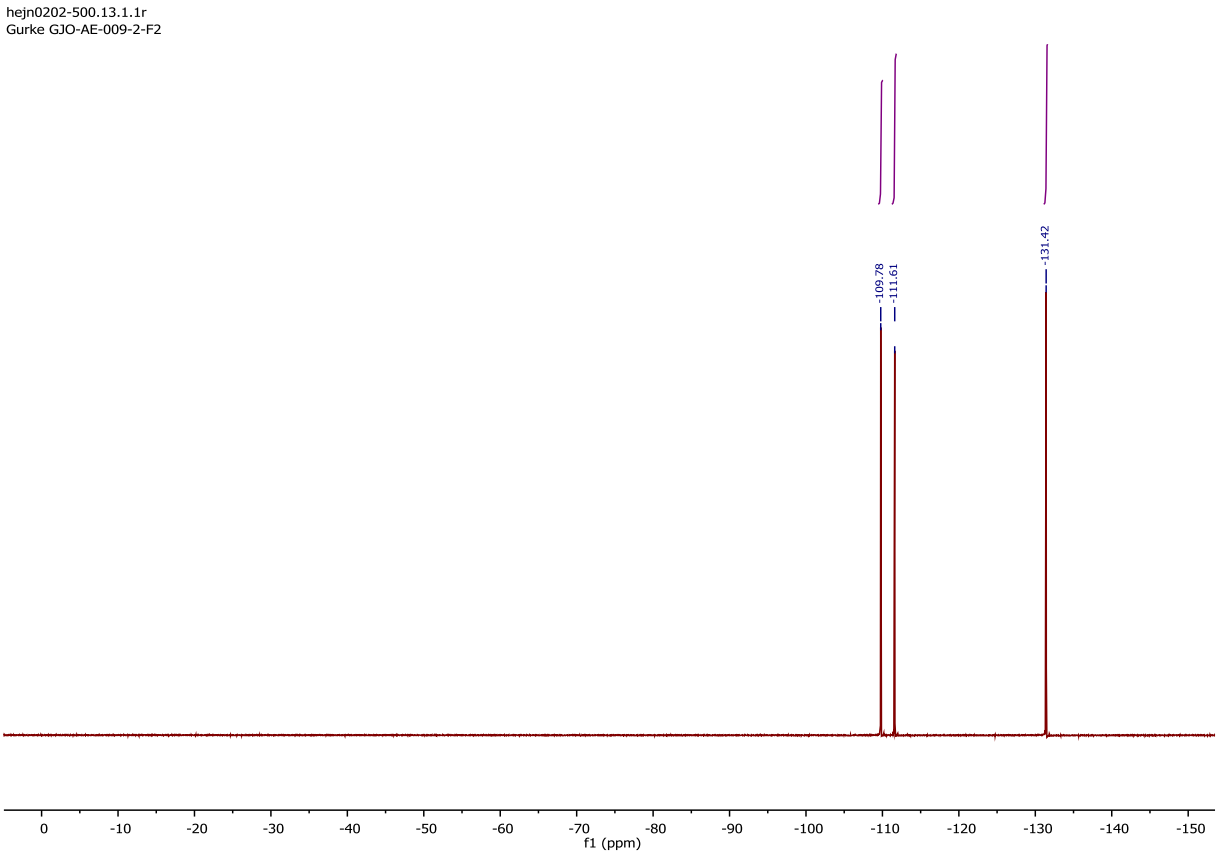

*Figure 7-15 ^{19}F-NMR spectrum of compound **4-13** in deuterated chloroform (25 °C).*

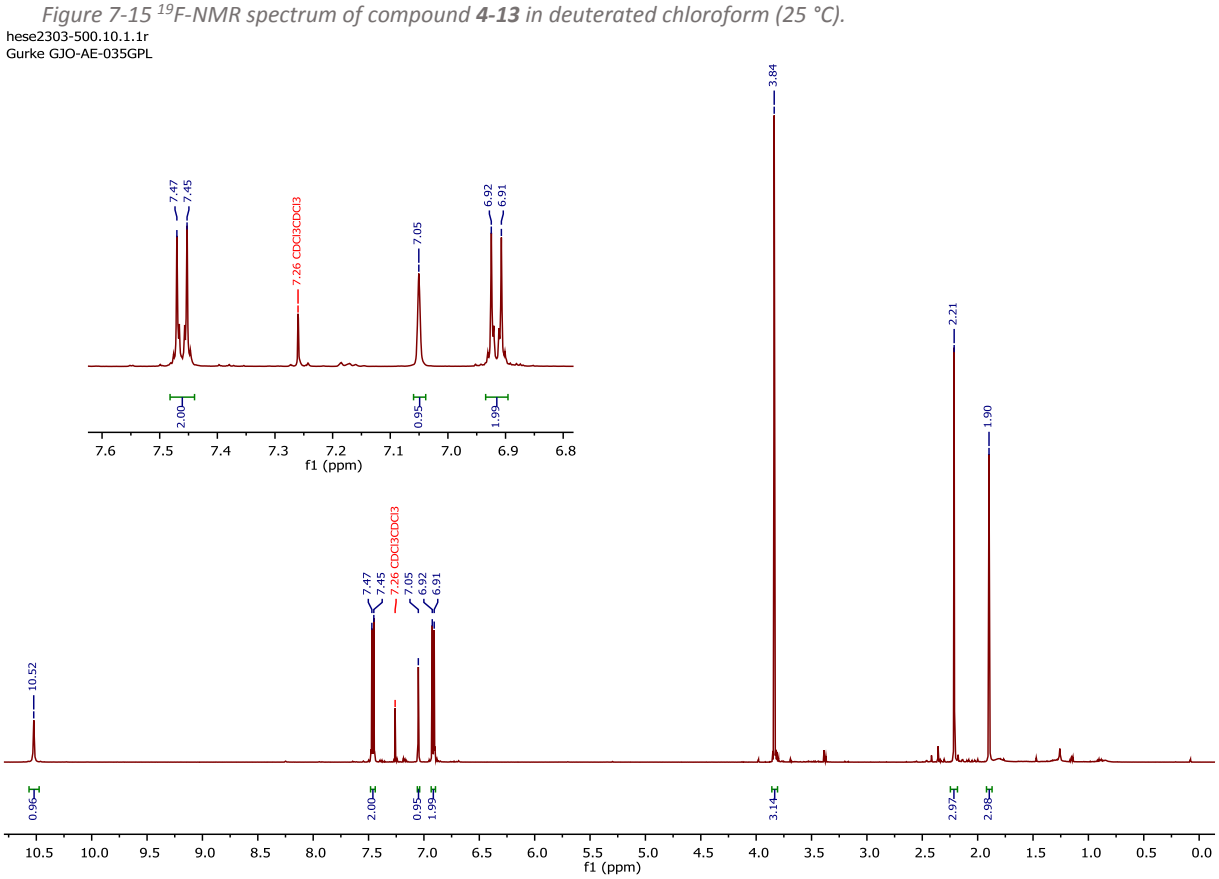

*Figure 7-16 1H-NMR spectrum of compound **4-3oH** in deuterated chloroform (25 °C).*

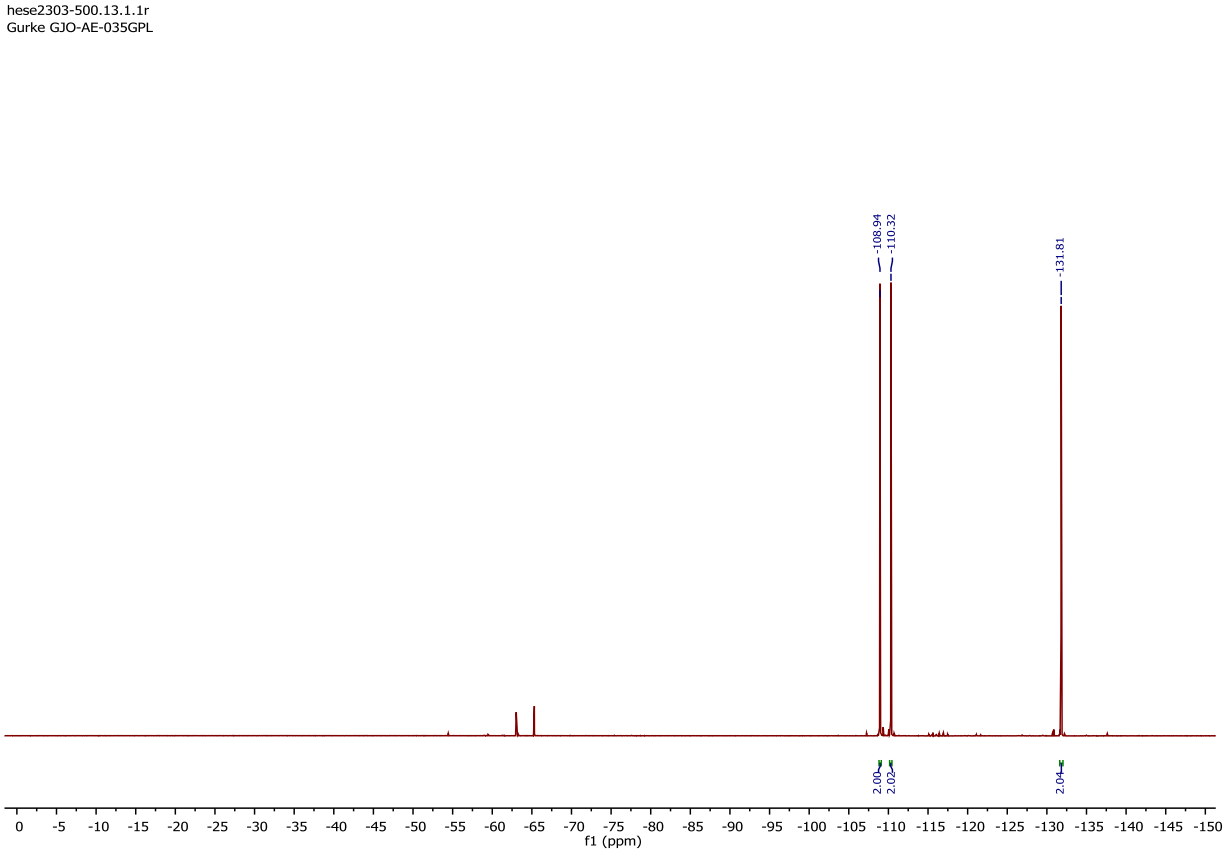

*Figure 7-17 ^{19}F-NMR spectrum of compound **4-3oH** in deuterated chloroform (25 °C).*

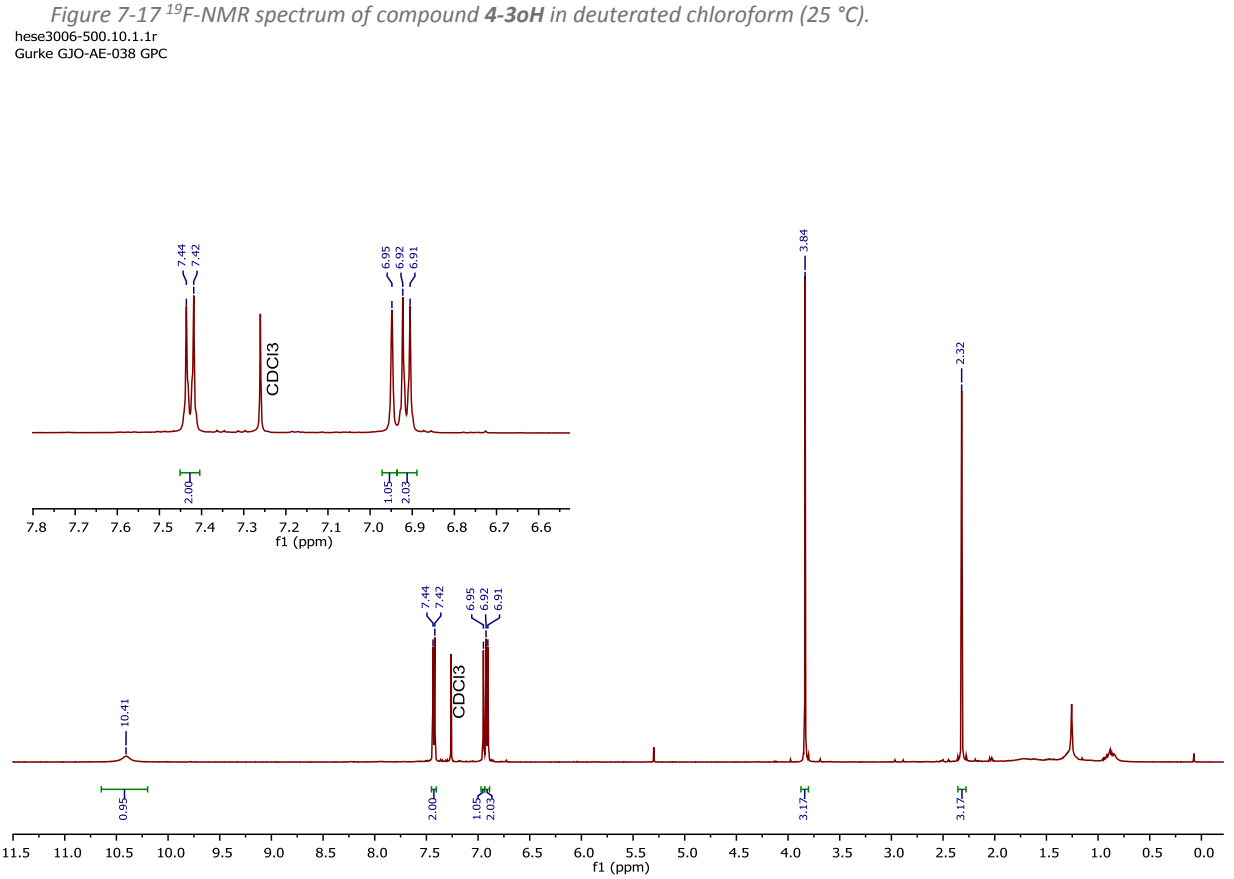

*Figure 7-18 ^{1}H-NMR spectrum of compound **4-4oH** in deuterated chloroform (25 °C).*

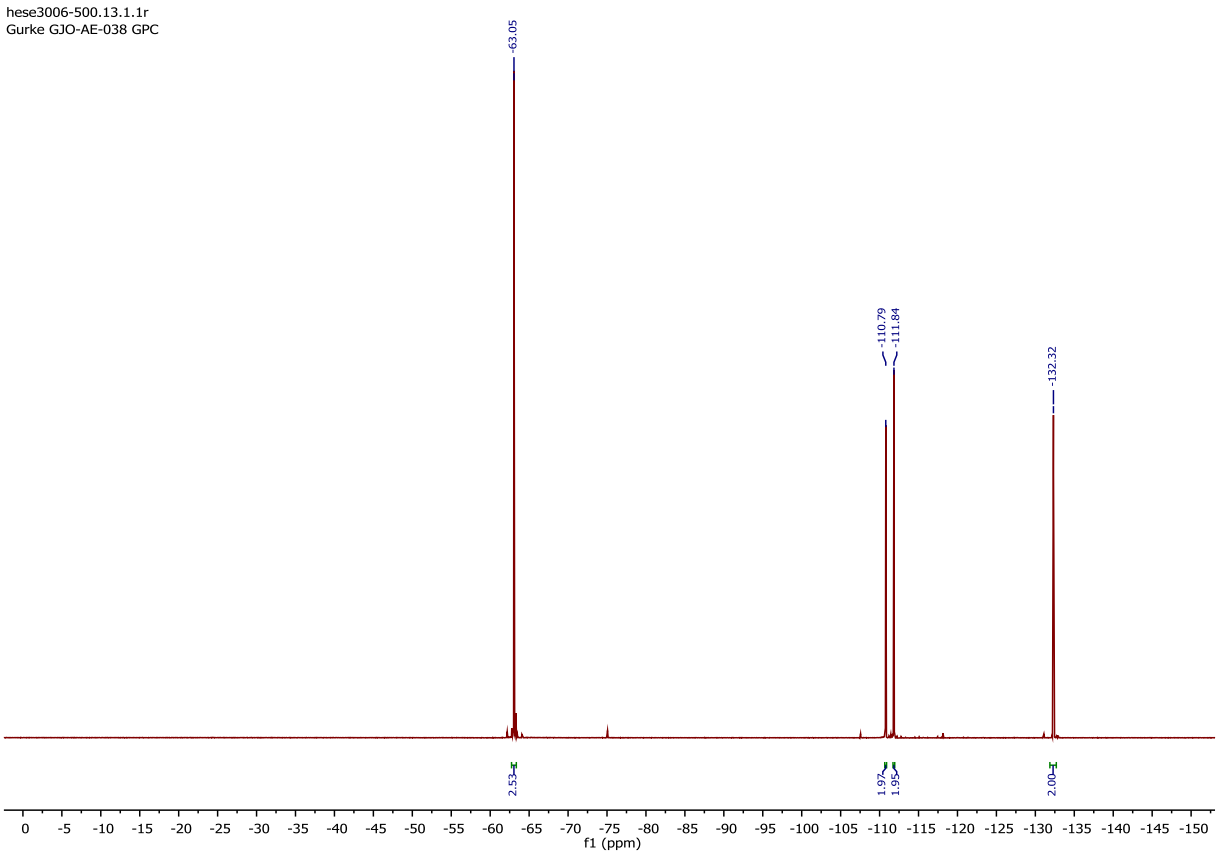

*Figure 7-19 ^{19}F-NMR spectrum of compound **4-4oH** in deuterated chloroform (25 °C).*

7.4 Computational Details, Calculated Structures and Detailed Results

7.4.1 Acid-catalyzed Cycloreversion

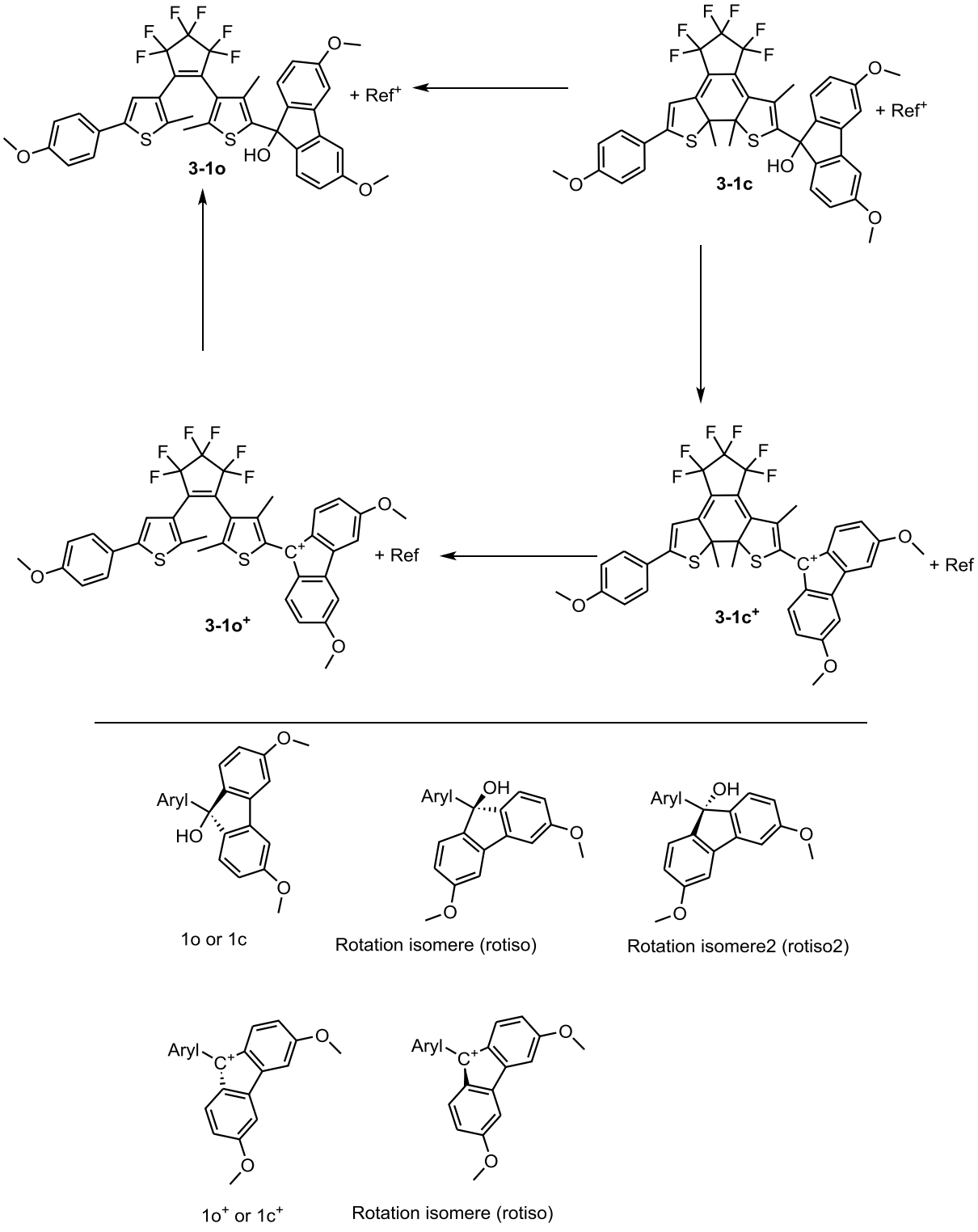

Scheme 7-1 All calculated structures.

Table 7-3 Total energy of all calculated structures.

in Hartree/Particle	*Opt*		*Freq*	*MeCN/aq*	
	ε_{gas}	G_{corr}	ΔG_{solv}	$E_{gas}+G_{corr}=G_{gas}$	$E_{gas} + G_{corr} +\Delta G_{solv}=G_{sol}$
3-1o	-3162.4767	0.5118	-0.0432	-3161.9649	-3162.0082
3-1o_rotiso	-3162.4729				
3-1o_rotiso2	-3162.4735				
3-1o⁺	-3086.4326	0.5024	-0.0939	-3085.9302	-3086.0241
3-1o⁺_rotiso	-3086.4299				
3-1c	-3162.4545	0.5191	-0.0437	-3161.9354	-3161.9791
3-1c_rotiso	-3162.4518				
3-1c_rotiso2	-3162.4522				
3-1c⁺	-3086.4200	0.5075	-0.0880	-3085.9125	-3086.0005
3-1c⁺_rotiso	-3086.4185				
3-1c_ts	-3162.4011	0.5141	-0.0425	-3161.8870	-3161.9295
3-1c⁺_ts	-3086.3872	0.5053	-0.0907	-3085.8819	-3085.9726
Ref	-808.8988	0.2497	-0.0230	-808.6490	-808.6721
Ref⁺	-732.8420	0.2386	-0.0747	-732.6034	-732.6781

Table 7-4 Calculated energetic of the reaction paths in kJ/mol.

REACTION	ΔG_{GAS}	ΔG_{SOL}
Closed dehydration (**3-1c** → **3-1c⁺**)	-22	-2
Charged cycloreversion (**3-1c⁺** → **3-1o⁺**)	-46	-62
Open hydration (**3-1o⁺** → **3-1o**)	-9	-12
Open dehydration (**3-1o** → **3-1o⁺**)	9	12
Uncharged cycloreversion (**3-1c** → **3-1o**)	-78	-76
Transition state charged cycloreversion (**3-1c⁺** → **3-1TS⁺**)	80	73
Transition state uncharged cycloreversion (**3-1c** → **3-1TS**)	127	130

Uncharged open 1o

```
Charge = 0 Multiplicity = 1
 Symbolic Z-Matrix:
 C          -1.66456  2.09451  1.35302
 C          -0.49658  1.52613  1.75871
 C          -2.59906  1.64375  0.30982
 C           0.02907  0.18863  1.42209
 C          -0.70536 -0.95457  1.68621
 S           0.19826 -2.37558  1.2849
 C           1.57321 -1.4383   0.75323
 C           1.34657 -0.08786  0.88346
 C          -4.01581  1.51706  0.5225
 C          -4.71322  1.08413 -0.57688
 S          -3.61082  0.85647 -1.92228
 C          -2.22206  1.31907 -0.98224
 C           2.79057 -2.17233  0.21693
 C          -2.08112 -1.09393  2.27376
 C          -0.86673  1.35545 -1.62299
 C          -6.15511  0.83538 -0.70708
 C          -0.92548  3.36348  3.28186
 C          -6.66658 -0.14313 -1.58444
 C          -8.03096 -0.37947 -1.68699
 C           0.19146  2.40719  2.78478
 C          -8.93654  0.35513 -0.9058
 C          -8.45131  1.33443 -0.02914
 C          -1.9203   3.39103  2.09324
 C          -7.07692  1.56906  0.0562
 C           4.12401 -1.72865  0.82712
 C           5.04331 -1.37662 -0.18215
 C           4.37562 -1.51728 -1.49081
 C           3.05968 -1.95424 -1.27676
 C           4.86246 -1.2863  -2.78128
 C           4.00028 -1.5102  -3.86517
 C           2.68211 -1.95626 -3.65181
 C           2.21026 -2.17689 -2.35843
 C           4.49957 -1.68207  2.15914
 C           5.80144 -1.27976  2.49952
 C           6.712   -0.92674  1.49163
 C           6.33369 -0.97429  0.13725
 O           2.52811 -3.56591  0.49602
 O           4.34801 -1.3239  -5.17291
 O           7.99579 -0.52011  1.72365
 O         -10.25619  0.04632 -1.07267
 C          -11.2229  0.74549 -0.29851
 C           5.66179 -0.87062 -5.4743
 C           8.45439 -0.43286  3.0674
 F           0.74093  1.70268  3.8118
 F           1.20422  3.16535  2.24525
 F          -0.47203  4.58629  3.63098
 F          -1.53588  2.81203  4.36684
 F          -3.20553  3.52848  2.53838
 F          -1.67001  4.48052  1.29882
 H          -4.48638  1.70043  1.48063
 H          -2.28588 -0.28938  2.9877
 H          -2.85745 -1.05257  1.49967
 H          -2.18809 -2.04645  2.80341
 H          -0.24684  2.13077 -1.16227
 H          -0.3388   0.40035 -1.51106
 H          -0.93896  1.57633 -2.6932
 H          -5.98321 -0.74163 -2.18161
 H          -8.4183  -1.13843 -2.36019
 H          -9.12566  1.92854  0.57751
 H          -6.72031  2.35369  0.71779
 H           5.88041 -0.94376 -2.93077
 H           2.04836 -2.12086 -4.51803
 H           1.19183 -2.52377 -2.20186
 H           3.79636 -1.95097  2.94341
 H           6.08723 -1.24228  3.54442
 H           7.06175 -0.69258 -0.61817
 H           3.2473  -4.08943  0.10651
 H         -12.18992  0.33212 -0.5897
 H         -11.06489  0.58433  0.77591
 H         -11.20564  1.8215  -0.51558
 H           5.70565 -0.79472 -6.56201
 H           6.41971 -1.58507 -5.12728
 H           5.8549   0.11508 -5.0312
 H           8.42437 -1.41189  3.56306
 H           9.48814 -0.08897  3.00447
 H           7.86295  0.28999  3.64405
 C           2.33477  0.98049  0.4851
 H           1.82503  1.89797  0.17998
 H           3.00367  1.2429   1.31365
 H           2.95789  0.65415 -0.35082
```

Charged open 1o$^+$

Input

```
Charge = 1 Multiplicity = 1
Symbolic Z-Matrix:
C          -2.48328  2.01742  1.27635
C          -1.34435  2.42305  0.65215
C          -2.9527   0.65535  1.54475
C          -0.17514  1.59657  0.28348
C           0.48083  0.81115  1.23643
S           1.80983 -0.03692  0.5505
C           1.56785  0.71426 -1.02907
C           0.44604  1.56292 -1.00342
C          -3.42968  0.22788  2.83198
C          -3.81422 -1.09033  2.87814
S          -3.62883 -1.81492  1.28917
C          -2.99991 -0.35429  0.59178
C           2.47217  0.41133 -2.08825
C           0.20171  0.6814   2.70184
C          -2.68059 -0.30782 -0.87303
C          -4.33311 -1.85593  4.01551
C          -4.14054 -3.24962  4.12496
C          -4.62758 -3.96029  5.21132
C          -5.3277  -3.29799  6.23492
C          -5.53315 -1.91289  6.14393
C          -5.04307 -1.21121  5.04247
C           3.0583  -0.88455 -2.37089
C           3.9035  -0.76816 -3.5111
C           3.89162  0.64788 -3.93361
C           3.00908  1.34873 -3.05591
C           4.5974   1.304   -4.90987
C           4.44389  2.71571 -5.03244
C           3.6171   3.42621 -4.14269
C           2.91433  2.74226 -3.1495
C           2.85035 -2.15478 -1.79752
C           3.5058  -3.2574  -2.32161
C           4.36013 -3.12409 -3.43837
C           4.55145 -1.85902 -4.05331
F          -3.84807  3.14513  2.91716
O           5.15806  3.27184 -6.01898
O           4.93801 -4.25598 -3.86055
O          -5.76321 -4.08008  7.25519
C          -6.49327 -3.48143  8.32468
C           5.10097  4.69028 -6.23864
C           5.82409 -4.24345 -4.98982
C          -1.31585  3.92981  0.50371
F          -4.3823   3.36877  0.80183
F          -2.97742  5.56963  1.15753
C          -2.36618  4.43187  1.53072
F          -1.74673  4.63896  2.72366
F          -0.08084  4.4582   0.73206
C          -3.33084  3.22206  1.6615
F          -1.69177  4.34768 -0.75089
H          -3.44203  0.87101  3.70287
H          -0.15132  1.63226  3.11236
H          -0.57871 -0.0673   2.88688
H           1.09733  0.37824  3.25213
H          -2.84136  0.7002  -1.26765
H          -1.63843 -0.58851 -1.07735
H          -3.32203 -0.99038 -1.43978
H          -3.58572 -3.78224  3.35642
H          -4.47396 -5.03175  5.2949
H          -6.08265 -1.37676  6.9092
H          -5.2415  -0.14528  4.97296
H           5.28659  0.80243 -5.58232
H           3.53092  4.50392 -4.20844
H           2.31431  3.30948 -2.44699
H           2.17891 -2.29157 -0.95676
H           3.37079 -4.24637 -1.89656
H           5.18016 -1.75541 -4.93032
H          -6.73256 -4.29676  9.00819
H          -5.88626 -2.73138  8.84667
H          -7.42123 -3.02314  7.96125
H           5.75526  4.87478 -7.08984
H           4.07897  5.00153 -6.4791
H           5.4702   5.23072 -5.36065
H           6.15559 -5.27487 -5.1044
H           5.29505 -3.92205 -5.89345
H           6.68632 -3.59596 -4.79791
C          -0.14526  2.2312  -2.21652
H          -1.22925  2.08317 -2.23789
H           0.01486  3.31379 -2.20703
H           0.27106  1.83179 -3.14277
```

Uncharged closed 1c

```
Charge = 0 Multiplicity = 1
 Symbolic Z-Matrix:
 C          -2.61523  1.07408  1.11122
 C          -3.06846  0.20005  0.16514
 C          -2.01928 -0.4183  -0.7616
 C          -0.75668 -0.75203  0.06582
```

C	-0.23535	0.53368	0.74232
C	-1.19497	1.3128	1.34561
S	0.64774	-1.38034	-0.9724
C	1.76631	-0.25577	-0.20221
C	1.20112	0.66959	0.64202
C	-4.39288	-0.2297	-0.1382
C	-4.47173	-1.30235	-0.98933
S	-2.87745	-1.9071	-1.50297
C	3.23395	-0.39664	-0.59747
C	-5.68739	-1.96115	-1.46495
C	-1.7559	0.5823	-1.91937
C	-1.00395	-1.80536	1.1802
C	-1.05986	2.44862	2.32051
C	-5.65309	-3.2469	-2.04913
C	-6.81018	-3.8755	-2.48367
C	-2.45989	2.54647	3.00872
C	-8.05334	-3.23556	-2.35434
C	-8.11339	-1.95387	-1.78593
C	-3.45606	1.96306	1.96892
C	-6.9427	-1.33435	-1.35317
O	-9.13127	-3.93089	-2.81
C	-10.42393	-3.3433	-2.70195
C	4.21741	-0.50141	0.57231
C	5.2514	0.44842	0.43769
C	4.98574	1.26144	-0.76432
C	3.79754	0.80859	-1.35813
C	5.70926	2.3244	-1.31298
C	5.21843	2.92795	-2.48087
C	4.02908	2.46981	-3.07916
C	3.31688	1.41057	-2.51898
C	4.22977	-1.40095	1.62515
C	5.27347	-1.35572	2.56393
C	6.29575	-0.40364	2.4306
C	6.28874	0.50782	1.3587
O	7.34862	-0.2803	3.29167
O	5.82539	3.97162	-3.11715
C	7.42925	-1.15931	4.40738
C	7.02703	4.50243	-2.57165
O	3.28404	-1.58517	-1.41528
F	-2.76732	3.80113	3.40165
F	-2.45854	1.74601	4.11113
F	-4.50454	1.33428	2.5884
F	-4.0156	3.00118	1.25276
F	-0.09828	2.28111	3.27712
F	-0.78864	3.65757	1.70961
H	-5.26451	0.21172	0.33062
H	-2.70318	0.82787	-2.40686
H	-1.31662	1.50774	-1.53314
H	-1.07979	0.15563	-2.66332
H	-1.78372	-1.46721	1.86922
H	-1.30496	-2.76558	0.75453
H	-0.08094	-1.94923	1.74869
H	-4.70578	-3.76885	-2.15226
H	-6.77689	-4.8666	-2.92576
H	-9.05654	-1.42887	-1.68538
H	-7.01173	-0.33389	-0.93738
H	-11.1165	-4.07773	-3.11571
H	-10.68307	-3.14463	-1.65426
H	-10.48732	-2.41352	-3.28151
H	6.62301	2.66788	-0.84064
H	3.68385	2.96495	-3.98159
H	2.39968	1.06275	-2.98719
H	3.44267	-2.14322	1.73166
H	5.27524	-2.06149	3.38665
H	7.09491	1.23193	1.28394
H	8.3355	-0.87271	4.9434
H	6.56127	-1.04394	5.06925
H	7.5107	-2.20551	4.08522
H	6.86498	4.89694	-1.56021
H	7.82258	3.74627	-2.54979
H	7.31841	5.31681	-3.23684
H	4.17403	-1.64482	-1.79951
C	1.97553	1.7709	1.3213
H	1.45185	2.72651	1.22697
H	2.10245	1.57268	2.39087
H	2.96381	1.89795	0.88263

Charged closed 1c^{+}

```
Charge = 1 Multiplicity = 1
 Symbolic Z-Matrix:
```

C	-2.96063	1.35388	1.94387
C	-3.26585	0.28984	1.0838
C	-2.19851	-0.0755	0.06357
C	-0.82306	-0.07945	0.78225
C	-0.5687	1.33231	1.35075
C	-1.66477	1.90887	2.01809
S	0.59327	-0.38191	-0.37496
C	1.52868	0.98128	0.305
C	0.73253	1.82571	1.12952
C	-4.41368	-0.48874	1.01417
C	-4.31444	-1.60861	0.16978
S	-2.73909	-1.73639	-0.5919
C	2.88636	1.13998	-0.04694
C	-5.3445	-2.5869	-0.07149
C	-2.28932	0.92506	-1.1223
C	-0.73225	-1.12211	1.92758
C	-1.70562	3.10154	2.95727
C	-5.10528	-3.73026	-0.87019
C	-6.09035	-4.67534	-1.10884
C	-3.02907	2.91823	3.77058
C	-7.37123	-4.5019	-0.54554
C	-7.63388	-3.3681	0.25542
C	-3.93201	2.05521	2.84468
C	-6.64497	-2.43663	0.48592
O	-8.39765	-5.34794	-0.70996
C	-8.23498	-6.52778	-1.50982
C	3.94542	1.69068	0.78984
C	5.15921	1.70767	0.05108
C	4.88267	1.14381	-1.27997
C	3.51018	0.75143	-1.31092
C	5.70484	0.98171	-2.3719
C	5.17049	0.40318	-3.55115
C	3.82042	0.02021	-3.60426
C	2.99451	0.19995	-2.48967
C	3.98049	2.02255	2.15701
C	5.16663	2.44987	2.73274
C	6.35129	2.52712	1.96808
C	6.35403	2.12831	0.61258
O	7.43871	2.96502	2.63009
O	6.04673	0.2711	-4.56668
C	8.69586	3.06506	1.95262
C	5.61279	-0.29629	-5.80692
F	-3.58756	4.08925	4.12035
F	-2.74998	2.21084	4.89566
F	-4.72157	1.20561	3.56726
F	-4.78328	2.86765	2.13985
F	-0.64633	3.17689	3.80574
F	-1.76711	4.28419	2.26848
H	-5.29247	-0.28576	1.61224
H	-2.05321	1.93887	-0.78654
H	-1.59063	0.65067	-1.91499
H	-3.3037	0.92505	-1.52939
H	-1.50459	-0.95112	2.68416
H	-0.83927	-2.14033	1.54618
H	0.24326	-1.04114	2.41327
H	-4.1254	-3.8875	-1.31229
H	-5.86402	-5.53777	-1.72448
H	-8.62685	-3.25073	0.67717
H	-6.882	-1.57392	1.09871
H	-9.20271	-7.02765	-1.48385
H	-7.98124	-6.26367	-2.54217
H	-7.46771	-7.18264	-1.08269
H	6.74715	1.28606	-2.37242
H	3.40396	-0.41672	-4.50387
H	1.95398	-0.09518	-2.56784
H	3.09782	1.92874	2.77912
H	5.21732	2.71692	3.78325
H	7.2698	2.12553	0.03246
H	9.39336	3.45339	2.69455
H	9.0336	2.08068	1.6089
H	8.62979	3.76039	1.1081
H	5.26312	-1.32495	-5.66295
H	4.8214	0.31306	-6.25815
H	6.49235	-0.29292	-6.45052
C	1.15598	3.22953	1.49243
H	1.32405	3.35586	2.5642
H	2.06489	3.51825	0.96637
H	0.36851	3.93422	1.20968

Reference (Triphenylmethanol)

```
Charge = 0 Multiplicity = 1
 Symbolic Z-Matrix:
```

C	0.01877	-0.01125	0.66973
C	-0.23485	1.43636	0.20949
C	-1.14749	-0.91869	0.22303
C	1.39009	-0.54805	0.20378
C	-0.70528	1.71295	-1.08244
C	-0.89403	3.02944	-1.50876
C	-0.62368	4.09506	-0.64569
C	-0.16109	3.82871	0.64471
C	0.03537	2.51059	1.06853
C	-1.11115	-1.65923	-0.96723
C	-2.2094	-2.42792	-1.36592
C	-3.36216	-2.46985	-0.57875

```
C          -3.40882 -1.73296  0.60838
C          -2.31302 -0.96239  1.00281
C           1.72518 -1.88676  0.47651
C           2.98668 -2.39379  0.16276
C           3.94202 -1.57115 -0.44244
C           3.62    -0.24304 -0.72477
C           2.35659  0.26441 -0.40146
O           0.04426  0.04817  2.11462
H          -0.93382  0.89851 -1.76304
H          -1.26022  3.2199  -2.51467
H          -0.77635  5.11994 -0.97474
H           0.04957  4.64748  1.32864
H           0.39539  2.30891  2.07056
H          -0.21913 -1.64721 -1.58702
H          -2.15784 -2.9976  -2.29069
H          -4.21443 -3.07069 -0.8861
H          -4.30136 -1.75492  1.22907
H          -2.35341 -0.38752  1.92259
H           0.986   -2.5502   0.92128
H           3.21961 -3.43272  0.38303
H           4.9242  -1.96395 -0.69273
H           4.35235  0.40753 -1.19643
H           2.12848  1.30111 -0.62449
H           0.38439 -0.79867  2.44413
```

Reference⁺ (Triphenylmethyl cation)

```
Charge = 1 Multiplicity = 1
 Symbolic Z-Matrix:
C           0.00016  0.0004   0.00103
C          -0.73689  1.2488   0.00085
C          -0.71282 -1.26298 -0.00013
C           1.45058  0.01433  0.00083
C          -0.23537  2.38759 -0.68504
C          -0.95228  3.57725 -0.69667
C          -2.1653   3.67127 -0.00125
C          -2.67034  2.56505  0.69522
C          -1.97717  1.36125  0.68489
C          -1.95309 -1.3963  -0.68089
C          -2.62463 -2.61228 -0.69227
C          -2.0977  -3.71081  0.00006
C          -0.88421 -3.59698  0.69163
C          -0.18804 -2.39492  0.68055
C           2.16751  1.03142  0.68617
C           3.5566   1.02967  0.69721
C           4.26243  0.03975  0.00001
C           3.57481 -0.96271 -0.697
C           2.18603 -0.98954 -0.68529
H           0.68741  2.30827 -1.25049
H          -0.57383  4.43152 -1.24994
H          -2.71778  4.60678 -0.00255
H          -3.60122  2.64828  1.24812
H          -2.35369  0.51616  1.25153
H          -2.34786 -0.55646 -1.243
H          -3.55552 -2.71124 -1.24257
H          -2.63357 -4.65595  0.00098
H          -0.48967 -4.44542  1.24259
H           0.73485 -2.30121  1.24343
H           1.62452  1.78178  1.25193
H           4.09332  1.79371  1.25155
H           5.34884  0.04924  0.00068
H           4.12535 -1.7166  -1.25171
H           1.65714 -1.7504  -1.24992
```

Uncharged transition state TS

```
Charge = 0 Multiplicity = 1
 Symbolic Z-Matrix:
C          -2.55869  1.26761  1.01909
C          -3.02753  0.52849 -0.13616
C          -2.04447  0.01473 -1.08844
C          -0.75908 -0.89538  0.25546
C          -0.26636  0.28806  0.95566
C          -1.26897  1.18357  1.51729
S           0.62239 -1.66662 -0.5669
C           1.73846 -0.42776 -0.02711
C           1.12496  0.53258  0.77463
C          -4.31245 -0.01332 -0.29638
C          -4.43983 -0.9478  -1.32211
S          -2.90096 -1.1407  -2.1645
C           3.18353 -0.51882 -0.49082
C          -5.61134 -1.73453 -1.67531
C          -1.13722  0.95962 -1.85978
C          -1.65722 -1.90758  0.95236
C          -1.11416  2.10619  2.69469
C          -5.53361 -2.82994 -2.56823
C          -6.6519  -3.58045 -2.89645
C          -2.57298  2.40526  3.14155
C          -7.90447 -3.26542 -2.34519
C          -8.01196 -2.18121 -1.46189
C          -3.40461  2.18637  1.84907
C          -6.88058 -1.43343 -1.13982
O          -8.94292 -4.06218 -2.72801
C          -10.238  -3.79832 -2.2008
C           4.2101  -0.56916  0.64731
C           5.21071  0.40702  0.46025
C           4.88392  1.18345 -0.75131
C           3.69287  0.6818  -1.29797
C           5.56007  2.25404 -1.34369
C           5.01983  2.81647 -2.51002
C           3.82904  2.30912 -3.06357
C           3.16551  1.24226 -2.45919
C           4.275   -1.43853  1.72342
C           5.34288 -1.34085  2.63003
C           6.33434 -0.36526  2.44294
C           6.27151  0.51846  1.34972
O           7.40668 -0.19163  3.27077
O           5.57866  3.86252 -3.18631
C           7.54139 -1.03892  4.40571
C           6.78452  4.4318  -2.69159
O           3.23434 -1.72529 -1.2841
F          -2.72736  3.63682  3.67452
F          -2.94861  1.49237  4.07959
F          -4.64687  1.68758  2.15319
F          -3.6303   3.39119  1.22725
F          -0.38386  1.57719  3.72004
F          -0.5127   3.30495  2.36919
H          -5.12444  0.21329  0.38309
H          -0.61766  1.64542 -1.18729
H          -0.38862  0.40363 -2.43355
H          -1.73095  1.55707 -2.5612
H          -2.50949 -1.42491  1.43422
H          -2.03762 -2.65008  0.24302
H          -1.08803 -2.43654  1.72543
H          -4.57673 -3.10447 -3.00381
H          -6.57905 -4.42218 -3.57861
H          -8.9656  -1.90692 -1.02487
H          -6.9975  -0.59052 -0.46554
H          -10.89414 -4.55206 -2.63888
H          -10.24951 -3.89428 -1.10737
H          -10.58825 -2.79808 -2.48679
H           6.47675  2.63311 -0.90556
H           3.44489  2.77071 -3.96815
H           2.24935  0.85466 -2.89689
H           3.50823 -2.19447  1.87357
H           5.38614 -2.02278  3.47144
H           7.05402  1.2631   1.23506
H           8.45391 -0.71474  4.90867
H           6.68899 -0.92922  5.08846
H           7.64209 -2.09065  4.10795
H           6.64632  4.84487 -1.68396
H           7.5975   3.69411 -2.67928
H           7.03585  5.2376  -3.3831
H           4.14216 -1.82812 -1.61324
C           1.8464   1.73433  1.3328
H           1.43477  2.66506  0.92709
H           1.74856  1.78306  2.42132
H           2.90915  1.7124   1.09837
```

Charged transition state TS⁺

```
Charge = 1 Multiplicity = 1
 Symbolic Z-Matrix:
C          -2.95344  1.48603  1.9736
C          -3.29066  0.54491  0.90148
C          -2.31114  0.29052 -0.13466
C          -0.74388 -0.20663  1.10193
C          -0.50813  1.11966  1.70227
C          -1.66789  1.75016  2.34356
S           0.68472 -0.63542  0.16015
C           1.55434  0.86757  0.56729
C           0.71192  1.70162  1.39154
C          -4.35936 -0.33919  0.92023
C          -4.31652 -1.327   -0.09082
S          -2.90177 -1.1076  -1.08218
C           2.85261  1.06687  0.10538
C          -5.25483 -2.40137 -0.29342
C          -1.76182  1.40681 -1.00964
C          -1.26483 -1.3679   1.93673
C          -1.6525   2.70698  3.52068
C          -5.04953 -3.3929  -1.2816
C          -5.95738 -4.42006 -1.48697
C          -3.10068  2.62649  4.08972
C          -7.12341 -4.48747 -0.69698
C          -7.34987 -3.50806  0.29477
C          -3.94847  2.19347  2.85729
C          -6.43741 -2.49336  0.49126
O          -8.06805 -5.43285 -0.80918
```

C	-7.93345	-6.46756	-1.79327
C	3.92782	1.79686	0.7862
C	5.08258	1.7931	-0.03636
C	4.7684	1.04253	-1.25999
C	3.43329	0.55759	-1.14945
C	5.53987	0.79375	-2.37685
C	4.98968	0.03375	-3.43307
C	3.67105	-0.44153	-3.34859
C	2.8966	-0.17173	-2.21378
C	4.03555	2.29925	2.09493
C	5.2277	2.86618	2.52223
C	6.34792	2.92037	1.66605
C	6.28327	2.35569	0.37694
O	7.44778	3.50587	2.18622
O	5.81568	-0.17219	-4.48376
C	8.63903	3.59549	1.40066
C	5.35161	-0.92355	-5.60681
F	-3.51758	3.77625	4.64346
F	-3.15162	1.6436	5.02554
F	-4.99592	1.40389	3.23827
F	-4.48547	3.28551	2.23834
F	-0.72047	2.38474	4.45245
F	-1.4158	3.99903	3.1331
H	-5.12455	-0.32108	1.68393
H	-1.43943	2.25697	-0.40601
H	-0.90832	1.05693	-1.5997
H	-2.53468	1.75966	-1.70055
H	-2.14107	-1.09028	2.52423
H	-1.51662	-2.23098	1.31371
H	-0.47887	-1.67663	2.6341
H	-4.15787	-3.36438	-1.90221
H	-5.7594	-5.16012	-2.25332
H	-8.25405	-3.57415	0.89123
H	-6.6461	-1.75339	1.25625
H	-8.81878	-7.0918	-1.67661
H	-7.91035	-6.0418	-2.80235
H	-7.03283	-7.06335	-1.60876
H	6.55444	1.16648	-2.48038
H	3.23765	-1.01889	-4.1566
H	1.87783	-0.5432	-2.19185
H	3.21088	2.22977	2.79489
H	5.33062	3.26339	3.5269
H	7.15357	2.33231	-0.26893
H	9.36186	4.11689	2.0283
H	9.0204	2.59831	1.15127
H	8.462	4.17195	0.48509
H	5.08798	-1.94643	-5.31271
H	4.49111	-0.43369	-6.07795
H	6.18746	-0.94757	-6.30628
C	1.03012	3.15251	1.66358
H	1.19197	3.35064	2.72757
H	1.91687	3.47519	1.12008
H	0.19461	3.78395	1.34708

7.4.2 Light-induced pK_a Modulation

The protonated (**4-4oH** and **4-4cH**) and deprotonated forms (**4-4o** and **4-4c**) of open and closed DAE molecules were studied by means of Density Functional Theory (DFT) and Complete Active Space (CAS) methods. First, the full structures were optimized at the ωB97X-D/6-31G(d) level of theory and the excitations energies were calculated (PBE0/6-311+G(2d,p) level, acetonitrile solvent) at the stationary points. The predicted excitation energies for the closed forms are 490 nm (neutral) and 503 nm (anionic), and in both cases, this first state is well separated from the S_2 excited state (S_2: 355 nm and 355 nm for **4-4cH** and **4-4c**). The absorption spectrum of the open forms is, as expected, hypsochromically shifted, with the first excited state of **4-4oH** form at 405 nm (low oscillator strength) and the S_1 of **4-4o** at 413 nm with 10-times higher oscillator strength. The S_2 states of the open forms are at 324 nm and 352 nm for **4-4oH** and **4-4o** forms.

The transformation between closed and open forms in the ground state is prevented by existence of large barrier: $\Delta G^{\neq}$ = 41.5 kcal/mol for neutral molecule and an even larger value of 46.9 kcal/mol is found for the deprotonated switch. In both cases, the open form is thermodynamically preferred: neutral ΔG_r = -6.9 kcal/mol, deprotonated ΔG_r = -10.0 kcal/mol. This is in line of typical differences in DAE.

We calculated the pKa change between open and closed form at a similar level of theory and we found the change of 2.3 in line with experimental observation.

In order to elucidate the observed differences in photochemistry of protonated/deprotonated forms we performed static calculations on excited-state energy hypersurface. Unlike in previous case we used a smaller (=truncated) model system (see Figures 1 and 2). The geometry optimizations were performed using spin-flip TD-DFT (SF-TD-PBE0, SF-TD-BHHLYP), a method used before in the literature for DAE and giving results compatible with CAS (at least in "standard" DAE). Below we summarize our findings:

4-4cH→4-4oH

After electron excitation to the first excited state the system reaches S_1 hypersurface (FC-C-S_1) and relaxes to Min-C-S_1. This minimum is characterized by elongated C-C bond distance (1.62 Å). We found a small barrier (~1 kcal/mol, TS-C-S_1) on the path between Min-C-S_1 and the minimum energy conical intersection (MECI S_1/S_0) which is localized at C-C distance 2.01 Å near the TS for ground-state reaction. We expect that system after reaching this point can relax to both **4-4cH** and **4-4oH** forms.

4-4oH→4-4cH

The experimental setup suggests excitation to S_2 of protonated open form, which decays to S_1. This excited state has very low oscillator strength and thus is, most probably, populated indirectly (=IC from S_2). The system relaxes on S_1 surface in barrierless fashion toward MECI S_1/S_0. We did not localize any stationary point on the path between FC region and MECI. In the MECI not only are the S_1 and S_0 states becoming degenerate but this holds also for the T_1 triplet. This fact along with presence of two sulphur atoms in the structure (higher spin orbit coupling) can qualitatively explain the observed population of long-living triplet state.

Slightly lower quantum yield (5.3 ring closure *versus* 6.7 ring opening) can be probably attributed to dynamical effects. The **4-4oH** in FC-S_1 experiences larger gradients and thus can explore larger part of PES without necessarily ending in MECI. On the other hand the **4-4cH→4-4oH** photoreaction is hindered by smaller barrier which can "focus" the system more effectively toward MECI. In any case, one should be cautious with such interpretations w/o fully dynamic studies.

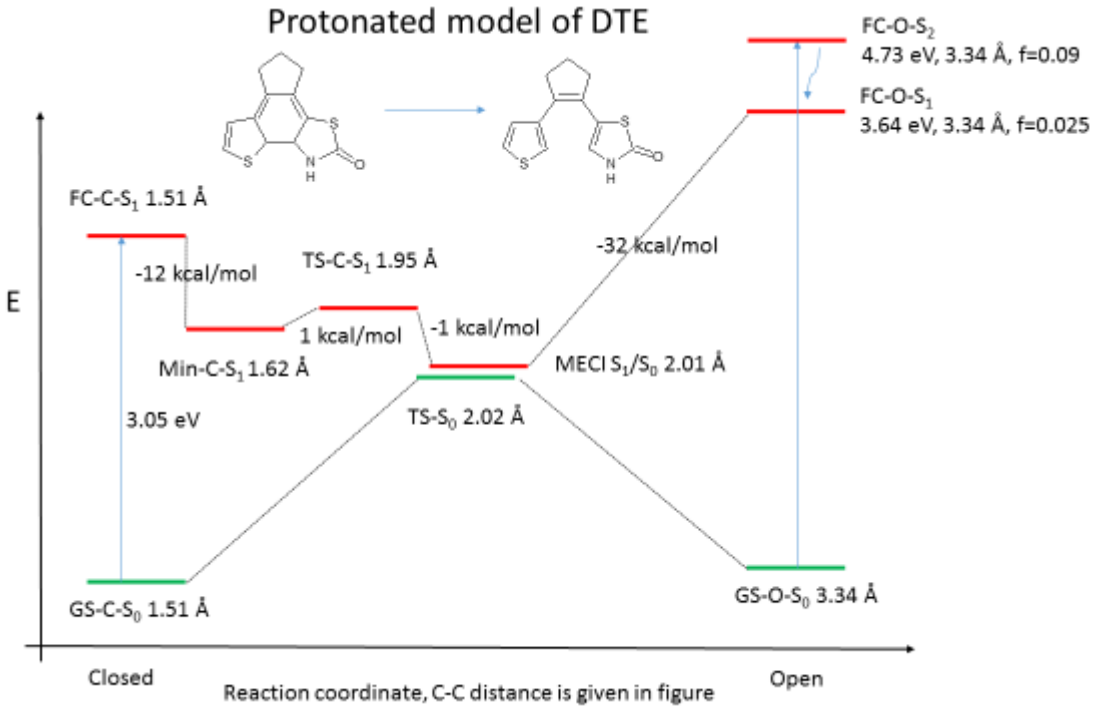

Figure 7-20 Important points on GS/ES PES for model of protonated photoswitch.

4-4o→4-4c

Experimentally, high yield 90 % was observed here. According to our calculation the system reaches the S_1 excited state surface and relaxes unlike **4-4oH** to Min-O-S_1 (see Figure 2). This structure is structurally distant from the MECI (C-C distance 2.77 Å for Min-O-S_1 vs. 2.01 MECI S_1/S_0). Following the above logic, one could suggest that tge presence of small, but non negligible, barrier on S_1 surface can be reason for higher quantum yield as it "exhausts" a part of the energy of the system and prevents it from exploring larger parts of PES. As shown by Boggio-Pasqua et al.

in their early work[17] the photochromism of diarylethene cannot be explained purely by reaction paths but the dynamic effects has to be accounted. Once more, this is quite speculative.

We did not localize state denoted as X in experimental analysis – several higher excited states exist nearby the ring-closing S_1, in the CAS calculations the strongest candidate for X is n→π* state localized on keto group (+oxygen and sulphur lone pairs). This state relaxes toward C=O bond elongation.

4-4c→4-4o

We found comparable structural features of S_1 PES in case of deprotonated closed form (**4-4c**) as for the protonated form including small barrier separating S_1 from the S_1/S_0 MECI. We note that several DFT functionals tend to predict larger OC-S distances (more than 2.0 Å).

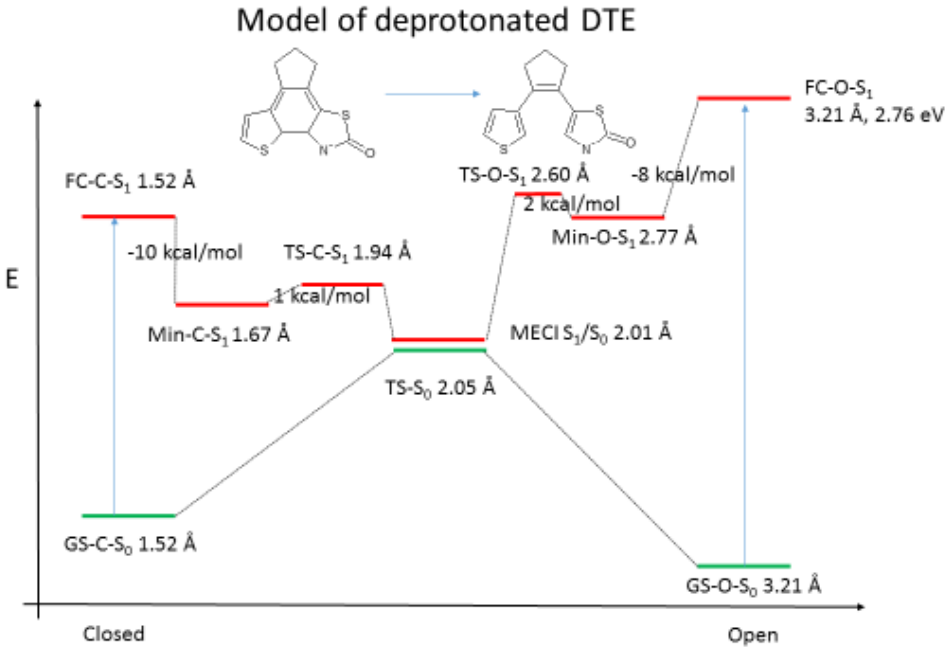

Figure 7-21 Important points on GS/ES PES for model of protonated photoswitch.

7.5 Transient Absorption Measurements[9]

7.5.1 Acid-catalyzed Cycloreversion

7.5.1.1 Transient Absorption (TA)

The TA setup with applications has been described elsewhere.[143] It provides spectral coverage 275 – 690 nm with a 0.1 ps instrumental response and timing precision of 0.02 ps over the full probe range. A solution of **3-1o** in TFA was flown through a sample cell of 0.4 mm internal thickness. Transient absorption spectra $\Delta A(\lambda, t)$ of **3-1o** were recorded upon 563 nm excitation.

[9] Conducted by Dr. Martin Quick and Dr. Sergay Kovalenko

10 – 20 pump-probe scans were averaged to improve the signal-to-noise ratio. All TA spectra were recorded at the magic angle between pump- and probe polarizations.

7.5.1.2 Spectral Corrections

The recorded absorption spectra contain both, the signal of the chromophore and the solvent. Transient absorption spectra of the solvent were recorded separately and subtracted to obtain the pure spectra of the chromophore.

To obtain a uniform time-zero for all frequencies (chirp-correction) the time-zero correction-function is determined independently from the transient absorption measurement of the solvent.

Spectral contributions that remain constant throughout a scan, before and after time-zero (fluorescence, scattering), are subtracted by an averaged spectrum that is calculated from the spectra of negative delay times.

7.5.1.3 Kinetic Evaluation

To obtain time constants and Decay-associated spectra (DAS) a global fit is performed with a sum of exponential time-functions $\sum_i A_i(\lambda)e^{-\frac{t}{\tau_i}}$. The integer i refers to the number of time-functions, τ_i is the time-constant and $A_i(\lambda)$ is the wavelength-dependent factor which is also known as DAS. It contains the spectral components that decay with τ_i.

7.5.1.4 Species-associated Spectra (SAS)

The spectral evolution can be described by migrating population that moves between virtual levels or energetic sinks on the potential-energy surface (PES). Each virtual level is characterized by a SAS. The technical implementation is done by solving a system of differential equations (rate equation). For the very example in the main text the kinetic scheme is chosen to be:

A → B → C → D → E

A, B and C refer to virtual levels on the excited-state. D and E refer to hot and vibrationally cool S_0. Within this scheme there is also implemented that there is direct access to D from B. The differential equations to solve are:

$$[\dot{A}] = -k_1[A] \quad \textbf{(E6-20)}$$

$$[\dot{B}] = +k_1[A] - k_2[B] - k_5[B] \quad \textbf{(E6-21)}$$

$$[\dot{C}] = +k_2[B] + k_3[C] \quad \textbf{(E6-22)}$$

$$[\dot{D}] = +k_5[B] + k_3[C] - k_4[D] \quad \textbf{(E6-23)}$$

$$[\dot{E}] = +k_4[D] \quad \textbf{(E6-24)}$$

k_1…k_5 refer to the rate-constants and are the inverted time-constants.

7.5.1.5 Results

Transient absorption spectra of **3-1o** in TFA are measured with 563 nm excitation. Spectra were detected in the range 275 – 690 nm and are shown in Figure 7-22. The spectrum develops within the convolution time of the pump- and probe-pulse. Negative bands at 310 nm and between 470 and 605 nm refer to bleach while positive bands correspond to Excited-state absorption (ESA). Stimulated emission is hardly detected at > 600 nm and short-living (< 100 fs). The initially populated Franck-Condon (FC) region is left within tens of femtoseconds, which is seen as development of vibrational structure on ESA in the region 320 – 470 nm (a). This evolution is outlined with the kinetic trace associated with the peak at 445 nm (Figure 7-23f). Figure 7-22b and c, show that the subsequent radiationless relaxation to the vibrationally hot electronic ground-state proceeds in two steps. The major fraction relaxes with a time-constant of 0.3 ps (b). The remaining (smaller) fraction still moves on the potential energy surface of S_1, but then follows awhile later with τ = 2 ps (c). This bi-exponential behaviour is also drawn in the kinetic traces of Figure 7-23a, d for bleach-decay and c, e for ESA-decay. Cooling in S_0 is indicated by the typical dispersive line-shape on the low-frequency region of the $S_1 \leftarrow S_0$ absorption band in Figure 7-22d. Here, the final relaxation to cold S_0 proceeds with an 11 ps time-constant (see also Figure 7-23b).

Species associated spectra (SAS) correspond to virtual levels (or base-spectra) that are populated by wave-packets throughout the relaxation process. They are considered as stable thermodynamic sinks between which the migration of population leads the temporal changes that are seen in the measured absorption spectra. All the SAS that are obtained are shown in Figure 7-24. The FC-spectrum represents the situation in which population just reached S_1 without any further relaxation (a). After relaxation from the FC-region the population reaches two stable sites in S_1. A first site from where the major fraction relaxes radiationless to S_0. And a second site, which is populated by only the remaining excited fraction and from where S_0 is populated in a second tranche (b). Both sites have similar base-spectra whereby a big change in the molecule's conformation is therefore not expected. The vibrationally hot S_0-state is indicated by the dispersive line-shapes that are located on the red flank of bleach (c).

7.5.1.6 Conclusion

The molecule **3-1o** quantitatively converts the initial photon-energy into heat. Within this process there is no big change in the molecules conformation registered.

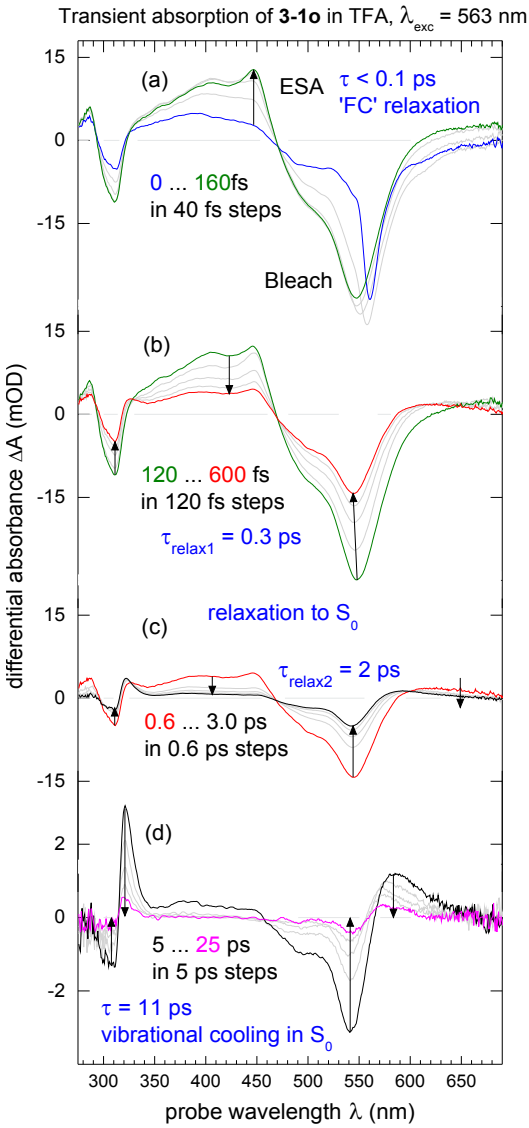

Figure 7-22 Transient absorption spectra of 3-1o in TFA measured with 563 nm excitation. a – The spectrum develops within the convolution time of the pump- and probe-pulse. Bleaching appears with a negative sign and is seen at 310 nm and in the region 470 – 605 nm. Positive bands are attributed to ESA that develops structure on an ultrafast time-scale when population leaves the Franck-Condon site of the excited state. b and c – Radiationless relaxation to S_0 follows immediately with two time-constants: 0.3 ps and 2 ps. d – Dispersive line-shapes around the bleach regions indicate the molecule is in a vibrationally hot state in S0. Cooling proceeds with 11 ps.

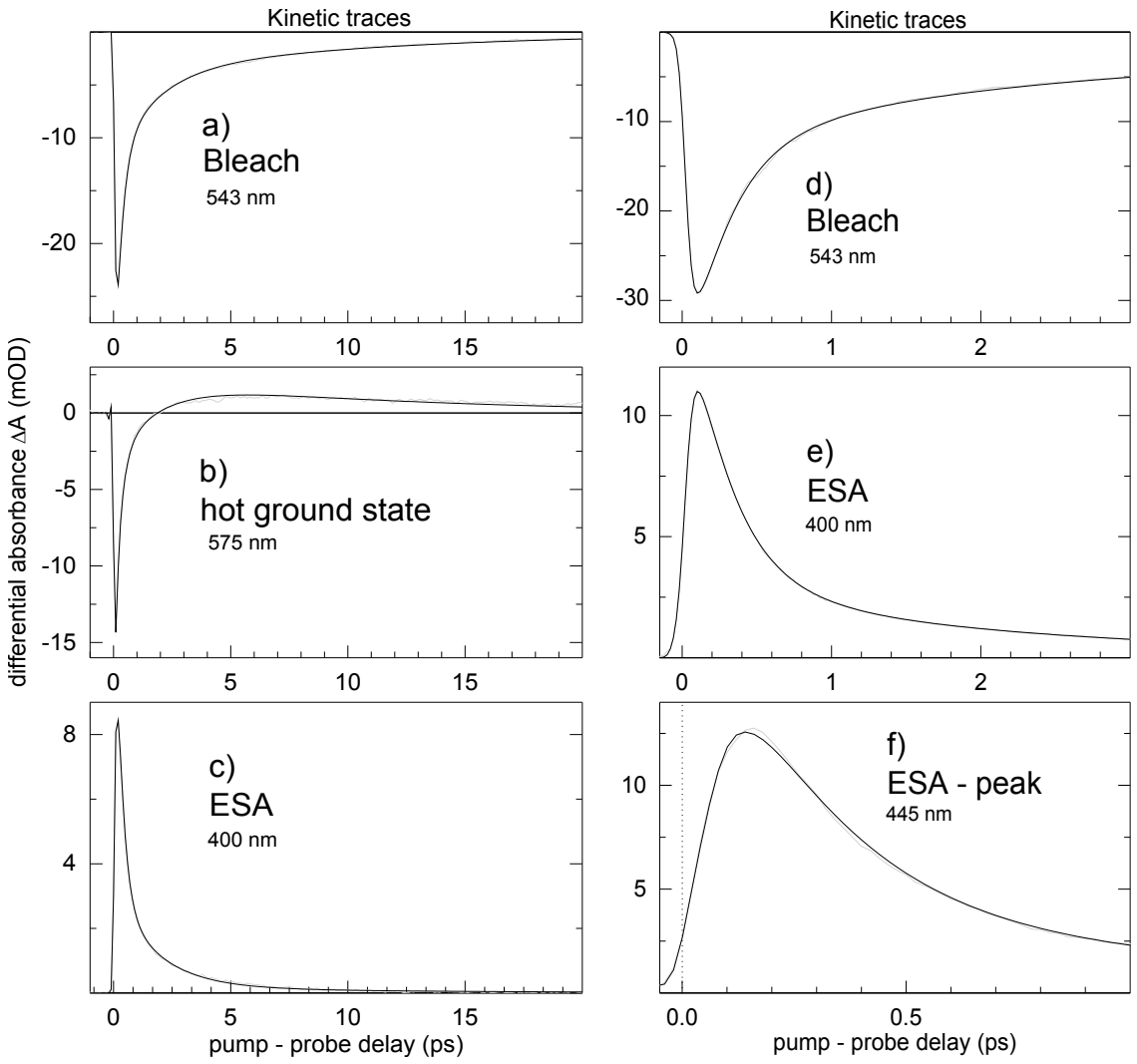

Figure 7-23 Kinetic traces (grey line) and the result of a global fit (black line) with 4 exponential time-functions. a and d – The relaxation into the electronic ground state proceeds in two tranches, with $\tau = 0.3$ ps and $\tau = 2$ ps. c and e – The bi-exponential decay of ESA with the same time-constants is represented with the kinetic trace at 400 nm. b – Vibrational cooling in S_0 proceeds with an 11 ps time-constant. f - The initial relaxation away from the FC-region is best seen in the development of structure in the ESA band between 320 and 470 nm, at 445 in particular.

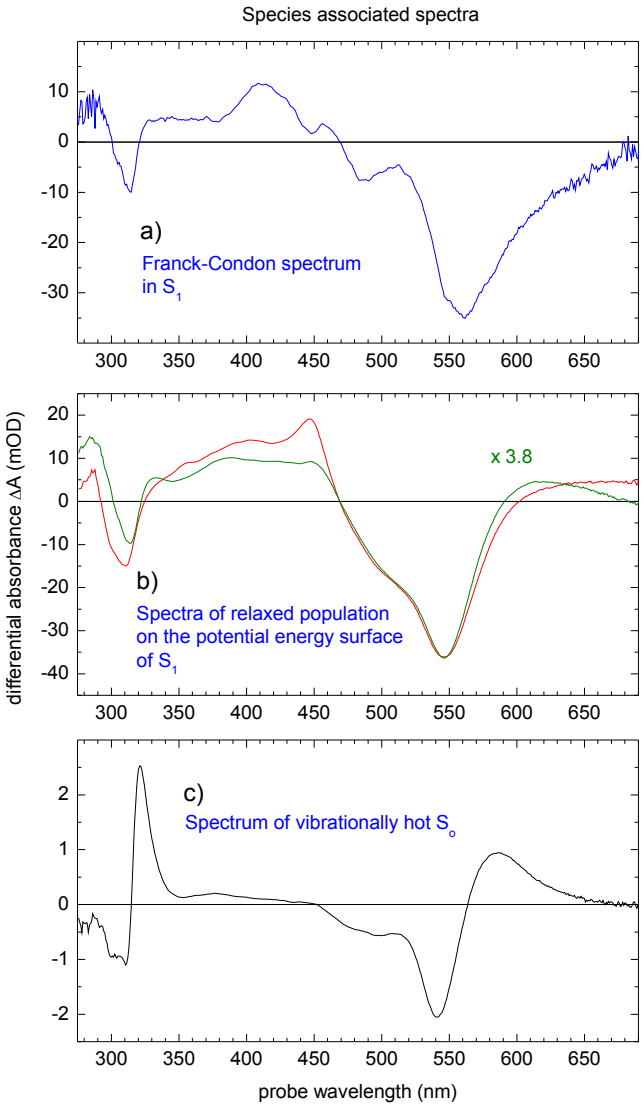

Figure 7-24 Species associated spectra (SAS) of 1o in TFA upon 563 nm excitation. a – FC spectrum in S_1. b – The second SAS corresponds to the relaxed state, away from the FC region (red). While the major part of the population already reaches the hot electronic ground-state within 1 ps the remaining fraction still moves in S_1, giving the third SAS (green). c – The hot S_0 is populated in two tranches. The corresponding SAS contains the typical dispersive line-shapes around the bleach-regions.

7.5.2 Light-induced pK_a Modulation

7.5.2.1 Abstract

Ring-opening and –closure of the protonated and deprotonated DAEs (**4-4oH**, **4-4cH**, **4-4o** and **4-4c**), respectively, are monitored with transient absorption (TA). Relaxation schemes are established to summarize the observations from TA and characteristic time-constants, as well as quantum yields for the photo-reaction are collected. One remarkable observation is that the ring-closure proceeds ultrafast (τ = 60 fs) and almost quantitatively when the nitrogen is deprotonated.

For comparison the protonated open DAE performs the photo-reaction with a quantum yield of only 5%. One possible explanation for this huge difference in reactivity might be the stronger delocalization of π-electrons in the deprotonated thiazole-ring. The attained large angles at nitrogen and carbonyl-C-atom compensate for the steric stress within the hexa-diene ring after ring-closure. With a proton attached to the nitrogen the delocalization is suppressed and no formation of **4-4cH** is observable. A three times larger quantum yield for the ring-opening is observed in case of the deprotonated isomer. The N-H stretching mode might open an additional deactivation channel for the thermal deactivation of S_1, whereby less photo-products are formed upon excitation of **4-4cH**.

7.5.2.2 Stationary extinction spectra

The extinction coefficient spectra of the diarylethenes (DAE) are shown in the left panel of Figure 7-22. For the protonated (**4-4cH**) and deprotonated (**4-4c**) closed form of the DAEs the $S_1 \leftarrow S_0$ transition is far red-shifted by ~ 10.000 cm^{-1} compared to higher transitions. While for the anionic open DAE (**4-4o**) the lowest electronic transition is also well separated from higher transition there is a superposition of the S_2-S_0- and S_1-S_0-absorption bands in case of the protonated (**4-4oH**) open DAE.

A reaction scheme for the ring-opening and –closure of the different DAEs is depicted in the right panel of Figure 7-25. At pH-values that favor the protonated DAEs photo-isomerization can occur from **4-4oH** to **4-4cH** and vice versa. **4-4oH** and **4-4cH** can be individually interconverted into the deprotonated forms when the proton-concentration is decreased. Photo-isomerization can now occur between **4-4o** and **4-4c** by irradiation with light.

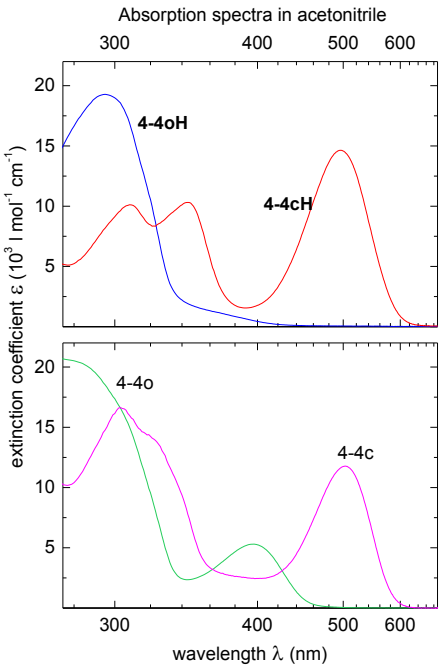

*Figure 7-25 Left: Top - Extinction coefficient spectra of protonated open (**4-4oH**) and closed form (**4-4cH**) of a diarylethene (DAE) derivative. Bottom - Extinction coefficient spectra of deprotonated open (**4-4o**) and closed Form (**4-4c**). Right: Reaction scheme of the interconversion between **4-4oH**, **4-4cH**, **4-4o** and **4-4c**.*

7.5.2.3 Transient absorption spectra

Let us first discuss the evolution of protonated diarylethene (DAE) outgoing from the open (**4-4oH**) and closed (**4-4cH**) isomer, respectively. The results shall be summarized in a relaxation scheme in terms of a potential energy diagram. The theoretically predicted barriers and pathways will be compared.

4-4oH → 4-4cH

Transient absorption (TA) spectra of **4-4oH** in acetonitrile were recorded upon 325 nm optical excitation and are shown in Figure 7-26. *a* – The spectrum shows up within the response time (~ 80 fs) where negative signals denote bleach and stimulated emission (SE), respectively while a positive sign corresponds to excited-state absorption (ESA). Temporary occurring narrow features in the spectral vicinity of the excitation wavelength denote S_0 Raman signals. They originate from a simultaneous interaction of pump- and probe field (time zero) with the sample and will be termed "coherent artifact". Due to the overlap of $S_1 \leftarrow S_0$ and $S_2 \leftarrow S_0$-bands in the extinction spectrum both states, S_1 and S_2, are populated simultaneously. Corresponding bands are seen at 440 nm (S_1-ESA) and 500 nm (S_2-ESA). *b* – Ultrafast conversion of S_2 to S_1 proceeds with $\tau = 50$ fs where the corresponding S_2-ESA decays while S_1-ESA rises further, accordingly. *c* – Vibrational relaxation in S_1 proceeds bi-exponentially with two time-constants: 140 fs and a 640 fs. Both τ can be expressed with one effective time-constant by considering their significances:

0.7·140 fs + **0.3**·640 fs ~ 300 fs. Band refinement of S_1-ESA is the main observation during this time, where a new peak at 450 nm is established. *d* – The ground-state recovers with a 30.8 ps time-constant which is seen in a vanishing bleach-band and S_1-ESA decay. The barrier that must be passed over from S_1 to S_0 can be estimated from $E = k_B T \cdot \ln(\tau/\tau_0)$, where $k_B T$ equals 210 cm^{-1} at RT and τ_0 is approximated to 0.01 ps, when stretching modes (1600 cm^{-1}) are considered the reactive coordinate for thermal deactivation. The barrier is estimated to 1687 cm^{-1} (20.1 kJ mol^{-1} or 4.8 kcal mol^{-1}). From a TA spectrum at infinite delay time a quantum yield of 5.3% is determined for the ring-closure of **4-4oH** to **4-4cH** (see Figure 7-26, *a*).

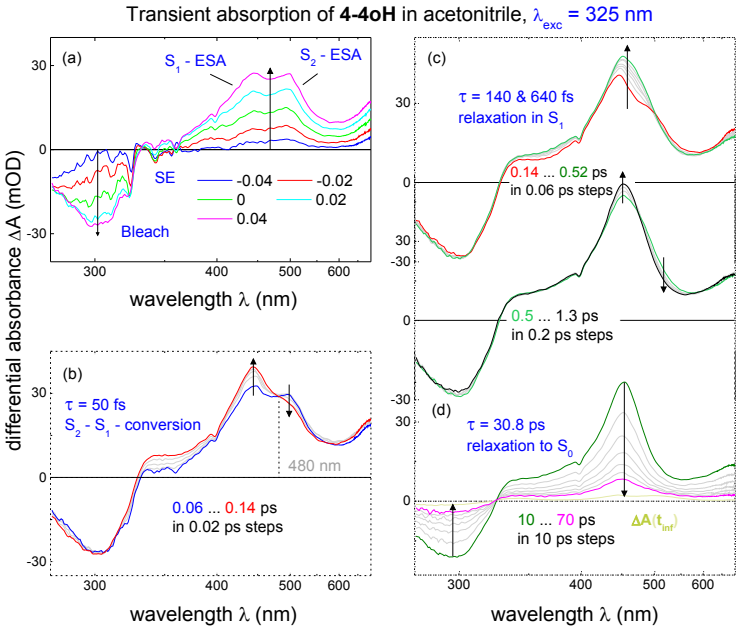

*Figure 7-26 TA spectra of **4-4oH** in acetonitrile are recorded upon 325 nm excitation. a – S_1 and S_1 are simultaneously populated and corresponding ESA bands show up at 440 nm (S_1-ESA) and 500 nm (S_2-ESA). b – Ultrafast conversion from S_2 to S_1 proceeds with τ = 50 fs. c – Relaxation in S_1 takes place with two subsequent steps that can be expressed with an effective time-constant of 300 fs. d - Decay to the electronic ground-state proceeds with τ = 30.8 ps.*

An estimate for the quantum yield of the ring-closure and representative time traces are shown in Figure 7-27. The time-constants that describe the spectral evolution are obtained from a global fit with a sum of three exponential time-functions and heavi-side function. These functions are convoluted with a Gaussian shape to take into account the finite duration of pump- and probe yielding a cross-correlation time of ~ 80 fs. To model the coherent artifact another Gaussian function of same duration plus an optional number of its derivatives with increasing order is added. Note, that the time-constant of 50 fs is determined aside from the global analysis because the corresponding ultrafast evolution is consumed by the aforementioned Gaussian function. The quality of the global fit is presented with band-integrals that are calculated over a spectral region for both, the data and the fit. *a* – Decay of S_1-ESA and bleach follow a time-constant of 30.8 ps. *b* – The bi-exponential character of the relaxation in S_1 is best seen for the region

between 475 and 500 nm. In here, a rise with τ = 140 fs is followed by a decay with τ = 640 fs. *c* - The quantum yield $Y_{\mathbf{4\text{-}4oH \rightarrow 4\text{-}4cH}}$ of the ring closure of **4-4oH** to form **4-4cH** is estimated from the TA spectrum at infinite time delay $\Delta A(t_{inf})$. Therefore, a difference spectrum is modelled from the extinction spectra of **4-4oH** and **4-4cH** until it fits the spectral pattern in $\Delta A(t_{inf})$. Only 5.3% of the initially excited population carries out the ring-closure, while the remainder simply returns to its original ground-state. An equally low value of 2.1% is obtained from stationary experiments.

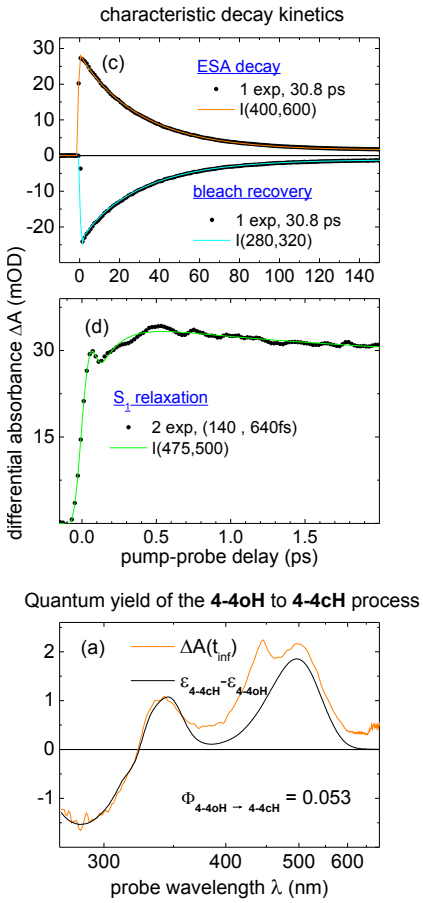

Figure 7-27 An estimate for the quantum yield of the ring-closure and representative time traces are shown. a – The evolution of spectra is presented in the form of band-integrals : $I(\lambda_1, \lambda_2; t) = \int_{\lambda_2}^{\lambda_1} \frac{\Delta A(\lambda,t) d\lambda}{\lambda}$

Decay of S_1-ESA and bleach proceed with a time-constant of 30.8 ps. *b* – Relaxation in S_1 takes place in two steps: 140 fs and 640 fs. *c* - A quantum yield of 5.3% is estimated for the ring-closure of **4-4oH** to form **4-4cH**.

4-4cH → 4-4oH

Transient absorption (TA) spectra of **4-4cH** in acetonitrile were recorded upon 544 nm optical excitation and are shown in Figure 7-28. *a* – The transient spectrum builds up within the cross-correlation time of pump and probe. Strong S_1-ESA bands are located around 400 nm and at 600 nm. *b* – Relaxation away from the Franck-Condon (FC) region proceeds with a 50 fs time-

constant. In this time the S_1-ESA band around 400 nm is getting vibrationally pronounced at 450 nm while a simultaneous peak-shift is observed in the red border of the spectrum. Note, that the signal at 450 nm does not represent excited **4-4oH** which also peaked at 450 nm because their decay times do not match. *c* – With a time-constant of 300 fs S_1-ESA completely decays until dispersive spectral structure remains (at 0.7 ps). This band-shape typically arises when excited vibrational states are populated in S_0. The barrier for the S_1-S_0 transition is estimated to 714 cm^{-1} (8.6 kJ mol^{-1} or 2 kcal mol^{-1}). *d* – Cooling or vibrational relaxation in S_0 is seen as vanishing dispersive structure and goes on with τ = 8.4 ps until no further changes are noticeable. *e* – Decay of S_1-ESA and bleach recovery, both follow a 300 fs time-constant. *f* – Cooling in S_1 is best seen with a band-integral that is calculated over the region 550 – 690 nm. Here, the decay of the positive part of the dispersive band-shape is depictured. *g* – The quantum yield $Y_{\mathbf{4\text{-}4cH \rightarrow 4\text{-}4oH}}$ is estimated from $\Delta A(t_{inf})$ and amounts 6.7% (stationary: 3.6%). Again, the actual photo-reaction (here ring-opening) remains ineffective and the vast majority of the initially excited population of **4-4cH** returns to the original electronic ground-state.

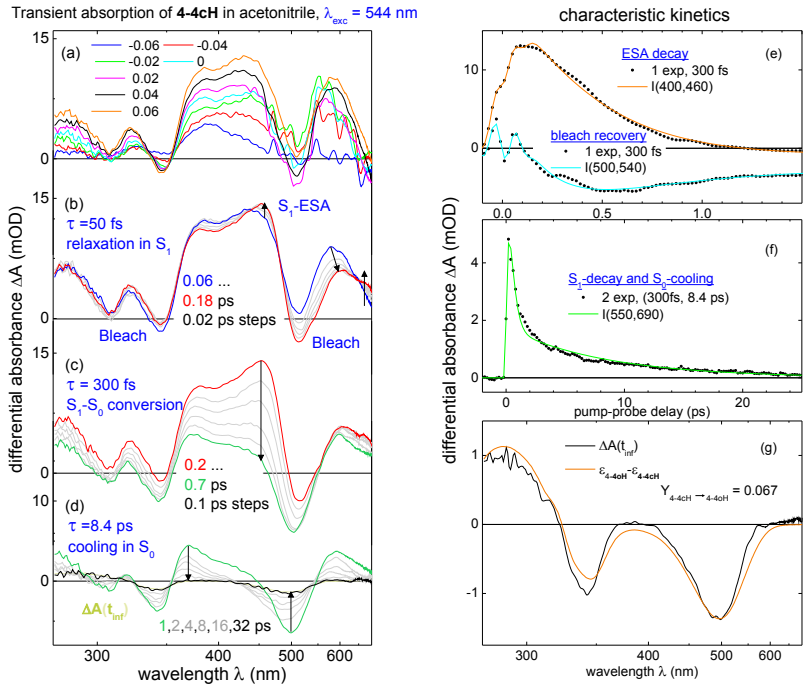

*Figure 7-28 TA spectra of **4-4cH** in acetonitrile are measured with optical pumping at λ_{exc} = 544 nm. a – The spectrum builds up within the cross-correlation time. b – FC relaxation proceeds ultrafast with τ = 50 fs. c – Conversion to S_0 follows a 300 fs time-constant. d – Subsequent cooling to the vibrational ground-state of S_0 is completed after 30 ps (τ = 8.4 ps). e, f – Time traces for the decays of S_1 and cooling in S_0 are the dominant contributions to the spectral evolution. g – Spectral decomposition at $\Delta A(t_{inf})$ yields 6.7% for the ring-opening of **4-4cH**.*

7.5.2.4 Model for excited-state dynamic

The ring-closure or –opening, respectively, is displayed by a diagram where the potential energy follows the ring-closing coordinate. The results so far shall be summarized with such a diagram in due consideration of a theoretically established scheme (see Scheme 7-2). Starting with

excited **4-4oH** (**4-4oH***) on the left side, population is equally transferred into S_1 and S_2. Ultrafast internal conversion (IC) from S_2 to S_1 follows a 50 fs time-constant and the entire population reaches the point of conical intersection (CI, red circle) with τ = 300 fs. At the point of CI the configuration of the excited DAE is closer to relaxed **4-4oH** than to **4-4cH**. In Scheme 7-2this case is pictured by the CI being located on the left side of the ground-state barrier that separates both isomers. Therefore, transition to S_0 mainly repopulates the ring-open DAE (94.7%), here with τ = 30.8 ps corresponding to a barrier of 4.8 kcal mol^{-1}. Next, the relaxation scheme of excited **4-4cH** (**4-4cH***) is outlined on the right of Scheme 7-2. Relaxation away from the FC region into a local minimum proceeds with a time-constant of 50 fs. From there, fast IC into vibrationally excited **4-4cH** follows a 300 fs time-constant. Almost no population manages to overcome the barrier to reach the CI, evident by the low quantum yield for the ring-opening. Subsequent cooling in S_0 takes place with a characteristic time of 8.4 ps.

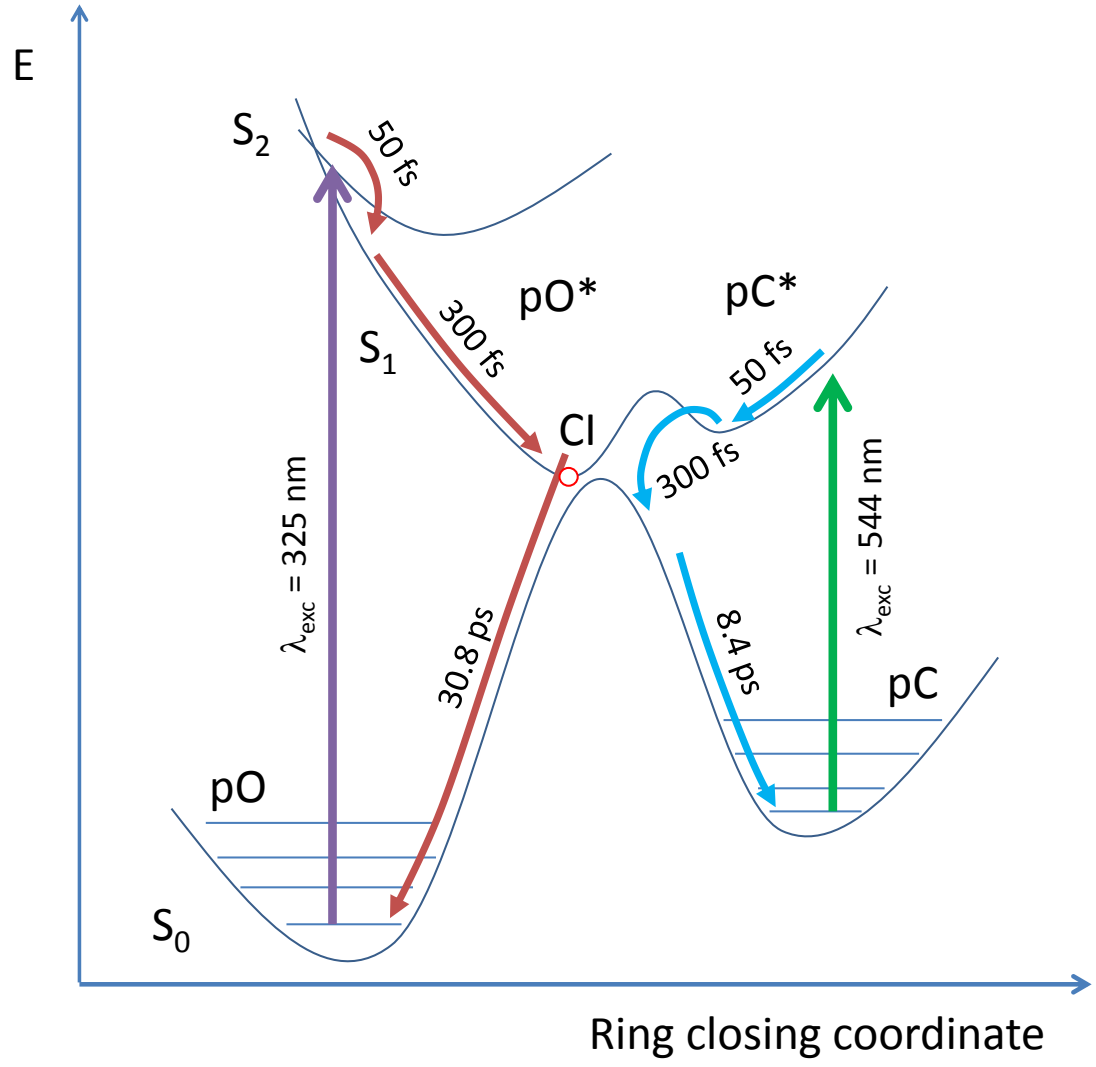

*Scheme 7-2 Potential energy diagram for the ring-opening and -closure of **4-4c** and **4-4o**, respectively.*

4-4o → 4-4c

The following interpretation of TA is, on one side, concluded directly from the spectra and on the other side from decay-associated spectra (DAS). The latter is one possibility to describe TA evolution by assuming that spectral changes can be expressed by an exponential decay of optical density via $A_i(\lambda, t) \cdot exp(-t/\tau_i)$. Here, $A_i(\lambda, t)$ equals the i-th DAS that corresponds to decay-time τ_i (see Figure 7-30). For example, if one DAS contains a region with negative sign, it either means an exponential decay of negative optical density or an exponential rise of an absorption band.

TA spectra of **4-4o** in acetonitrile are measured upon 400 nm excitation and are shown in Figure 7-29 together with kinetic traces and an estimate for the quantum yield of the ring-closure. *a* – Shortly after optical excitation (τ = 60 fs) the open isomer does perform the ring-closure with a quantum yield of 90%. Corresponding amounts of SE (**4-4o**-SE) and S_1-ESA (**4-4o**-ESA) decay between 400 and 690 nm. At the same time, ground-state absorption bands of vibrationally excited (hot) **4-4c** appear. This attribution follows from a comparison with the TA spectrum at infinite delay times where bands of the stationary **4-4c**-spectrum are located at the same positions (see Figure 7-29, *g*). *b* – The time-window up to 1.5 ps is dedicated to the excited-state evolution of remaining **4-4o**. Vibrational relaxation in S_1 is seen as a S_1-ESA blue-shift around 330 nm. Simultaneous changes in oscillator-strengths of upward and downward transitions may lead to a renewed visibility of **4-4o**-SE around 640 nm. *c* – Coming back to **4-4c**, cooling of the hot ground-state takes place with τ = 10.5 ps, which is of the same order of magnitude as cooling in **4-4cH** (8.4 ps). The determining sign for vibrational relaxation is the narrowing of the $S_1 \leftarrow S_0$ absorption band. *d* – The final step in TA evolution marks the return of the remaining **4-4o** to the electronic ground-state which is best seen in a vanishing S_1-ESA band. Barely visible, however, is the very small amount of bleach recovery in the blue edge of the spectral window. Altogether, the latest relaxation proceeds with a 140 ps time-constant until the TA spectrum reaches its stationary shape. *e* – The evolution of the **4-4o**-SE band is illustrated with a calculated band-integral over the region 620 – 690 nm. *f* – Recovery of bleach is barely visible for **4-4o** because the amount left in the excited state is very little. *g* – The TA spectrum at infinite delay times is used to estimate the quatum-yield for the conversion of **4-4o** to **4-4c**, here 90% (stationary: 47%). In addition, the TA spectrum at 0.3 ps is added with a dashed line to compare the early spectrum with the stationary spectrum after relaxation. The similarity in shape, position and signal height indicates a very fast and almost quantitative product formation (< 300 fs, 90%).

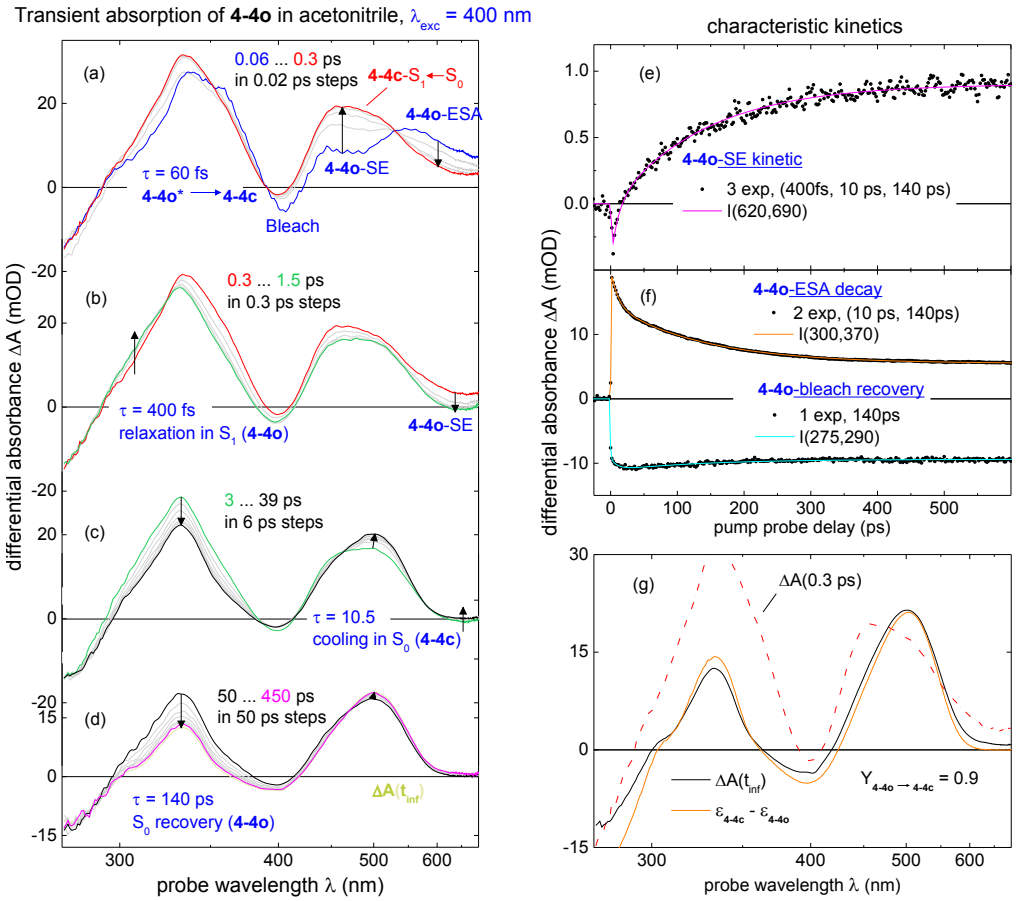

*Figure 7-29 TA spectra of **4-4o** in acetonitrile are measured upon 400 nm excitation. a – Ultrafast conversion of the open isomer to the closed form **4-4c** (with τ = 60 fs). b – Relaxation in S_1 of the remaining **4-4o** is seen as a shift of S_1-ESA around 330 nm and as a change of oscillator-strength in the red part of the spectrum where **4-4o**-SE dominates (both with τ = 400 fs). c – After the ring-closure all hot **4-4c**-molecules relax into the vibrational ground-state of S_0 with a 10.5 ps time-constant. d – S_1-ESA decay and recovery of bleach indicate that unconverted **4-4o** also return to the electronic ground-state. e – The band-integral, calculated for the region 620 – 690 nm is presumed to describe the **4-4o**-SE decay on a long time-scale (up to 600 ps). f – **4-4o**-ESA- and bleach decay on a long time-scale indicates the return of the remaining **4-4o** to the electronic ground-state. g – The quantum-yield for the ring-closure is estimated to 90%. The similarity in shape, position and signal height indicates a very fast and almost quantitative product formation (< 300 fs, 90%).*

As stated before, the interpretation of the TA spectra that monitor the evolution of **4-4o** is partly based on the involved Decay associated spectra (DAS). We assume two independently evolving species: formed **4-4c** and remaining **4-4o**. Therefore, it is reasonable to associate all obtained DAS to either species. This association is pictured in Figure 7-30. Once again, the upper part denotes the ultrafast formation of the photo-product **4-4c** in S_1 and the subsequent transition to S_0 (see also Figure 7-29, *a*). The middle part of Figure 7-30 contains the DAS for any further evolution of the hot **4-4c**-molecules. Vibrational relaxation in S_0 is usually accompanied by a narrowing of the absorption band (green DAS). This DAS exhibits a dispersive structure around the maximum of $S_1 \leftarrow S_0$ absorption. In accordance with the interpretation of DAS a negative sign describes a gain of intensity at the peak (upward arrow) while the two adjacent lobes of positive sign indicate loss of intensity around the peak (downward arrow). In total, narrowing of this band

is observed. The TA spectrum at infinite delay times (orange DAS) contains the stationary spectrum of **4-4c** (positive signal) that resembles absorption bands visible at ~ 0.3 ps. This similarity confirms the ultrafast ring-closure. The bottom part of Figure 7-30 contains two DAS that correspond to relaxation in S_1 (cyan DAS) and ground-state recovery (red DAS), respectively. Vibrational relaxation in the excited-state is usually seen as a blue-shift of ESA. Such a shift can be regarded as gain on the blue side and loss on the red side of ESA, which is realized with a dispersive band-shape around 320 nm in the corresponding DAS. Ground-state recovery of **4-4o** is accompanied by the decay of bleach, ESA and SE.

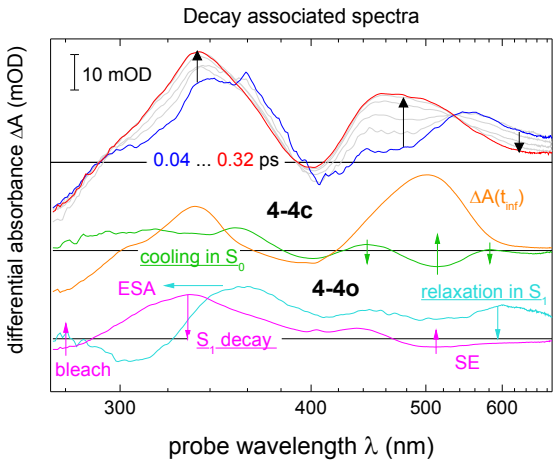

*Figure 7-30 Decay associated spectra (DAS) reflect the spectral changes when a system evolves between two virtual states. Illustrated on top is the ultrafast ring-closure of **4-4o** to **4-4c** (compare with **figure 4**, a). The middle part shows the (green) DAS that is attributed to ground-state cooling of hot **4-4c**. At the bottom two DAS reflect relaxation and decay of S_1 (blue and red DAS).*

4-4c → 4-4o

TA spectra of **4-4c** in acetonitrile are measured upon 544 nm optical excitation are shown in Figure 7-31 together with kinetic traces and an estimate for the quantum yield of the ring-opening. *a* – The spectrum builds up within the response time and FC relaxation takes place shortly after with τ = 100 fs. This is seen as a sharpening of ESA, a little above 400 nm. *b* – Similar to **4-4cH**, a quick return to the electronic ground-state is observed, here with a 500 fs time-constant. Again, dispersive features on the low-frequency side of stationary transitions indicate that the molecule is vibrationally excited. *c* – Cooling in S_0 proceeds with τ = 7.2 ps, which is getting in line with the corresponding relaxation time observed with **4-4cH** (8.4 ps). *d* – Return to the (hot) electronic ground-state is seen by the decay of ESA between 350 and 430 nm. *e* – The entire return to vibrationally relaxed S_0 (decay of S_1 and cooling in S_0) is reflected by the evolution of bleach. *f* – The quantum yield for the ring-opening of **4-4c** to **4-4o** is determined to 18% (stationary: 9.6%),

which is more than twice as much as the corresponding yield obtained from the protonated isomers (~ 7%).

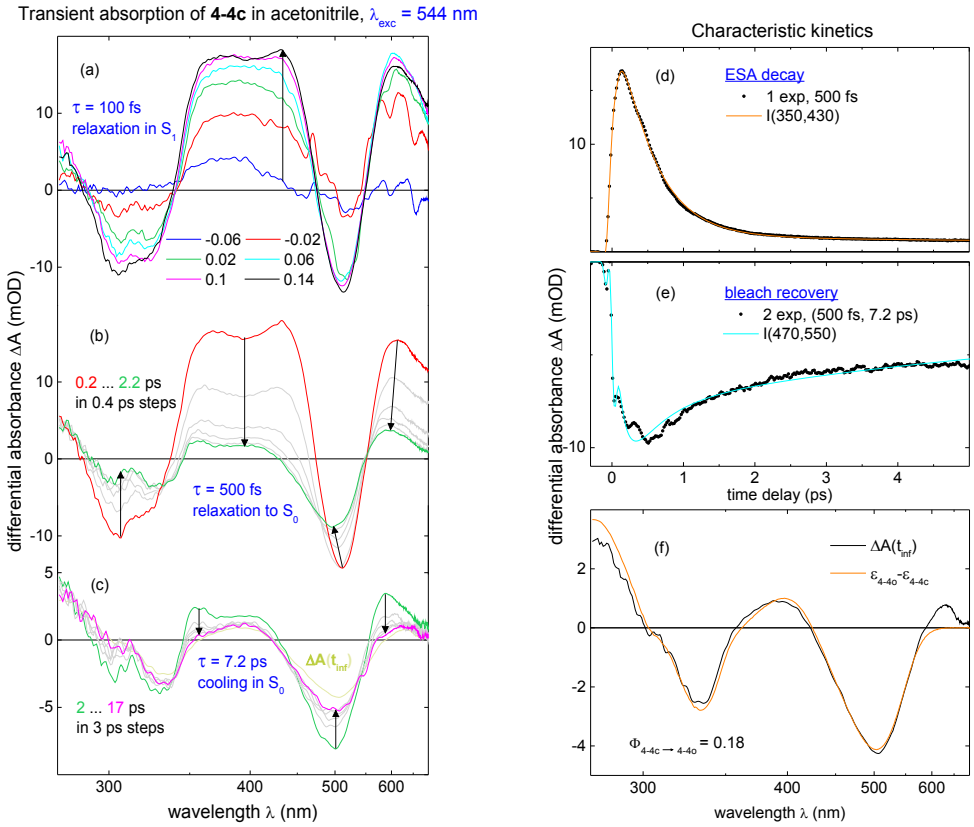

*Figure 7-31 TA spectra of **4-4c** in acetonitrile upon 544 nm excitation. a – FC relaxation in S_1 proceeds with τ = 100 fs. b – Fast relaxation to the vibrationally excited ground-state (τ = 500 fs). c – Cooling in S_0 proceeds with a 7.2 ps time-constant. d – Decay of ESA reflects internal conversion to S_0. e – Ground-state recovery proceeds bi-exponentially with the decay of S_1 and subsequent cooling in S_0, both seen as spectral evolution in the bleach-region. f – A quantum yield of 18% is determined for the ring-opening.*

Scheme 7-3 summarizes the evolution of excited **4-4o** and **4-4c**, respectively. Starting with **4-4o**, upon optical excitation the photoproduct **4-4c** is formed on a very short time-scale (60 fs) where almost 90% of the excited population strides through the conical intersection (CI, red circle). The remainder of ~ 10% that does not possess enough ballistic energy and resides on S_1 until the original ground-state is re-populated with τ = 140 ps. Note, that the point of CI is located on the right side of the ground-state energy barrier to suggest a closer similarity of **4-4o*** with **4-4c**. When the closed isomer **4-4c** is excited a relaxation pattern very similar to **4-4cH** is observed: vibrational relaxation in S_1 (100 fs), fast internal conversion to the hot ground-state (500 fs) and subsequent cooling in S_0 (~ 10 ps). The biggest difference in the ring-opening process between the protonated and deprotonated DAE is that the amount of photo-product is three times larger for **4-4c**.

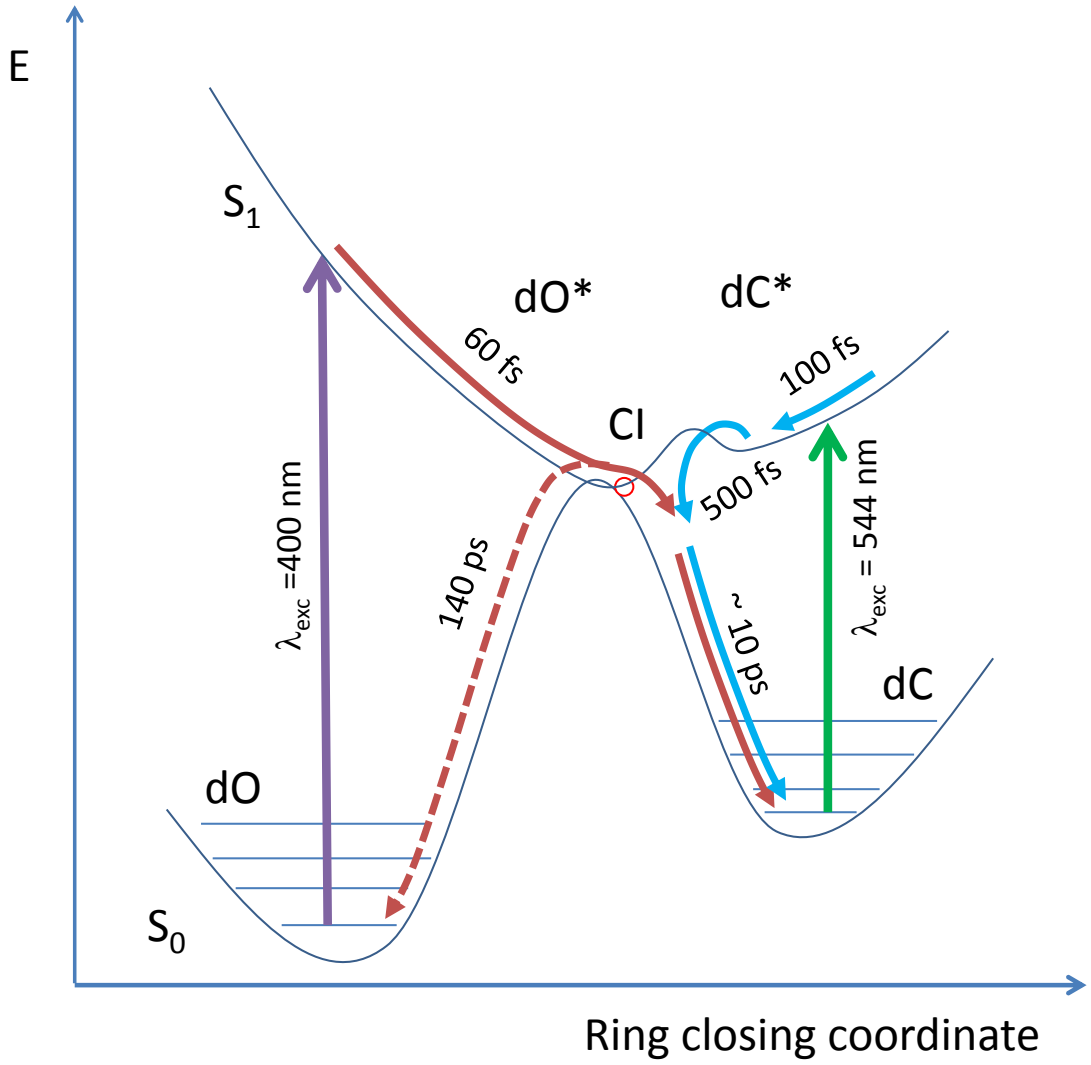

*Scheme 7-3 Potential energy diagram for the ring-opening and –closure of **4-4c** and **4-4o**, respectively.*